Complex structure of Piton de la Fournaise and its underlying lithosphere revealed by magnetotelluric 3D inversion

Lydie-Sarah Gailler, Anna Martí, Jean-François Lénat

▶ **To cite this version:**

Lydie-Sarah Gailler, Anna Martí, Jean-François Lénat. Complex structure of Piton de la Fournaise and its underlying lithosphere revealed by magnetotelluric 3D inversion. Journal of Volcanology and Geothermal Research, 2018, 356, pp.200-210. ⟨10.1016/j.jvolgeores.2018.03.006⟩. ⟨insu-03708972⟩

HAL Id: insu-03708972

https://insu.hal.science/insu-03708972v1

Submitted on 17 Jun 2025

HAL is a multi-disciplinary open access archive for the deposit and dissemination of scientific research documents, whether they are published or not. The documents may come from teaching and research institutions in France or abroad, or from public or private research centers.

L'archive ouverte pluridisciplinaire **HAL**, est destinée au dépôt et à la diffusion de documents scientifiques de niveau recherche, publiés ou non, émanant des établissements d'enseignement et de recherche français ou étrangers, des laboratoires publics ou privés.

Distributed under a Creative Commons CC BY 4.0 - Attribution - International License

Complex structure of Piton de la Fournaise and its underlying lithosphere revealed by MT 3D inversion.

Lydie-Sarah Gailler[1], Anna Marti[2], Jean-François Lénat[1]

[1] Université Clermont Auvergne, Laboratoire Magmas et Volcans - CNRS, UMR 6524, IRD, R 163, 6 Avenue Blaise Pascal TSA 60026 – CS 60026, 63178 AUBIERE Cedex, FRANCE

[2] Departament de Geodinàmica i Geofísica, Universitat de Barcelona, Spain

Corresponding author: lydiegailler@hotmail.fr

Abstract

La Réunion is a large volcanic construction resting on Paleocene oceanic crust. Through the 3D inversion of a large set of magnetotelluric (MT) soundings, our results reveal the general resistivity structure of the western part of Piton de la Fournaise volcano down to its base and the first ten kilometers or so of the underlying lithosphere. The upper resistive layer is associated to a superimposition of unsaturated and probably water-saturated lava flows with an averaged thickness of 1.5 km overlying more or less continuous highly conductive patches which imply the presence of highly conductive fluids and/or minerals. In the summit area and Enclos, this conductor is unambiguously attributed to the presently active hydrothermal system. In the Plaine des Sables, it is tentatively associated with the hydrothermal alteration beneath the ancient volcanic center. A third widespread conductive patch is observed below the NW flank of Piton de la Fournaise resulting more likely from volcanic activity since it coincides with part of the N120 rift zone. In the area beneath the Plaine des Sables where a dense intrusive complex has been inferred from gravity models, the resistivity is not significantly higher. The upper lithosphere is markedly more resistive than the bulk of the

volcanic construction (except for the upper part of this latter) forming a virtual horizon around -4 km in depth. However, one main conductive anomaly is present in the crust beneath the NW flank along the N120 rift zone assumed to be linked with present day seismic and degassing activity. The NW flank therefore appears as a main area of interest in the study of Piton de la Fournaise activity and its evolution as well. We therefore demonstrate the capability of the method to image major shallow structures such as the hydrothermally altered zones, and deeper ones such as possibly the heterogeneity of the crust.

Keywords: Piton de la Fournaise; magnetotelluric data; 3D inversion; hydrothermal system; oceanic lithosphere; plumbing system.

1. Introduction

The architecture of volcanic systems is important to know because: (1) it provides information on the construction and evolution of the volcanic structures; (2) it has an influence on the magma paths (the conduits) and (3) it may generate its own volcano-tectonic activity through, for example, gravitational instabilities. The need of high resolution imagery of the interior of the volcanic systems is therefore obvious and is the main motivation for the application geophysical prospecting methods in volcanology. Several geophysical techniques can be used to image the structures and rocks physical properties at depth. The most common are seismics, gravity and electrical resistivity measurements. The magnetotelluric (MT) method has been used since the early 1980s in volcanic areas for both geothermal exploration and volcanological studies. It is particularly well suited for volcanic studies (Piña et al. 2014 and references therein) since the electrical conductivity is influenced by both temperature and compositional variations. But is has also the capability to probe deep in the crust and the mantle (Jones, 1999)

Electrical resistivity of crustal rocks generally varies over several orders of magnitude (1 10^{-4} to 100 kohm·m), depending on a wide range of petrological and physical parameters, such as bound versus free water, composition of the fluids, temperature, and the content of clay or metallic minerals. Resistivity is usually dominated by the ionic conductivity of the fluids present in the interconnected pores. In general, a basaltic shield consists predominantly of a pile of highly permeable lava flows. If not altered or water saturated, such formations generally have resistivity as high as 10–100 kohm-m. A large resistivity variation usually exists at the transition between the vadose zone, where rocks contain only some moisture, and the zone beneath the water table, where the rocks are fully water saturated. On oceanic islands, the basal water table consists of a lens of fresh water (Ghyben-Herzberg lens; e.g., see Vacher, 1988) floating over the seawater- saturated zone. The top of the freshwater lens generally takes place at an elevation of a few meters to a few tens of meters above the sea level. However, this model, initially derived for the Hawaiian Islands, may not apply when the hydraulic conductivity decreases significantly with depth. In this case, the water table forms a high elevation dome within the edifice. The latter model is preferred in the case of Piton de la Fournaise by Join et al. (2005).The resistivity of a basaltic pile saturated with fresh water is generally a few hundred ohm·m, but drops to a few tens of ohm·m or less when saturated with sea water. In addition to water saturation, the nature of the formation also plays a role in the resistivity distribution. In intrusion zones (central zone, rift zones), swarms of subvertical dikes can create impermeable barriers that impound bodies of water at high elevations (Stearns, 1942; Takasaki, 1981; Jackson and Kauahikaua, 1987). Alteration, particularly hydrothermal alteration, tends to lower the rock resistivity through the formation of highly conductive, hydrated minerals such as clay minerals and zeolites. Similarly, pyroclastic and breccia deposits generally have lower resistivity values than lava flows, because they typically contain hydrated minerals. Magma has a resistivity of only a few

74 ohm·m or less (Rai and Manghnani, 1977; Haak, 1982). The resistivity of the upper oceanic
75 lithosphere underlying a volcanic edifice may be different and more complex than regular
76 oceanic lithosphere. Constable and Cox (1996) indicate that the resistivity of an undisturbed
77 upper oceanic lithosphere is more than 100 ohm·m. Increasing compaction with depth causes
78 a decrease in the effective porosity and hence increases the resistivity. However, it may vary
79 significantly depending on its temperature, and hence often its age: a young, hotter,
80 lithosphere will be less resistive than its older counterpart (Nobes et al., 1992; Unsworth,
81 1994; MacGregor et al., 1998). The presence of conductive layers (e.g. fluid and/or mineral-
82 filled fractures, magma) will also contribute to lowering the rock resistivity. In the case of hot
83 spot volcanism, magmatic underplating is a common feature, and this has been suggested by
84 Charvis et al. (1999) and Gallart et al. (1999) for La Réunion. Therefore the presence of
85 magma beneath the crust can be investigated with the MT data. At greater depths, as the
86 temperature increases, the mantle becomes more conductive. Laboratory experiments on
87 basaltic and mantle rocks show the very low electrical conductivity of melts. For example, at
88 the scale of the Hawaiian hot spot swell, 2D electrical models have shown a resistive
89 lithosphere underlain by a conductive lower mantle, and a narrow conductive plume
90 connecting the surface of the island to the lower mantle (Constable and Heinson, 2004).
91 In this work, we focus on La Réunion volcanic edifice, which has been extensively studied
92 since decades, with a special interest given to Piton de la Fournaise volcano (see Lénat et al.
93 (2012a and reference therein)). However, the deep architecture of Piton de la Fournaise and
94 its underlying lithosphere remain poorly known. Previous geoelectrical studies carried out by
95 Lénat et al. (2000) focused on the first kilometer or so of the active part of the volcano. The
96 aim of the current study is to take advantage of a new large set of MT soundings acquired
97 during a geothermal reconnaissance of Piton de la Fournaise in order to image the resistivity
98 structure down to several to tens of kilometers. The good spatial coverage of the sites and the

lack of a preferred strike direction obtained from the dimensionality analysis allowed us to invert the data and obtain a 3D geoelectrical model of the volcanic edifice and its surrounding which is discussed it in terms of large scale structures.

2. Geological and geophysical structure of Piton de la Fournaise and its basement

Piton de la Fournaise is located on the southeast of La Réunion Island (Fig. 1a), and is one of the world's most active basaltic shield volcanoes. Its evolution can be reconstructed by means of its deep valleys. The evolution can be divided into two main periods: the Ancient Shield (> 0.15 Ma) and the Recent Shield (< 0.15 Ma). At the base of the deep valleys (Rivière des Remparts, Rivière de l'Est and Rivière Langevin) (Fig. 1a), a differentiated unit called Pintades Unit (Bachèlery, 1981; Bachèlery and Mairine, 1990; Merle et al., 2010) is evidenced. It is dated from at least 530 kyr to 400/450 kyr, and is inferred by Smetiana (2011) to belong to a volcano which predates Piton de la Fournaise called Les Alizés volcano (Rançon et al., 1989; Malengreau et al., 1999; Lénat et al., 2001). The Pintades Unit is observed up to 1000/1200 m in elevation in the Rivière des Remparts, and therefore Piton de La Fournaise, rising at 2632 m, must be a relatively thin edifice (Merle et al., 2010).

Since about 290 kyr, the geological history of Piton de la Fournaise is summarized as a sequence of volcano-tectonic events with alternating episodes of volcanic destruction and reconstruction (Merle et al., 2010). Two calderas have been identified during the Ancient Shield period: the Rivière des Remparts caldera at about 250 kyr and the Morne Langevin caldera at about 150 kyr. During the Ancient Shield period, the volcanic center is inferred to have been located in what is presently the Plaine des Sables (Fig. 1). Bachèlery and Mairine (1990) propose that the eastward displacement of the volcano to its present location (Fig. 1b) could have taken place at about 150 kyr, concurrently with the formation of the Morne

123 Langevin caldera, although it could be as young as the formation of the Plaine des Sables
124 caldera, which formed at about 65 and/or 40 kyr (Gillot and Nativel, 1989; Bachèlery, P. and
125 Mairine, 1990; Staudacher and Allègre, 1993; Merle et al., 2010). Letourneur et al. (2008)
126 suggest the possibility of an intermediate location before the present one. The formation of the
127 most recent, 8 km-wide caldera, called the Enclos Fouqué caldera (or, simply, Enclos), has
128 been dated at about 4.5 kyr (Bachèlery, 1981; Staudacher and Allègre, 1993; Mohamed-
129 Abchir, 1996), but the recent reappraisal of the existing radiocarbon data and new ages
130 suggest two younger collapse episodes at around 3700, 3100 and 2300 kyr (Morandi et al.,
131 2015). The present eruptive center is located on the Central Cone which has grown inside the
132 Enclos caldera, which is breached to the east (the Grandes Pentes and Grand Brulé areas). The
133 relationships between the Enclos Fouqué, the Grandes Pentes and the Grand Brûlé are still
134 debated (Bachèlery, 1981; Merle and Lénat, 2003; Michon and Saint-Ange, 2008).
135 The locations of the magma reservoirs and transfer structures have been recently reviewed by
136 Michon et al. (2016). Whereas most of the recent eruptive activity took place within the
137 Enclos, either on the Central Cone or along the NE and SE rift zones, the presence of eruptive
138 fissures and pyroclastic cones in other areas of the edifice indicates that magmas have reached
139 the surface via different paths. In addition to the NE and SW rift zones that radiate from the
140 Central Area of Piton de la Fournaise and extend beyond the Enclos (Fig 1a), a broad, diffuse
141 N120 rift zone occurs between Piton des Neiges and Piton de la Fournaise volcanoes. It is
142 marked by numerous (~160) cinder cones and lava flows. The age of this rift zone is not well
143 defined, but eruptions began at least 29 ky ago (McDougall, 1971) and the last eruption is
144 dated at 0.140 kyr (Morandi et al., 2015). Another concentration of cones is observed at the
145 base of the subaerial south flank of Piton de La Fournaise. Michon et al. (2016) name this area
146 the "South Volcanic Zone". Michon et al. (2016) propose to interpret the deep seismicity
147 observed at La Réunion in connection with the distribution of the volcanic zones at the

surface. They use a compilation of the volcano-tectonic (VT) seismicity from 1993 to 2013. Below a depth of 10-11 km (base of the crust, according to (Gallart et al., 1999)), most of the VT events are located beneath the northwestern part of Piton de la Fournaise and beneath the NW flank of Piton de la Fournaise and the Plaine des Cafres areas. They are generally deeper (up to about 30 km) to the NW and become progressively shallower (up to 10-11 km) near the presently active area of Piton de la Fournaise. No seismicity is observed from the base of the crust to a region above 8 km in depth. Michon et al. (2016) suggest that this aseismic zone could correspond to a zone of magma storage (underplating). They also propose that the deep northwestern seismicity is organized along a N30-40 axis at depths greater than 20 km and then rotates and concentrates beneath the N120 NW rift zone. Michon et al. (2016) link the deep seismicity with magma transfer, and suggest a vertical ascent of magma between 30 and 20 km in depth. Earthquakes are observed from about 8 km in depth to the surface before and during volcanic crises with an overall lateral migration of the seismic swarms along 10-11 km, from the Plain des Sables toward the presently active area of Piton de la Fournaise. In addition, a high resolution survey of soil CO_2 emissions carried out on the western flank of Piton de la Fournaise (Boudoire et al., 2017) has evidenced that narrow zones of high fluxes are aligned along a well-defined N135° axis coincident with seismic swarms detected during the reawakening of the volcano (2014–2015). The authors have called this alignment the Songit Lineament (Fig. 1a) which is consistent with the orientation of paleo-spreading axes. They also suggest that this latter could result from the inheritance of the oceanic lithosphere.

Receiver function techniques have also provided information in depth (Fontaine et al., 2015). A joint inversion of receiver function and surface wave dispersion suggests that thin magmatic underplating may be present below La Réunion. Lateral variations of its thickness suggest that this latter could result from an important interaction between the plume and

172 lithosphere. In addition, a low velocity layer interpreted as a zone of partial melt beneath the
173 active volcano is evidenced at a depth of about 33 km.

174 At Piton de la Fournaise, recent geophysical explorations using electromagnetic surveys have
175 provided new hydrogeological information (Join et al., 2005). Their hydrogeological model
176 suggests the presence of a continuous aquifer which domes at 1800 m asl below the central
177 active part. It deepens to between 1600 to 1400 m asl beneath the Plaine des Sables and is
178 even deeper beneath the Fond de la Rivière de l'Est depression. A recent synthesis of all
179 available data led Lénat et al. (2012 and reference therein) to propose a geological model of
180 the infrastructure of Piton de la Fournaise and its basement (Fig. 1b). We summarize here the
181 main points of this interpretative geological section, starting from the surface: (1) shallow
182 accumulation of dense lava flows in paleo depressions, (2) presence of pervasive
183 hydrothermal alteration, (3) the presumed interface with Les Alizés volcano, (4) presence of
184 hypo-volcanic complexes (gabbros, cumulates) beneath the Plaine des Sables area, (5)
185 possible ancient and recent magma reservoir at the interface between La Réunion and the
186 oceanic crust, (6) no significant flexure of the lithosphere, and (7) possible magma
187 underplating at the base of the crust.
188 The dense Ancient Shield hypovolcanic complex (ASC) beneath the Plaines des Sables-
189 Enclos area is a major feature inside the edifice that creates a positive gravity anomaly. The
190 location of the complex has been deduced from 2D ¾ and 3D gravity modelling (Gailler et al.,
191 2009). Gabbro and cumulate xenoliths found in lava flows and tephra above this complex
192 (Bachèlery, 1981) probably originated from it. The base of the volcanic edifice on the oceanic
193 crust is inferred to be around -4 km in elevation, which is the level of the oceanic floor around
194 La Réunion. This is a reasonable assumption given that seismic studies (De Voogd et al.,
195 1999; Gallart et al., 1999) suggest that there is no lithospheric flexure beneath La Réunion.

196 Lastly, we note that the estimated Curie depth, based on analysis of the magnetic anomalies
197 (Gailler et al., 2016), shows a bulge in the Curie surface below the island, with its top shifted
198 offshore to the NE of Piton de la Fournaise. Nevertheless, several features as well as the deep
199 structure, beyond the volcanic edifice sensu stricto remains poorly imaged.

200 # 3. Resistivity data

201 In order to investigate the deep structure of the edifice, we have compiled all available
202 electrical data, especially magnetotelluric (MT) soundings which provide the greatest depth of
203 investigation in the western part of Piton de la Fournaise area.

204 ## 3.1. Previous studies and new data

205 Electric and electromagnetic surveys have been carried out on La Réunion Island for
206 hydrogeologic studies (Courteaud, 1996; Schnegg, 1997), structural studies of Piton de la
207 Fournaise (Schnegg, 1997; Lénat et al., 2000) and geothermal prospecting (Benderitter and
208 Gérard, 1984; Benderitter, 1990; Smith, 1996). A compilation of these datasets has been
209 already provided by Gailler and Lénat (2012) to study the island at a larger scale. In this
210 study, we have mostly used new data acquired during a geothermal reconnaissance project
211 between 2001 and 2004. The main datasets (Fig. A1 in Supporting Information A) come from
212 a magnetotelluric (MT) survey carried out by Phoenix Geophysics in 2002 (34 collocated MT
213 soundings, AMT for audiomagnetotellurics and TDEM for Time Domain ElectroMagnetic
214 soundings) and an MT survey by PB Power (53 collocated MT and TDEM soundings). The
215 data were collected in the 10^{-3} to 10^{4} Hz frequency range. We have also used 24 AMT
216 soundings (in the range 1 to 10^{4} Hz) acquired by our group (here designated as UBP) in 2001
217 (7 collocated with shallow Direct Current (DC) older electrical soundings), 4 MT soundings
218 (in the range 10^{-3} to 10^{3} Hz) acquired in 2001 by University Pierre et Marie Curie (here
219 designated as Paris) and 3 old MT soundings acquired by the Bureau de la Recherche

220 Géologique et Minière (BRGM). The data of the latter (in the range 10^{-2} to 10^{2} Hz) were
221 digitized from paper copies.

222 ### 3.2. Data processing and analysis

223 The MT and AMT data were processed using WinGlink® software package from Geosystem.
224 When multiple sets of data were available for the same location (i.e. HF and LF for AMT and
225 MT data), the data were combined into a single sounding. A first quality inspection based on
226 the error bars and the consistency of the resistivity curves made us reduce the dataset to 108
227 sites located in figure 2. It can be observed that the density of soundings is much higher in the
228 Plaine des Sables, since this area was the target of the geothermal reconnaissance survey.
229 However, parts of the Fond de la Rivière de l'Est, Plaine des Remparts and even the NW
230 flank of Piton de la Fournaise Central Cone and Enclos are well enough covered by the data to
231 allow us to expand our study to these areas.

232 #### 3.2.1. Dimensionality analysis

233 We have carried out a dimensionality analysis using the WALDIM code from Martí et al.
234 (2009), which is based on the WAL invariants (Weaver et al., 2000).We used a threshold
235 value of 0.2 and assumed an error percentage of 5%. As shown in Figure 3, the distribution of
236 dimensionality shows a predominant 1D behavior for shorts periods (< 1s) and a few 2D and
237 mainly 3D as periods increases beyond 1s, which seem to be reasonable. The behavior
238 becomes fully 3D for periods longer than 10 s (Fig. 3), suggesting that a 3D inversion of the
239 data is needed for a consistent interpretation of the overall dataset.

240 In order to better investigate the quality of the data and to provide a first general view of the
241 resistivity distribution in depth, we provide maps of invariant phases for periods ranging from
242 10^{-4} to 10^{3} (Fig. 4a) using WINGLINK software. In such analysis, the invariant phase is
243 calculated as the arithmetic mean of the phases elements, provides an image of the variation

244 of resistivity with the period, and presents the strong advantage to be unaffected by static
245 shift. To complete the data analysis, Bostick resistivity inversions are also presented showing
246 the main distribution of resistivity at fixed elevations (Fig. 4b). An overall good coherency is
247 evidenced between both representations (Fig. 4a and b). For the shortest period (10^{-4}s), the
248 shallowest layer (2000 m asl) shows a very low invariant phase as well as high resistivity
249 values for most of the study area. At an intermediate range of periods (between 0.001 and 1s),
250 the invariant phase then progressively increases, especially in the area of Enclos Fouqué,
251 Plaine des Sables and Fond de la Rivière de l'Est. This feature could be correlated with the
252 decrease in resistivity observed from 1000 m to – 2000 m asl. Beyond a period of 100s and a
253 depth of -4000 m, the invariant phase scheme and the resistivity distribution are more
254 complex, with an overall increase in resistivity with depth.
255 Therefore, this analysis enables to delineate several interesting features: i) a resistive shallow
256 layer above 1000 m asl, ii) an intermediate conductive layer between 1000 and – 2000 m in
257 average, and iii) higher resistivity more in depth with both lateral and vertical heterogeneities
258 at depths greater than -4000 m asl. The 3D model will help depict the details of this general
259 description.
260
261 **3.2.2. Sea water and topography artifacts**
262 In an oceanic environment such as La Réunion with strong reliefs, it should be stressed that
263 the data artifacts associated to the sea, topography and bathymetry can be important. This is
264 especially the case for coastal soundings where the influence of the sea could be significant
265 and affect the interpretation of AMT and MT data. Pinã-Varas et al. (2014) have identified
266 such effects on the MT data by constructing a 3D conceptual geoelectrical model of Tenerife
267 Island, using known geological and geophysical data. Details on this synthetic test are given
268 in their study, suggesting that the MT responses are strongly distorted by topography and sea

effects at frequencies lower than 0.1 Hz. These effects will not be an issue as far as the bathymetry, topography and sea water are included in the model. A 3D approach should be, here again, preferred to provide reliable modeling of our dataset. 2D inversions have been also performed using Winglink software to investigate several profiles of interest. However, the structures are not fully reliable given the strong assumption of strike direction and TE and TM mode.

4. 3D inversion

4.1. Initial model

We have computed a 3D electrical resistivity model of Piton de la Fournaise area using the ModEm code (Egbert and Kelbert, 2012; Kelbert et al., 2014). The starting 3D mesh model was build using WINGLINK described by Mackie and Madden (1993) subsequently developed and implemented by Geosystem. The initial model was discretized onto a 79 (NS) x 70 (EW) x 78 (vertical) grid, where topography and bathymetry were defined and fixed using a digital elevation model. The resistivity value of the seawater was set to 0.33 ohm·m, and a thin layer of conductive sediments underwater was added in the initial model fixed at 200 ohm.m. The mesh was more refined in the first km (from 2600 m asl to -5000 m bsl) with the aim of obtaining a clear image of the area of hydrothermal alteration and eventually the presence of a magmatic reservoir more in depth. The inversions were undertaken using both the off-diagonal (Zxy, Zyx) and diagonal when available (Zxx, Zyy) components of the impedance tensor for a maximum of 15 periods in the period range between 0,0001 s to 1000 s, depending on the stations. A 5 % error floor in the impedance components was imposed during the inversion process. A smoothing of 0.2 was applied in all directions and an initial lambda value of 10 was chosen. The starting RMS was 9.45, while the final RMS is 1.50 after 63 iterations. Fig. B1 in the supplementary material B shows the comparison between the raw

293 data and model responses as apparent resistivity and phases curves for each site used in
294 inversion. Figure 5 shows an example for one site showing that the fits of the diagonals are
295 not perfect but acceptable. Several tests have been also done inverting either the full tensor or
296 only the off-diagonals. The resulting models are very similar, which confirms the overall good
297 consistency of the final 3D model described hereafter.

298 **4.2. The 3D final model**

299 In order to better visualize the 3D model, we present here two multi-segments sections
300 crossing the main areas of interest, i.e. Plaine des Sables, Enflos Fouqué, Fond de la Rivière
301 de l'Est and NW flank of Piton de la Fournaise (Fig. 6a and b). The geological studies
302 described above and in figure 1b constitute a good reference model to start interpreting our
303 3D resistivity model. To the first order, the general structure can be described as follows:

304 (1) In the shallow resistive layer, the interface between the highly and moderately
305 resistive values more or less mimics the topography.

306 (2) A very conductive layer, not continuous in the model is more superficial and thinner
307 below the Plaines des Sables, western of the dense hypovolcanic complex modeled
308 from gravity data (Gailler, 2010), and below the Enclos.

309 (3) In the deeper part of the edifice, the hypovolcanic complex is not individualized by a
310 resistivity contrast.

311 (4) The lithosphere is globally moderately resistive but not fully homogeneous.

312 **4.2.1. The shallow resistive layer**

313 In detail, the shallow resistive layer can be separated into a highly resistive layer (~1000 to
314 10000 ohm·m) with a thickness of 1 km – 1.5 km, overlying a thinner and less resistive one
315 (~100 to 1000 ohm·m). The shallower resistive layer is easily identified to piles of unsaturated
316 lava flows. The underlying layer has resistivity values compatible with that of water-saturated

317 lava flows, although it is observed at a relatively high elevation, slightly higher than that of
318 the regional water-table calculated by Join et al. (2005).

319 **4.2.2. The intermediate conductive layer**

320 A very conductive layer (~ 4 ohm·m or less to about 30 ohm·m) is observed below, with an
321 average thickness of about 1 km. In the model, it does not form a continuous layer but appears
322 as elongated patches. It is not possible to assume whether this discontinuous appearance is
323 real or an artefact of the model due to the distribution and quality of the data. This very
324 conductive layer is present in two different zones. The first one is at high elevation below the
325 Enclos (we have to keep in mind that the Central Cone is less resolved because it is not
326 covered by MT soundings), the Plaine des Sables, the Plaine des Remparts and the Fond de la
327 Rivière de l'Est. The second one is just above the inferred oceanic floor on the NW flank of
328 Piton de la Fournaise.

329 This conductor has been found in all the previous resistivity surveys (e.g. (Benderitter and
330 Gérard, 1984; Courteaud et al., 1997; Schnegg, 1997; Lénat et al., 2000)), in the different
331 areas of Piton de la Fournaise. Various interpretations have been proposed to explain the
332 presence of this conductor. Benderitter and Gérard (1984) attribute the very low resistivity to
333 hydrothermal alteration whereas Courteaud et al. (1997) explain it by the presence of clay-
334 rich brecciated material resulting from volcano-tectonic processes (caldera and flank
335 collapses). For Lénat et al. (2000), the conductor, rising to a depth of about 300 m beneath the
336 summit, is caused by the central hydrothermal activity within the Enclos. They suggest that in
337 the Plaine des Sables it could also be associated with the hydrothermal activity of Piton de la
338 Fournaise's old active center until the volcano center shifted to its present location in the
339 Enclos (Bachèlery and Mairine, 1990). In the other zones, the geological nature of the
340 conductor has not been identified.

341 Since the conductor is well above the expected level of sea water, the presence of which could
342 explain low resistivity values, such low resistivity values suggest the presence of hydrated
343 minerals, which could be found in landslide breccias, in hydrothermally altered zones, or in
344 thick pyroclastic layers. Therefore, the nature of the conductor may be different in each zone.
345 Below the NW flank of Piton de la Fournaise, the conductor above the preexisting sea floor
346 coincides with the N120 rift zone (Michon et al., 2016; Chevallier and Bachèlery, 1981;
347 Villeneuve and Bachèlery, 2006) characterized by a high density of large cinder cones. These
348 are fed by primitive magmas through deeply rooted intrusions (Michon et al., 2016). The
349 hydrothermal alteration caused by the swarm of the dikes in the rift zone is a possible
350 explanation of this resistivity anomaly.

351 **4.2.3. The base of the edifice and the transition with the crust**

352 As indicated above, the base of the volcanic edifice on the oceanic crust is inferred to lie at
353 around -4 km in elevation and the lithosphere does not show any significant flexure. A -4 km
354 resistivity transition is clear in two areas only. The first one is beneath La Plaine des Sables-
355 Fond de la Rivière de l'Est where the oceanic crust is more resistive (> 150 ohm.m) than the
356 base of the volcanic construction (< 100 ohm.m). The second one is at the NW, where, as
357 indicated above, a very conductive layer is present at the base of the volcanic construction. A
358 third transition is suggested beneath the Rivière des Remparts, but in this area the model is
359 poorly constrained by MT soundings.
360 The hypovolcanic dense complex of the Ancient Shield (ASC) of Piton de la Fournaise
361 revealed by gravity in the interior of the edifice (Fig. 6 a and b) would be expected to show a
362 higher resistivity that its surrounding, as it is the case for another intrusive complex beneath
363 Piton des Neiges volcano (Gailler and Lénat, 2012). Here, the dense complex does not show a
364 resistivity contrast with the rest of the lower part of the edifice. This lack of correlation
365 between the resistivity distribution and the gravity model may be explained by two types of

366 reasons. The geometry and density distribution of gravity model may be biased by the fact
367 that constant density is assumed for both the intrusive complex and its surrounding. This
368 could be a too large simplification of the reality and the geometry of the dense body could be
369 significantly different if large density variations exist within the dense body and within its
370 surrounding. A second type of explanation would be to consider that parts of the dense body
371 are fractured and/or hydrothermally altered, and therefore less resistive. As a whole, the deep
372 part of the edifice seems rather homogeneous in resistivity and no structural features, such as
373 the transition with Les Alizés, is observed.

374 **4.2.4. The oceanic lithosphere**

375 The upper oceanic lithosphere beneath La Réunion is globally resistive with values up to
376 several thousand ohm·m (Fig. 6a and b). The boundary between the crust and the upper
377 mantle, estimated to be around –12 km (Gallart et al., 1999), is not marked in the model. At
378 this range of depth, resistivity contrasts are suggested only below Plaine des Sables and
379 Enclos area on the Bostick analysis (Fig. 4b). Beneath the NW flank, a pronounced
380 conductive anomaly of the crust extends at large depth. It starts at the NW of the Plaines des
381 Sables-Fond de la Rivière de l'Est area and deepens down to about 8 km at the border of the
382 model. It seems to more or less follow the N120 rift zone comprising a very conductive (< 5
383 ohm.m) zone in the upper 2 km that is distinct from a similar feature observed above in the
384 volcanic construction.

385 High resistivity values (>1000 ohm.m) below the W flank and the Rivière des Remparts from
386 about -8 to -16 km in depth, are not reliable, because this area is only covered by a few
387 number of soundings and lies at the edge of the model. The highly conductive area at a depth
388 of -16 km covering a large area below the Plaine des Sables-Fond de la Rivière de l'Est and
389 even part of the Enclos and the NW flank of Piton de la Fournaise on the Bostick analysis

390 (Fig. 4b) is also not reliable, because our study area is relatively narrow and may be not
391 adequate to resolve the resistivity distribution in this range of depths (Bhattacharya and
392 Shalivahan, 2002).

393 5. Discussion and conclusion

394 The interior of Piton de la Fournaise has been investigated by numerous geophysical and
395 geological studies. However, the information for all the methods become less precise with
396 depth and therefore the deep part of the volcanic construction and its interaction with the
397 lithosphere are poorly known. Our MT study offers the advantages of being able to probe both
398 the volcanic construction and the upper lithosphere and to use a different physical parameter
399 than those of the previous seismic, gravity and magnetic studies. An interpretative scheme is
400 presented in figure 6c, based on our 3D resistivity model and results from other studies.
401 The upper part of the edifice is very typical of basaltic shield volcanoes predominantly built
402 by highly permeable lava flows. Accordingly, the first layer of water unsaturated lava flows is
403 highly resistive. The fact that it evolves at depth to a more conductive layer (water saturated
404 lava flows) supports the hydrogeological model of Join et al. (2005) that postulates the
405 presence of a continuous high water table at Piton de la Fournaise. This contrasts with the
406 classical Hawaiian hydrogeological model where high elevation groundwater bodies are
407 disconnected and impounded by dike swarms or impervious layers.
408 At depth, within the edifice, the presence of more or less continuous highly conductive (< 5
409 ohm.m) patches is a special feature. Such low resistivity values imply the presence of highly
410 conductive fluids and/or minerals. High conductivity fluids should be hot and/or mineralized
411 ones. High conductivity minerals in this context are hydrated minerals commonly resulting
412 from hydrothermal alteration. The high conductivity layer is described in greater detail by
413 Lénat et al. (2000) beneath the Central Cone where it can be unambiguously linked to the

414 presently active hydrothermal system of the volcano. Beneath the Plaine des Sables-Fond de
415 la Rivière de l'Est, an hydrothermal origin of the conductor can only be presumed. Gravity
416 studies have shown that this area is underlain by a dense structure interpreted as a
417 hypovolcanic intrusive system (Gailler, 2010), source of heat and fluids for hydrothermal
418 activity. This complex would have formed during the Ancient Shield stage and, therefore, the
419 conductor beneath the Plaine des Sables would have developed during this period. The third
420 notable patch of high conductor in the study area is the one observed in the lower part of the
421 volcanic construction below the NW flank of Piton de la Fournaise (Fig. 6b). The fact that this
422 conductor is not a widespread but a localized structure suggests that it is not due to an
423 invasion of seawater but more likely to volcanic activity. Its location coincides with that of a
424 part of the N120 rift zone with numerous cinder cones. In this framework, it can be tentatively
425 explained by hydrothermalized and /or hot volume of rocks developing around a dense swarm
426 of cooling intrusions at the base of the edifice and, possibly in the upper part of the crust
427 where a similar conductor is observed. This system may be still active because a deep seismic
428 activity (between about 10 and 20 km) and CO_2 emanations are observed in this area (Liuzzo
429 et al., 2015; Michon et al.; 2016; Boudoire et al., 2017).
430 The dense hypovolcanic intrusive system found beneath the Plaine des Sable and the western
431 part of the Enclos by Gailler (2010) is not characterized by a resistivity contrast with the rest
432 of the edifice. Only overlying highly conductive layer may attest of its presence. Similarly, the
433 interface between Les Alizés and Piton de la Fournaise volcanoes inferred by Lénat et al.
434 (2012b) does not correspond to any obvious resistivity contrast in our model.
435 The upper lithosphere is markedly more resistive than the bulk of the volcanic construction
436 (except for the upper part of this latter). However, one main resistivity anomaly is present in
437 the crust, located beneath the NW flank. It spatially coincides, as indicated above, with the
438 N120 rift zone assumed to be linked with present day seismic and degassing activity. It is

439 therefore appealing to suggest that the lowering of the resistivity of the crust in this area may
440 be due to the magmatic activity (magma intrusion, hydrothermal activity, presence of hot fluids
441 …). The NW flank therefore appears as a main area of interest in the study of Piton de la
442 Fournaise activity and its evolution as well. Also note that, at the base of the crust, the
443 underplating is not imaged in our 3D resistivity model. For further investigations in depth, the
444 study should be extended to the whole island to study the structures beneath Piton des Neiges
445 and the whole of the Piton de la Fournaise area.

446 ## Aknowledgments

447 We are very grateful to the 'Conseil Régional de la Réunion' for its financial support for the
448 acquisition of gravity and electromagnetic data in the framework of a geothermal exploration
449 project and for its encouragement to use the data for academic research purposes. All the
450 Geothermal Project participants are also thanked for their various contributions (E. Delcher,
451 B. Robineau, P. Andrieu, F. Ranvier, T. Souriot, X. Pierre, B. Lapierre, D. Runavot, L.
452 Fornot, O. Odon). The dataset will be available from the authors of this manuscript. We thank
453 the staffs of the Observatoire Volcanologique du Piton de la Fournaise (Aline Peltier, Valérie
454 Ferrazini, Nicolas Villeneuve), of Université de la Réunion (Laurent Michon, Anthony
455 Finizola), and of University of Barcelona (Pilar Queralt, Juanjo Ledo and Alejandro
456 Marcuello) for their contribution and discussions about this study. We also thank Naser
457 Meqbel for its help around 3D Grid software. Last we acknowledge Michael Walter, Volker
458 Rath and an anonymous reviewer tor for very insightful comments and suggestions.

Figure captions

Figure 1: a) 3D view of Piton de la Fournaise showing the main structural features and the location of the main places discussed in the text. The study area is framed in red; **b)** Interpretive W–E geological section of Piton de la Fournaise by Lénat et al. (2012a). Coordinates in kilometers (WGS84, UTM40S).

Figure 2: Location of the resistivity soundings used in this study. The area of interest is framed in red. Coordinates in kilometers (WGS84, UTM40S). More details are given in Supporting Information (Fig. S1).

Figure 3: Map of dimensionality for six different period bands, using WALDIM code (Martı´ et al., 2009).

Figure 4: a) Map of invariant phases for periods ranging from 10^{-4} to 10^{3}, using WINGLING software. **b)** Bostick resistivity inversions are also presented showing the main distribution of resistivity at fixed elevation, using WINGLING software.

Figure 5: Comparison of the apparent resistivity and phases between the model responses and the raw data for the G10 sounding a) off-diagonal components; b) all components.

Figure 6: a) 3D model represented as a multi-segments section crossing the main area of interest, i.e. Plaine des Sables, Enflos Fouqué, Fond de la Rivière de l'Est and NW flank of Piton de la Fournaise. b) Interpretative scheme of the 3D model. ASC for Ancient Shield Complex.

480 ## References

481 Bachèlery, P. (1981), Le Piton de la Fournaise (Ile de la Réunion): étude volcanologique,
482 structurale et pétrologique, 255 pp., Univ. Blaise Pascal, Clermont-Ferrand.

483 Bachèlery, P., and P. Mairine (1990), Evolution volcano–structurale du Piton de la Fournaise
484 depuis 0.53 Ma, in Le volcanisme de la Réunion, Monographie, edited by J.-F. Lénat, pp.
485 213–242, Centre de Recherches Volcanologiques, Clermont-Ferrand.

486 Bachèlery, P. and P. Mairine (1990), Evolution volcano–structurale du Piton de la Fournaise
487 depuis 0.53 Ma, in Le volcanisme de la Réunion, Monographie, edited by J.-F. Lénat, pp.
488 213–242, Centre de Recherches Volcanologiques, Clermont-Ferrand.

489 Battaglia, J., V. Ferrazzini, T. Staudacher, K. Aki, and J. L. Cheminée (2005), Pre-eruptive
490 migration of earthquakes at the Piton de la Fournaise volcano (Réunion island),
491 Geophys. J. Int., 161, 549–558.

492 Benderitter, Y. (1990), Études géoélectrique et électromagnétiques à la Réunion, in Le
493 volcanisme de la Réunion, monographie, edited by J. F. Lénat, pp. 29–42 , Centre de
494 Recherches Volcanologiques, Clermont-Ferrand.

495 Benderitter, Y., and A. Gérard (1984), Geothermal study of Réunion Island:
496 audiomagnetotelluric survey, J. Volcanol. Geotherm. Res., 20, 311–332.

497 Bhattacharya B.B, Shalivahan (2002), The electric moho underneath Eastern Indian Craton,
498 Geophysi al Research Letters, Vol. 29, NO. 10, 1376, 10.1029/2001GL014062.

499 Boudoire G., Liuzzo M., Di Muro A, Ferrazzini V., Michon L., et al.. Investigating the
500 deepest part of a volcano plumbing system: Evidence for an active magma path below the

501 western flank of Piton de la Fournaise (La Réunion Island). Journal of Volcanology and
502 Geothermal Research, Elsevier, 2017, 341, pp.193-
503 207.<10.1016/j.jvolgeores.2017.05.026>.

504 Charvis, P., A. Laesanpura, J. Gallart, A. Hirn, J. C. Lepine, B. de Voogd, T. A. Minshull, Y.
505 Hello, and B. Pontoise (1999), Spatial distribution of hotspot material added to the
506 lithosphere under La Réunion, from wide-angle seismic data, J. Geophys. Res., B104,(2),
507 2875–2893.

508 Chevallier, L., and P. Bachèlery (1981), Evolution structurale du volcan actif du Piton de la
509 Fournaise. Ile de la Réunion, Océan Indien, Bull. Volc., 44 (4), 723–741.

510 Constable, S., and G. Heinson (2004), Hawaiian hot-spot swell structure from seafloor MT
511 sounding, Tectonophysics, 389, 111–124.

512 Constable, S. C., and C. S. Cox (1996), Marine controlled source electromagnetic sounding:
513 2. The PEGASUS experiment, J. Geophys. Res., 101, 5519–5530.

514 Courteaud, M. (1996), Etude des structures géologiques et hydrogéologiques du Massif de la
515 Fournaise par la méthode audiomagnétotellurique, 212 pp., Thèse d'Université, Univ. de
516 la Réunion.

517 Courteaud, M., P. Bachèlery, B. Robineau, and J. L. Join (1997), Les brèches de Saint-Gilles.
518 Note technique géologique, Laboratoire des Sciences de la Terre, Univ. de La Réunion. .

519 Egbert, G. D. and A. Kelbert, (2012), Computational recipes for electromagnetic inverse
520 problems, Geophysical Journal International, 189, 251-267.

521 Kelbert, A., N.M. Meqbel, G. D. Egbert & K. Tandon, 2014.ModEM: A modular system for
522 inversion of electromagnetic geophysical data,/Comp. Geosci./, 66, 40-53, ISSN 0098-
523 3004, http://dx.doi.org/10.1016/j.cageo.2014.01.010.

524 Fontaine, F.R., G. Barruol, H. Tkalčić, I. Wölbern, G. Rümpker, T. Bodin, M. Haugmard
525 (2015), Crustal and uppermost mantle structure variation beneath La Réunion hotspot
526 track, Geophysical Journal International, 203, Issue 1, 1, 107–126.

527 Gailler, L., J.F. Lénat, M. Lambert, G. Levieux, N. Villeneuve, and J. L. Froger (2009),
528 Gravity structure of Piton de la Fournaise volcano and inferred mass transfer during the
529 2007 crisis, J. Volcanol. Geotherm. Res., 184, 31–48,
530 doi:doi:10.1016/j.jvolgeores.2009.01.024.

531 Gailler, L., J.F. Lénat, and R.J. Blakely (2016), Depth to Curie temperature or magnetic
532 sources bottom in the volcanic zone of La Réunion hot spot, Earth Planet. Sci. Lett.

533 Gailler, L.S. (2010), Structure interne d'un système océanique volcanique, La Réunion
534 (Océan Indien) – Approches géophysiques, 471 pp., Université Blaise Pascal-Laboratoire
535 Magmas et Volcans, Clermont-Ferrand.

536 Gailler, L.S., and J.F. Lénat (2012), Internal architecture of La Réunion (Indian Ocean)
537 inferred from geophysical data, J. Volcanol. Geotherm. Res., 221-222, 83–98.

538 Gallart, J., L. Driad, P. Charvis, M. Sapin, A. Hirn, J. Diaz, B. de Voogd, and M. Sachpazi
539 (1999), Perturbation to the lithosphere along the hotspot track of La Réunion from an
540 offshore-onshore seismic transect, J. Geophys. Res., B, Solid Earth Planets, 104(2),
541 2895–2908.

542 Gillot, P. Y., and P. Nativel (1989), Eruptive history of the Piton de la Fournaise volcano,
543 Réunion Island, Indian Ocean, J. Volcanol. Geotherm. Res., 36, 53–65.

544 Haak, V. (1982), Electrical Conductivity of Minerals and Rocks at Temperatures and
545 Pressures, in Zahlenwerte und Funktionen aus Naturwissenschaften und Technik
546 /Landolt-Brrnstein, vol. V/1b, edited by G. Angenheister, pp. 291–307, Springer, Berlin.

547 Jackson, D.B., and J. Kauahikaua (1987), The high-level water table beneath Kilauea
548 Volcano, Hawaii. How Volcanoes Work, Hilo, Hawaii, January 19–25, 120.

549 Join, J.L., J. L.Folio, and B. Robineau (2005), Aquifers and groundwater within active shield
550 volcanoes. Evolution of conceptual models in the Piton de la Fournaise volcano, J.
551 Volcanol. Geotherm. Res., 147, 187–201.

552 Jones, A.G. (1999), Imaging the continental upper mantle using electromagnetic methods.
553 Lithos 48, 57– 80.

554 Lénat, J.F., P. Bachèlery, and O. Merle (2012a), Anatomy of Piton de la Fournaise volcano
555 (La Réunion, Indian Ocean), Bull. Volcanol, 74:1945–1961. doi:10.1007/ s00445-012-
556 0640-y.

557 Lénat, J.F., D. Fitterman, and D.B. Jackson (2000), Geoelectrical structure of the central zone
558 of Piton de la Fournaise volcano (Réunion), Bull. Volc., 62 (2), 75–89.

559 Lénat, J.F., B. Gibert-Malengreau, and A. Galdéano (2001), A new model for the evolution of
560 the volcanic island of Reunion (Indian Ocean), J. Geophys. Res., B, 106,(5), 8645–8663.

561 Lénat, J.F., P. Bachèlery, and A. Peltier (2012b), The interplay between collapse structures,
562 hydrothermal systems and magma intrusions: the case of the central area of Piton de la
563 Fournaise volcano, Bull. Volcanol., 74, 407–421, doi:10.1007/s00445-011-0535-3.

564 Letourneur, L., A. Peltier, T. Staudacher, and A. Gudmundsson (2008), The effects of rock
565 heterogeneities on dyke paths and asymmetric ground deformation: the example of Piton
566 de la Fournaise volcano, J. Volcanol. Geotherm. Res., 173, 289–302.

567 Liuzzo, M., A. Di Muro, G. Giudice, L. Michon, V. Ferrazzini, S. Gurrieri (2005), New
568 evidence of CO2 soil degassing anomalies on Piton de la Fournaise volcano and the link
569 with volcano tectonic structures, Geochem. Geophys.
570 Geosyst., 16, 10.1002/2015GC006032

571 MacGregor, L.M., S.C. Constable, and M. C.Sinha (1998), The RAMESSES experiment—III.
572 Controlled-source electromagnetic sounding of the Reykjanes Ridge at 57°45'N,
573 Geophys. J. Int., 135, 772–789.

574 Malengreau, B., J.F. Lénat, and J.L. Froger (1999), Structure of Reunion Island (Indian
575 Ocean) inferred from the interpretation of gravity anomalies, J. Volcanol. Geotherm.
576 Res., 88(3), 131–146.

577 Martı´ A, P. Queralt, J. Ledo (2009), WALDIM: a code for the dimensionality analysis of
578 magnetotelluric data using the rotational invariants of the magnetotelluric tensor.
579 Comput. Geosci. 35(12):2295–2303.

580 McDougall, I. (1971), The geochronology and evolution of the young volcanic island of
581 Réunion (Indian Ocean), Geochem. Cosmochim. Acta., 35(3), 261–288.

582 Merle, O., and J.F. Lénat (2003), Hybrid collapse mechanism at Piton de la Fournaise
583 volcano, Reunion Island, Indian Ocean, J. Geophys. Res., 108 (B3), 2166,
584 doi:doi:10.1029/2002JB002014.

585 Merle, O., P. Mairine, L. Michon, P. Bachèlery, and M. Smietana (2010), Calderas, landslides
586 and paleo-canyons on Piton de la Fournaise volcano (La Réunion Island, Indian Ocean),
587 J. Volcanol. Geotherm. Res., in press.

588 Michon, L., and F. Saint-Ange (2008), Morphology of Piton de la Fournaise basaltic shield
589 volcano (La Réunion Island): Characterization and implication in the volcano evolution,
590 J. Volcanol. Geotherm. Res., 113(B03203), 1–19, doi:doi:10.1029/2005JB004118.

591 Michon, L., V. Ferrazzini, A. Di Muro (2016), Magma intrusions paths of Piton de la
592 Fournaise. In: Bachèlery, P., Lénat, J.F., Di Muro, A., Michon, L. (Editor), Active
593 Volcanoes of the Southwest Indian Ocean: Piton de la Fournaise and Karthala. Active
594 Volcanoes of the World. Springer-Verlag Berlin and Heidelberg. pp. 91-106.

595 Mohamed-Abchir, A. (1996), Les Cendres de Bellecombe: un événement majeur dans le
596 passé récent du Piton de la Fournaise, Ile de la Réunion, 248 pp., Université de Paris VII.

597 Morandi, A., A. Di Muro, C. Principe, L. Michon, G. Leroi, F. Norelli, and P. Bachèlery
598 (2015), Pre-historic explosive activity at Piton de la Fournaise volcano, in Active
599 Volcanoes of the Southwest Indian Ocean: Piton de la Fournaise and Karthala. Active
600 Volcanoes of the World., edited by P. Bachèlery, J.F. Lénat, A. Di Muro, and L. Michon.

601 Nobes, D.C., L.K. Law, and R.N. Edwards (1992), Results of a sea-floor electromagnetic
602 survey over a sedimented hydrothermal area on the Juan de Fuca Ridge, Geophys. J. Int.,
603 110, 333–346.

604 Pinã-Varas P., L. Ledo, P. Queralt, A. Marcuello, F. Bellmunt, R. Hidalgo, M. Messeiller
605 (2014), 3-D Magnetotelluric Exploration of Tenerife Geothermal System (Canary
606 Islands, Spain), Surv. Geophys. 35:1045–1064, doi 10.1007/s10712-014-9280-4.

607 Rai, M.P., and M.H. Manghnani (1977), Electrical conductivity of basalts to 1550°C.
608 Chapman conference on partial melting in the earth's upper mantle proceedings. Oregon
609 Department of Geology and Mineralogy Bull. 96:219–232 ,

610 Rançon, J.P., P. Lerebour, and T. Augé (1989), The Grand Brûlé exploration drilling; new
611 data on the deep framework of the Piton de la Fournaise Volcano; Part 1,
612 Lithostratigraphic units and volcanostructural implications, J. Volcanol. Geotherm. Res.,
613 36(1-3), 113–127.

614 Schnegg, P.A. (1997), Electrical structure of Plaine des Sables caldera, Piton de la Fournaise
615 volcano (Réunion Island), Ann. Geofis., 40, 305–317.

616 Smith, D.K. (1996), Comparison of the shapes and sizes of seafloor volcanoes on Earth and
617 "pancake" domes on Venus, J. Volcanol. Geotherm. Res., 73(1-2), 47–64.

618 Staudacher, T., and C.J. Allègre (1993), Ages of the second caldera of Piton de la Fournaise
619 volcano (Réunion) determined by cosmic ray produced 3He and 21Ne, Earth Planet Sci
620 Lett, 119, 395–404.

621 Stearns, H.T. (1942), Hydrology of volcanic terranes, in Physics of the earth, vol IX.
622 Hydrology. Dover, New York, pp. 678–703.

623 Takasaki, K.J. (1981), Evaluation of major dike-impounded groundwater reservoirs, Island of
624 Oahu, US Geol. Surv. Open-File Rep. 81-1119146.

625 Unsworth, M.J. (1994), Exploration of a mid-ocean ridge with a frequency-domain EM
626 system, Geophys. J. Int., 116, 447–467.

627 Vacher, H.L. (1988), Dupuit-Ghyben-Herzberg analysis of strip-island lenses, Bull. Geol.
628 Soc. Am., 100, 580–591.

629 Villeneuve, N., and P. Bachèlery (2006), Revue de la typologie des éruptions au Piton de la
630 Fournaise, processus et risques volcaniques associés: Cybergeo: European Journal of
631 Geography (http://cybergeo.revues.org/2536).,

632 De Voogd, B., S. Pou Palomé, A. Hirn, P. Charvis, J. Gallart, D. Rousset, J. Danobeitia, and
633 H. Perroud (1999), Vertical movements and material transport during hotspot activity;
634 seismic reflection profiling offshore La Réunion, J. Geophys. Res. B, Solid Earth
635 Planets, 104,(2), 2855–2874.

636 Weaver, J.T., A.K. Agarwal, F.E.M. Lilley (2000), Characterization of the magnetotelluric
637 tensor in terms of its invariants. Geophys. J. Int. 141(2):321–336.
638 http://dx.doi.org/10.1046/j.1365-246x.2000.00089.x.

Figure 1

(a)

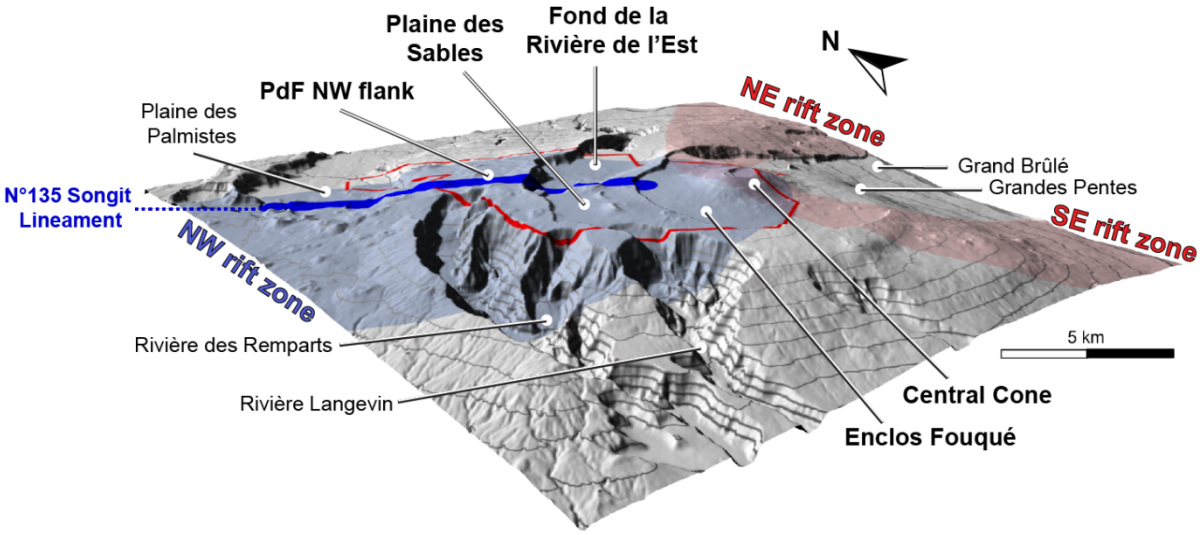
Plaine des Sables
Fond de la Rivière de l'Est
N
PdF NW flank
NE rift zone
Plaine des Palmistes
Grand Brûlé
Grandes Pentes
N°135 Songit Lineament
SE rift zone
NW rift zone
5 km
Rivière des Remparts
Central Cone
Rivière Langevin
Enclos Fouqué

(b)

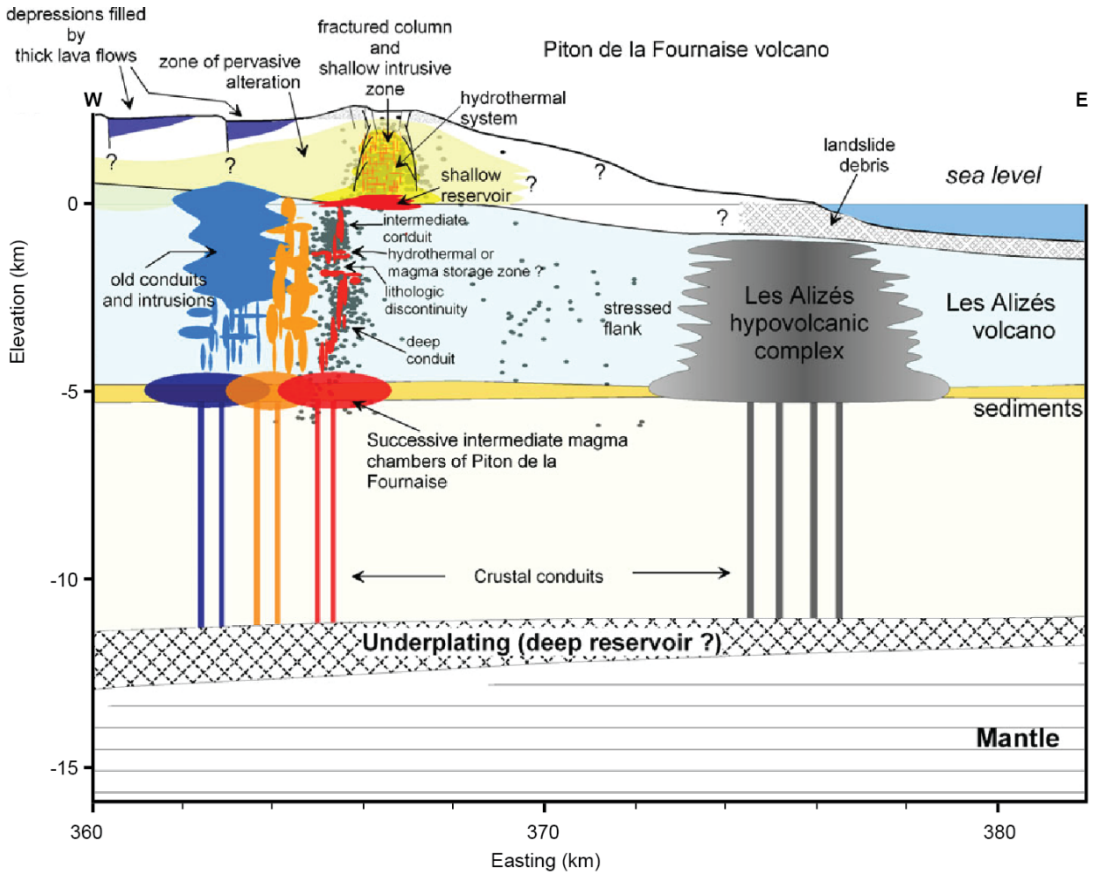
depressions filled by thick lava flows
zone of pervasive alteration
fractured column and shallow intrusive zone
Piton de la Fournaise volcano
W
E
hydrothermal system
landslide debris
sea level
shallow reservoir
intermediate conduit
hydrothermal or magma storage zone ?
lithologic discontinuity
deep conduit
old conduits and intrusions
stressed flank
Les Alizés hypovolcanic complex
Les Alizés volcano
sediments
Successive intermediate magma chambers of Piton de la Fournaise
Crustal conduits
Underplating (deep reservoir ?)
Mantle
Elevation (km)
0
-5
-10
-15
360
370
380
Easting (km)

Figure 2

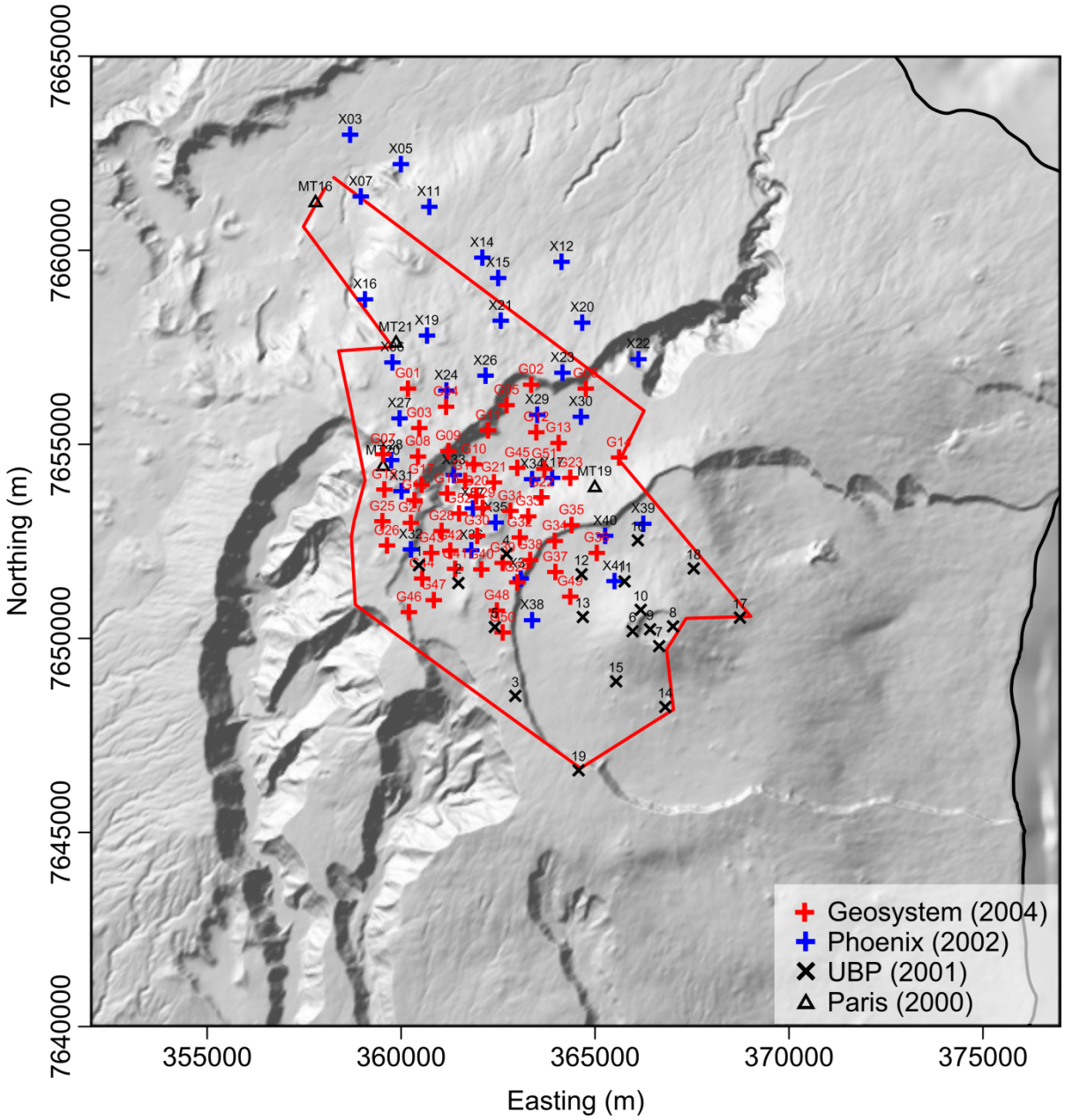
Northing (m)
7665000
7660000
7655000
7650000
7645000
7640000
355000
360000
365000
370000
375000
Easting (m)
Geosystem (2004)
Phoenix (2002)
UBP (2001)
Paris (2000)

Figure 3

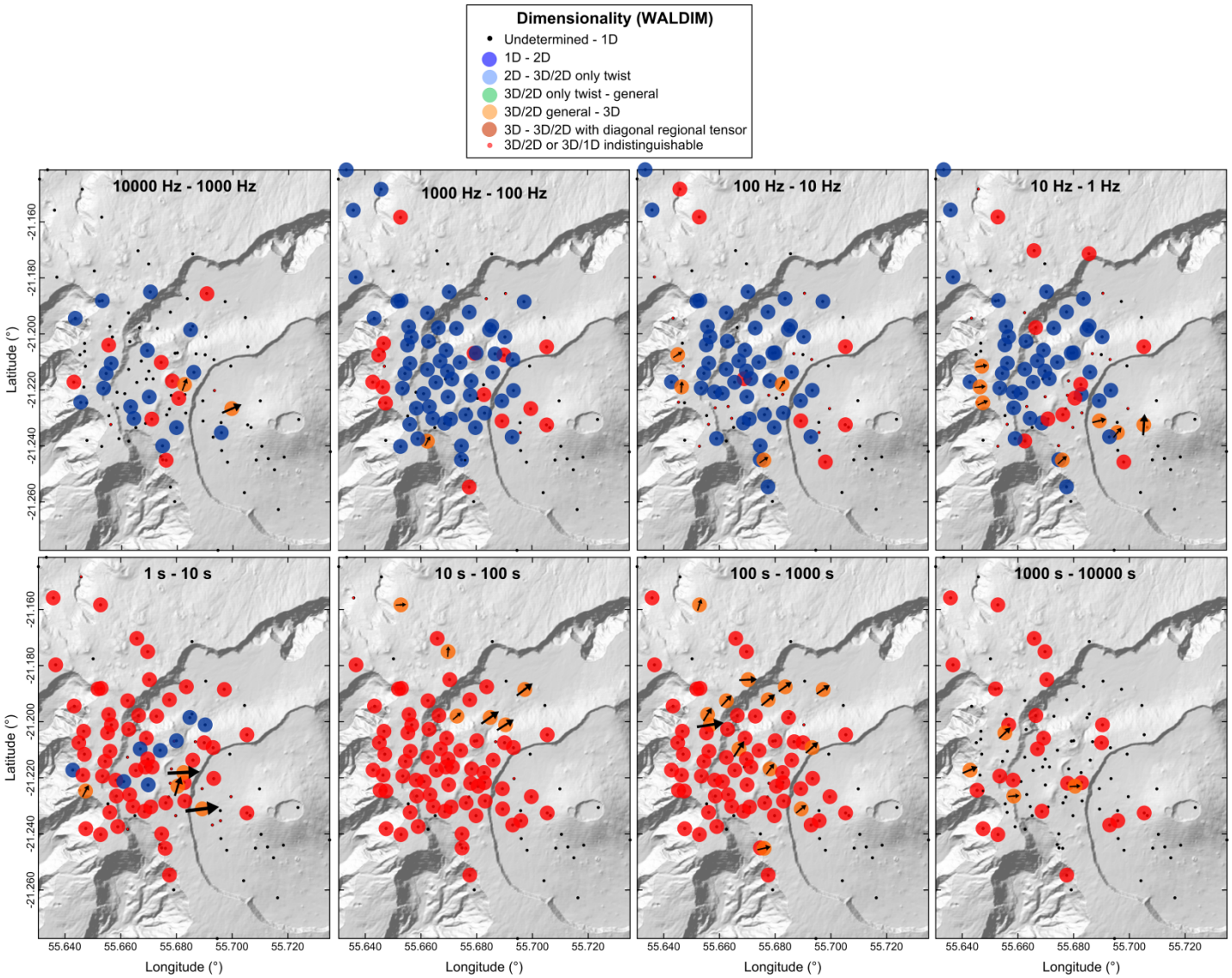
Dimensionality (WALDIM)
Undetermined - 1D
1D - 2D
2D - 3D/2D only twist
3D/2D only twist - general
3D/2D general - 3D
3D - 3D/2D with diagonal regional tensor
3D/2D or 3D/1D indistinguishable
10000 Hz - 1000 Hz
1000 Hz - 100 Hz
100 Hz - 10 Hz
10 Hz - 1 Hz
1 s - 10 s
10 s - 100 s
100 s - 1000 s
1000 s - 10000 s
Latitude (°)
-21.160
-21.180
-21.200
-21.220
-21.240
-21.260
Longitude (°)
55.640
55.660
55.680
55.700
55.720

Figure 4

(a)

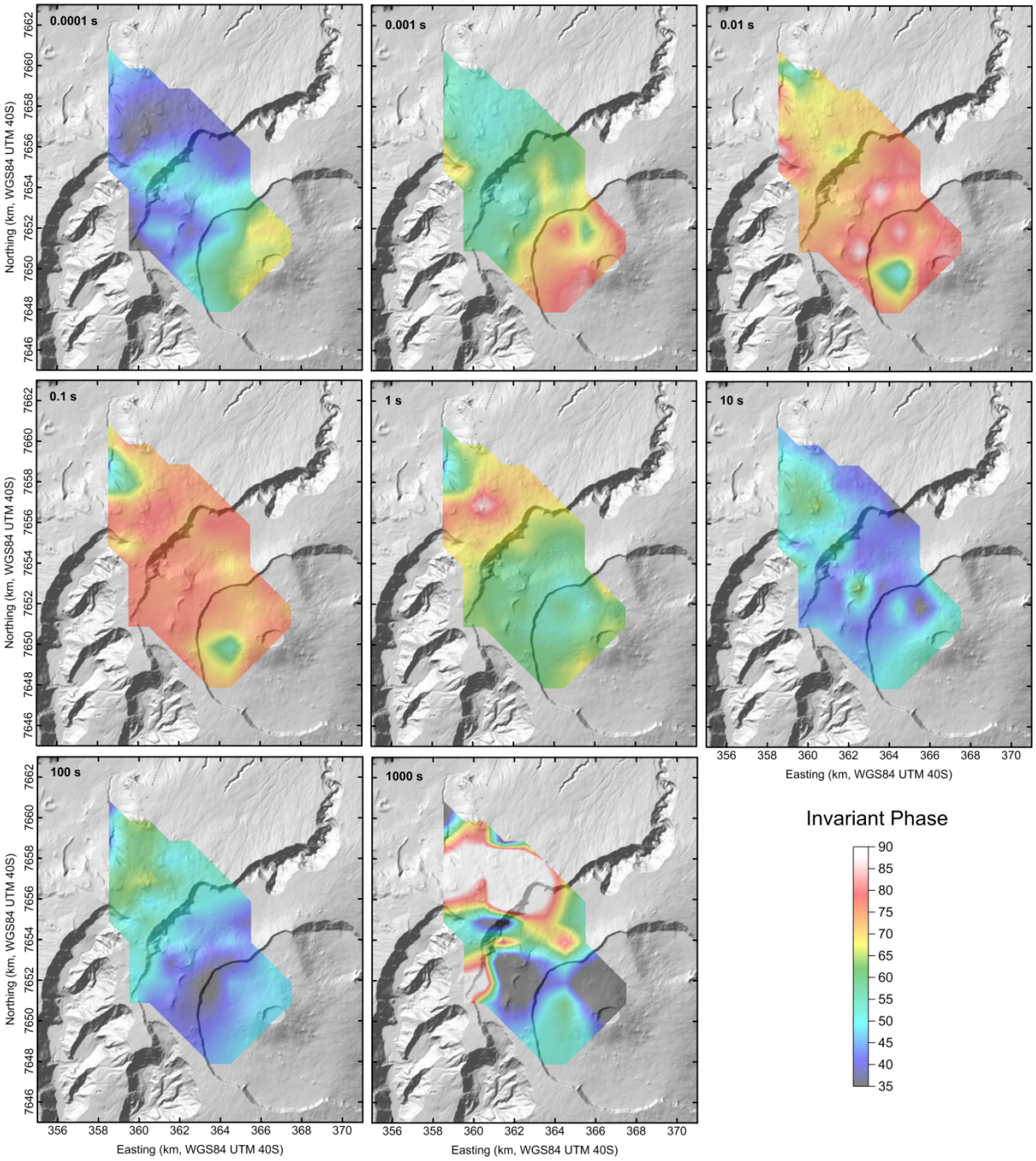
0.0001 s
0.001 s
0.01 s
0.1 s
1 s
10 s
100 s
1000 s
Northing (km, WGS84 UTM 40S)
Easting (km, WGS84 UTM 40S)
7646
7648
7650
7652
7654
7656
7658
7660
7662
356
358
360
362
364
366
368
370
Invariant Phase
90
85
80
75
70
65
60
55
50
45
40
35

(b)

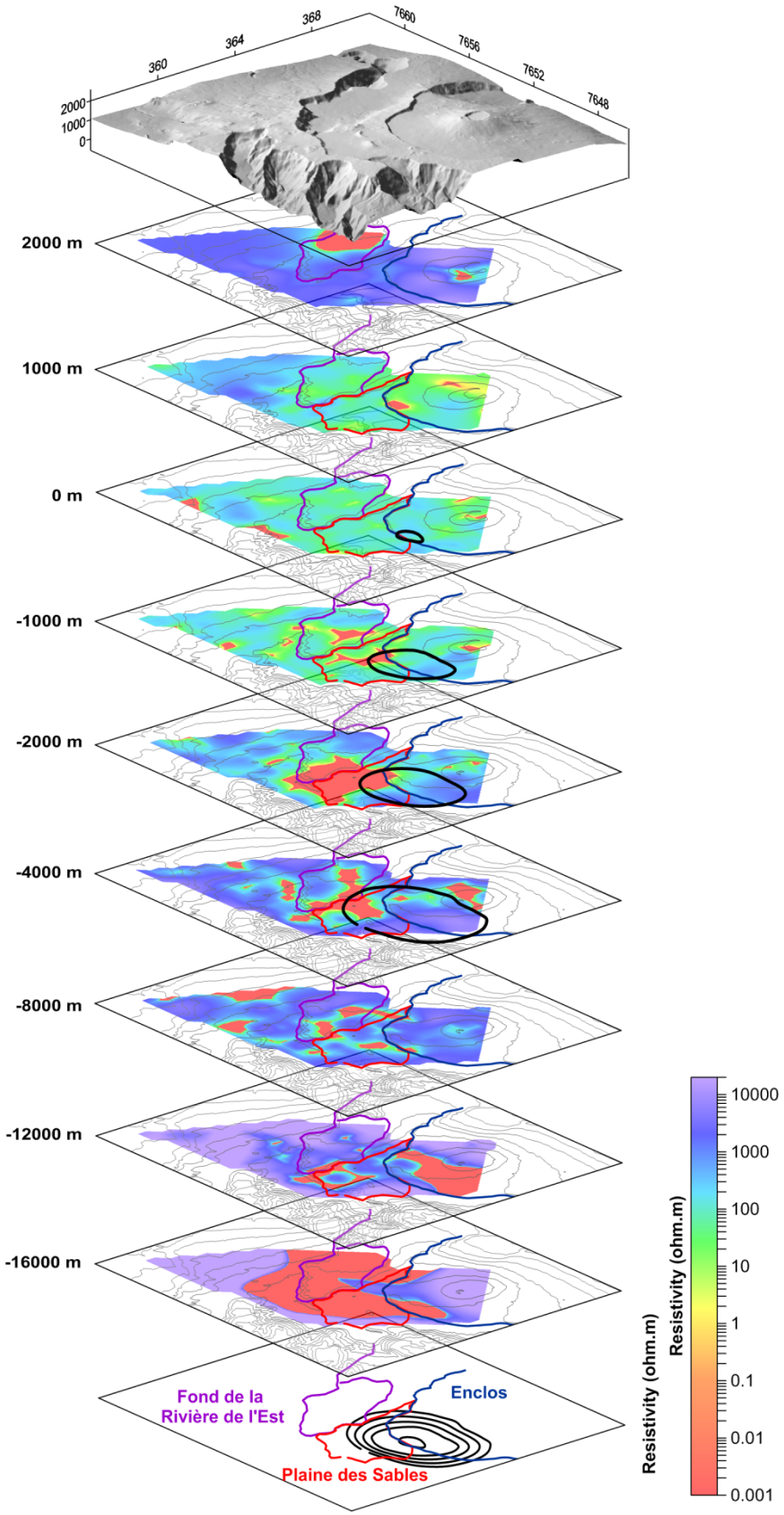
360
364
368
7660
7656
7652
7648
2000
1000
0
2000 m
1000 m
0 m
-1000 m
-2000 m
-4000 m
-8000 m
-12000 m
-16000 m
Fond de la
Rivière de l'Est
Enclos
Plaine des Sables
Resistivity (ohm.m)
Resistivity (ohm.m)
10000
1000
100
10
1
0.1
0.01
0.001

Figure 5

(a)

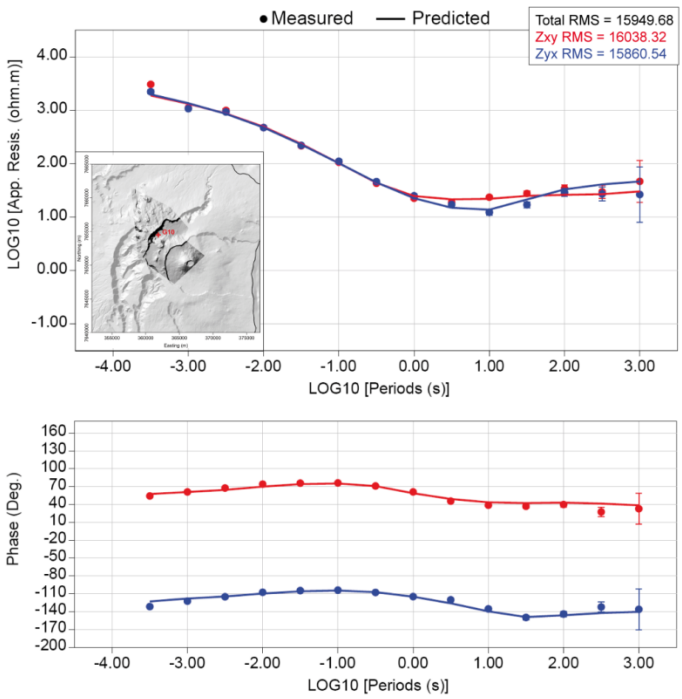
Measured
Predicted
Total RMS = 15949.68
Zxy RMS = 16038.32
Zyx RMS = 15860.54
LOG10 [App. Resis. (ohm.m)]
LOG10 [Periods (s)]
Phase (Deg.)
LOG10 [Periods (s)]

(b)

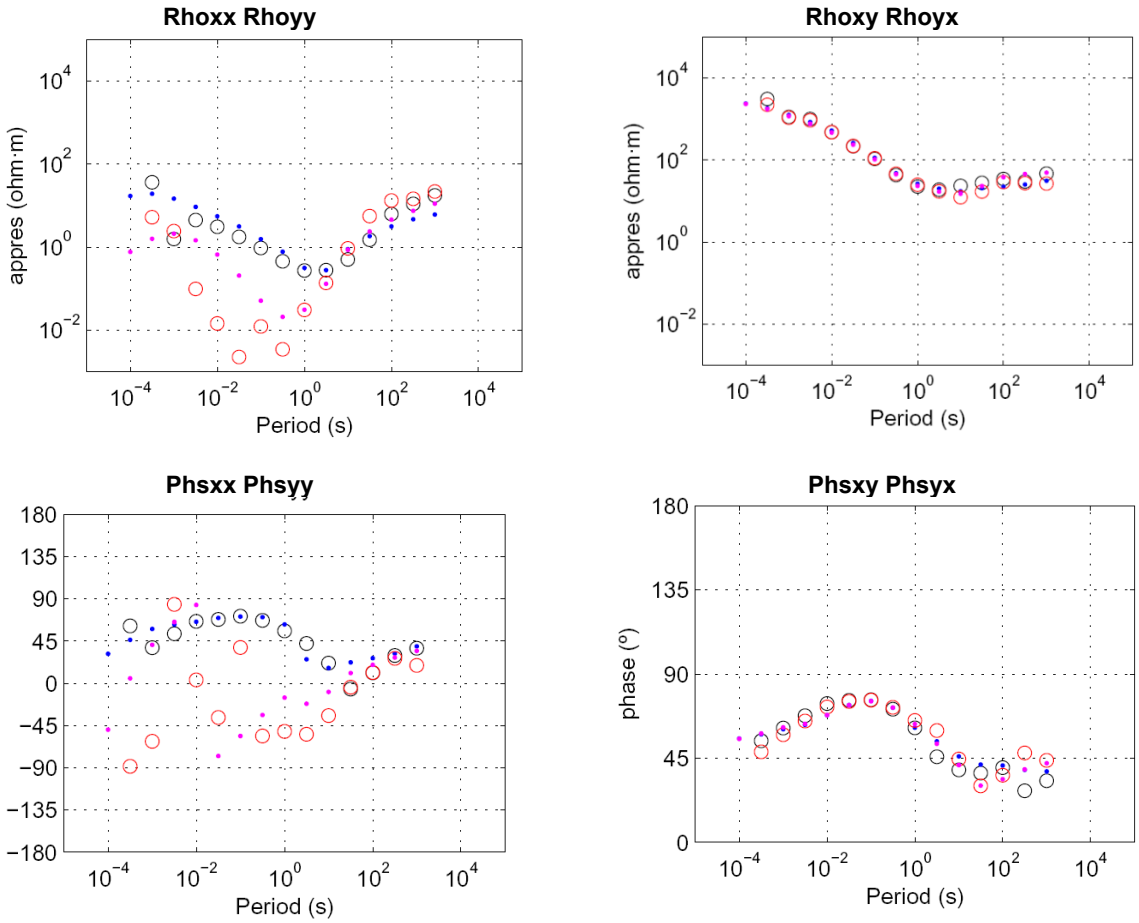
Rhoxx Rhoyy
appres (ohm·m)
Period (s)
Rhoxy Rhoyx
appres (ohm·m)
Period (s)
Phsxx Phsyy
phase (°)
Period (s)
Phsxy Phsyx
phase (°)
Period (s)

Figure 6

(a)

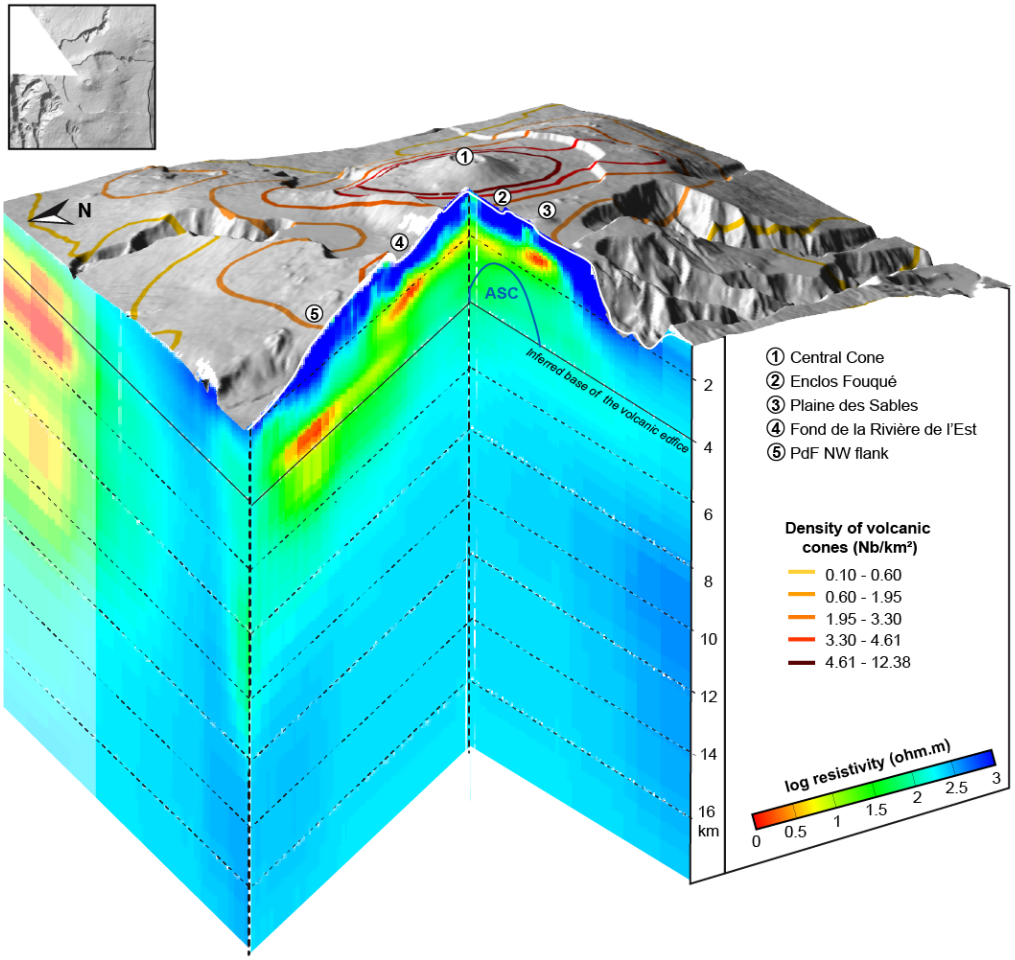
N
ASC
Inferred base of the volcanic edifice
① Central Cone
② Enclos Fouqué
③ Plaine des Sables
④ Fond de la Rivière de l'Est
⑤ PdF NW flank
Density of volcanic cones (Nb/km²)
0.10 - 0.60
0.60 - 1.95
1.95 - 3.30
3.30 - 4.61
4.61 - 12.38
log resistivity (ohm.m)
0 0.5 1 1.5 2 2.5 3
2 4 6 8 10 12 14 16 km

(b)

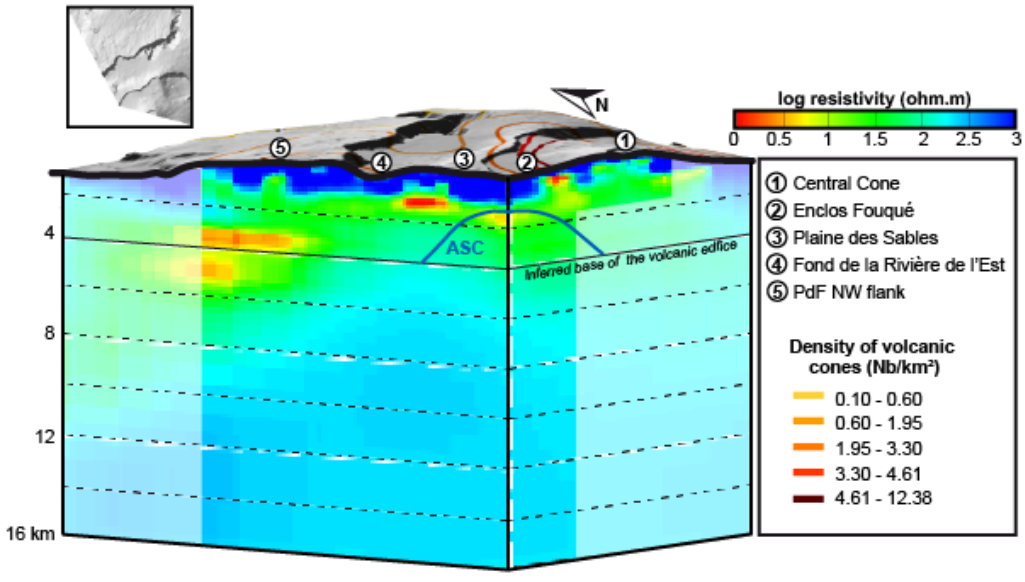
N
log resistivity (ohm.m)
0 0.5 1 1.5 2 2.5 3
ASC
Inferred base of the volcanic edifice
① Central Cone
② Enclos Fouqué
③ Plaine des Sables
④ Fond de la Rivière de l'Est
⑤ PdF NW flank
Density of volcanic cones (Nb/km²)
0.10 - 0.60
0.60 - 1.95
1.95 - 3.30
3.30 - 4.61
4.61 - 12.38
4 8 12 16 km

(c)

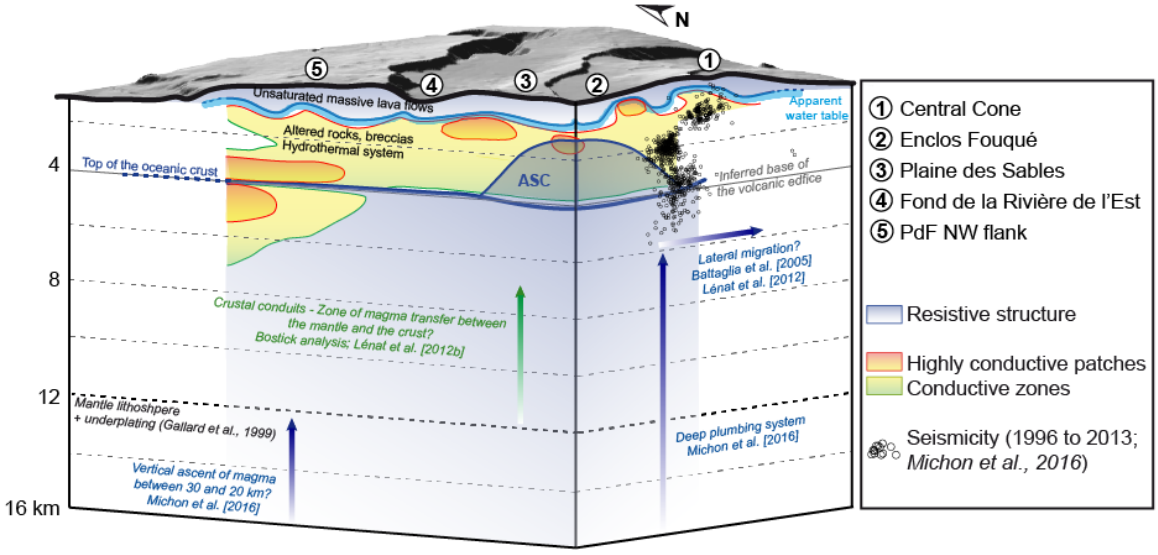
N
5
4
3
2
1
Unsaturated massive lava flows
Altered rocks, breccias
Hydrothermal system
Apparent water table
Top of the oceanic crust
ASC
Inferred base of the volcanic edifice
4
8
12
16 km
Lateral migration?
Battaglia et al. [2005]
Lénat et al. [2012]
Crustal conduits - Zone of magma transfer between the mantle and the crust?
Bostick analysis; Lénat et al. [2012b]
Mantle lithosphere
+ underplating (Gallard et al., 1999)
Vertical ascent of magma between 30 and 20 km?
Michon et al. [2016]
Deep plumbing system
Michon et al. [2016]
① Central Cone
② Enclos Fouqué
③ Plaine des Sables
④ Fond de la Rivière de l'Est
⑤ PdF NW flank
Resistive structure
Highly conductive patches
Conductive zones
Seismicity (1996 to 2013; Michon et al., 2016)

Supplementary Online material A

Details on MT-AMT data location

At the scale of the study area, the final dataset includes 118 MT and AMT soundings, and 17 electrical soundings from various organizations (Fig. A.1).

(a)

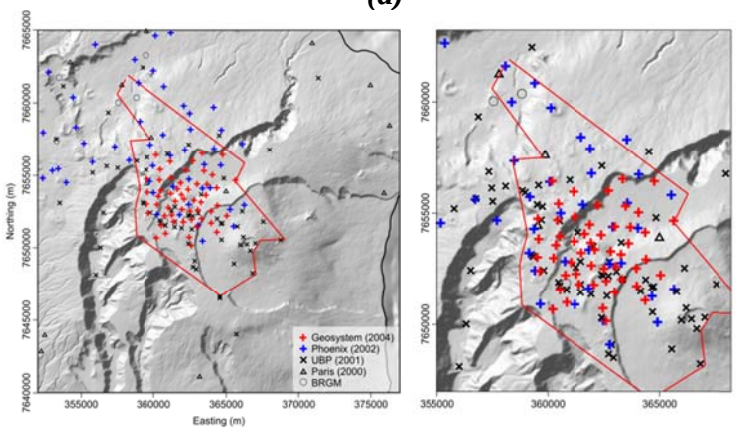

(b)

Geosystem (MT, 2004)

Phoenix (MT, 2002)

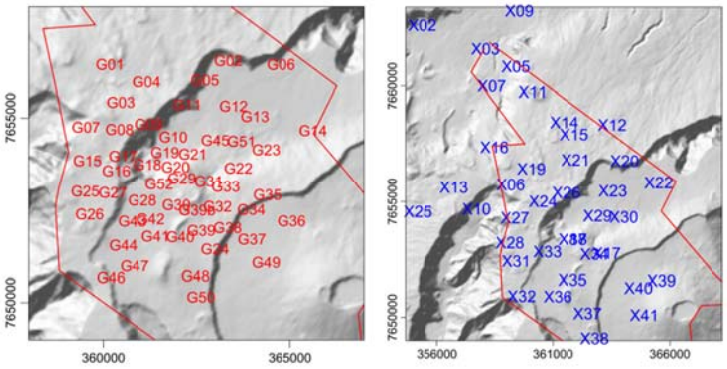

UBP (AMT, 2001)

Paris (MT, 2002), BRGM (MT)

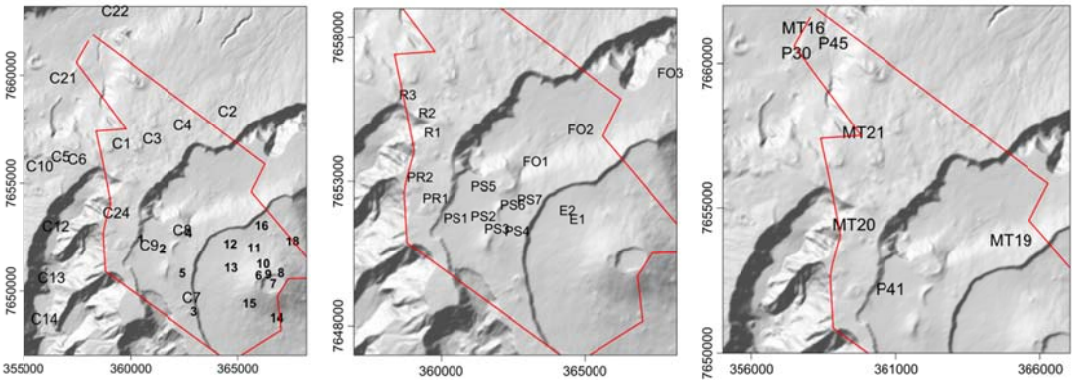

Figure A.1: a) *Location of the resistivity soundings used in this study at the scale of Piton de la Fournaise.* ***b)*** *Zoom on each set of soundings from various organizations. The study area is framed in red.*

The soundings have a typical spacing of 700 m in the center of the survey area (2 by km²), increasing to 1000 m towards the periphery.

The data, available as EDI files, were processed using WinGLink ™ Version 2.6.02 provided by Geosystem society. In addition to treatment and modelling options, this software also provides features of a geo-referenced database for all geophysical measurements. When multiple sets of data were available for a sounding (i.e. HF and LF for AMT and MT data), the combination of the data was also performed with this software.

Supplementary Online material B

Raw data versus model responses

Fig. B.1: Comparison between the raw data and model responses as apparent resistivity and phases curves for each site used in inversion.

Site: 2

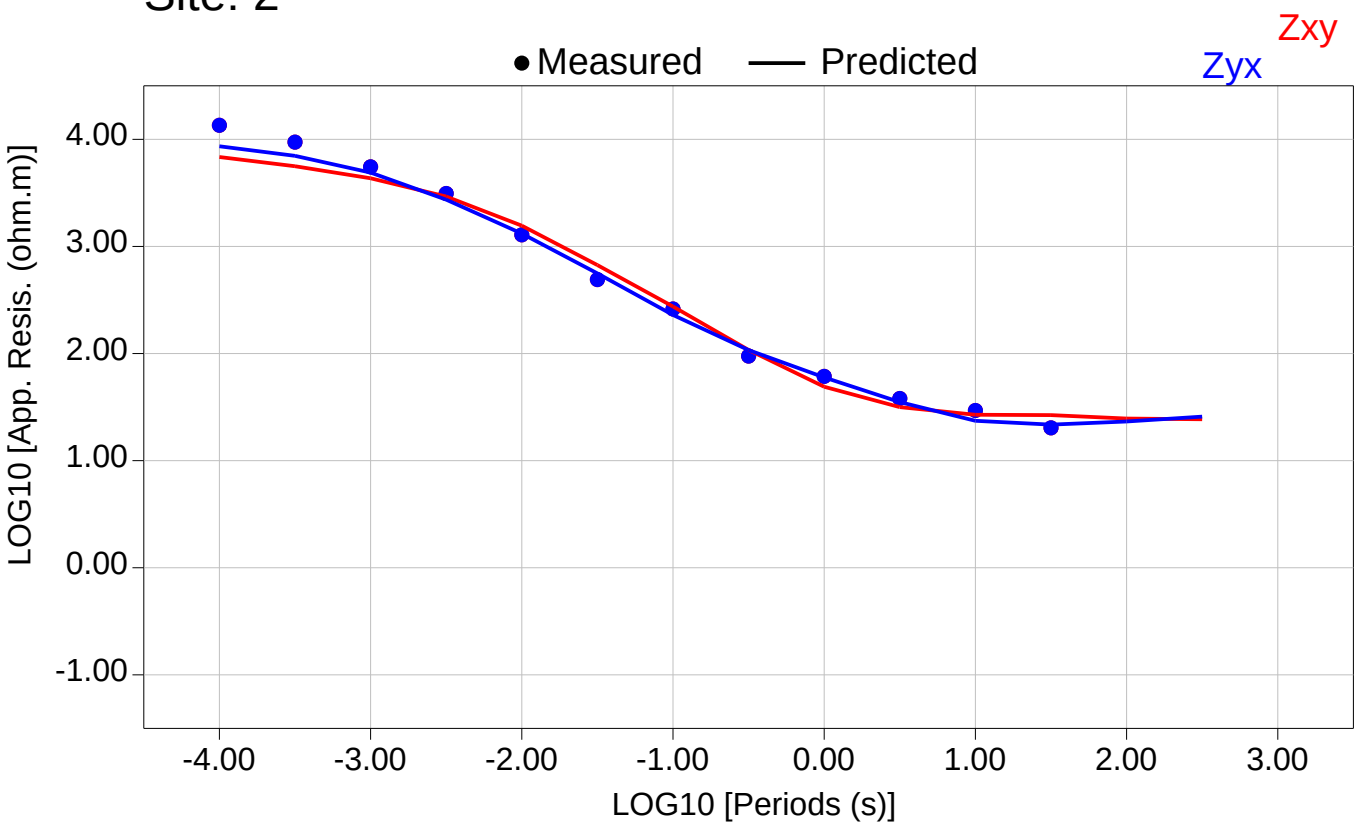

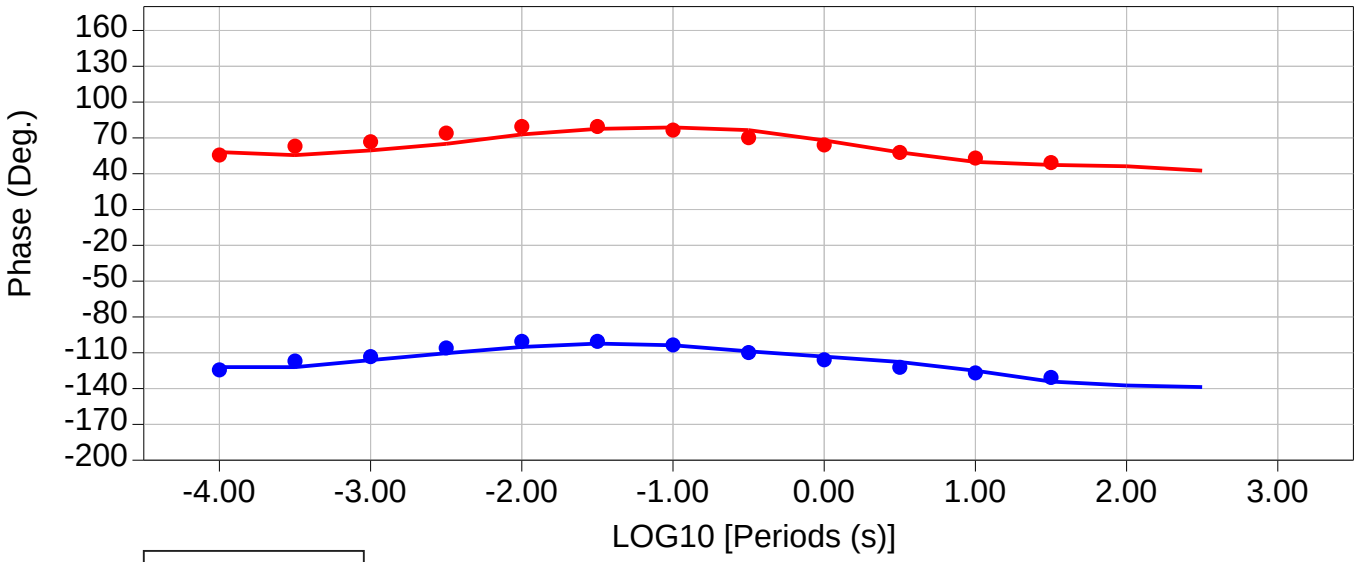

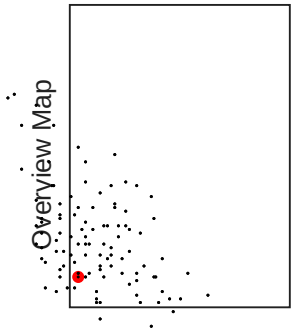

Total RMS = 20196.14

Zxy RMS = 20404.41
Zyx RMS = 19985.71

Site: 3

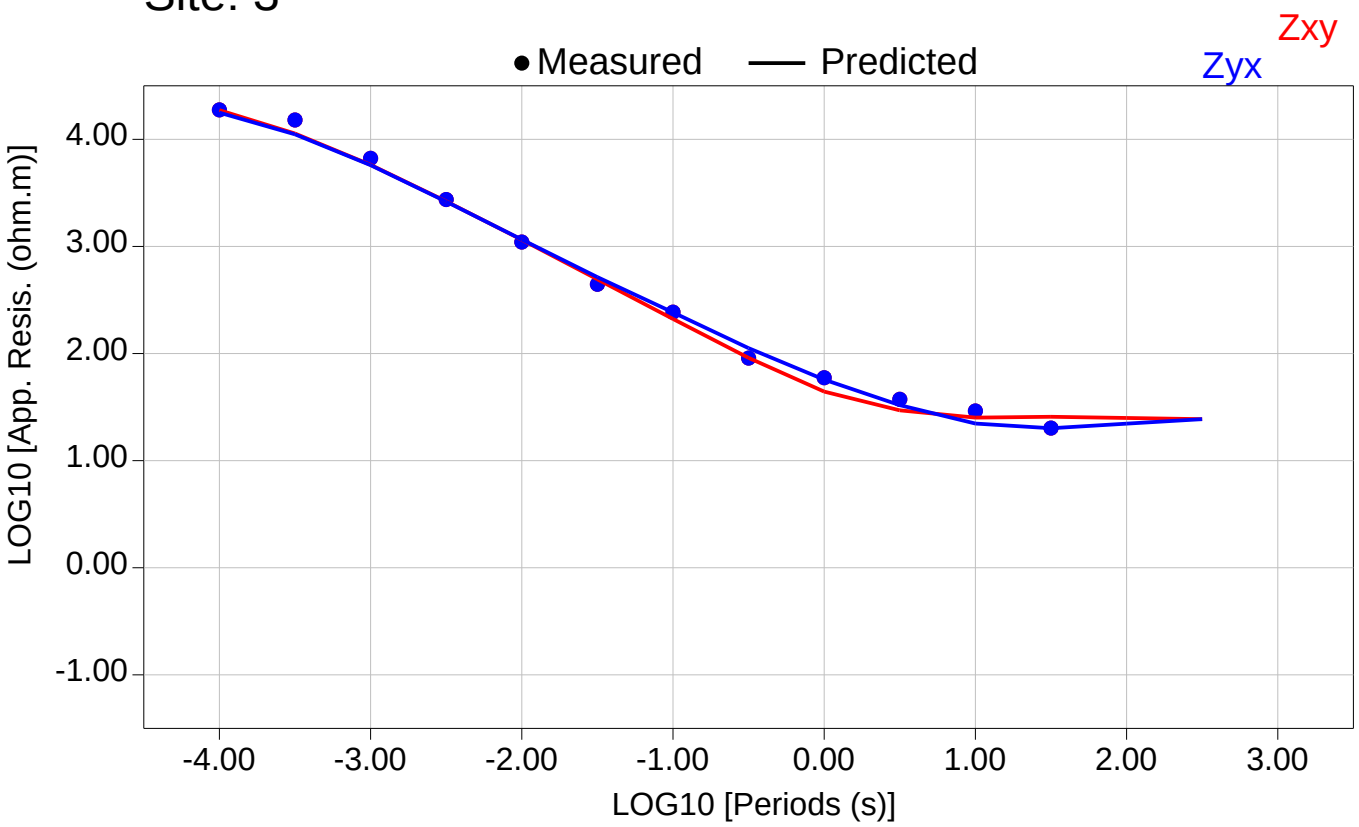

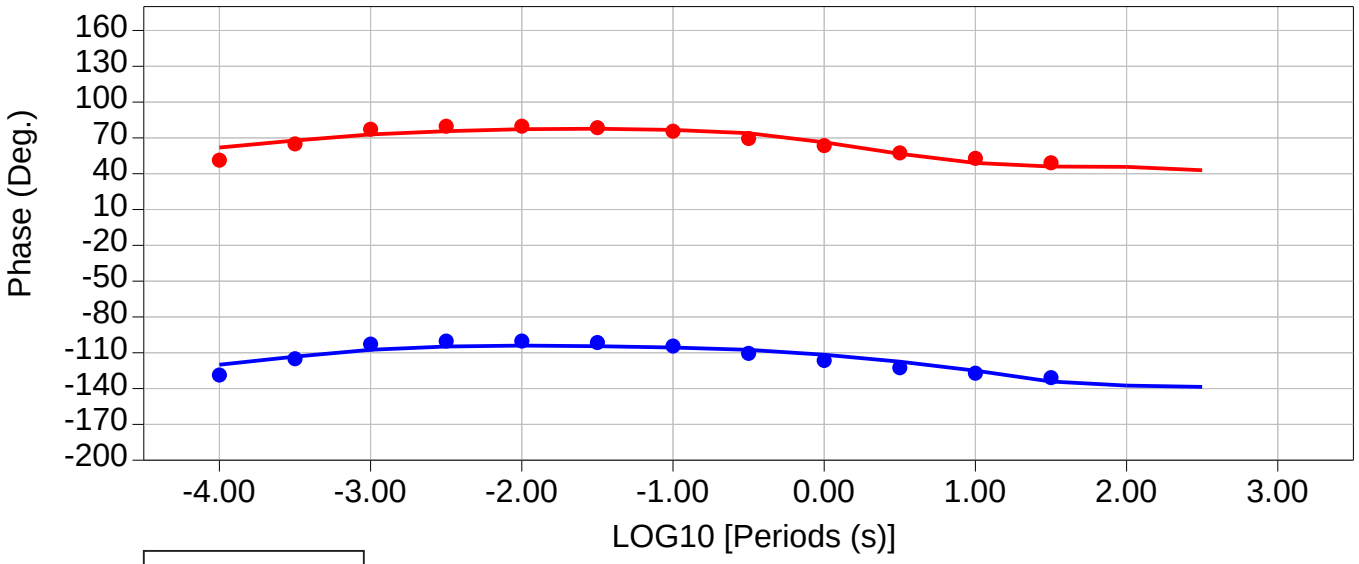

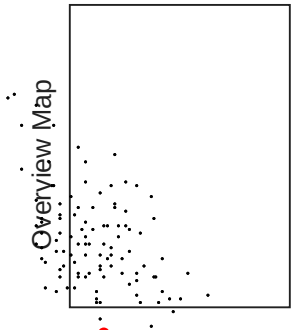

Total RMS = 20560.45

Zxy RMS = 20339.08
Zyx RMS = 20779.46

Site: 18

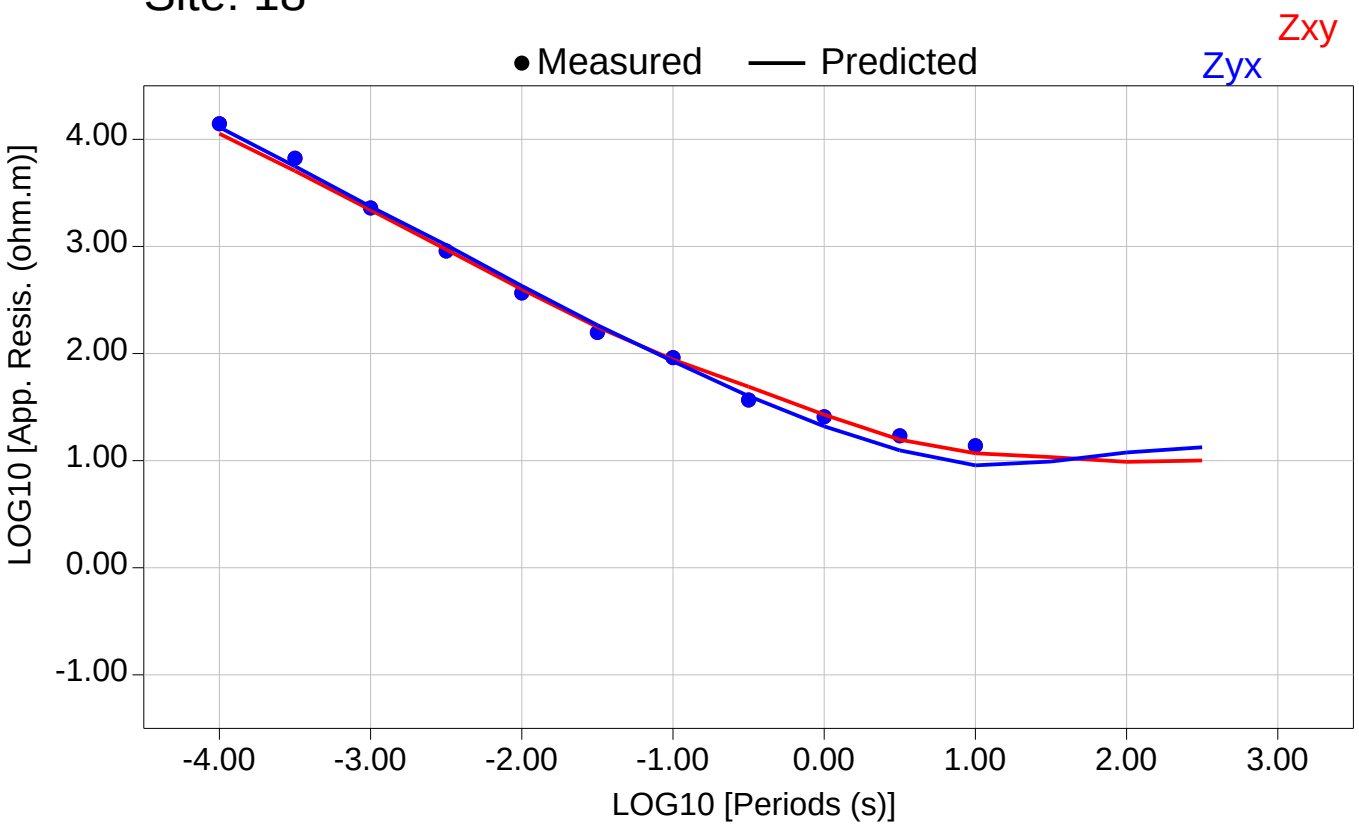

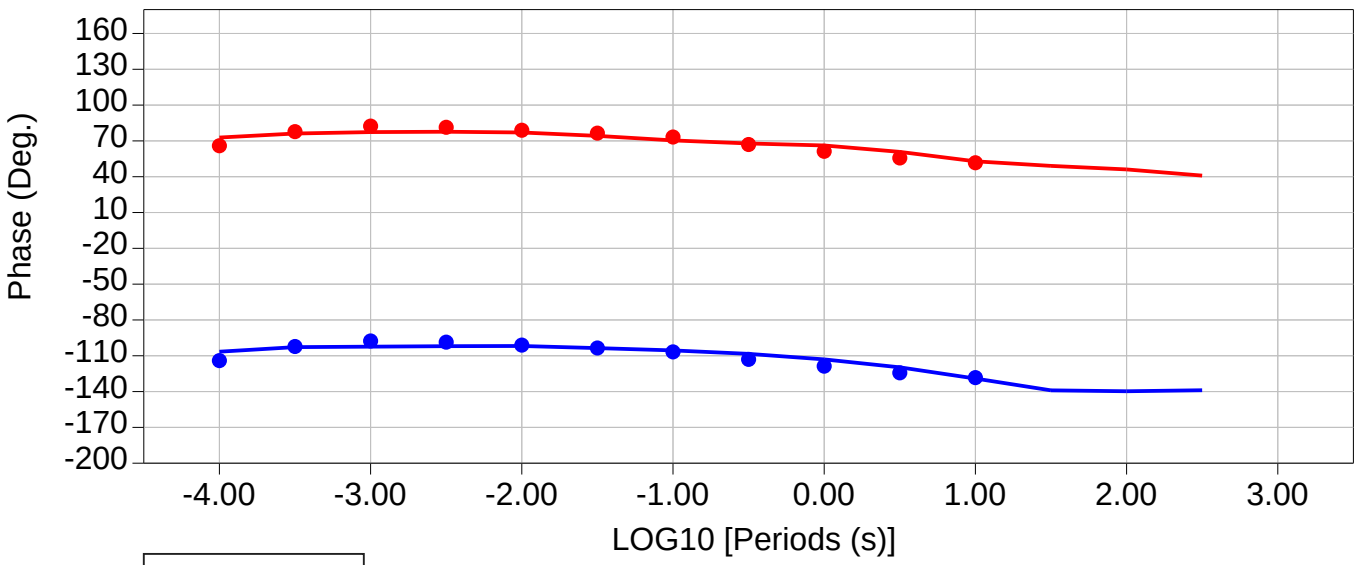

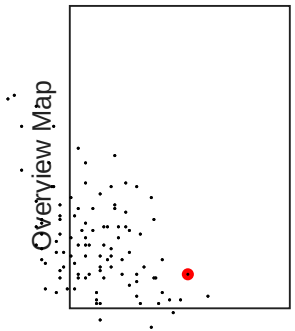

Total RMS = 21298.52

Zxy RMS = 21243.25
Zyx RMS = 21353.66

Site: G02

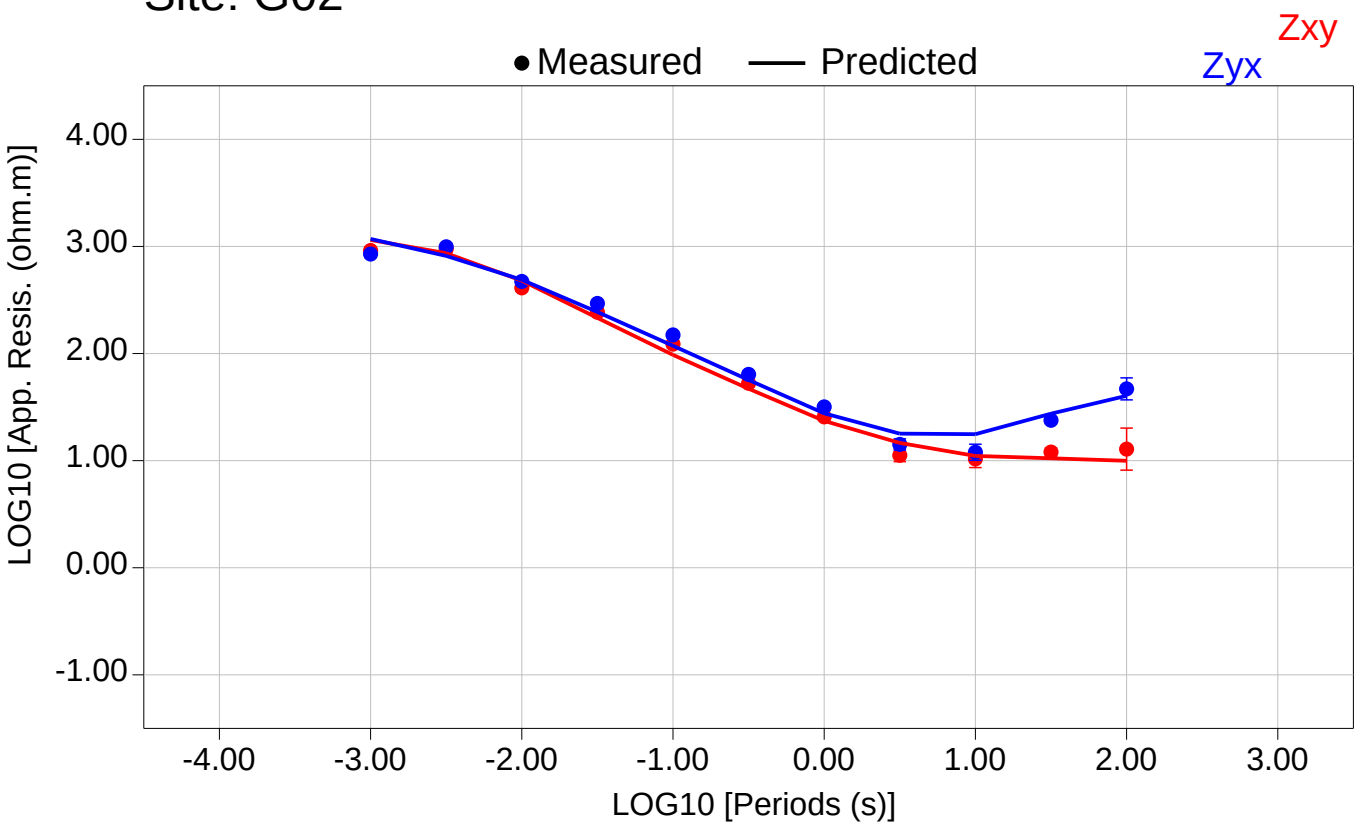

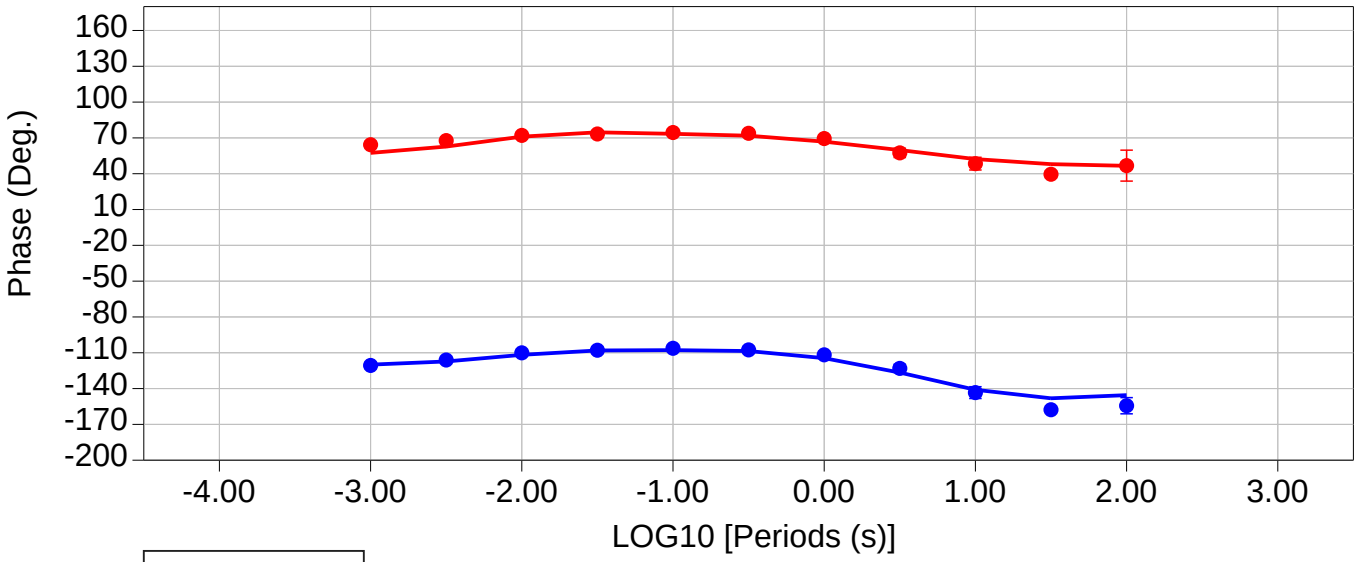

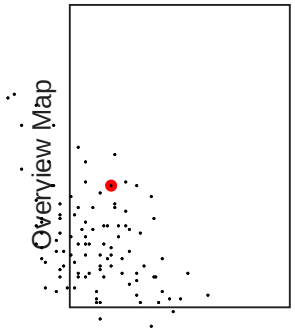

Total RMS = 16595.32

Zxy RMS = 16033.28
Zyx RMS = 17138.94

Site: G03

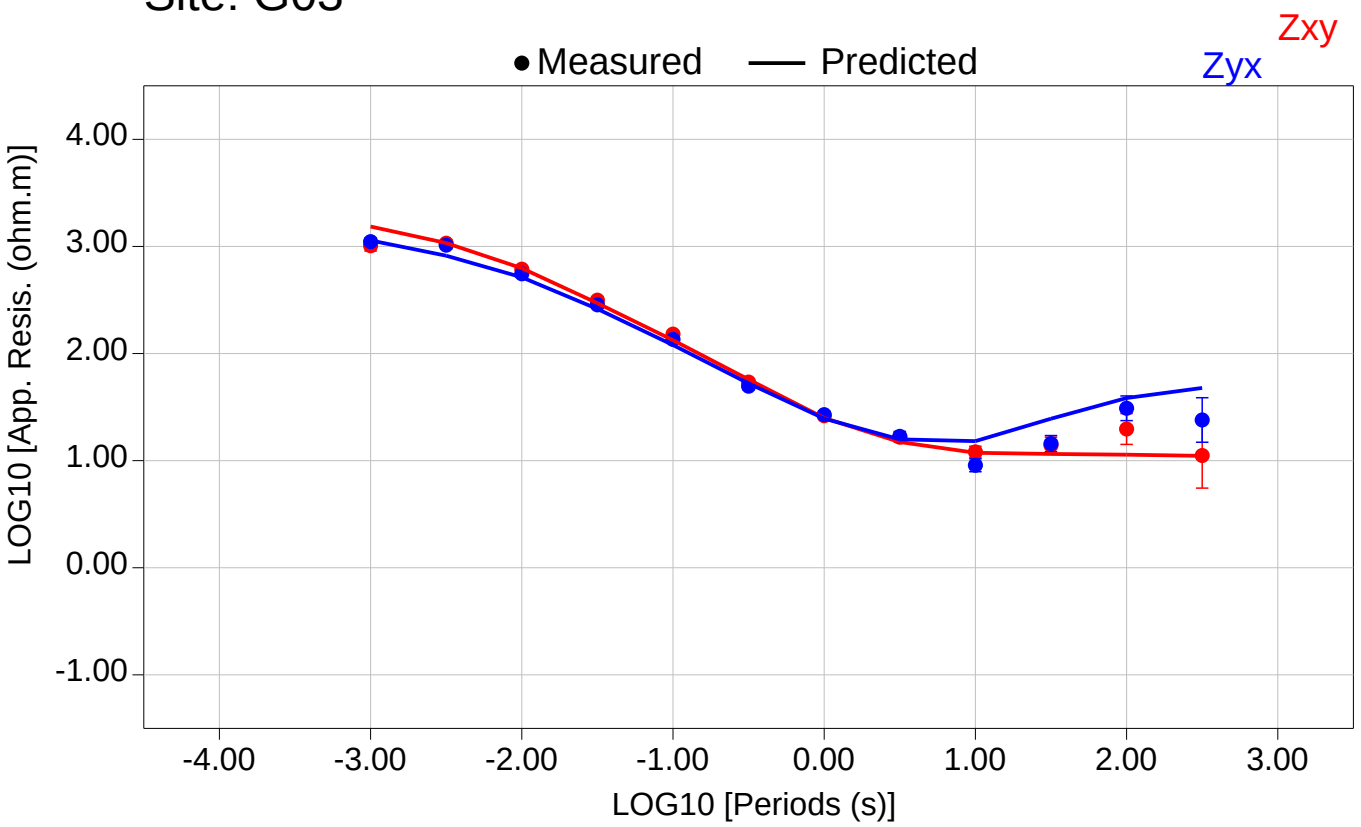

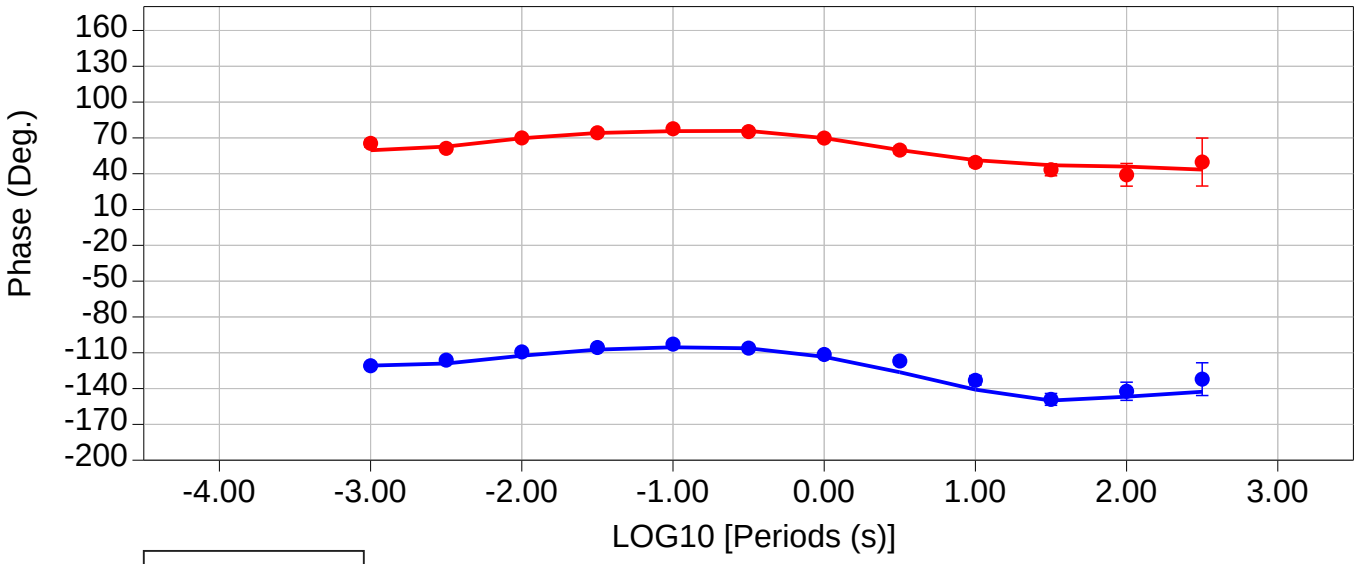

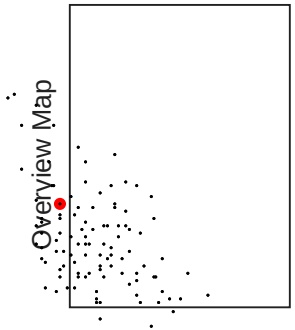

Total RMS = 16040.16

Zxy RMS = 16495.12

Zyx RMS = 15571.92

Site: G05

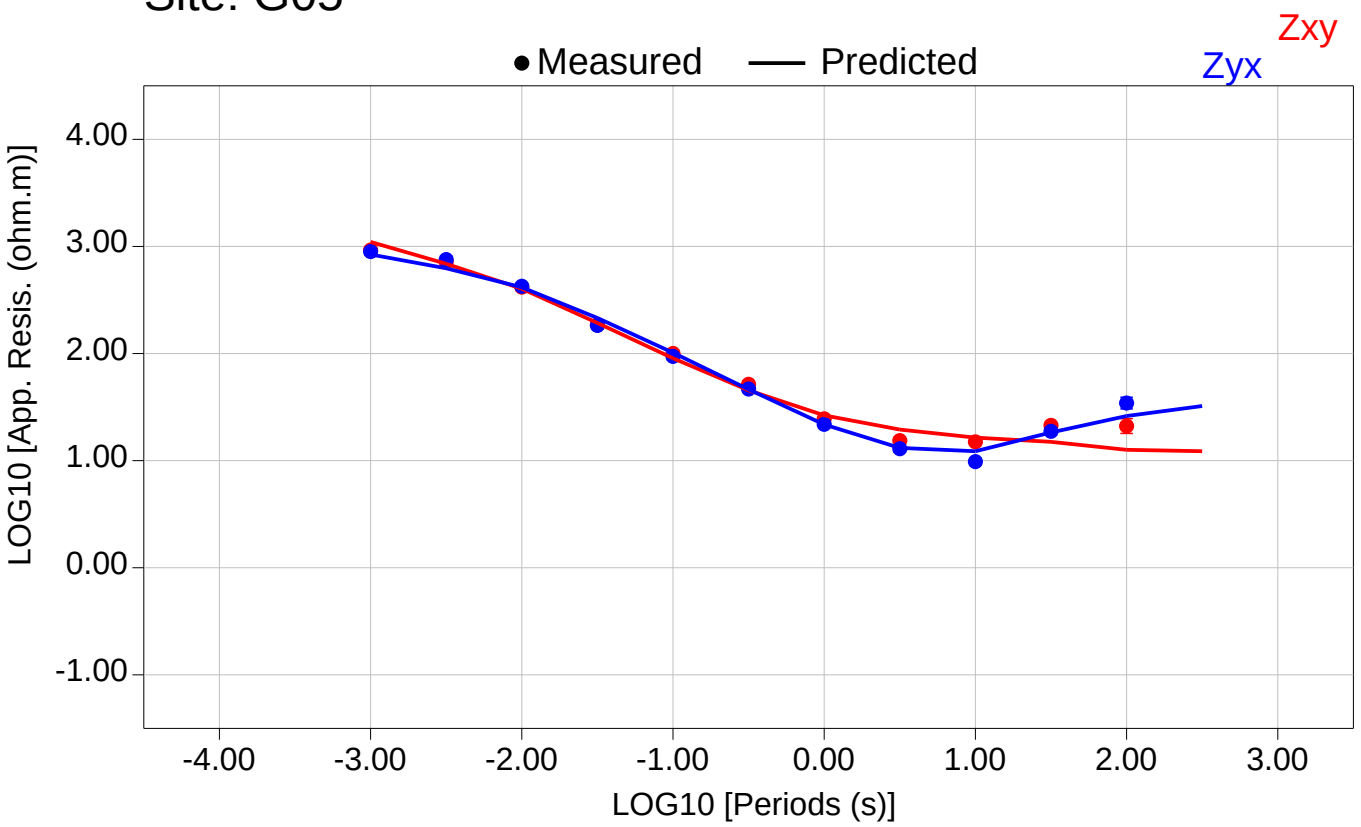

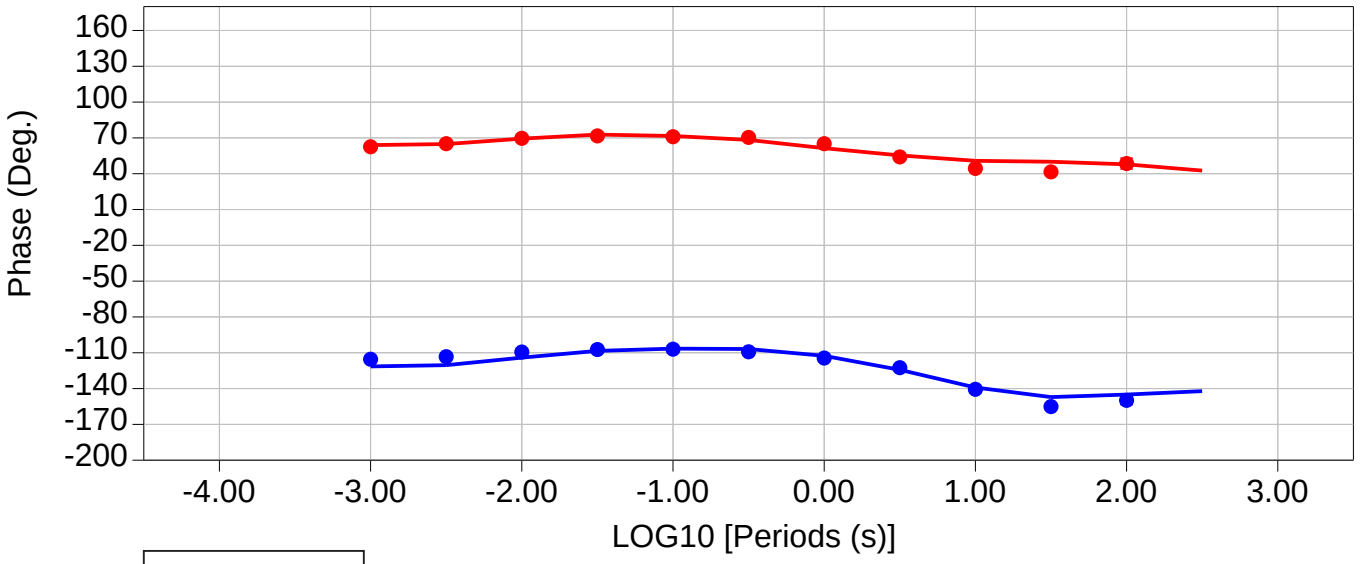

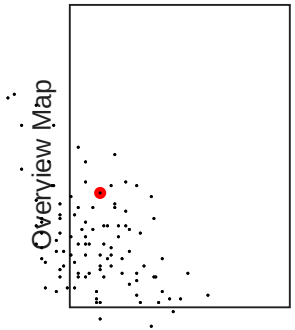

Total RMS = 18732.56

Zxy RMS = 19105.57

Zyx RMS = 18351.98

Site: G06

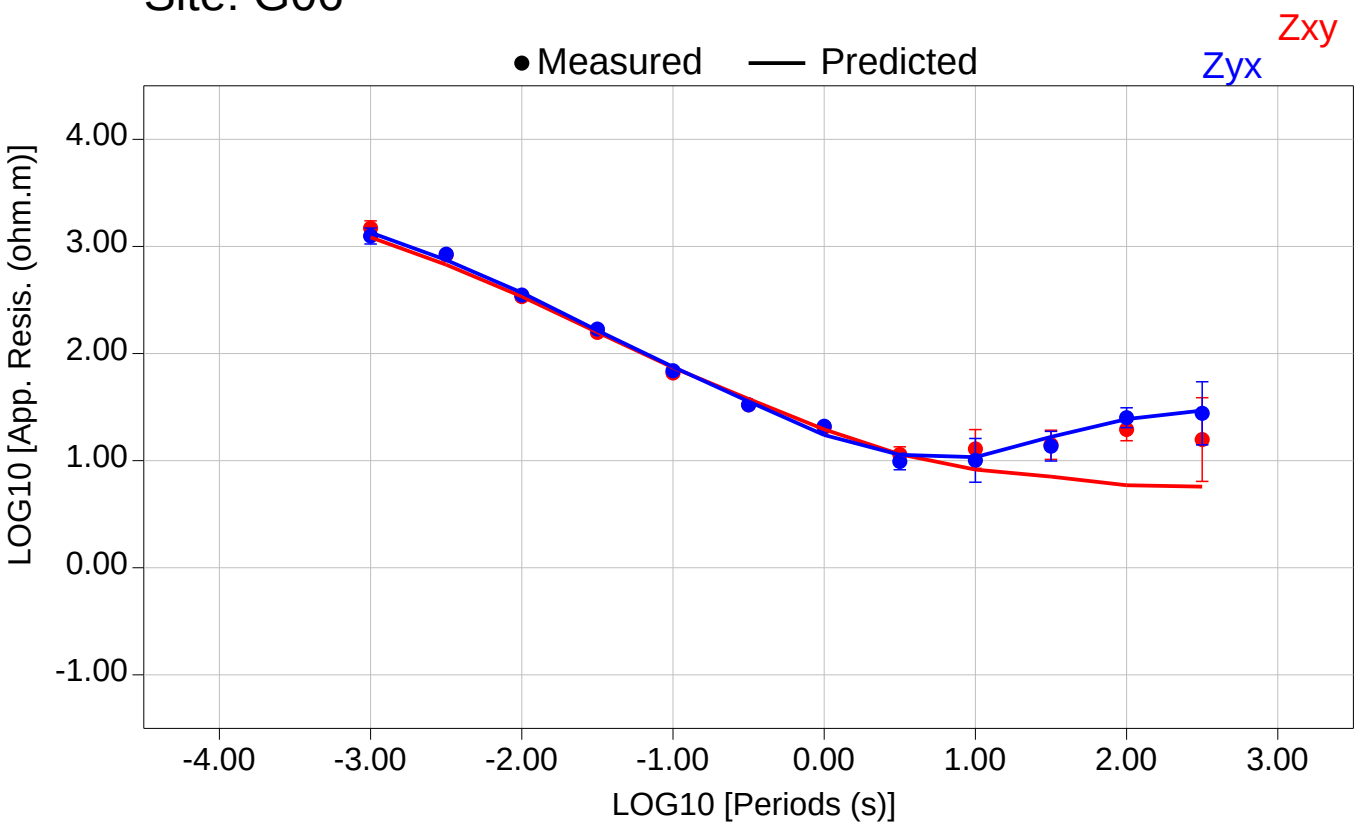

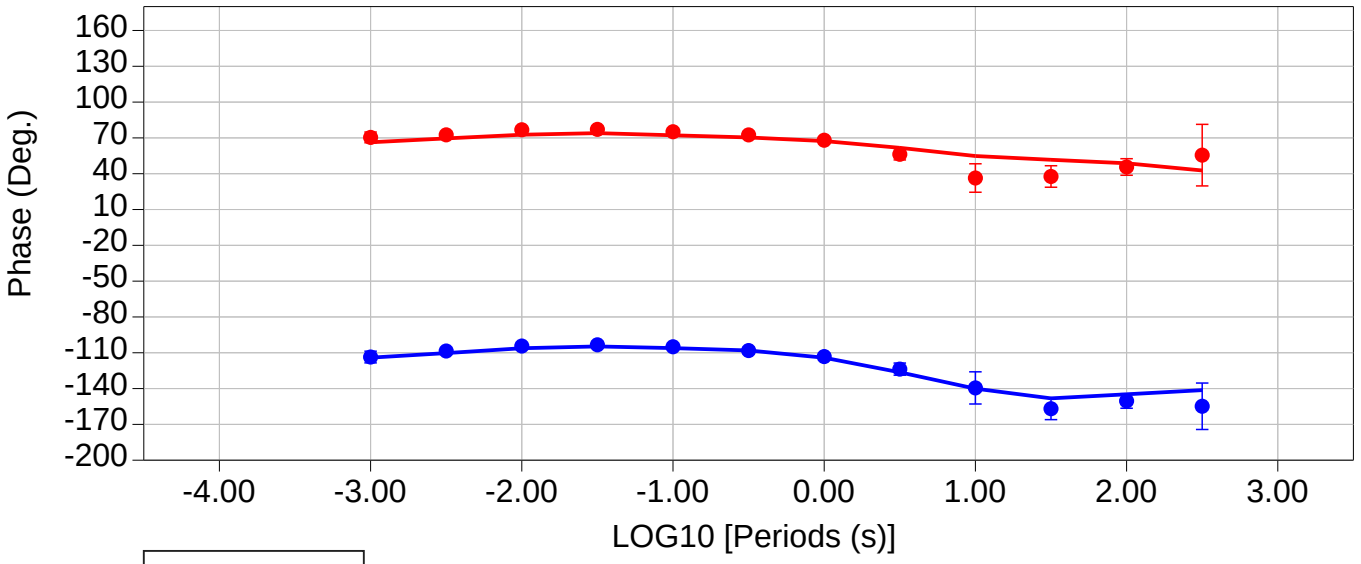

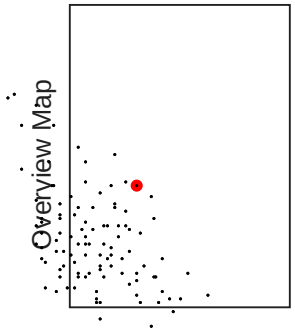

Total RMS = 15633.57

Zxy RMS = 15428.56

Zyx RMS = 15835.92

Site: G08

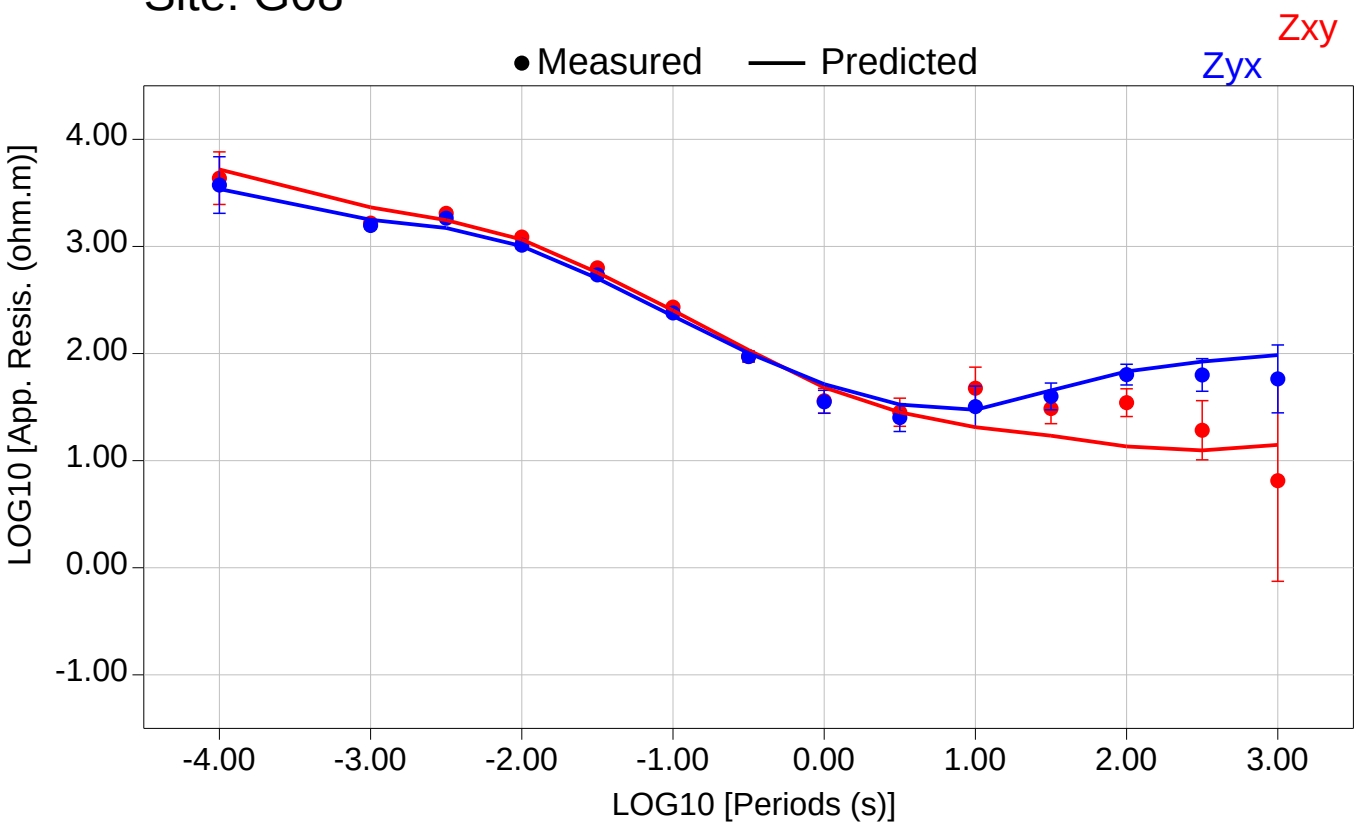

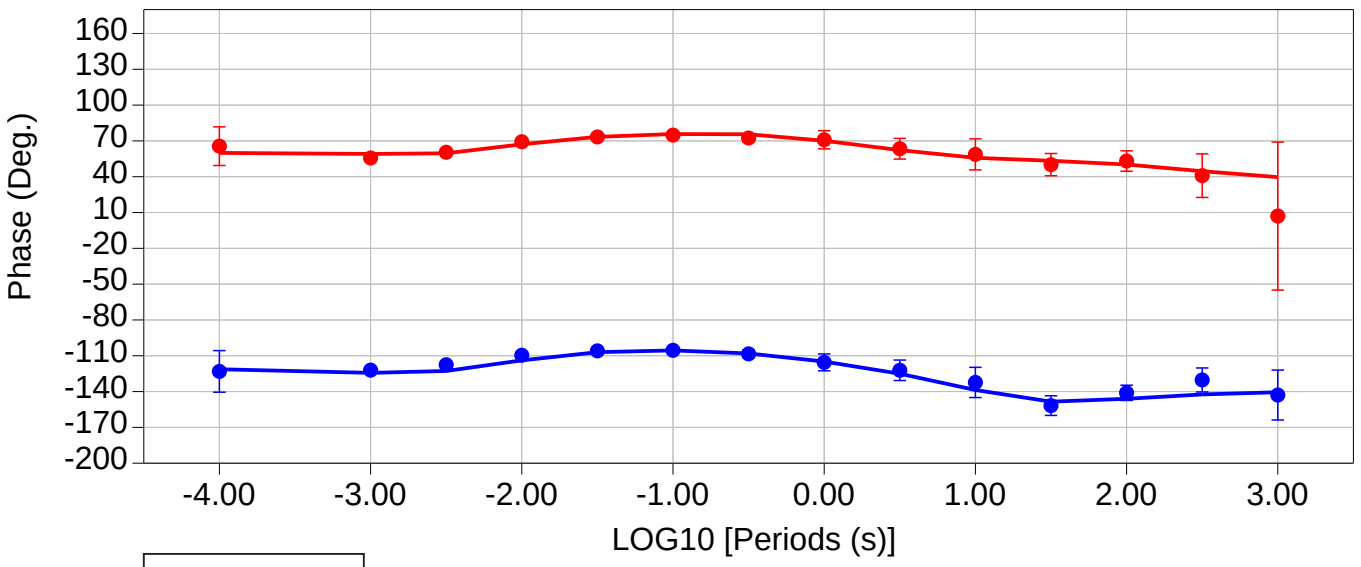

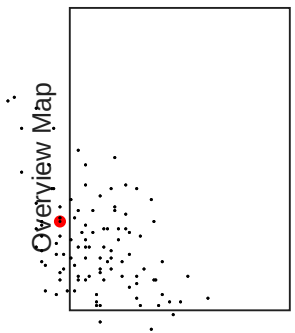

Total RMS = 12092.52

Zxy RMS = 12525.79

Zyx RMS = 11643.14

Site: G09

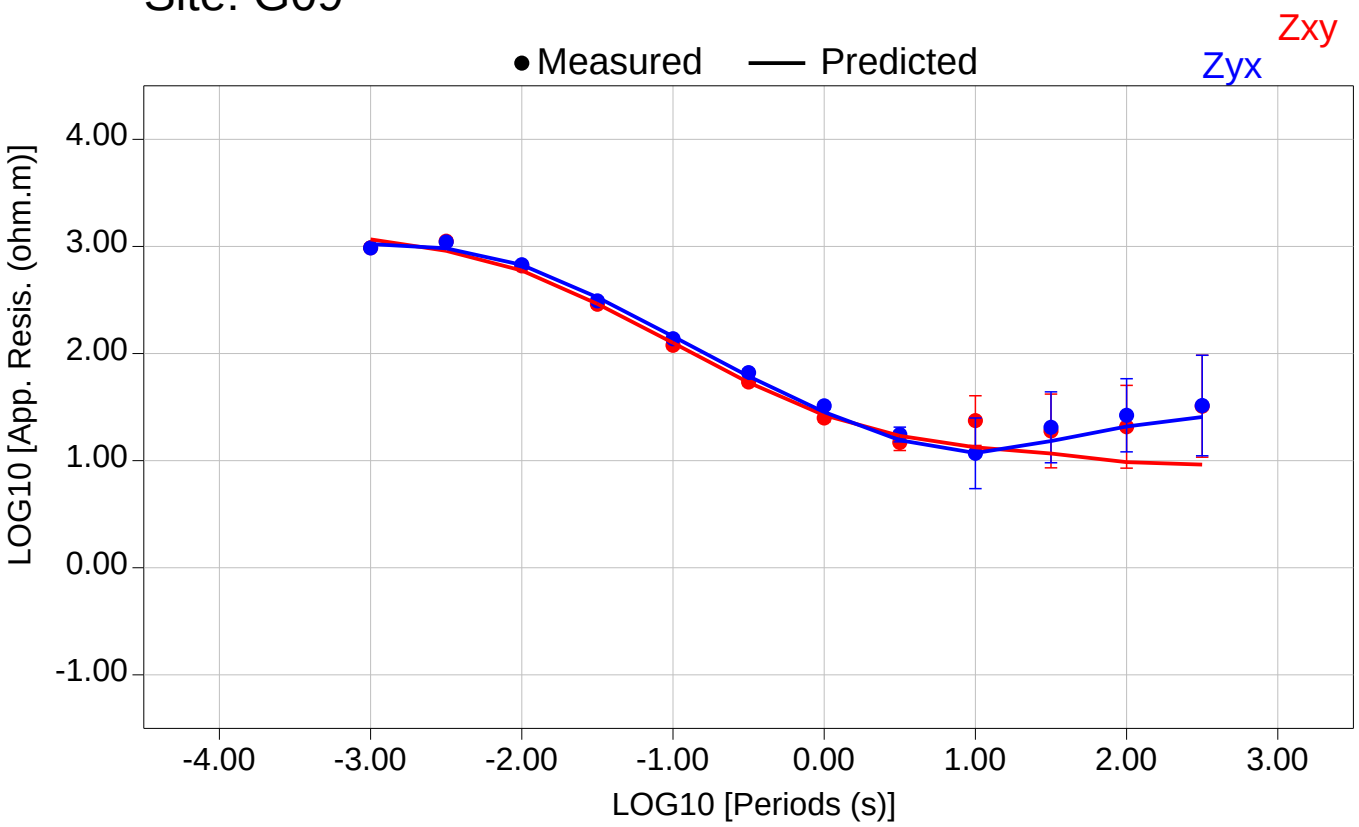

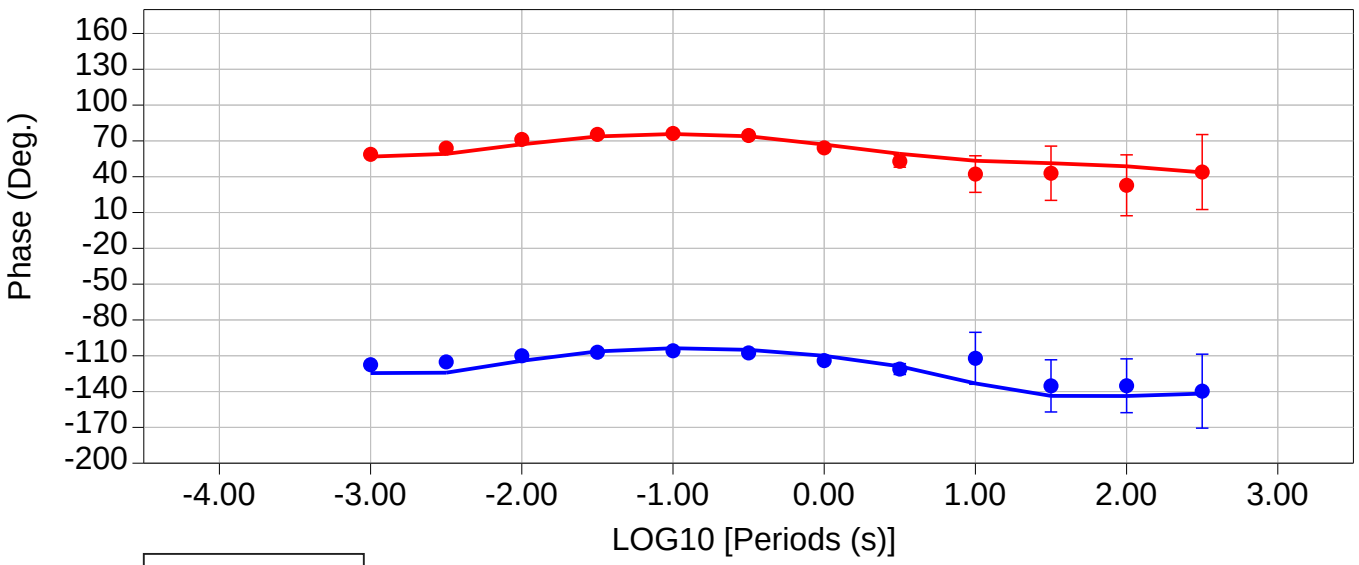

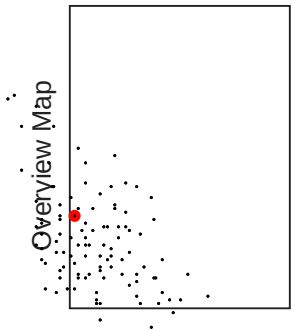

Total RMS = 15210.51

Zxy RMS = 14903.62

Zyx RMS = 15511.34

Site: G10

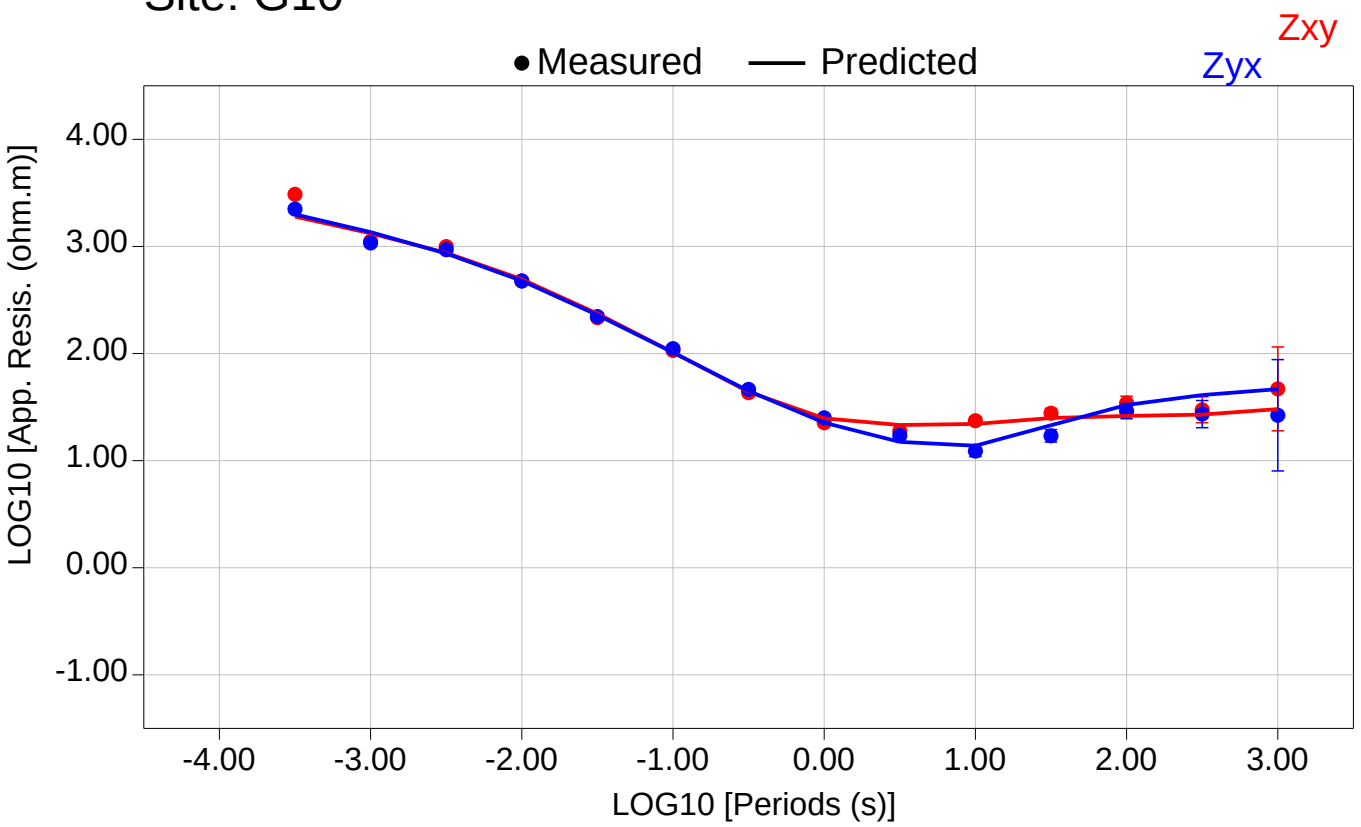

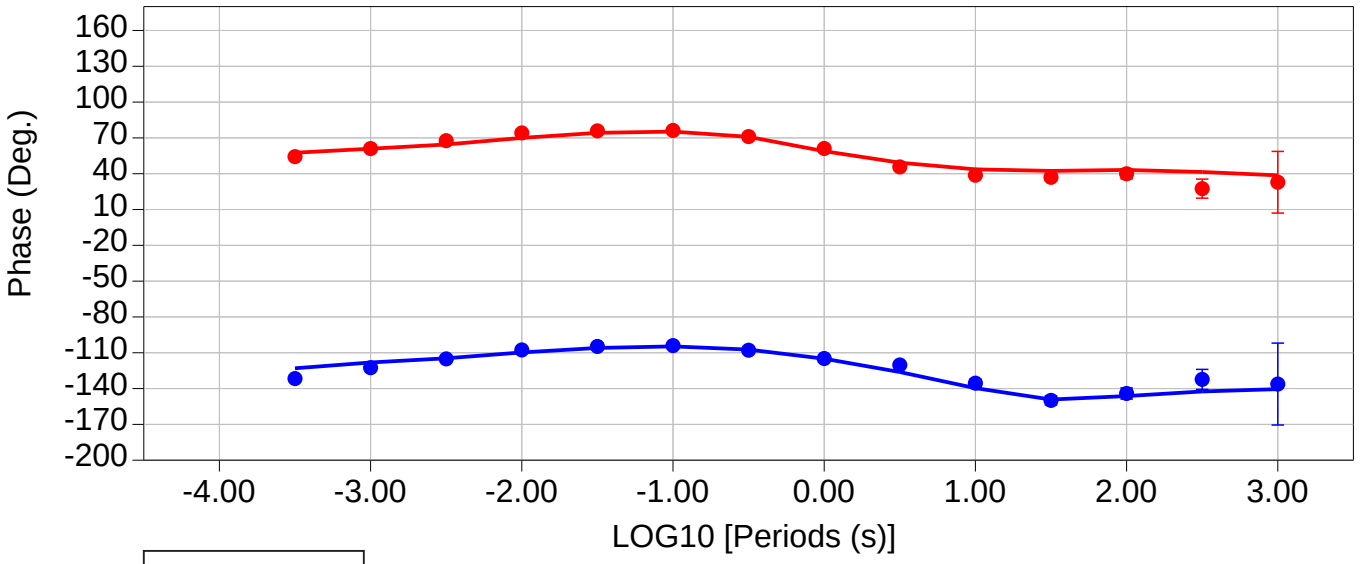

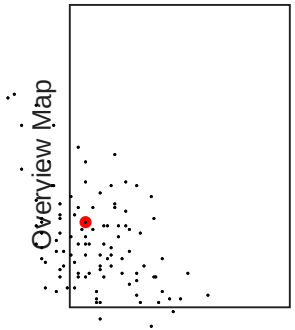

Total RMS = 15949.68

Zxy RMS = 16038.32

Zyx RMS = 15860.54

Site: G25

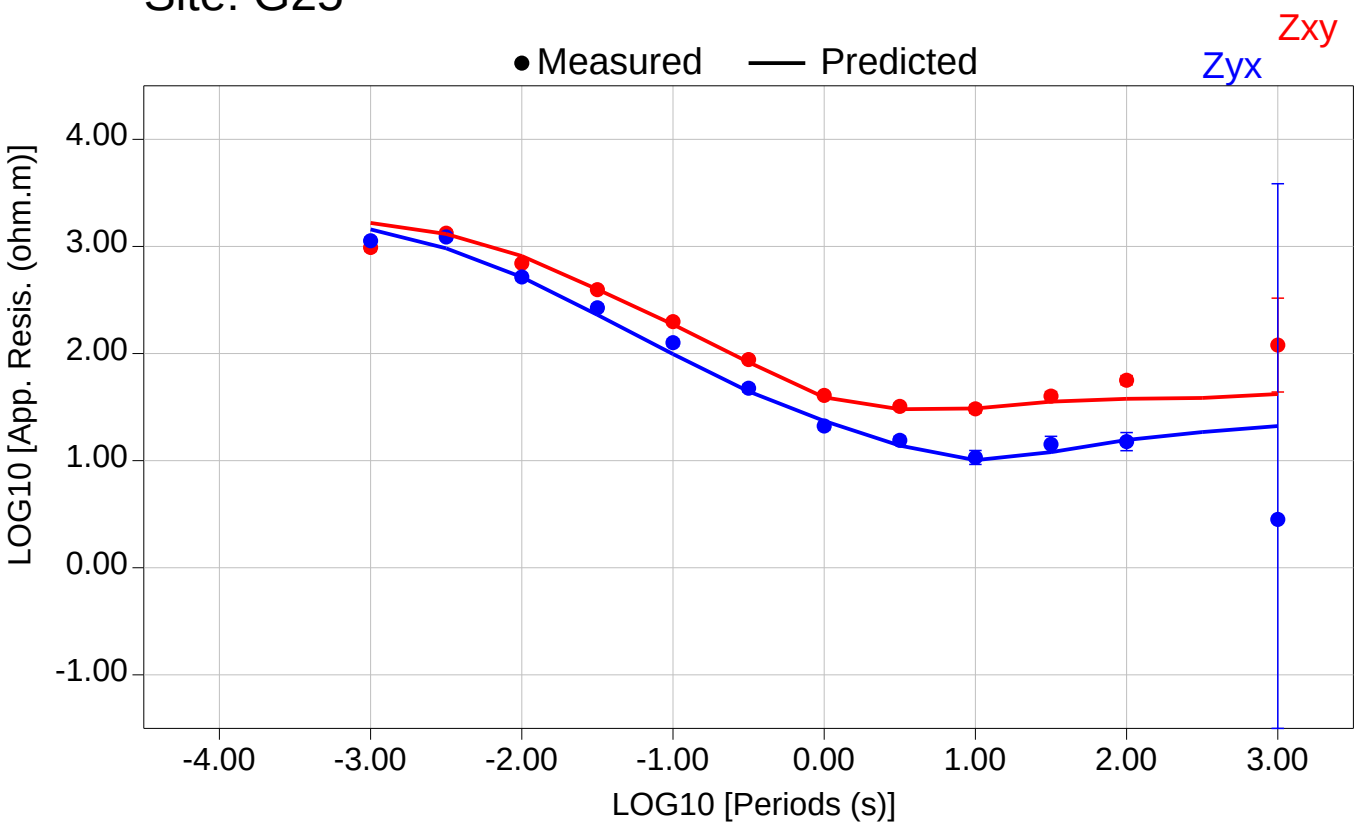

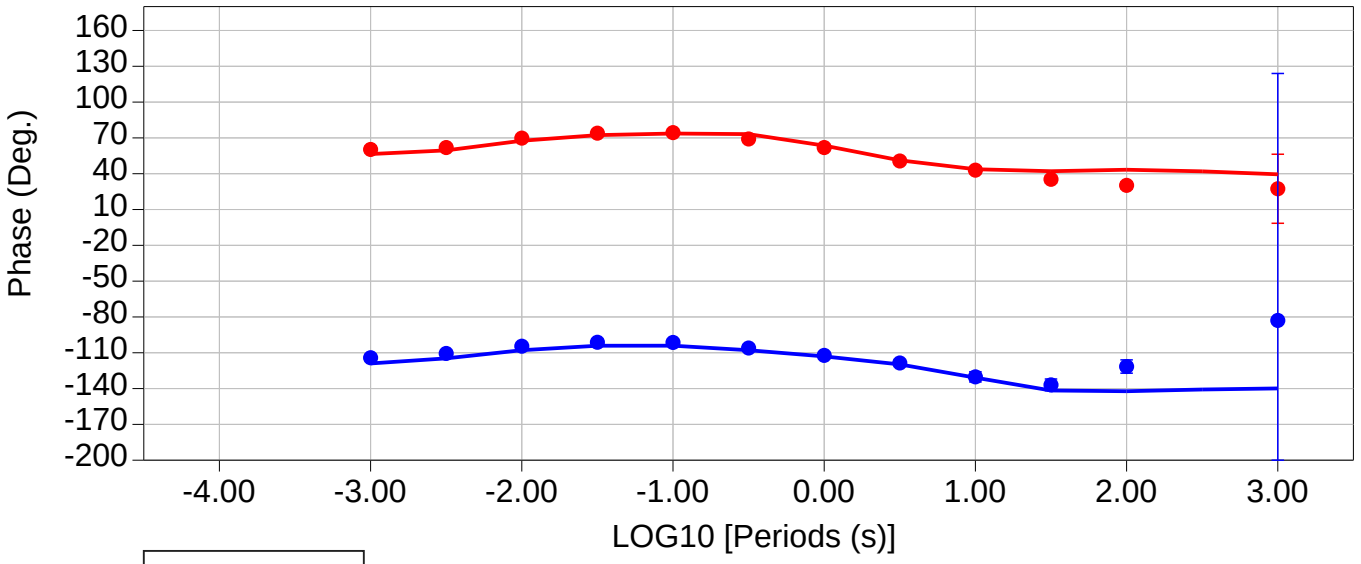

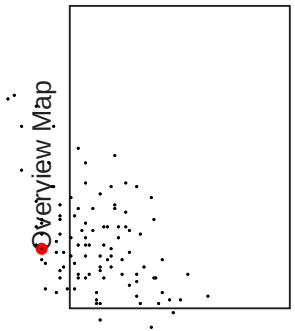

Total RMS = 16749.41

Zxy RMS = 18478.39
Zyx RMS = 14820.07

Site: G26

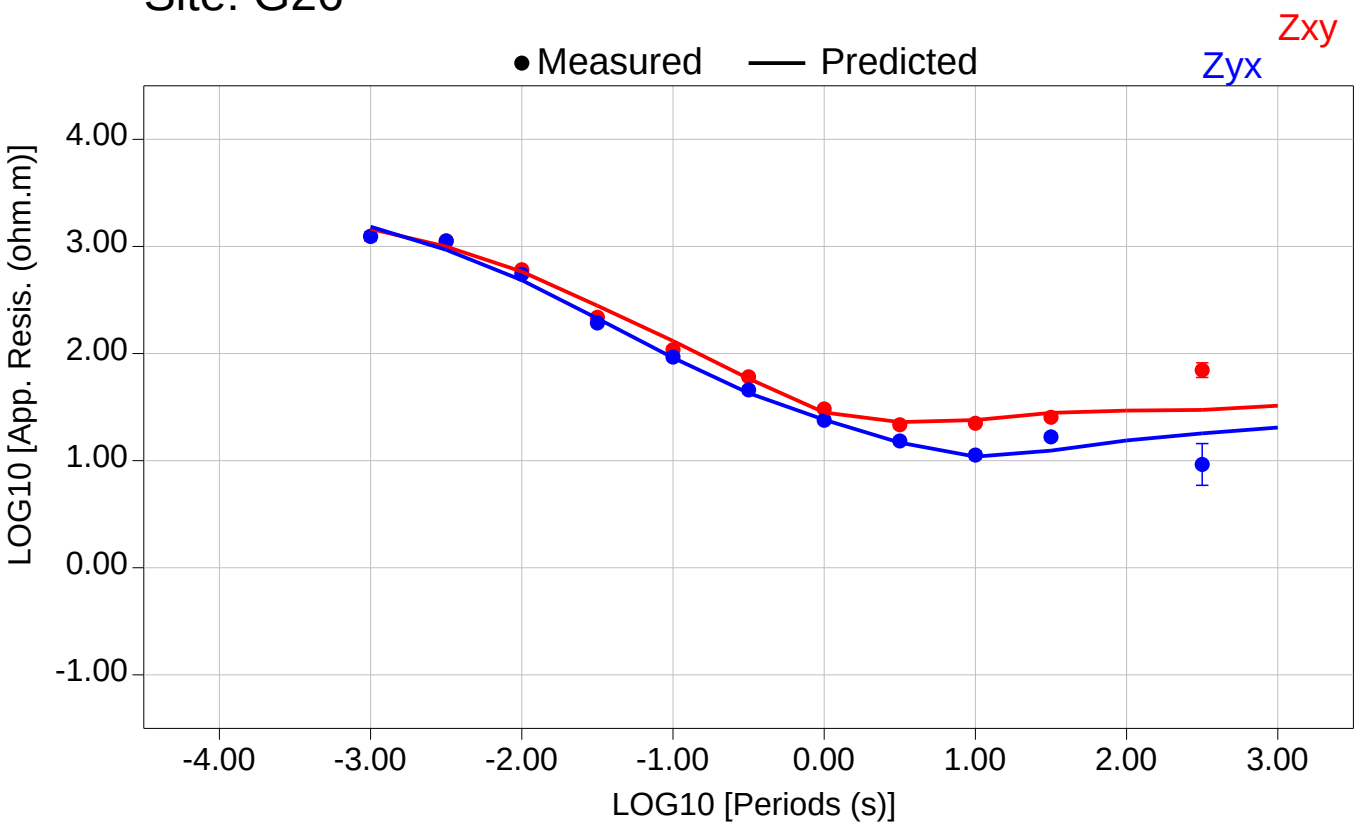

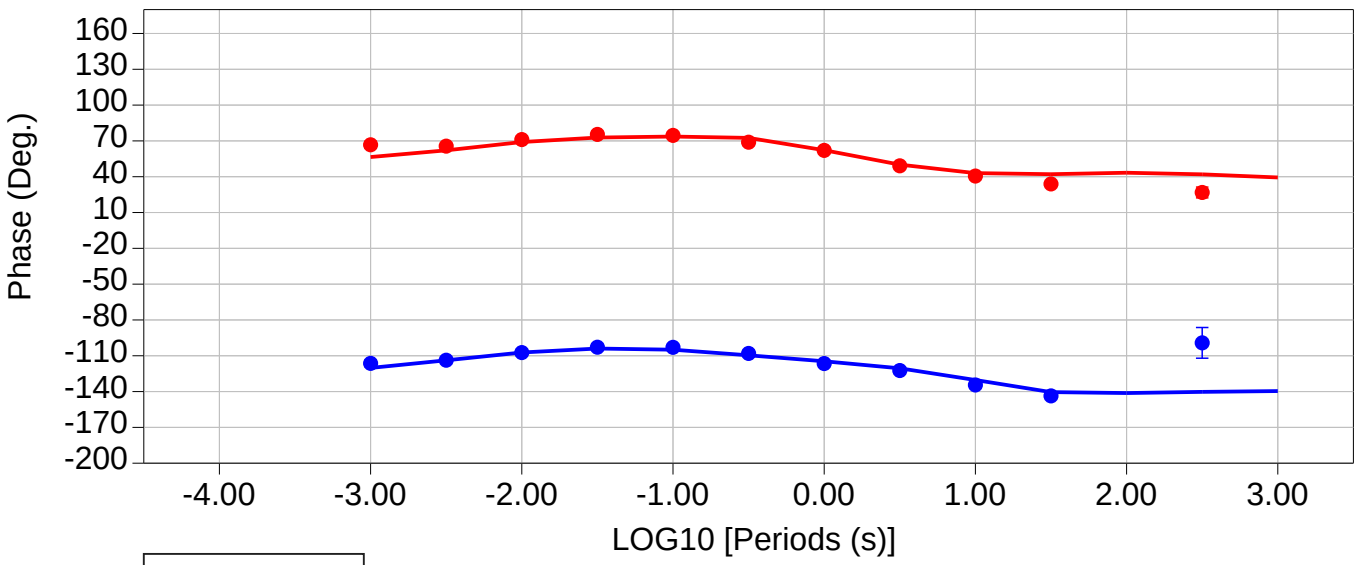

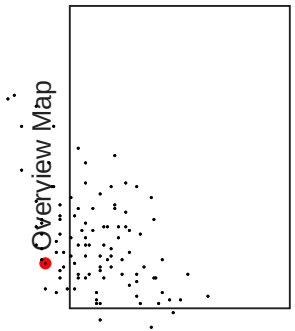

Total RMS = 18982.16

Zxy RMS = 20157.87
Zyx RMS = 17728.65

Site: G27

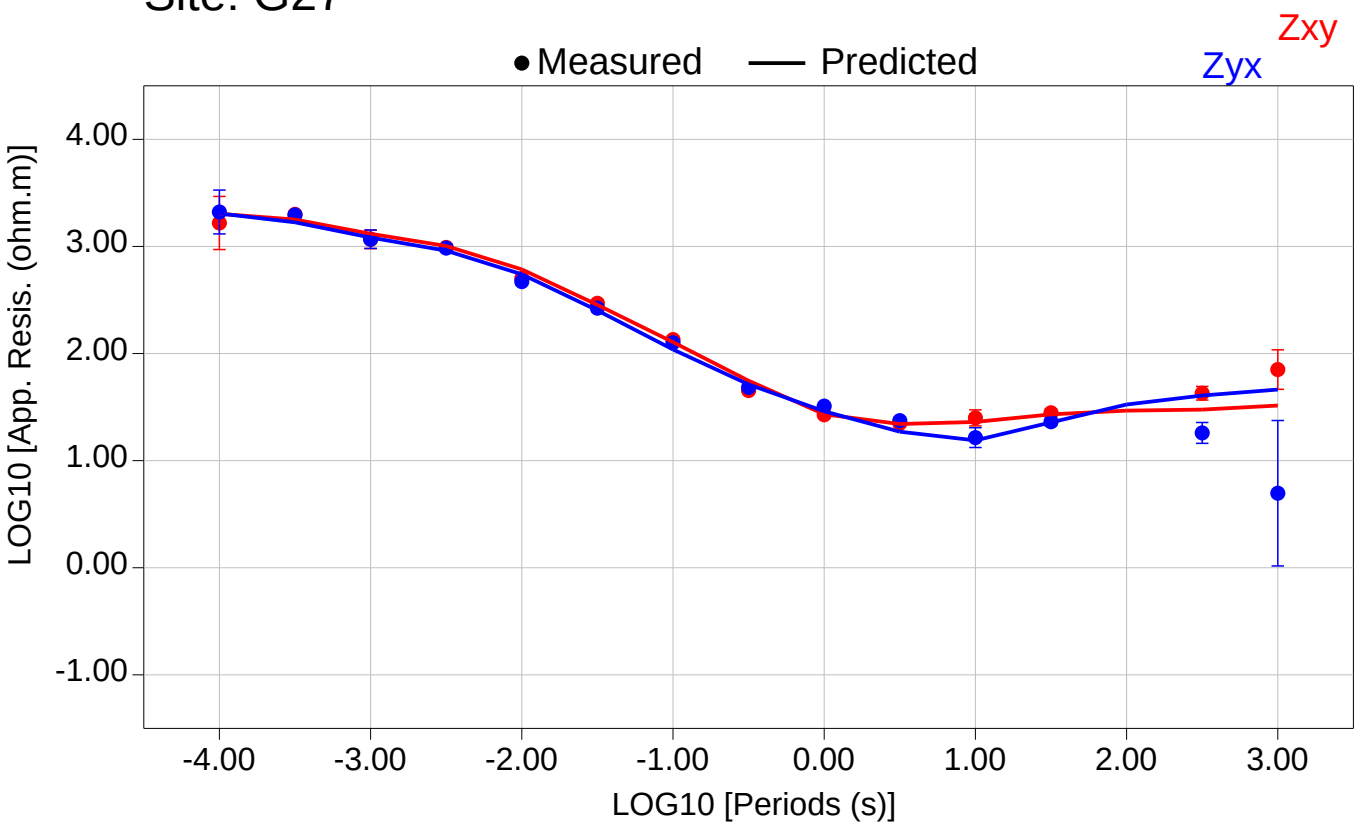

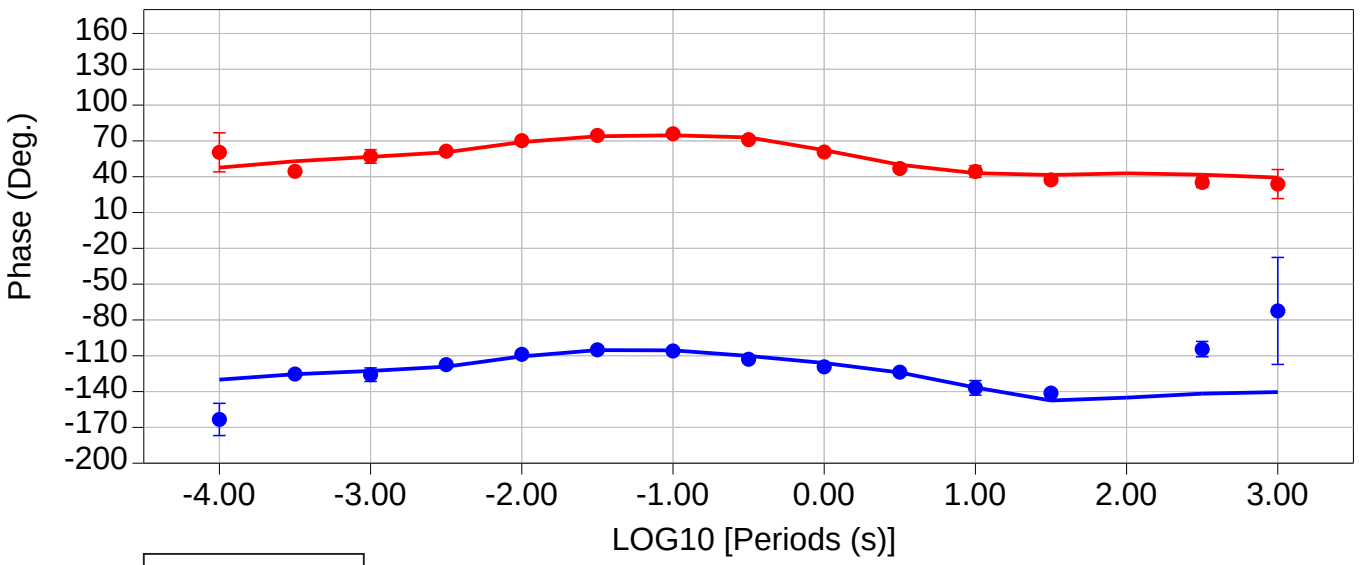

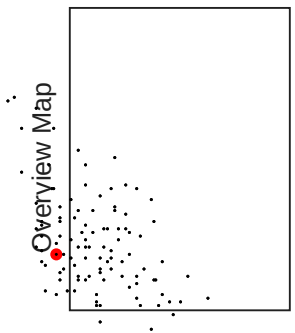

Total RMS = 16839.70

Zxy RMS = 17219.77
Zyx RMS = 16450.85

Site: G28

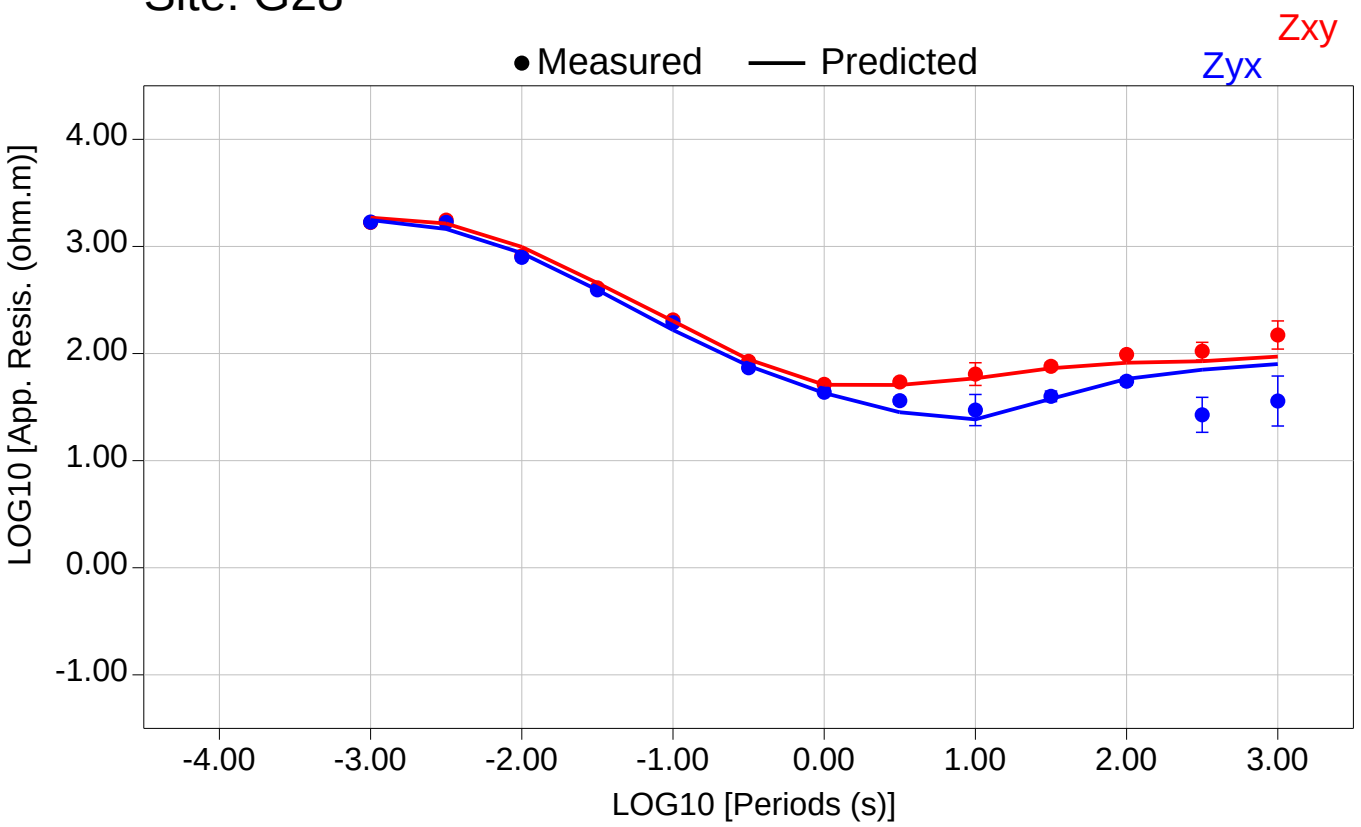

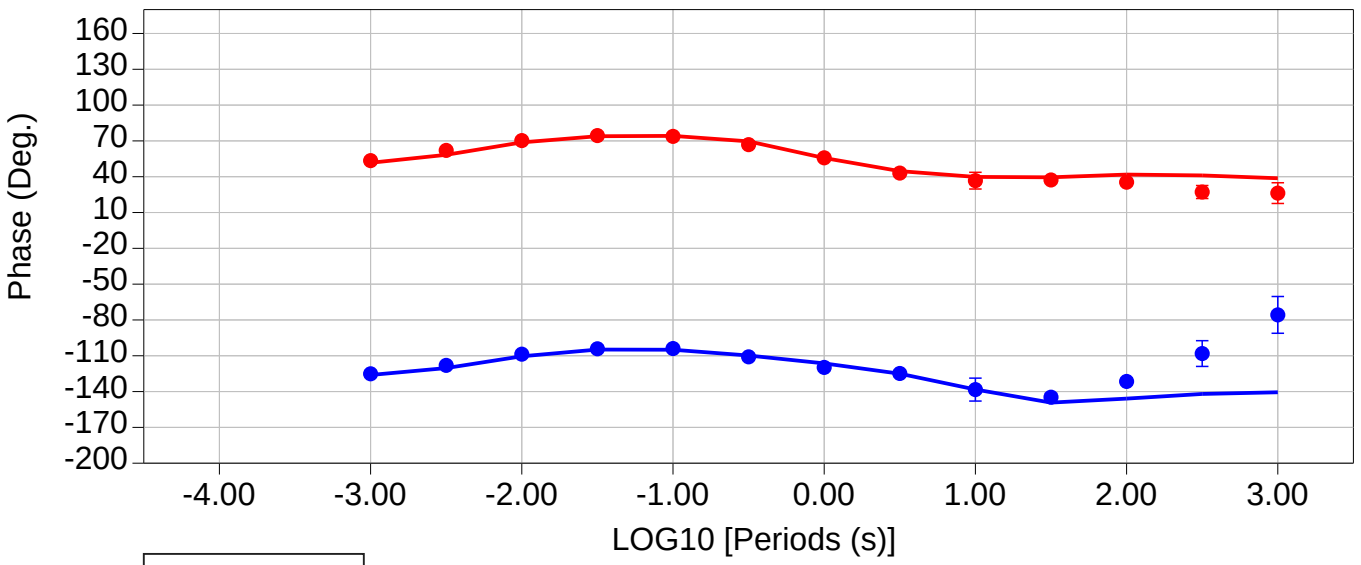

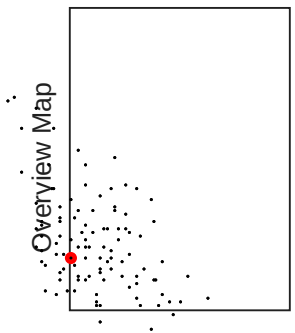

Total RMS = 16537.34

Zxy RMS = 17289.55

Zyx RMS = 15749.23

Site: G29

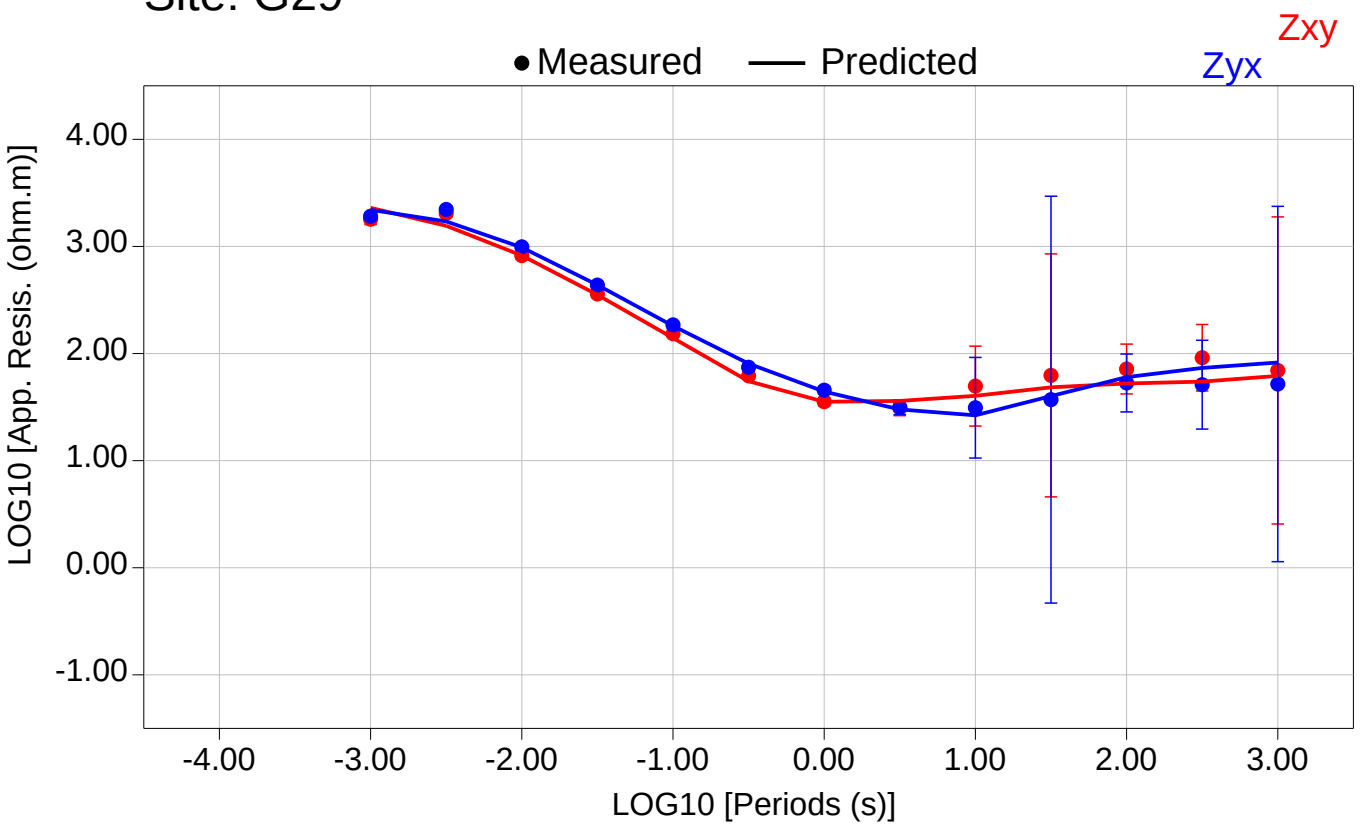

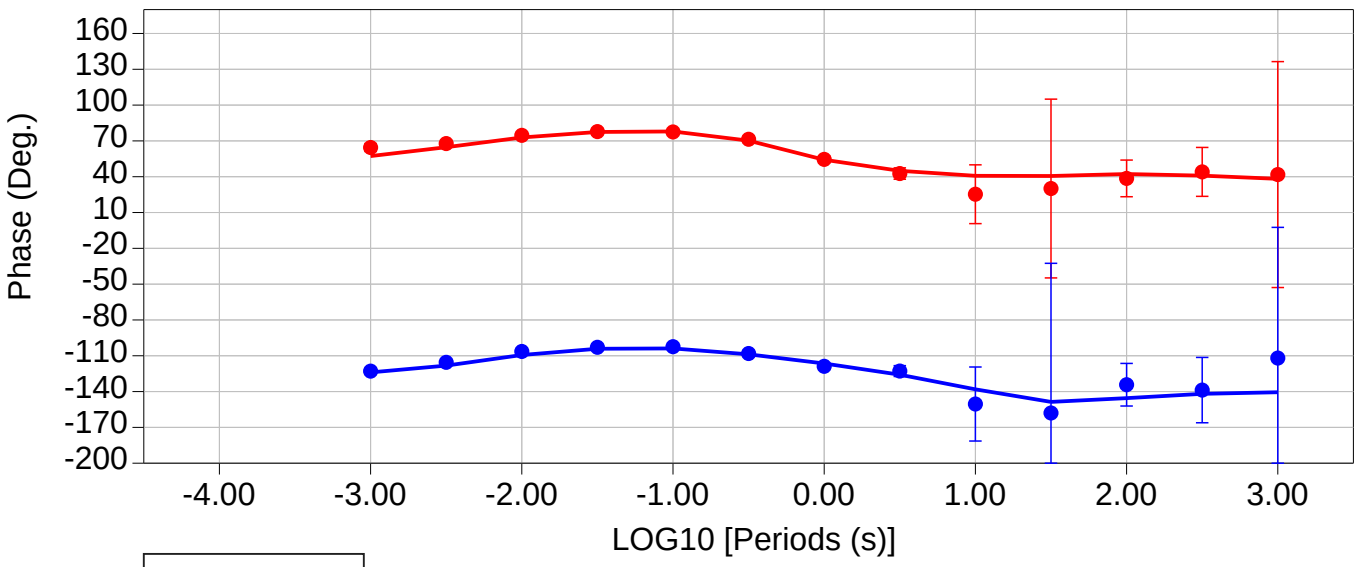

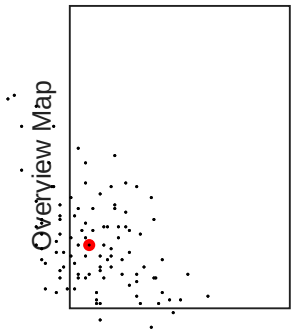

Total RMS = 14708.17

Zxy RMS = 13939.03
Zyx RMS = 15439.04

Site: G30

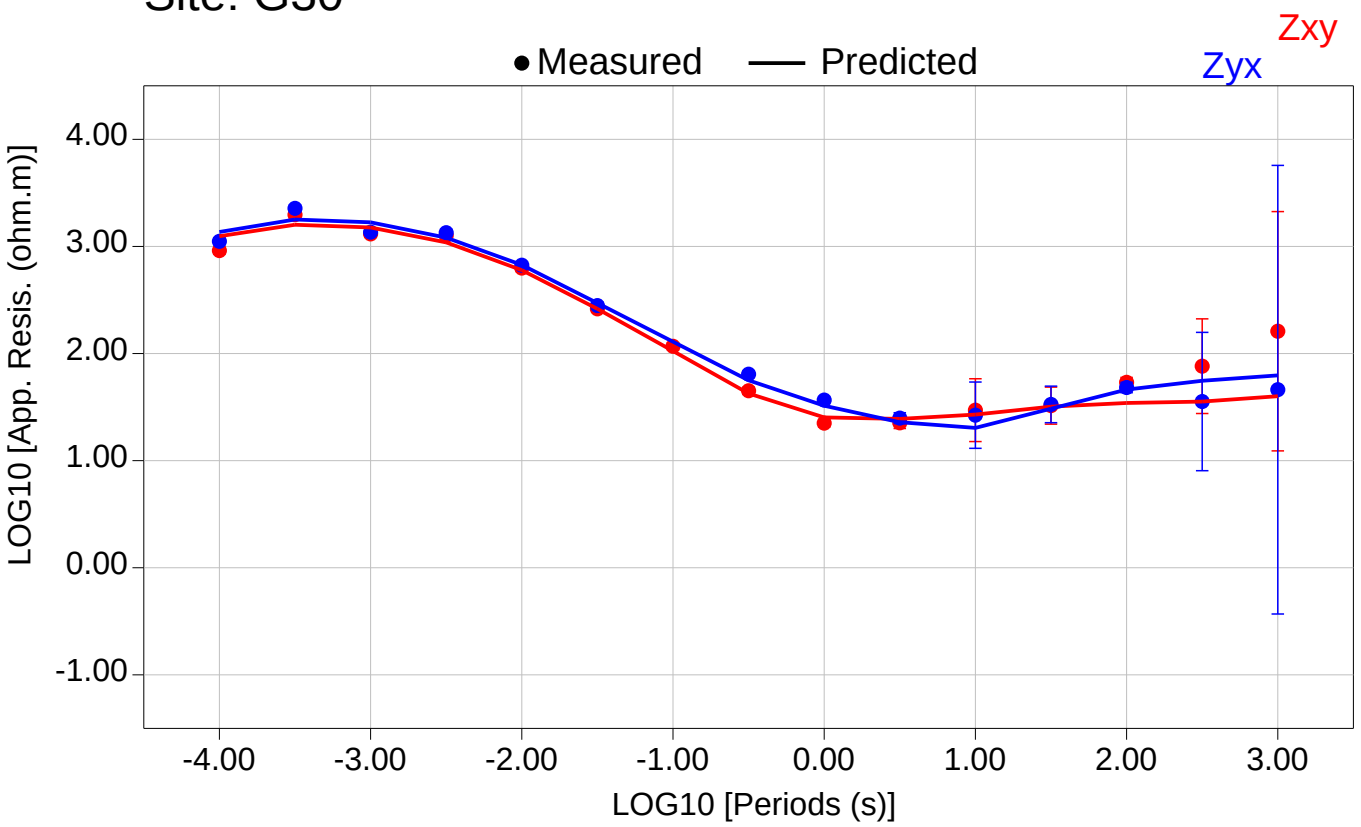

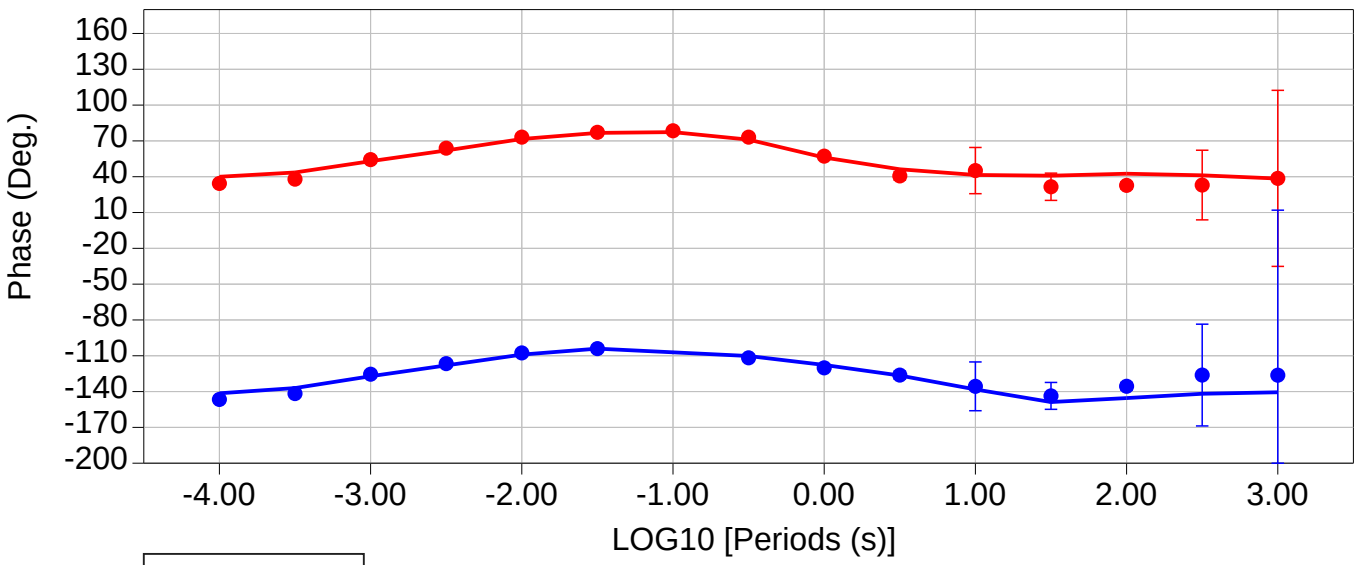

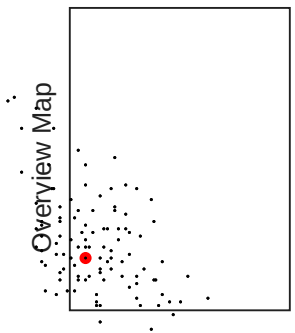

Total RMS = 14179.85

Zxy RMS = 14620.19

Zyx RMS = 13692.35

Site: G31

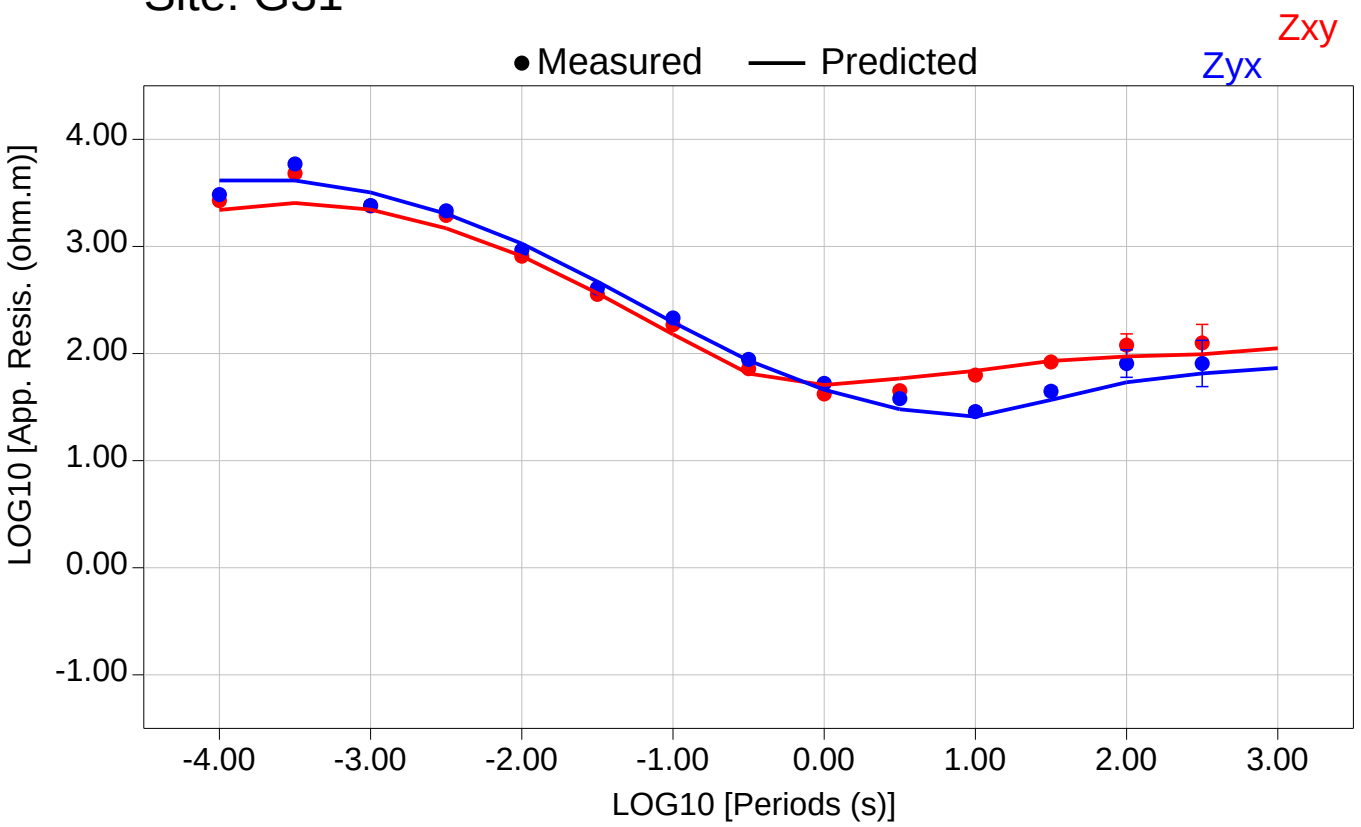

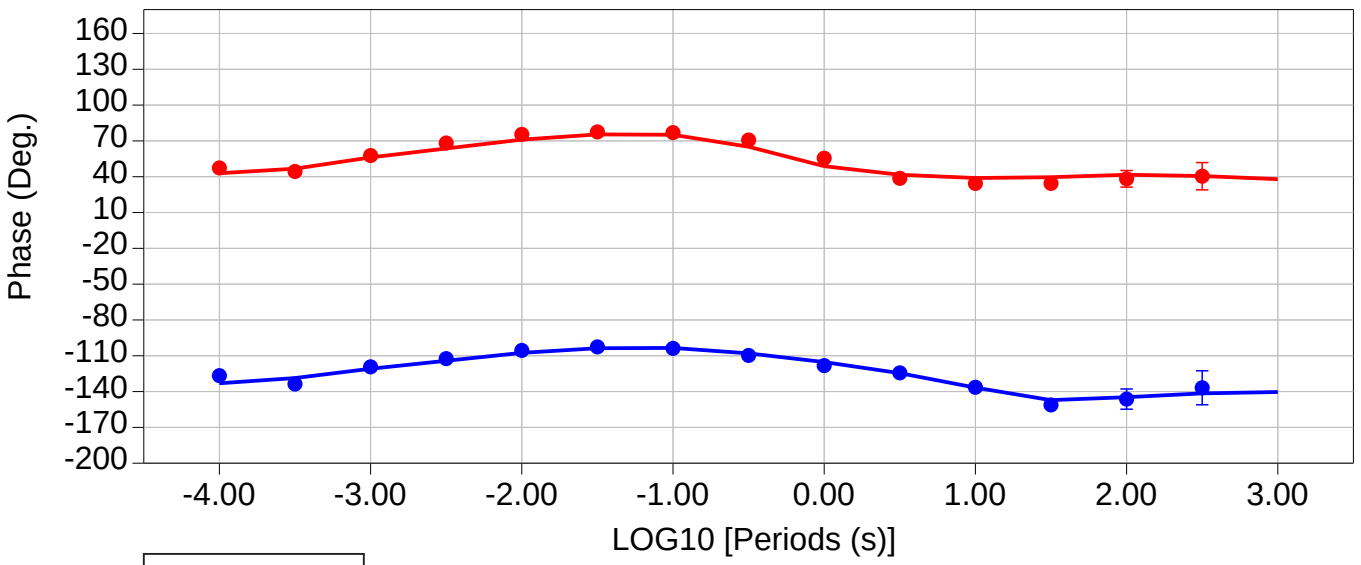

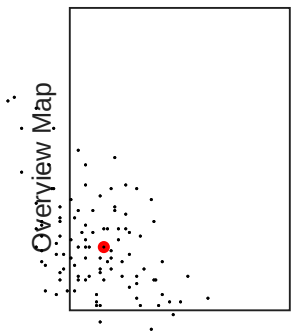

Total RMS = 17140.71

Zxy RMS = 16530.46

Zyx RMS = 17729.97

Site: G32

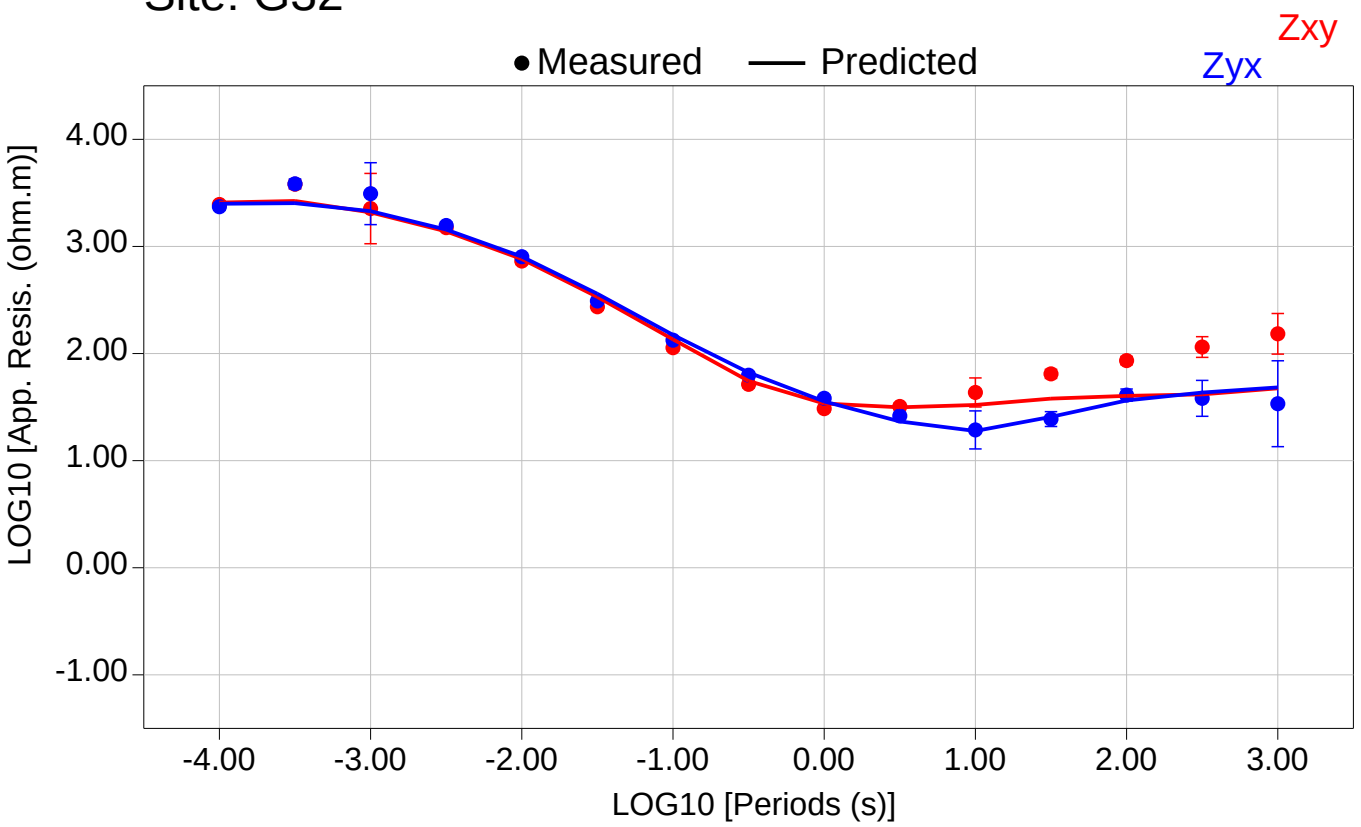

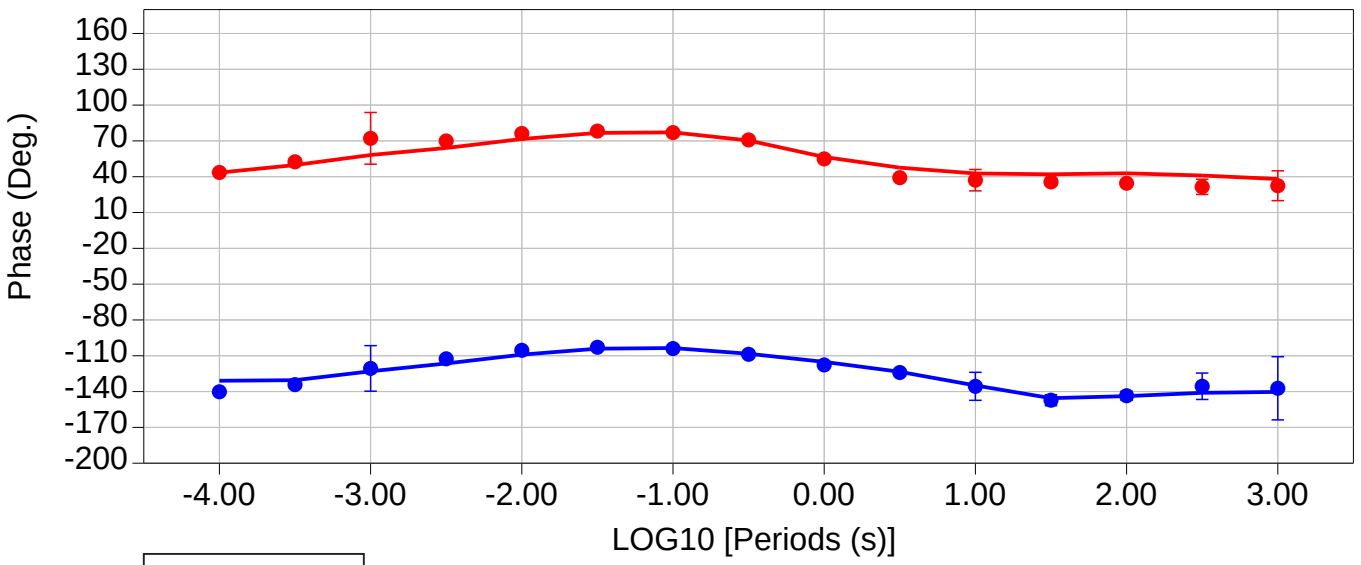

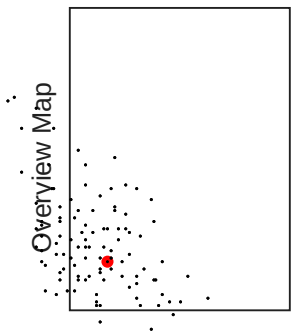

Total RMS = 16158.40

Zxy RMS = 16013.28
Zyx RMS = 16302.23

Site: G33

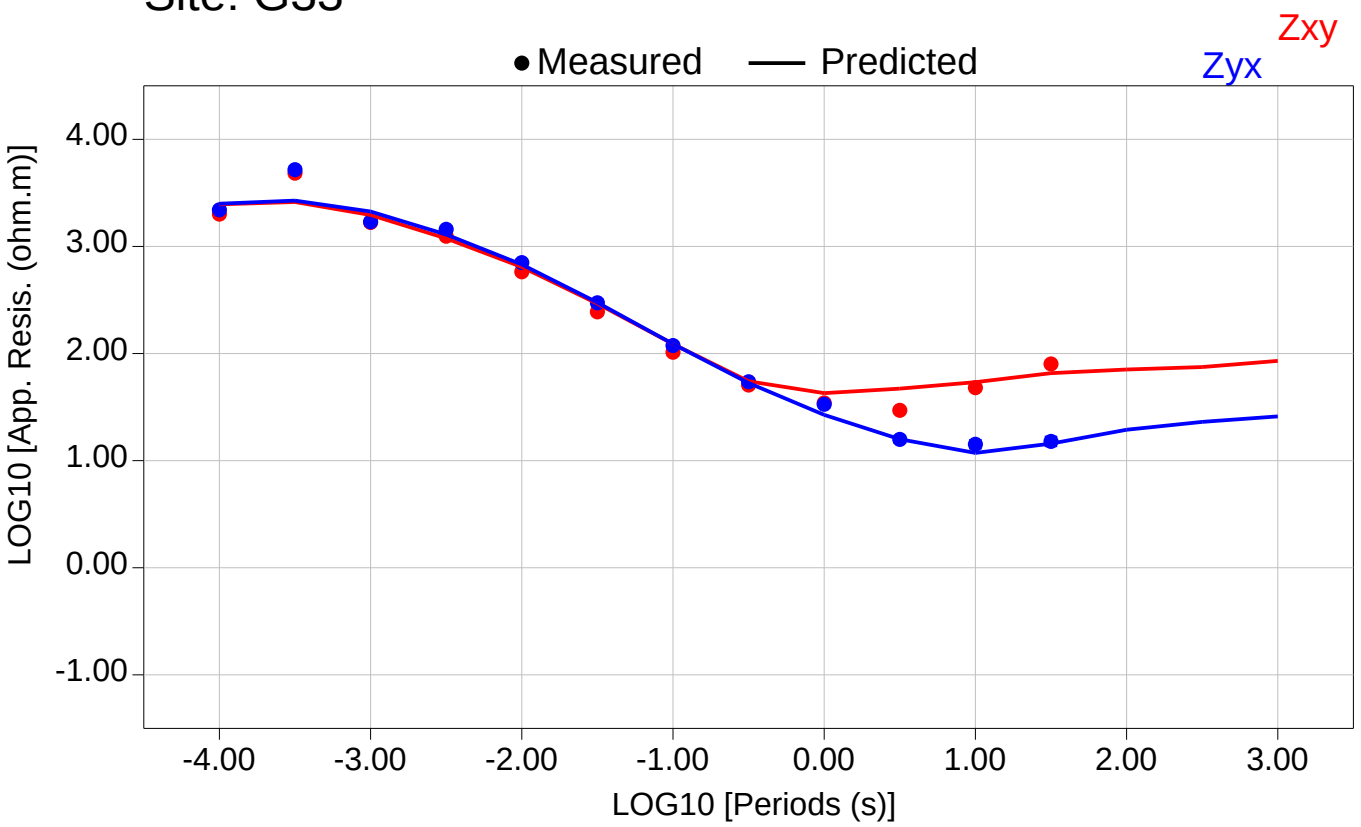

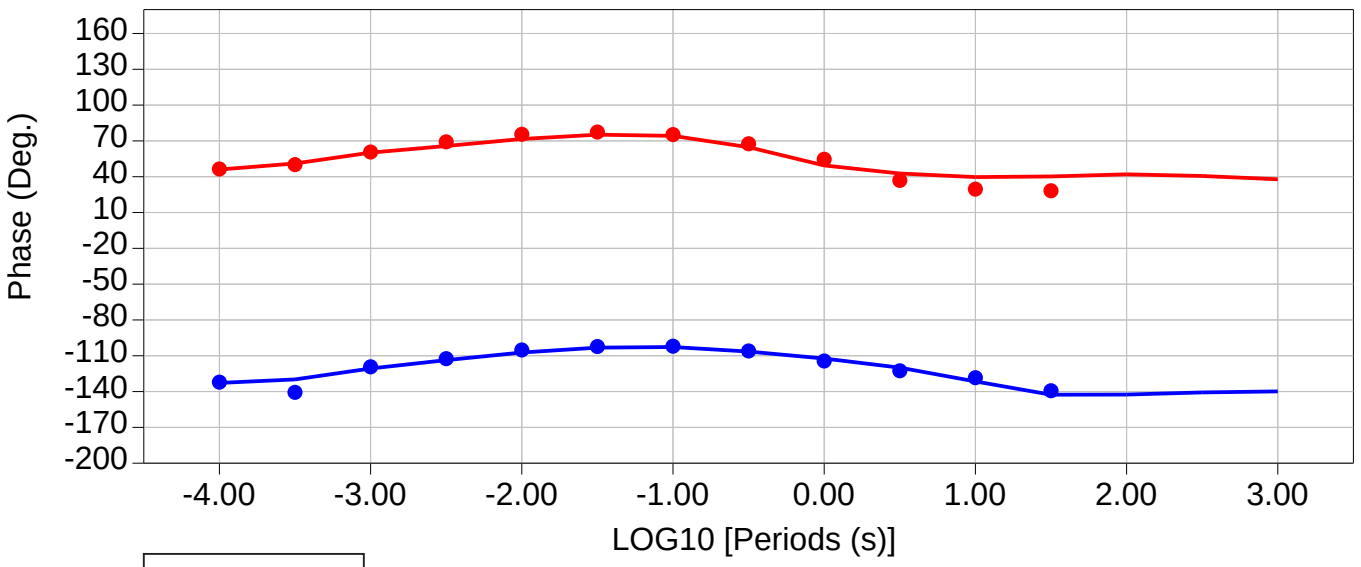

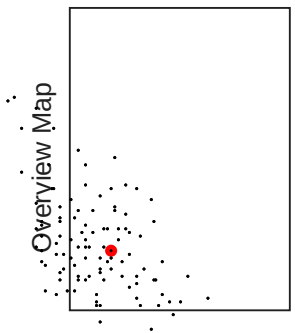

Total RMS = 19592.65

Zxy RMS = 20550.51
Zyx RMS = 18585.49

Site: G34

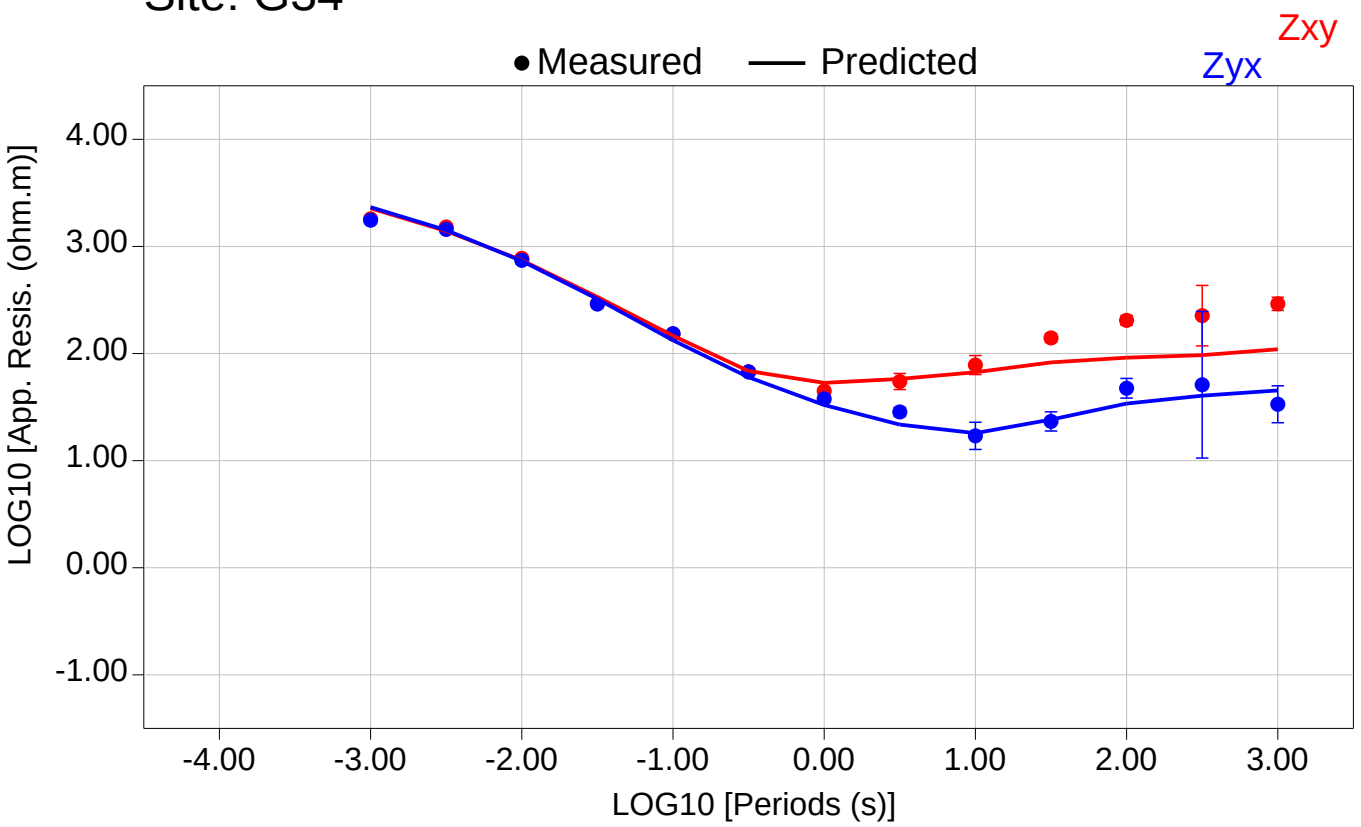

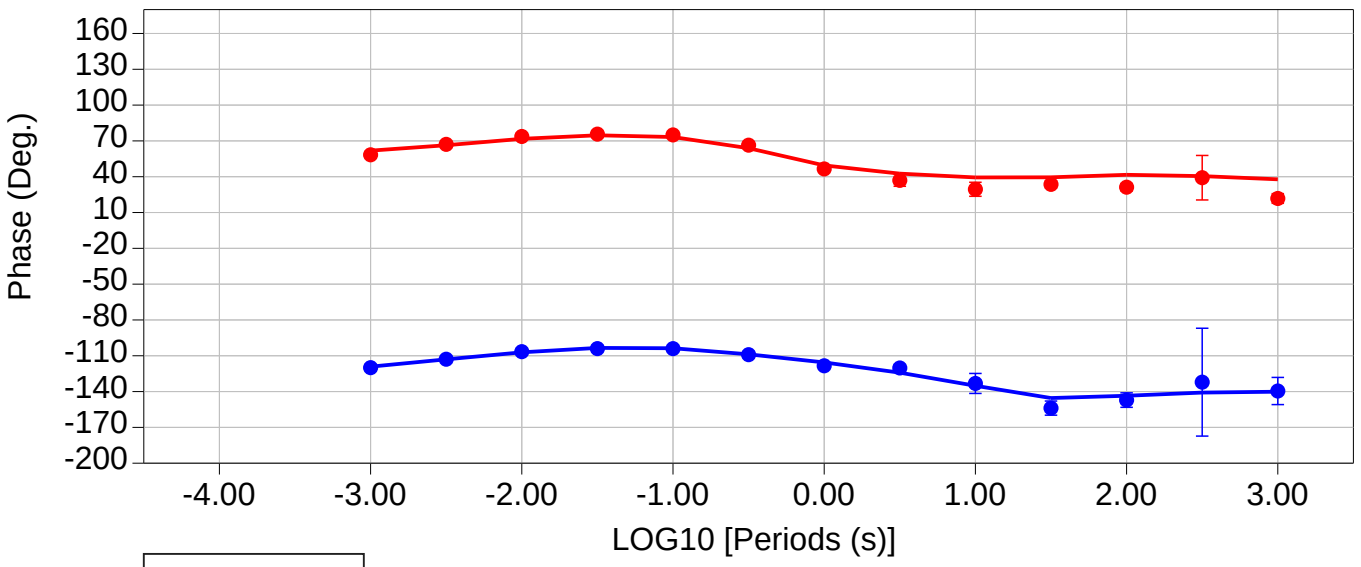

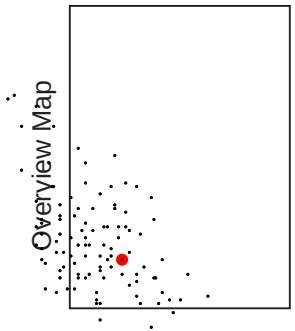

Total RMS = 15834.54

Zxy RMS = 15926.74

Zyx RMS = 15741.81

Site: G35

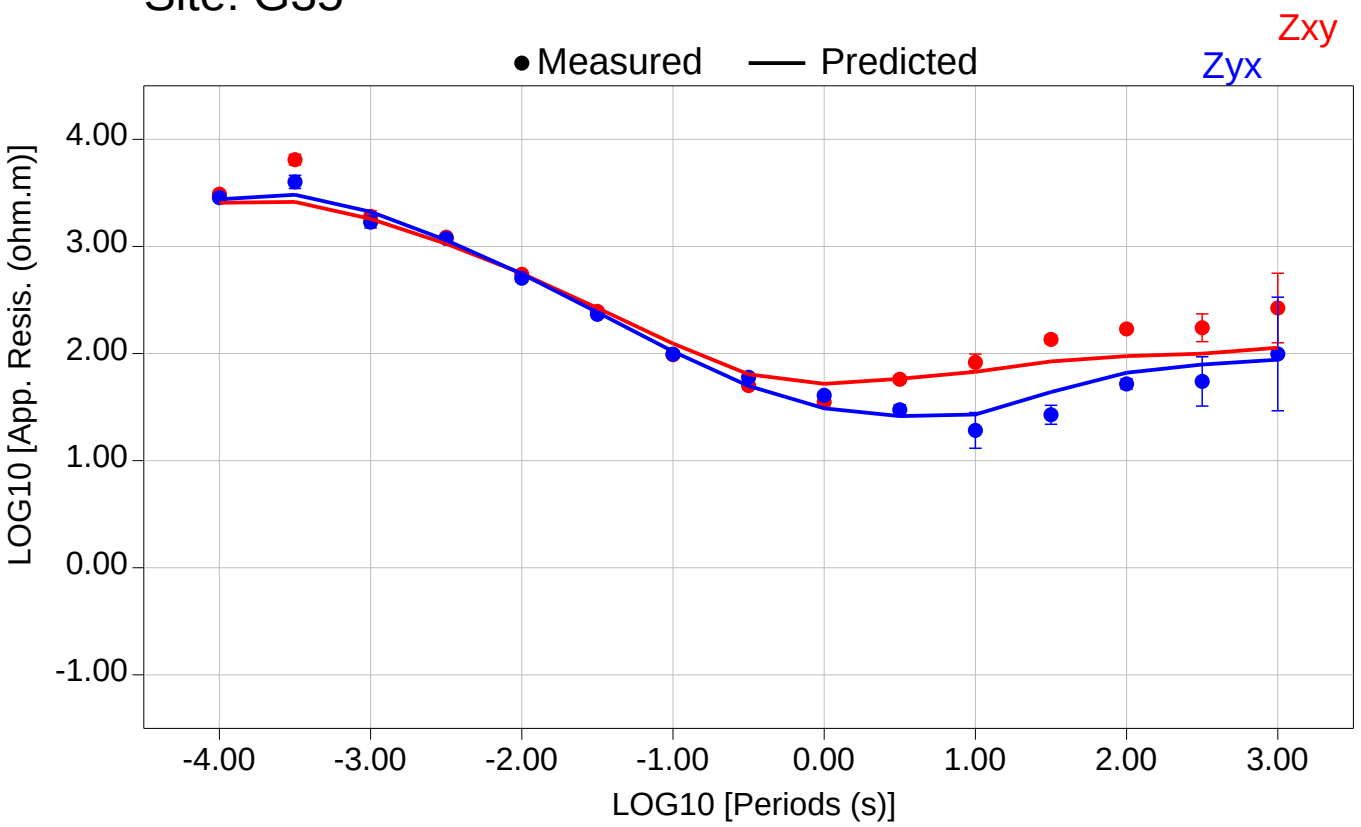

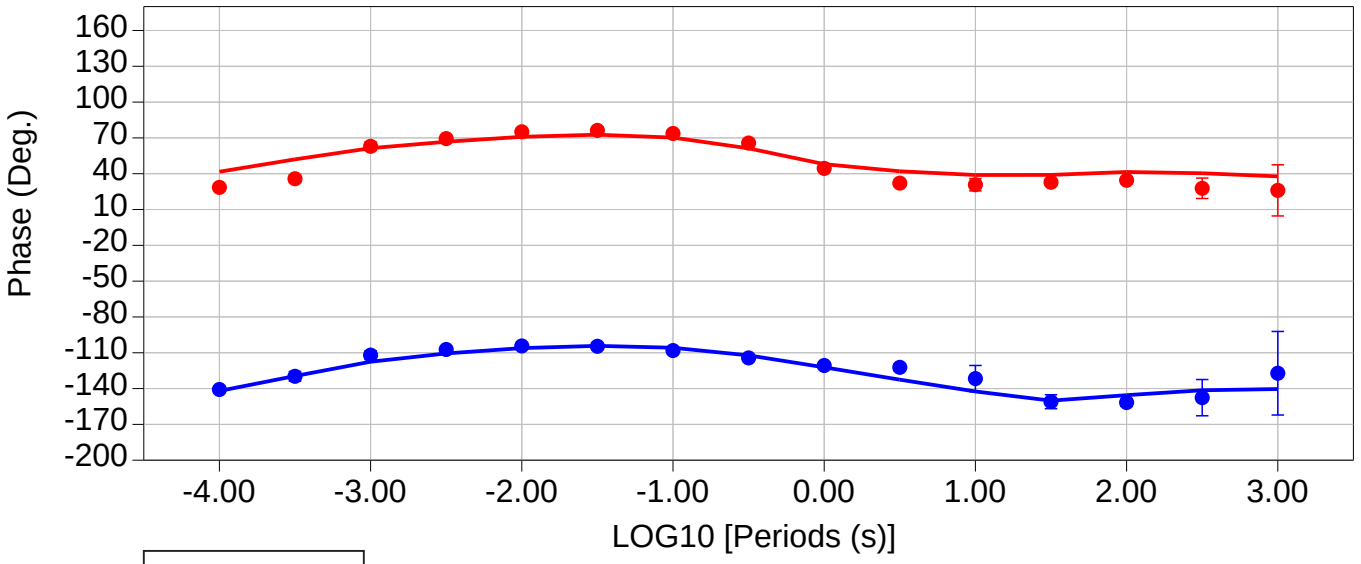

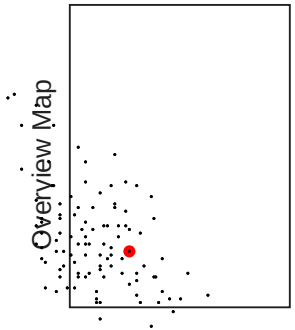

Total RMS = 15338.90

Zxy RMS = 15802.70

Zyx RMS = 14860.64

Site: G36

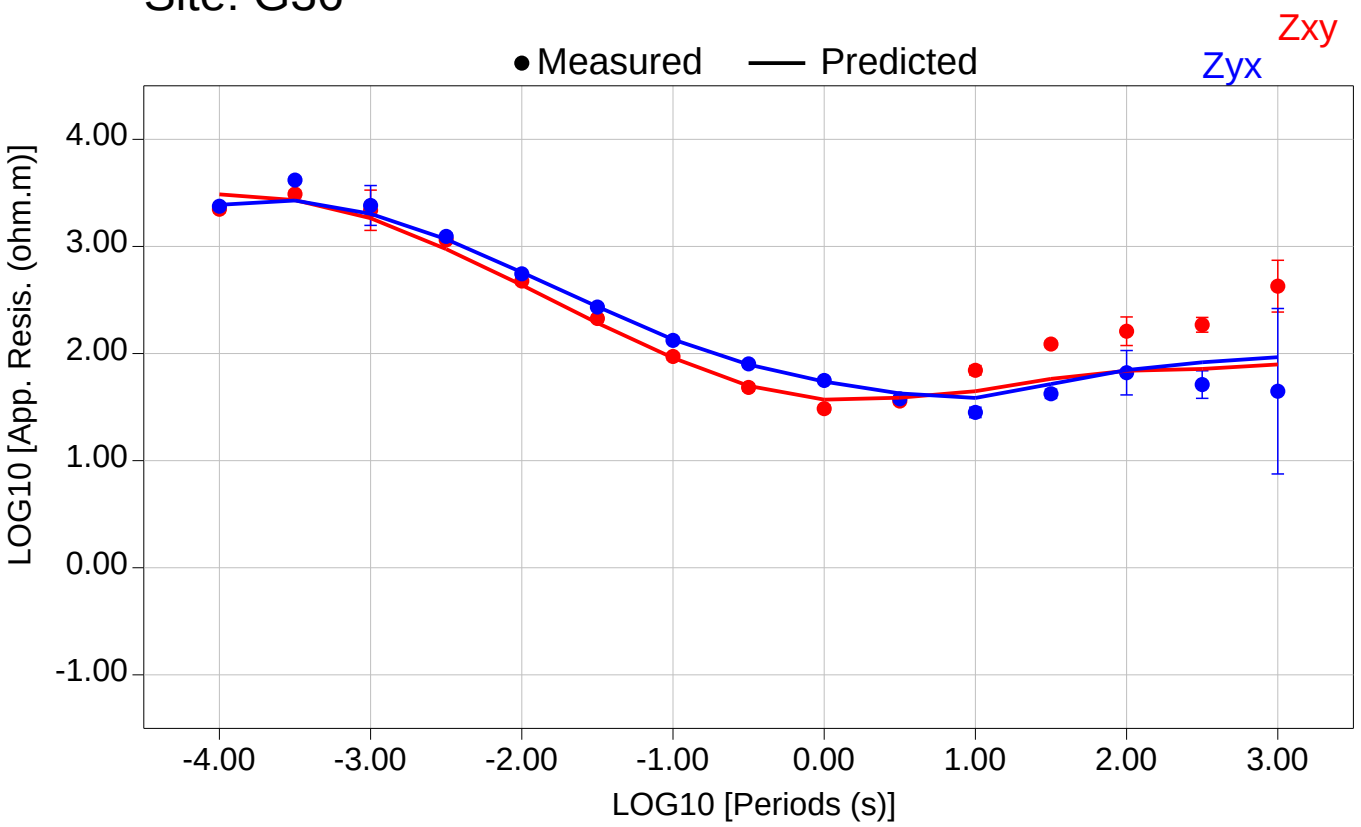

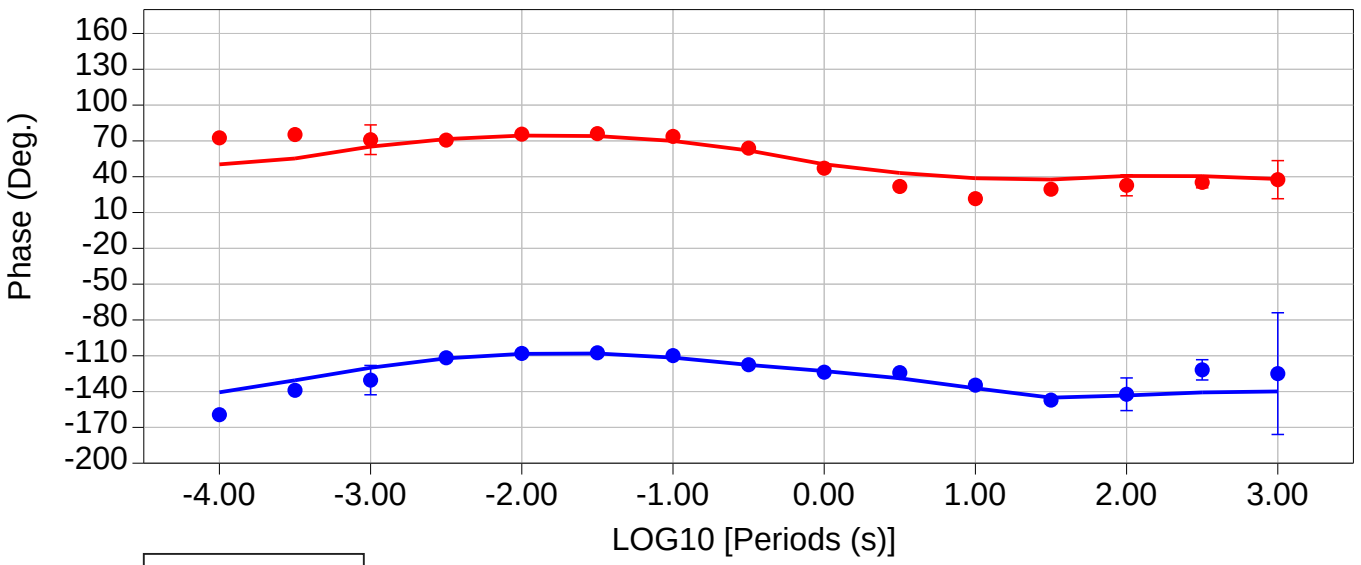

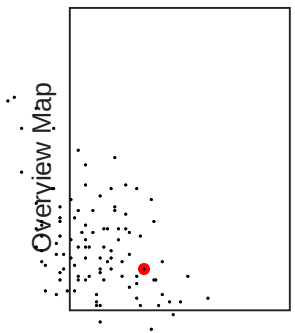

Total RMS = 15956.09

Zxy RMS = 15017.94
Zyx RMS = 16842.07

Site: G37

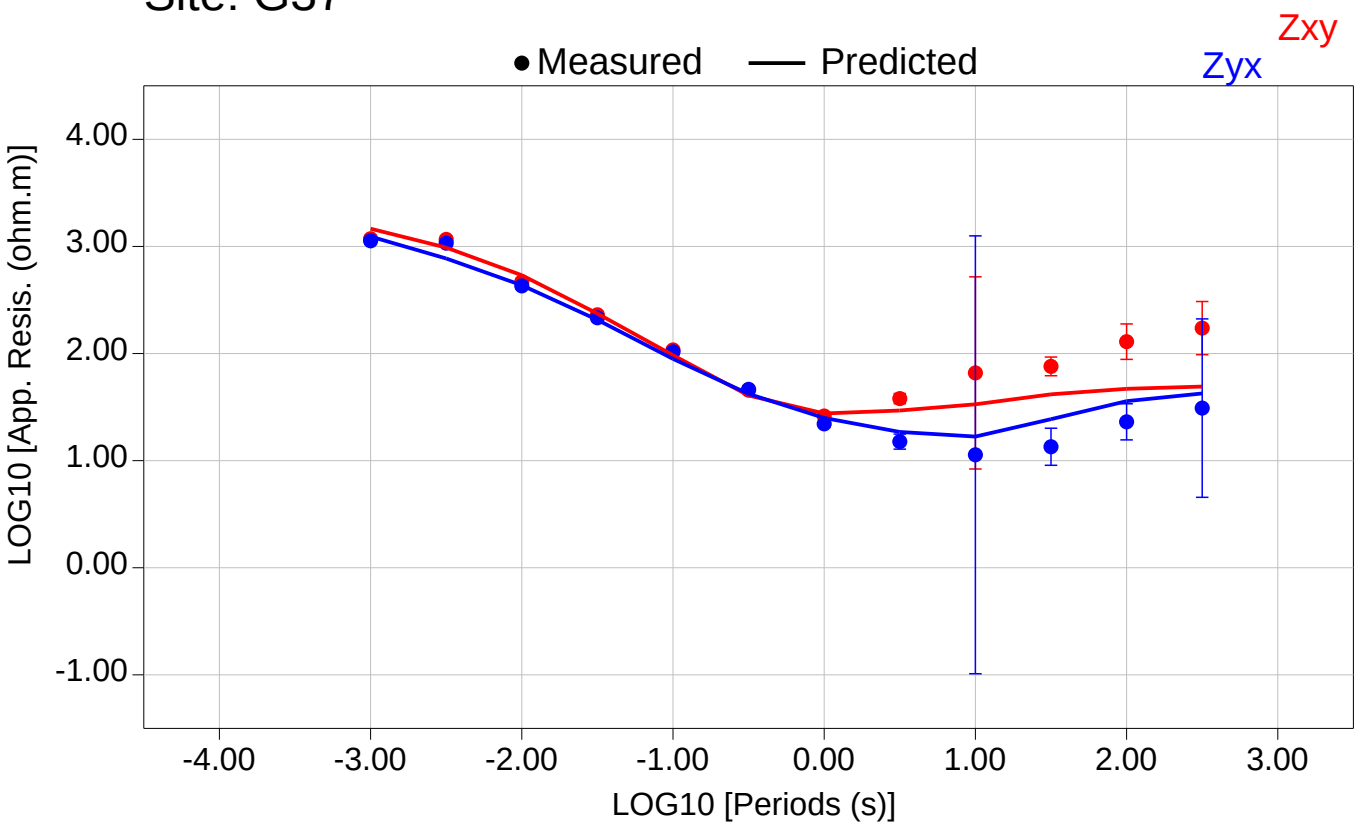

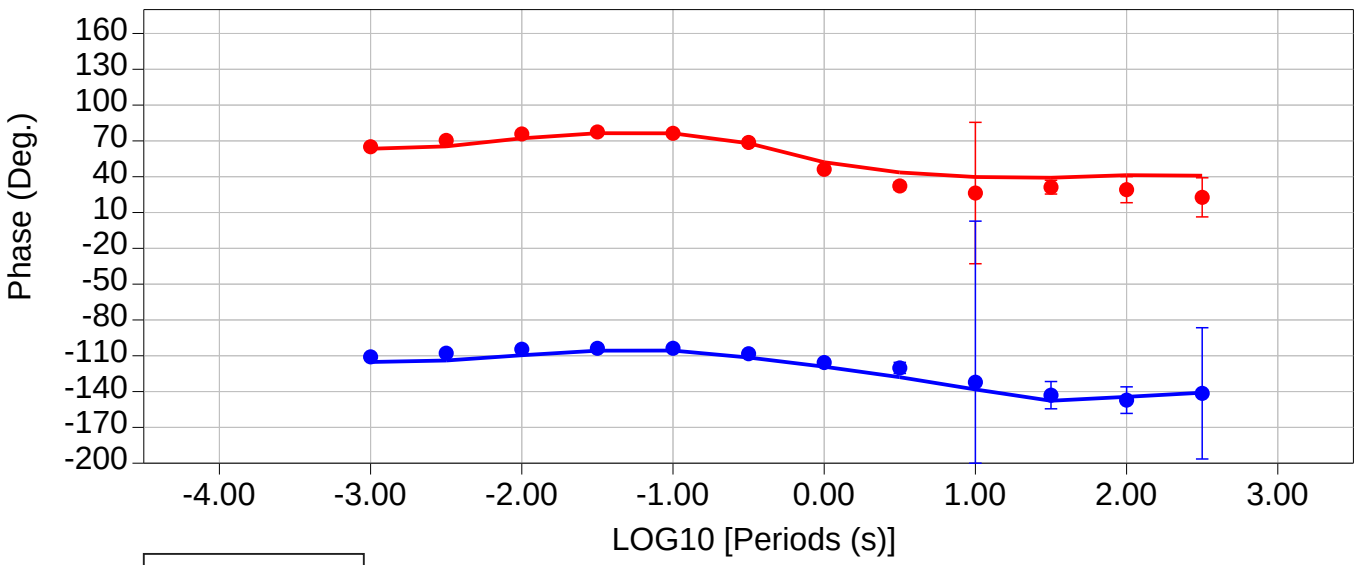

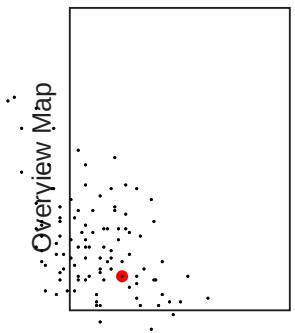

Total RMS = 15411.35

Zxy RMS = 15950.64

Zyx RMS = 14852.48

Site: G38

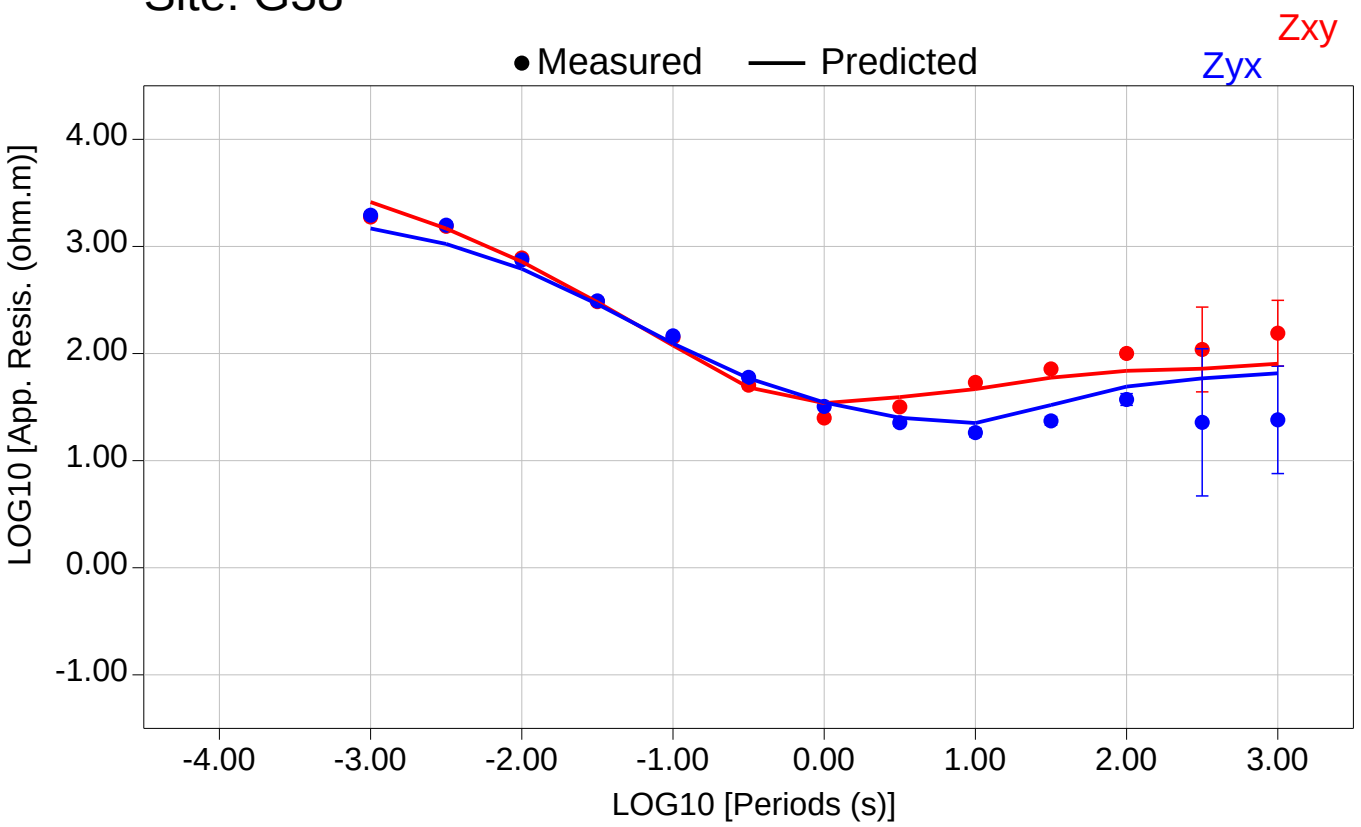

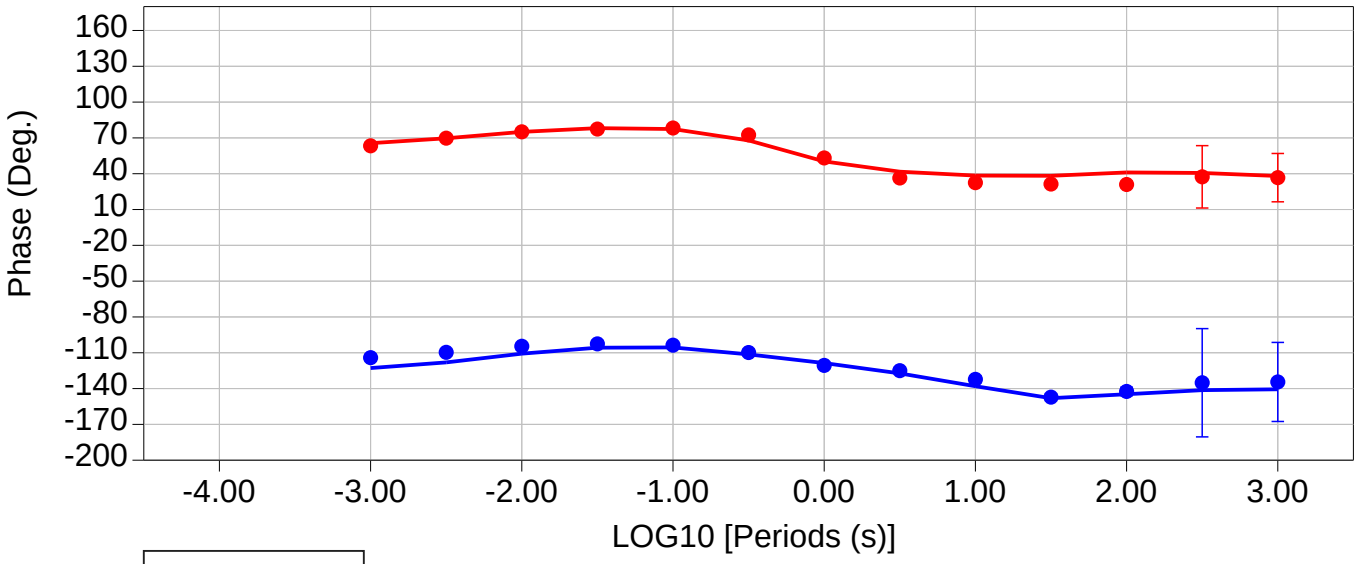

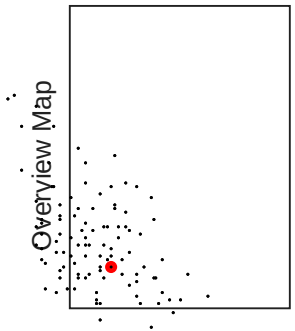

Total RMS = 17188.67

Zxy RMS = 18076.96

Zyx RMS = 16251.89

Site: G39

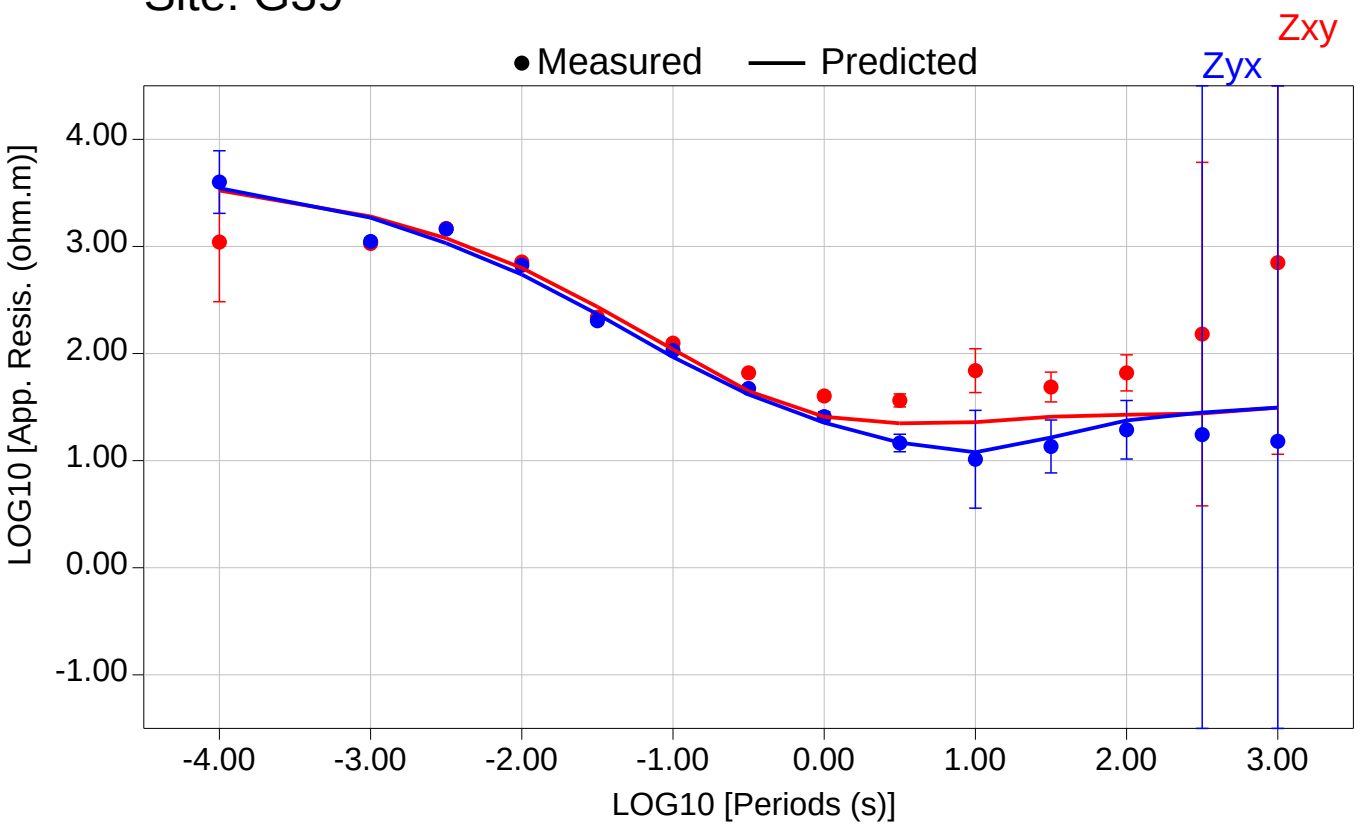

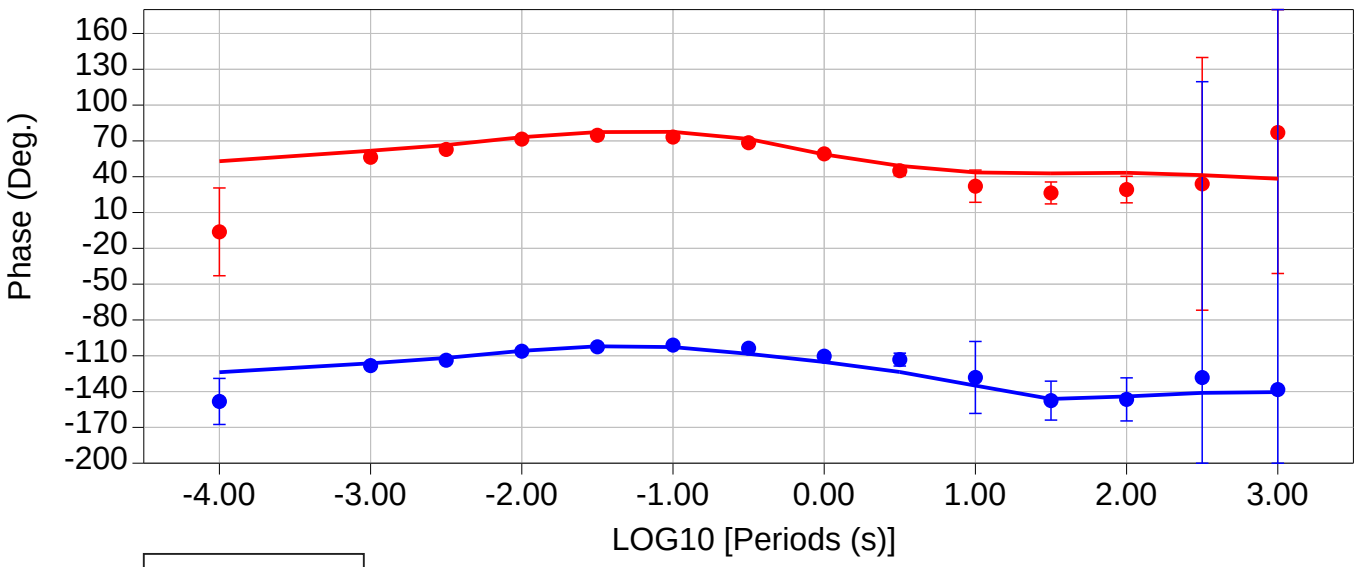

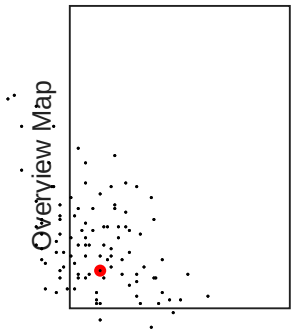

Total RMS = 14490.77

Zxy RMS = 14886.06

Zyx RMS = 14084.39

Site: G40

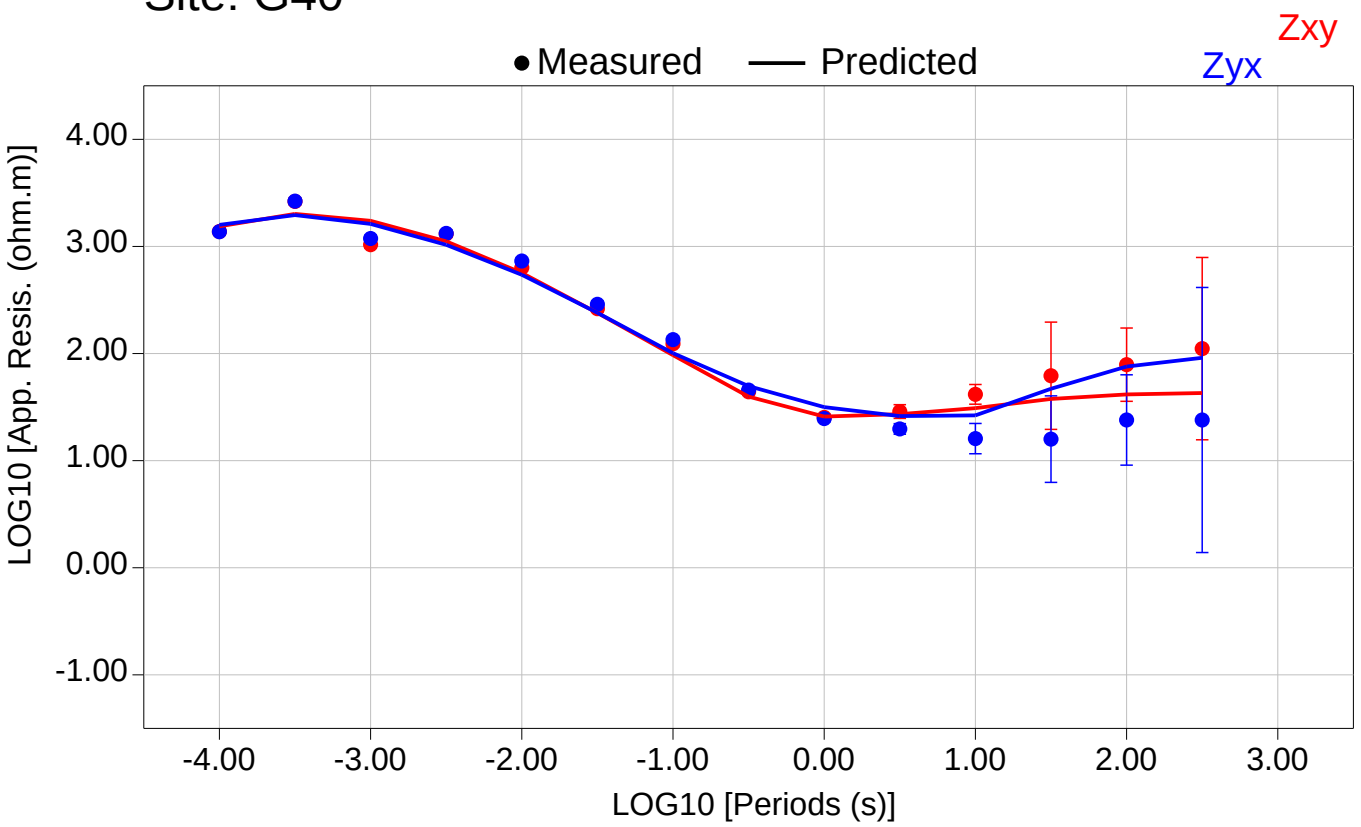

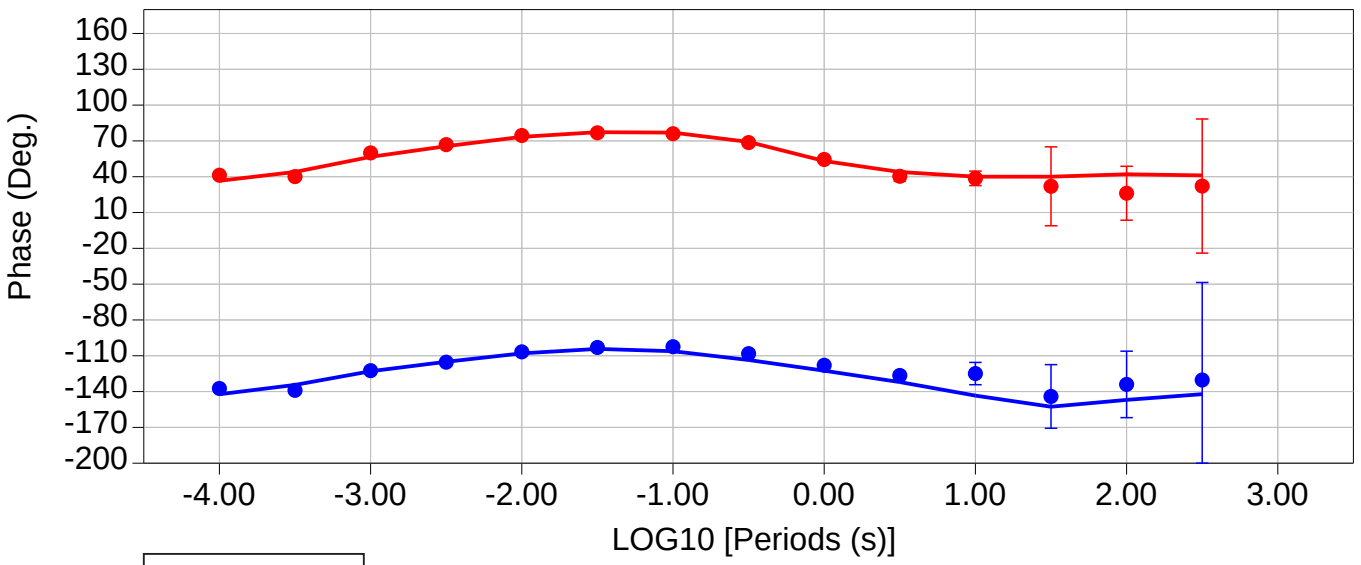

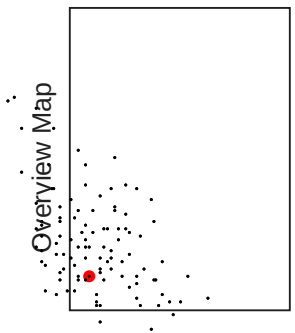

Total RMS = 15332.18

Zxy RMS = 15116.79
Zyx RMS = 15544.59

Site: G41

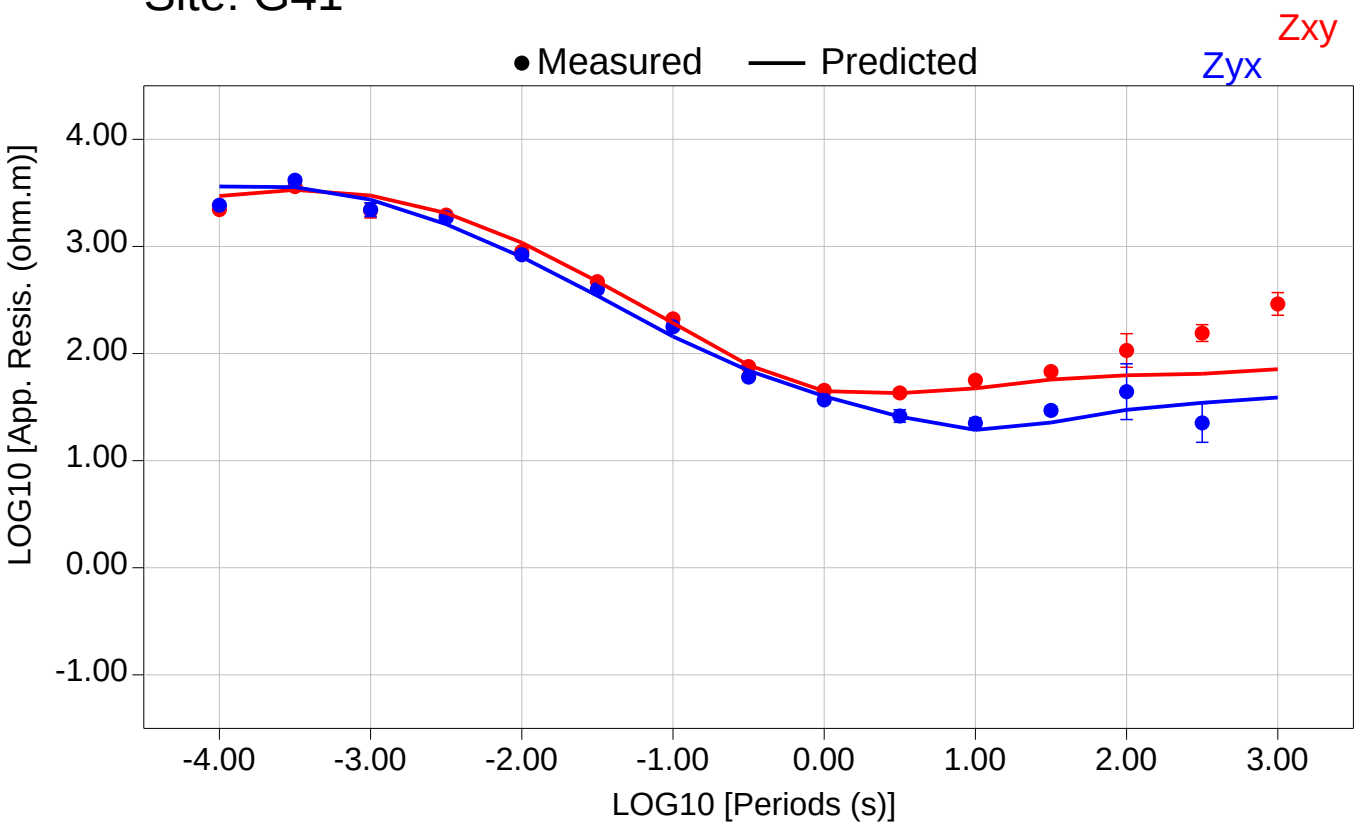

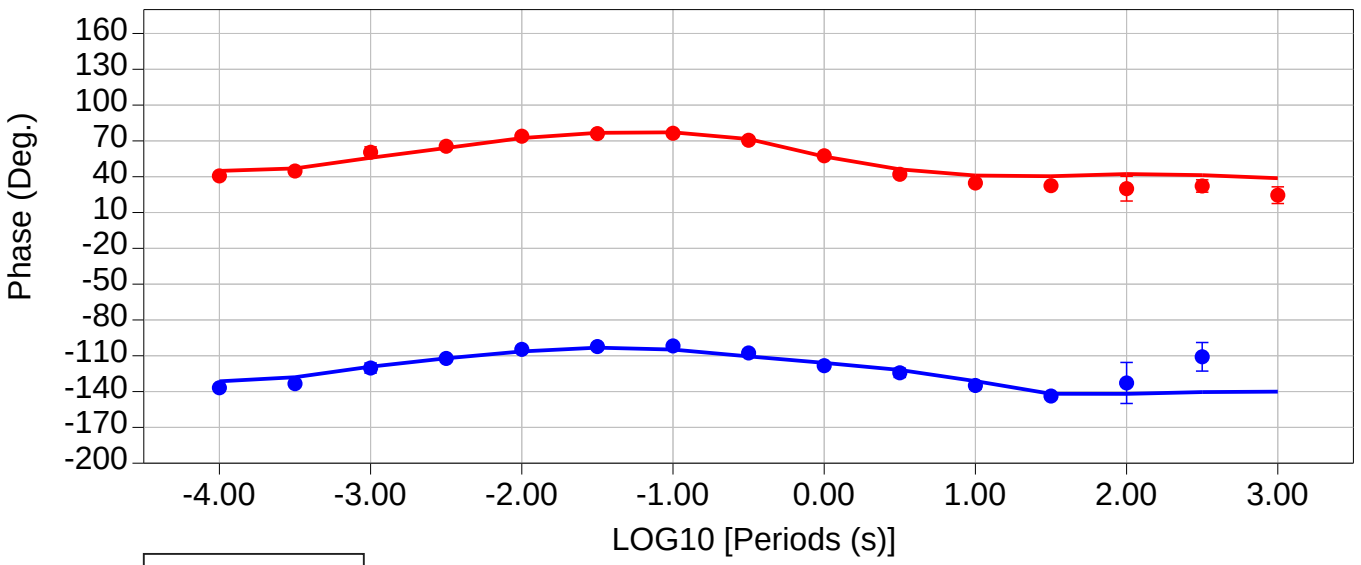

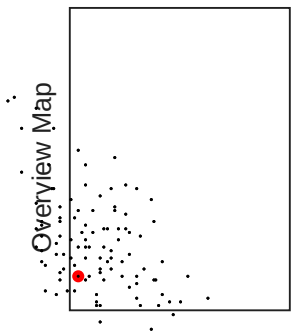

Total RMS = 16716.44

Zxy RMS = 17499.59
Zyx RMS = 15834.42

Site: G42

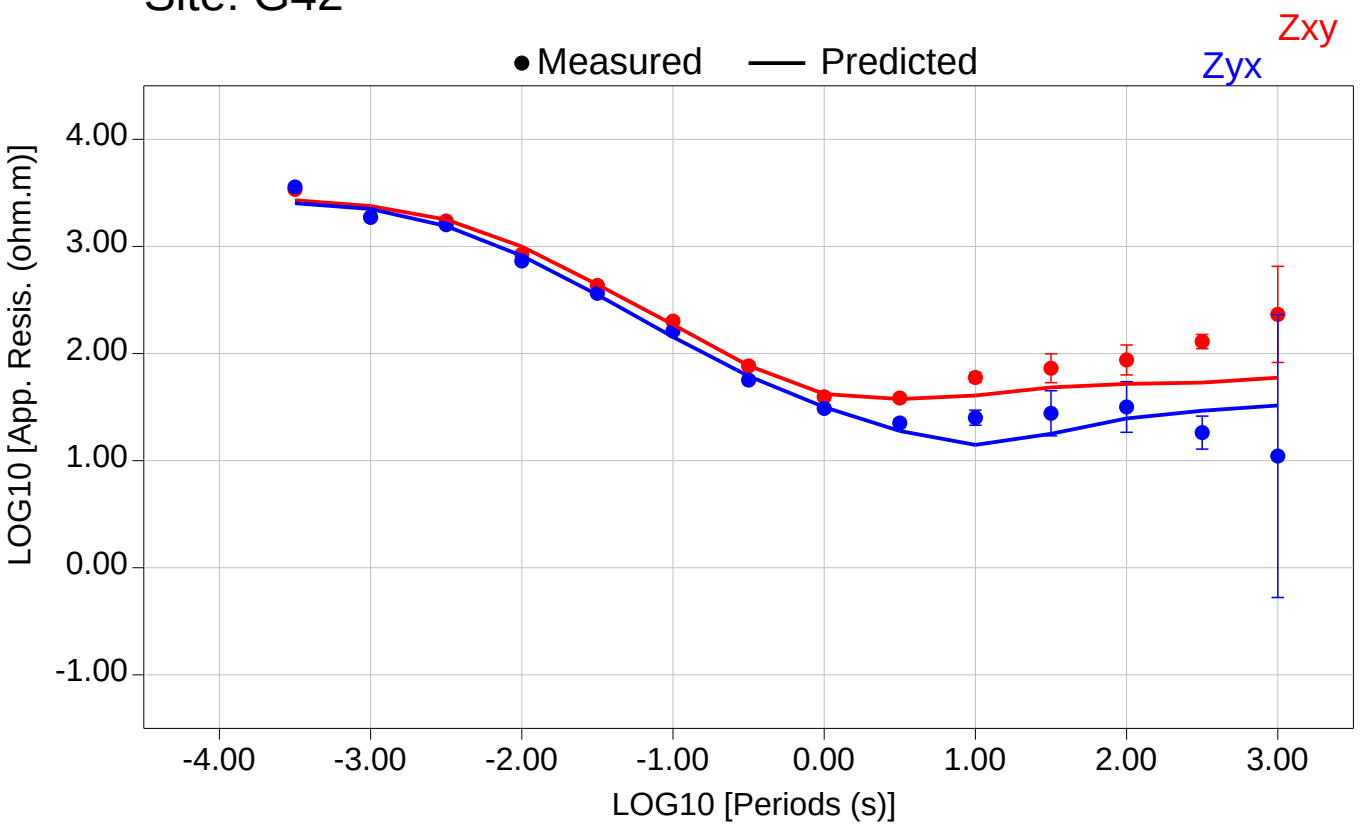

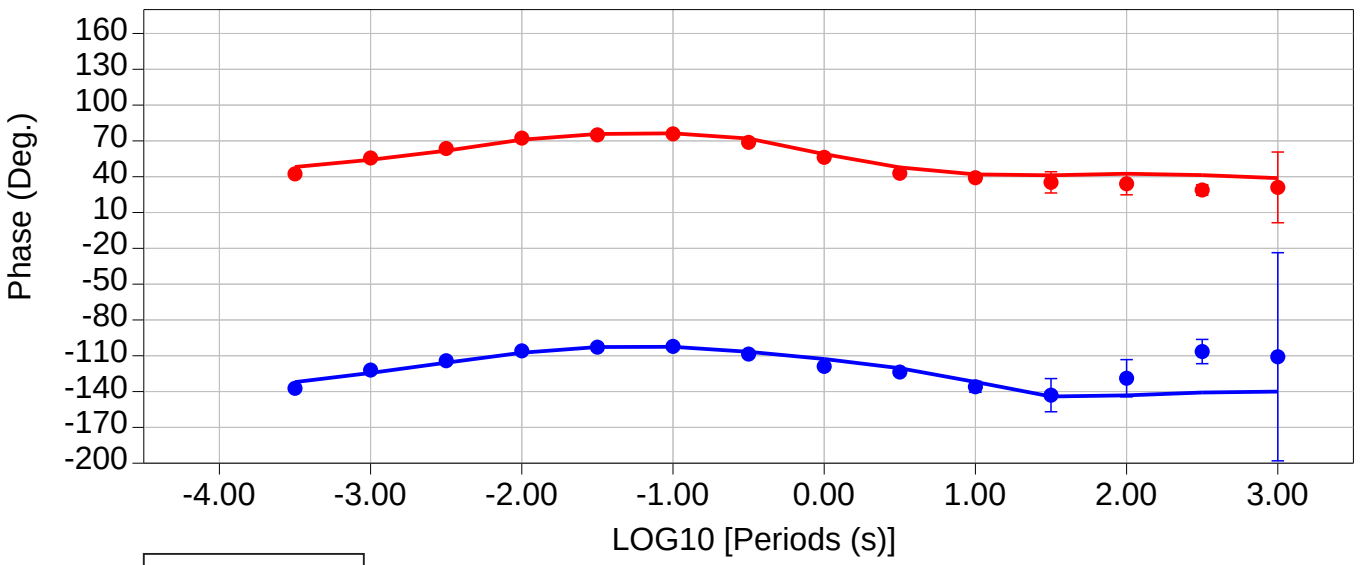

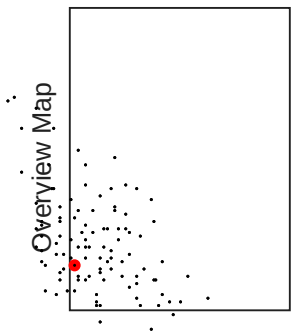

Total RMS = 15693.14

Zxy RMS = 16494.77

Zyx RMS = 14848.29

Site: G43

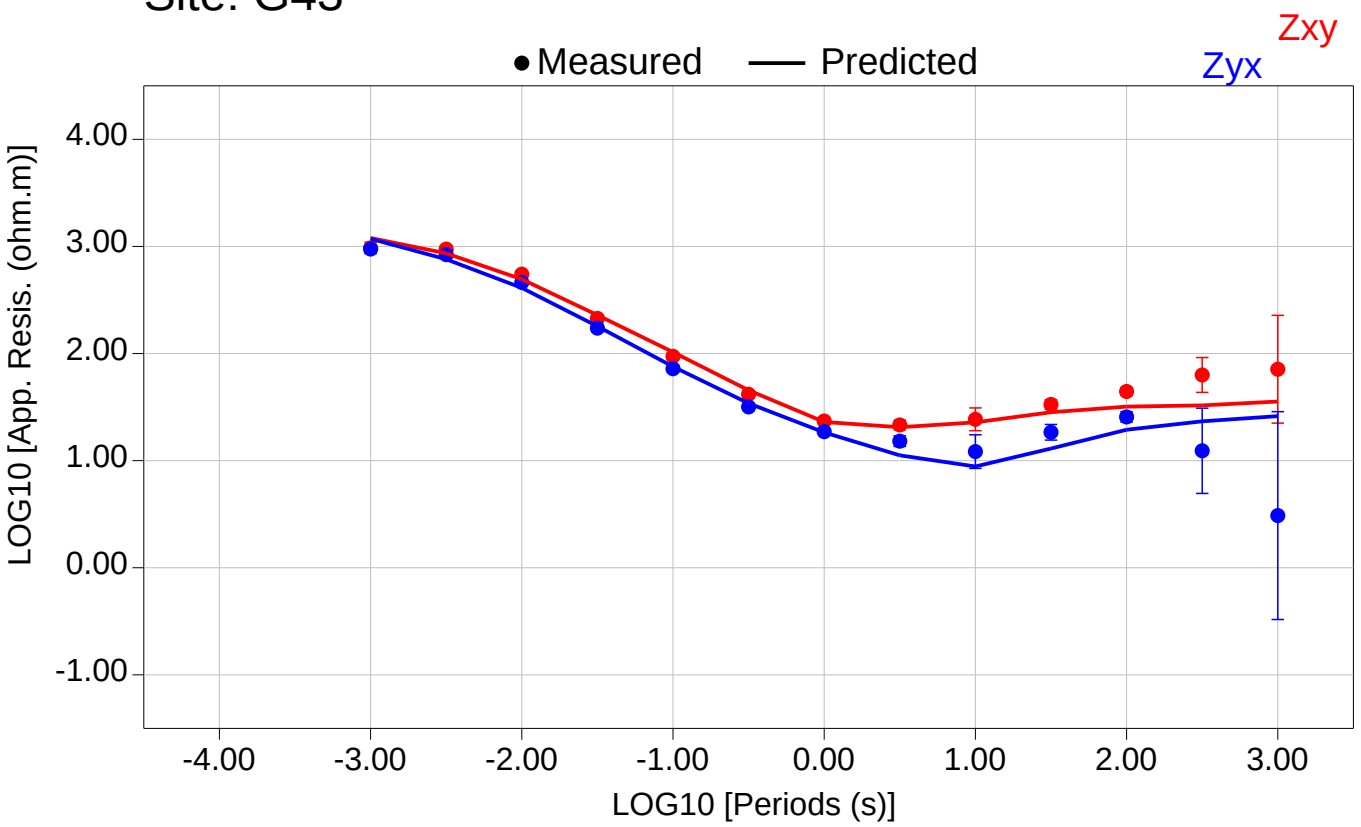

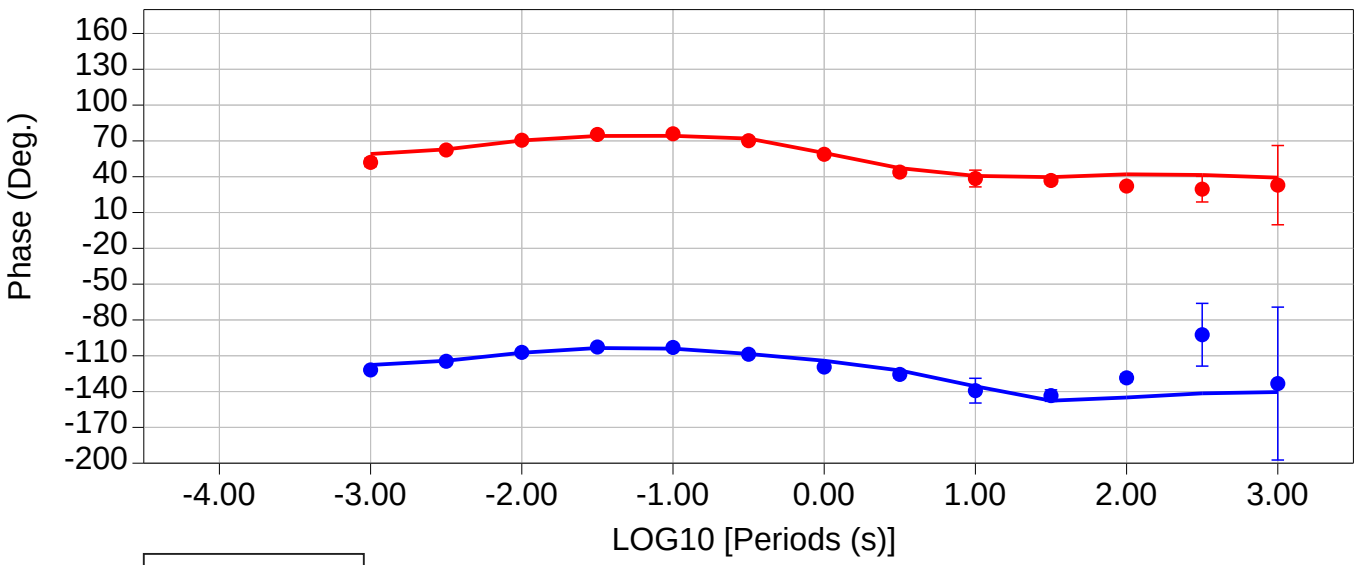

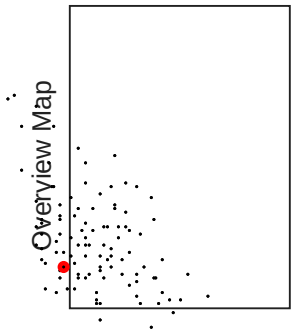

Total RMS = 15880.53

Zxy RMS = 16607.10
Zyx RMS = 15119.09

Site: G44

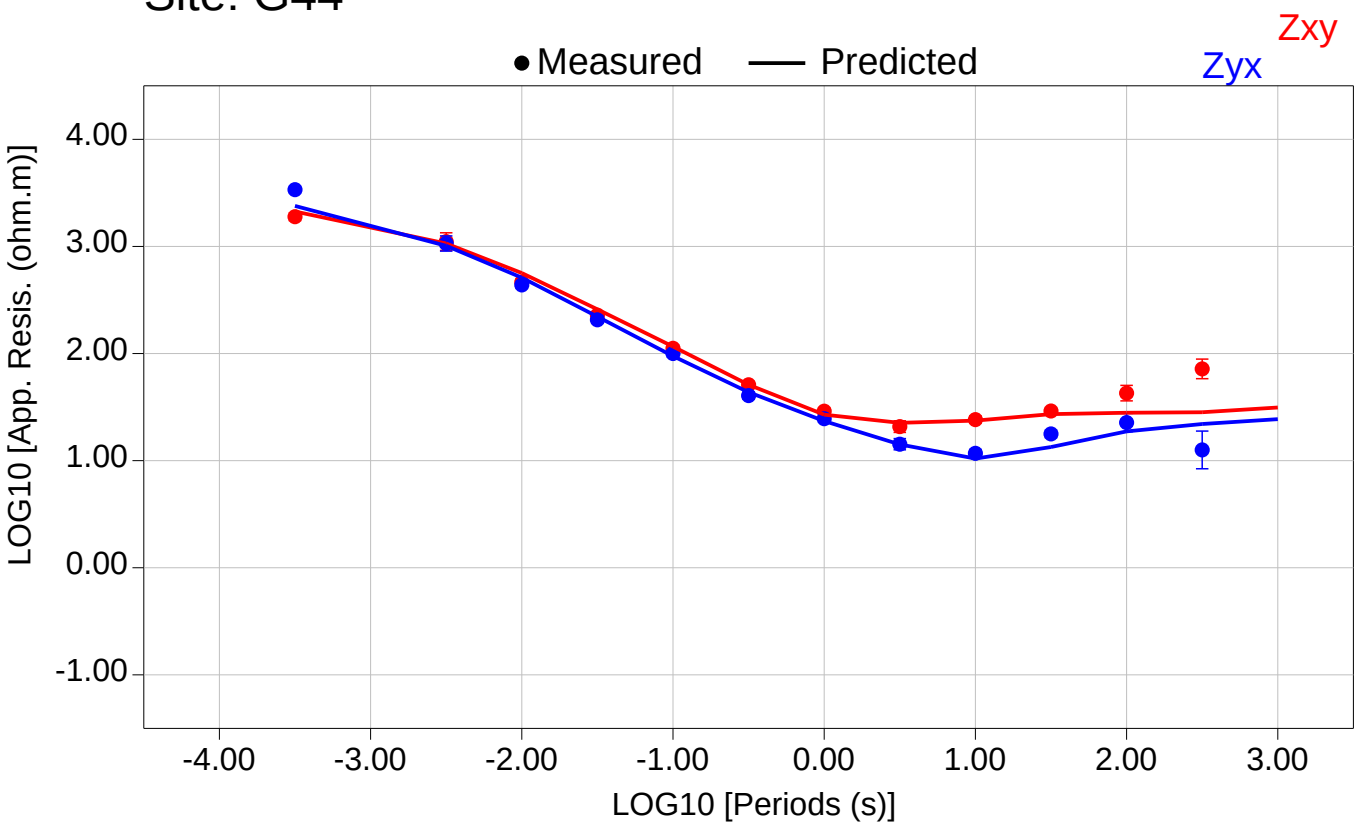

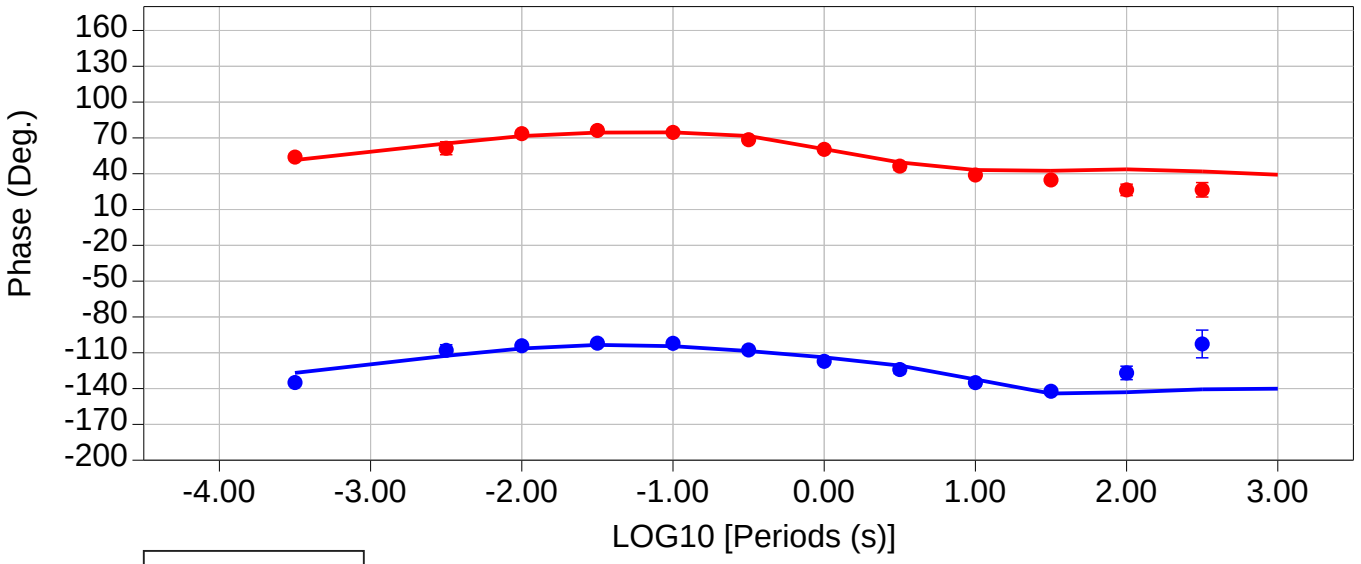

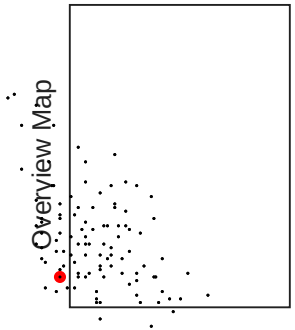

Total RMS = 15637.37

Zxy RMS = 16340.34
Zyx RMS = 14901.27

Site: G45

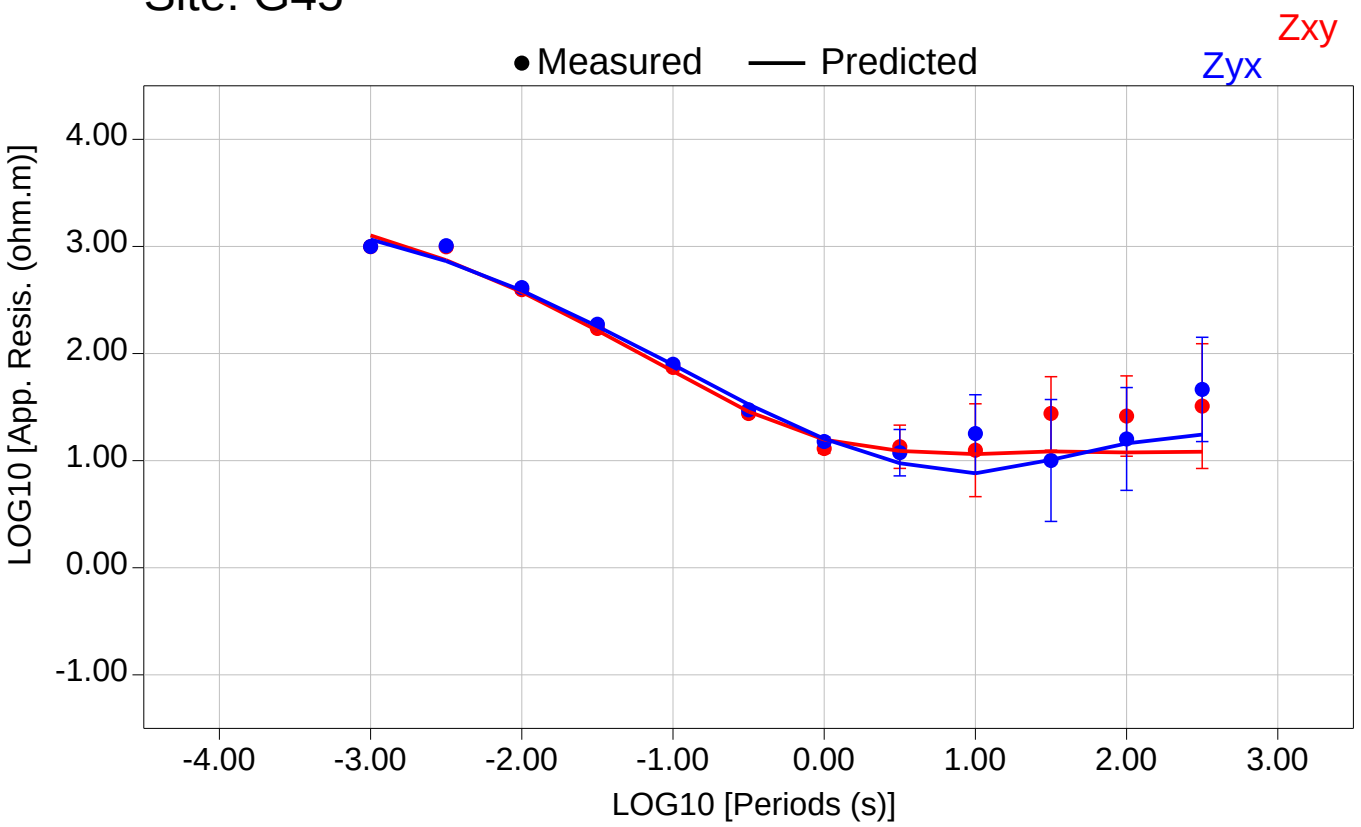

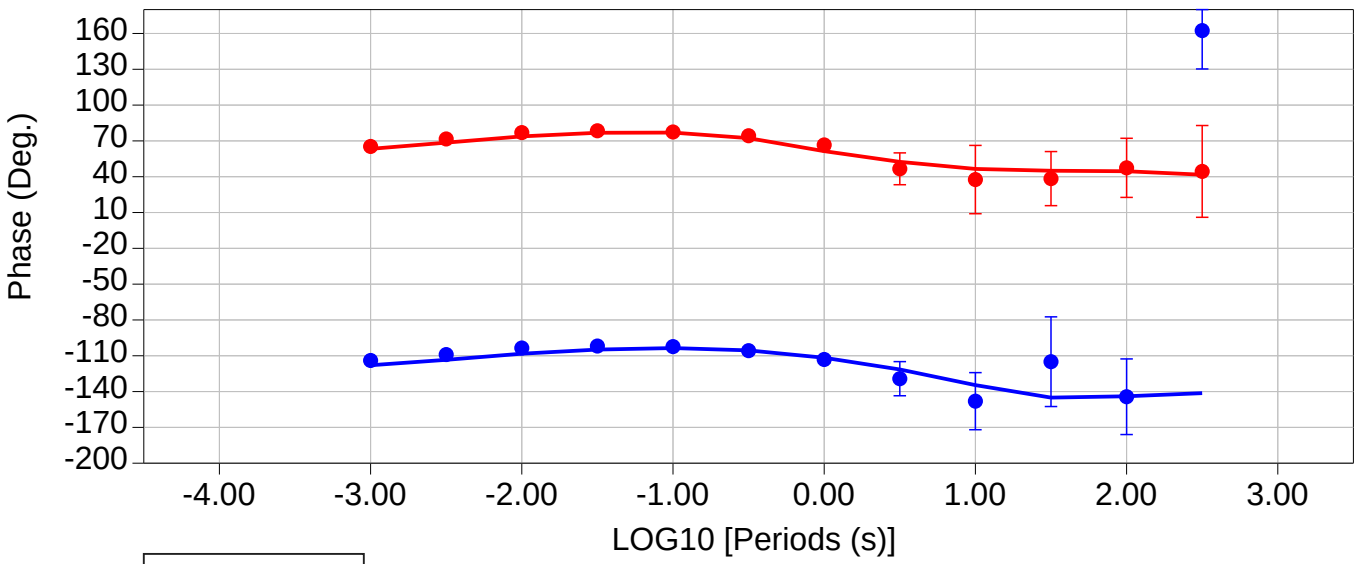

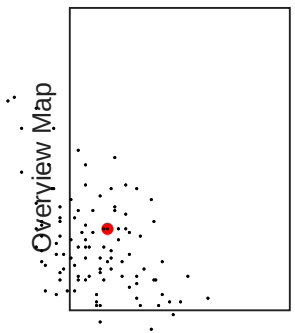

Total RMS = 15393.25

Zxy RMS = 15206.71

Zyx RMS = 15577.55

Site: G46

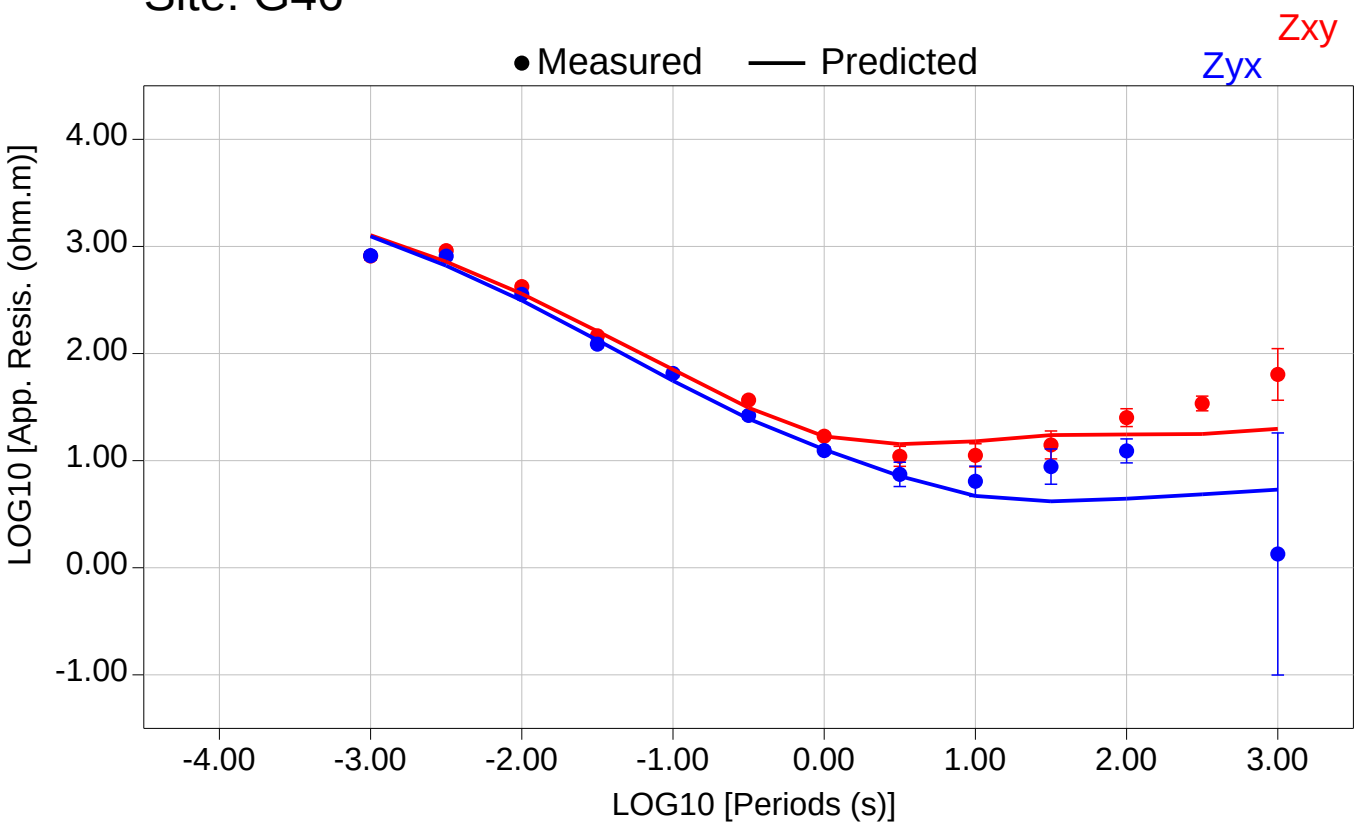

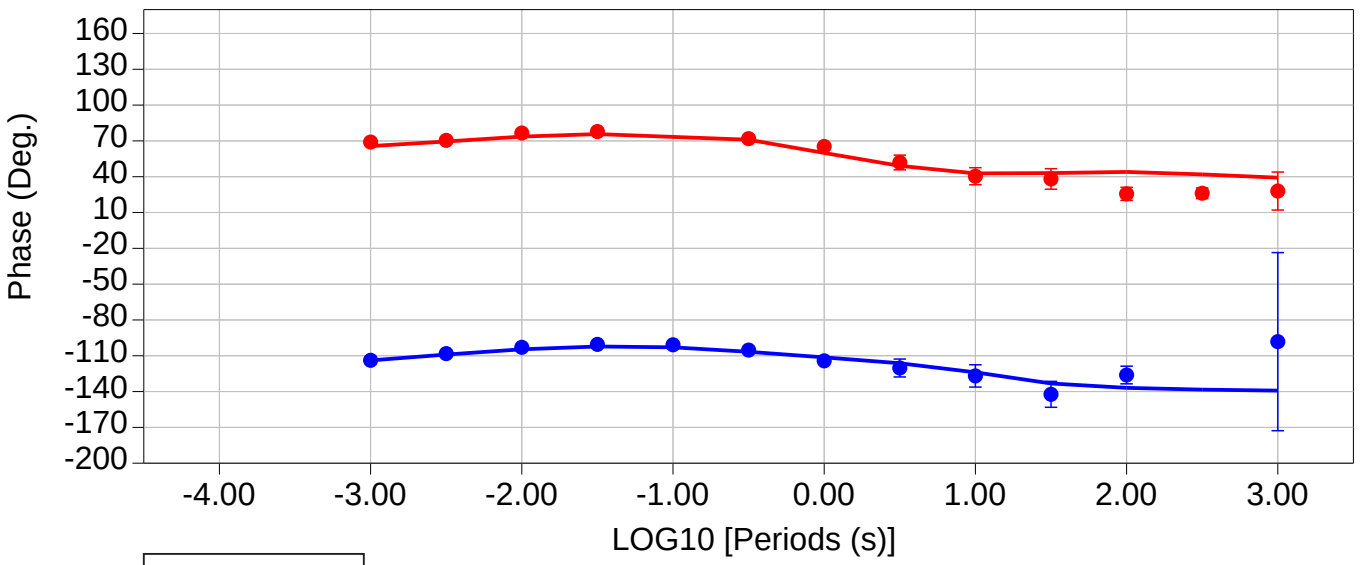

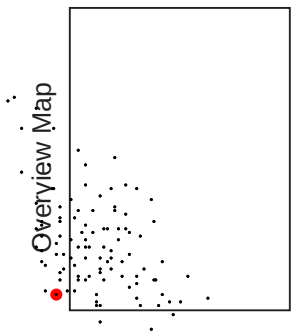

Total RMS = 14380.60

Zxy RMS = 13629.48

Zyx RMS = 15094.40

Site: G47

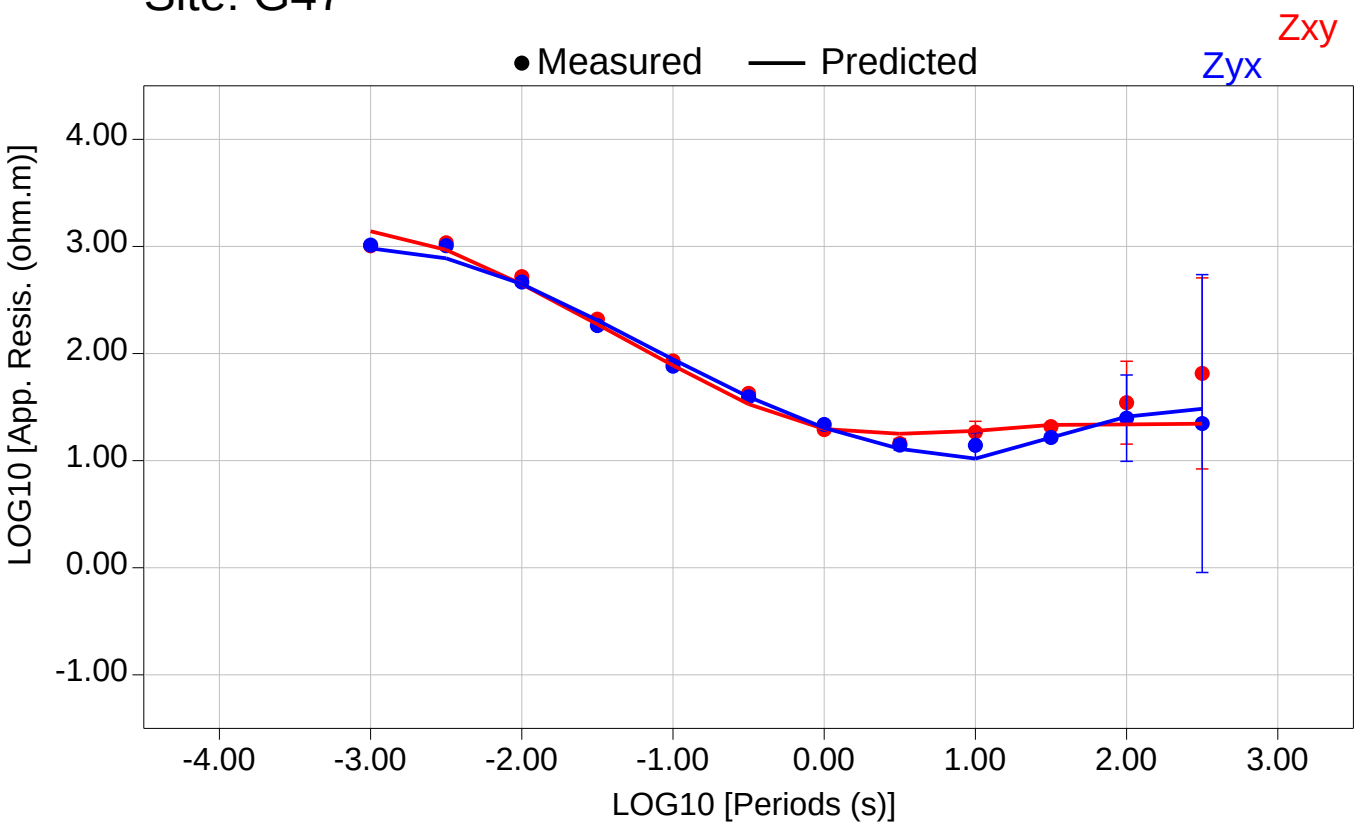

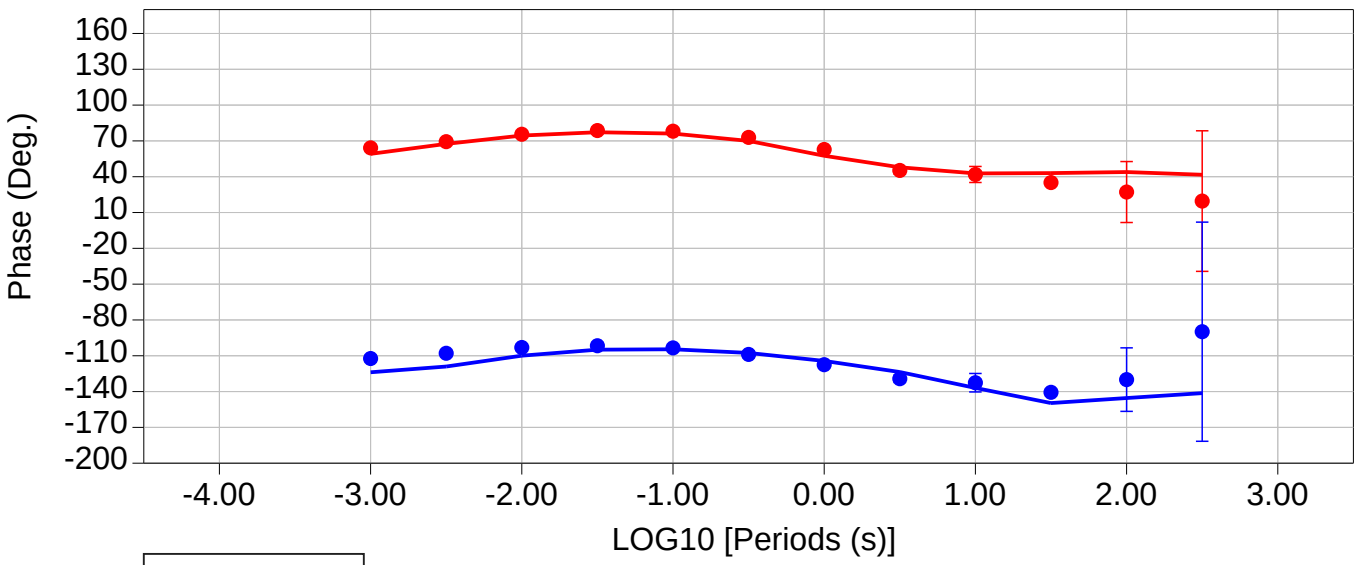

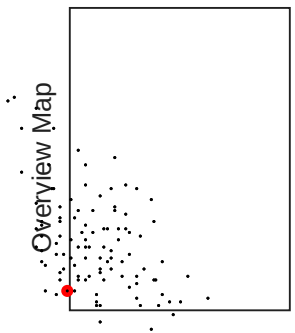

Total RMS = 16398.34

Zxy RMS = 16715.07

Zyx RMS = 16075.38

Site: G48

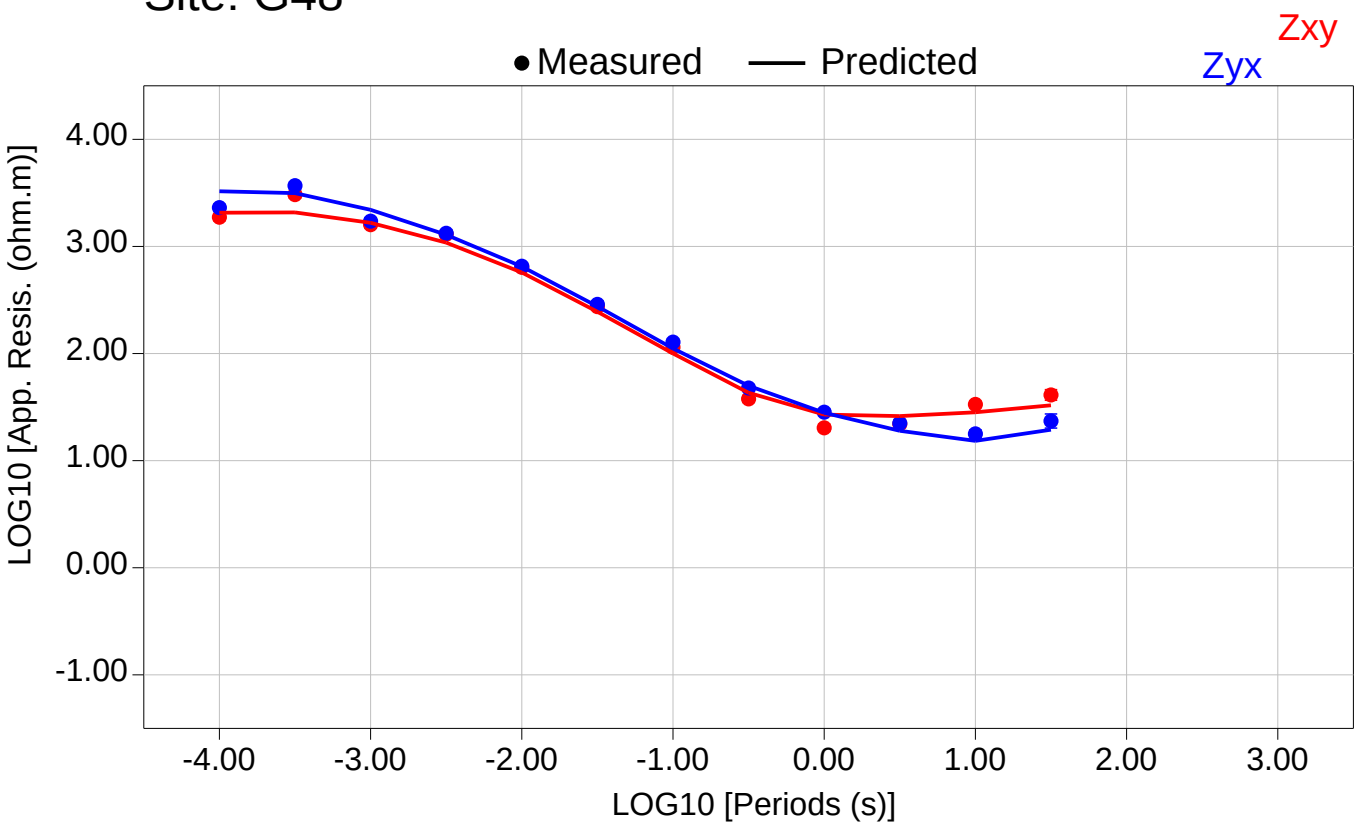

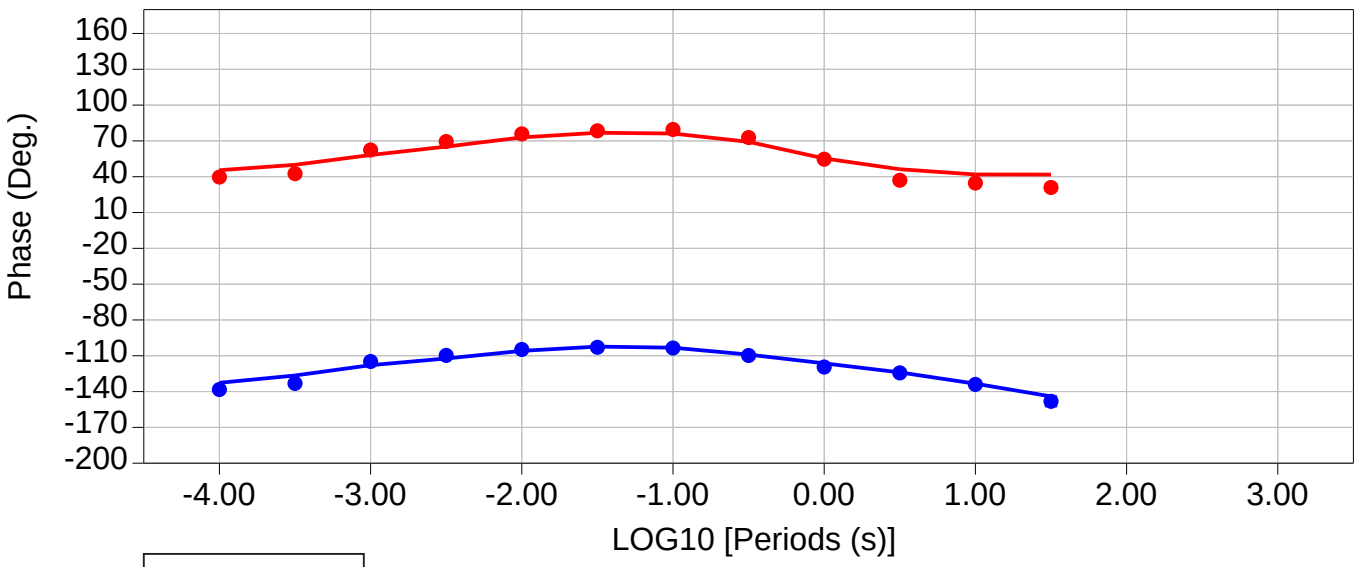

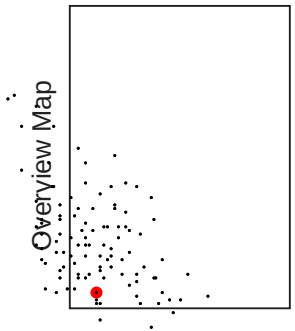

Total RMS = 18339.42

Zxy RMS = 17670.07

Zyx RMS = 18985.18

Site: G49

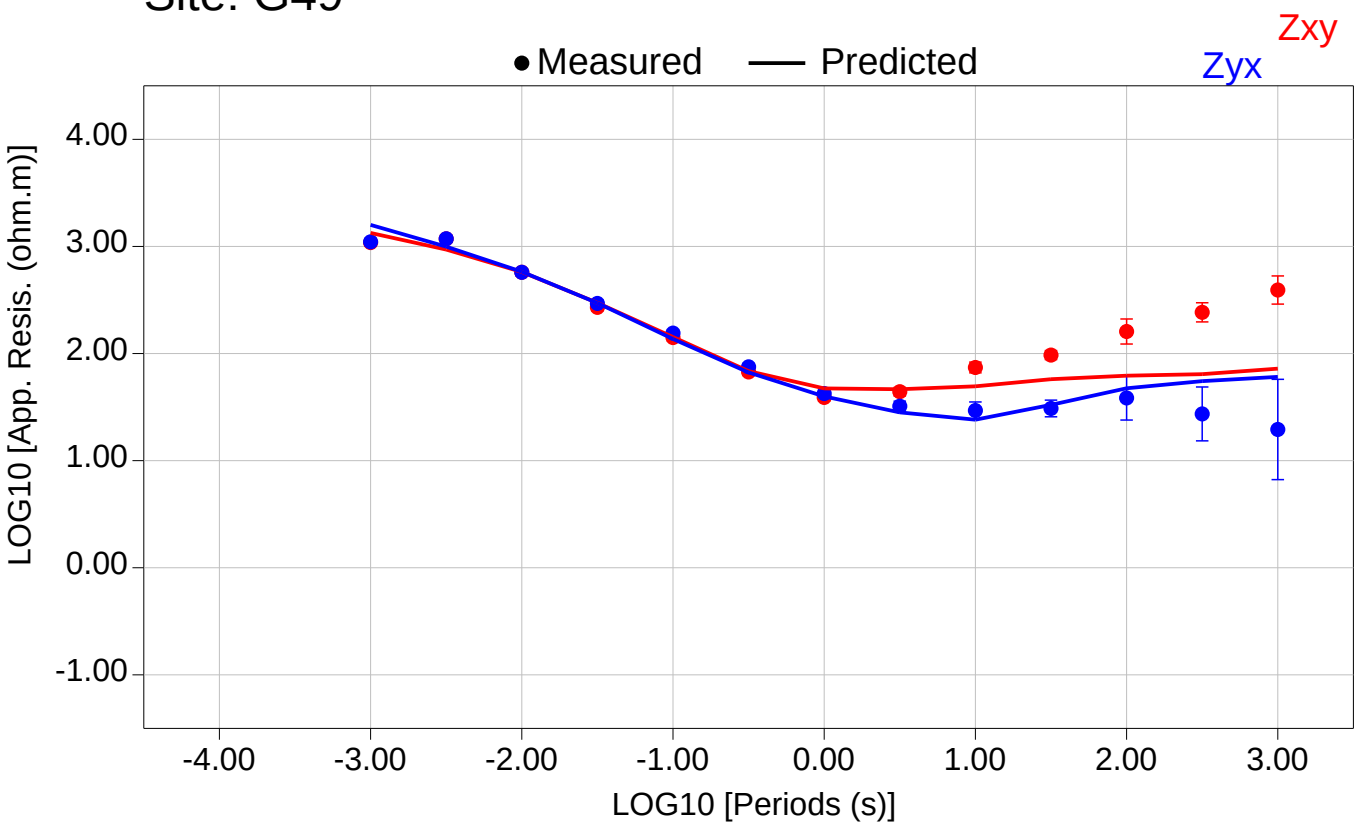

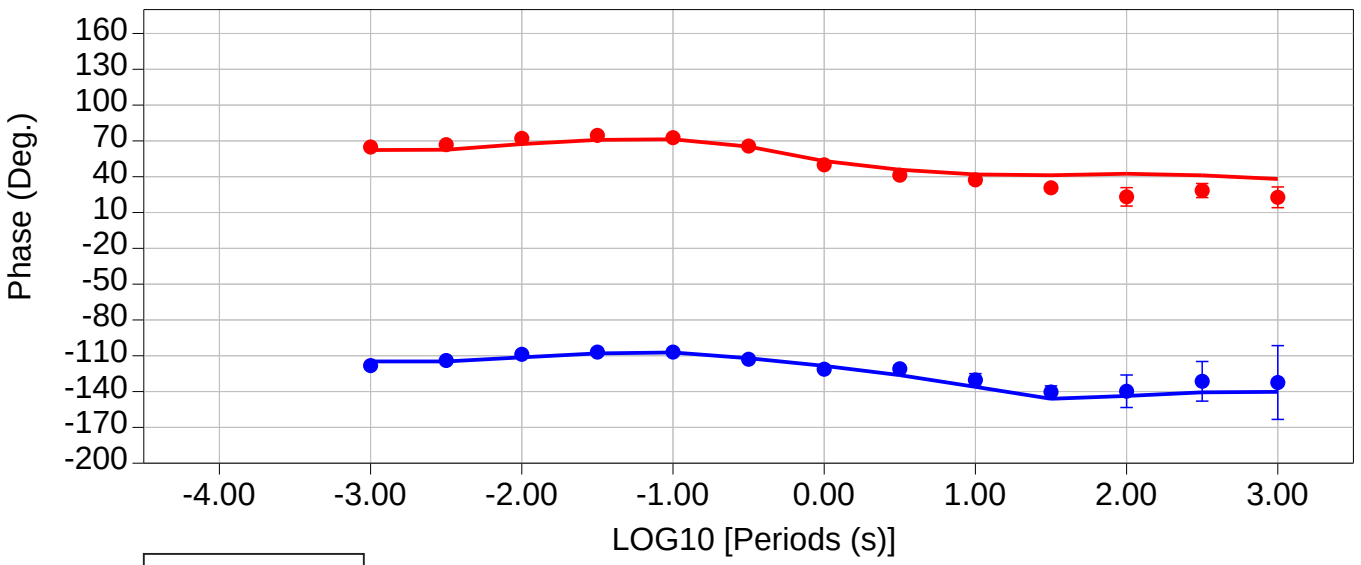

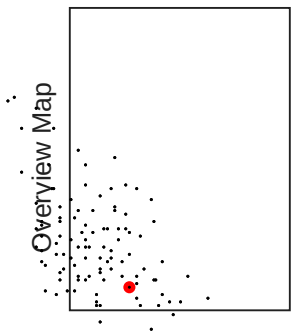

Total RMS = 15208.89

Zxy RMS = 15280.30

Zyx RMS = 15137.14

Site: G50

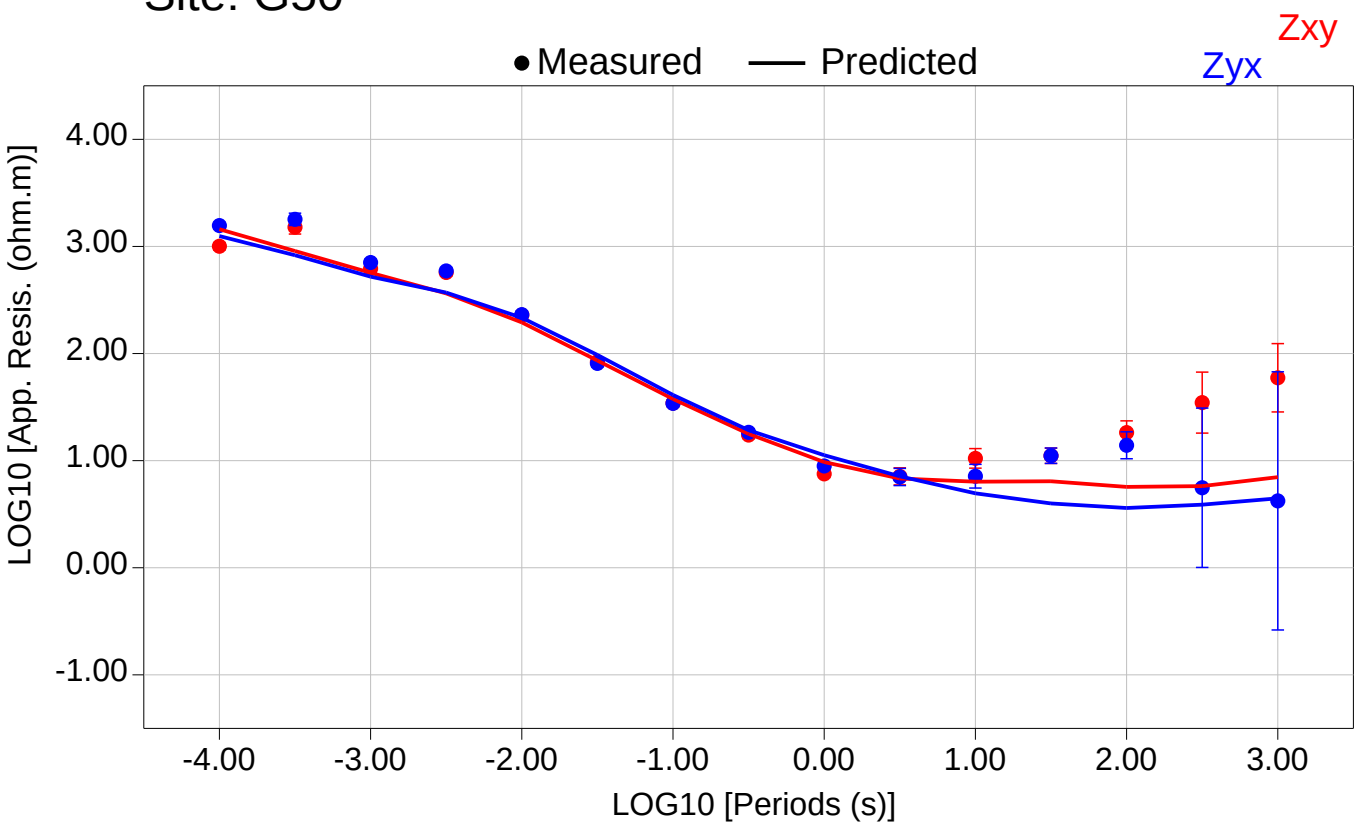

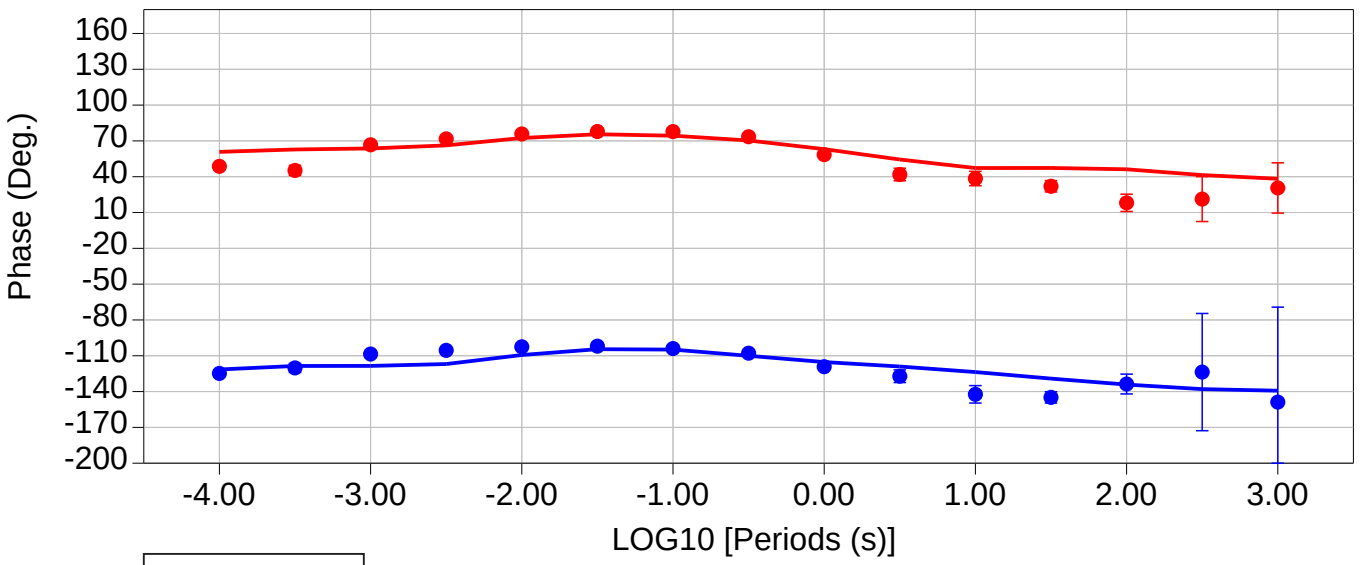

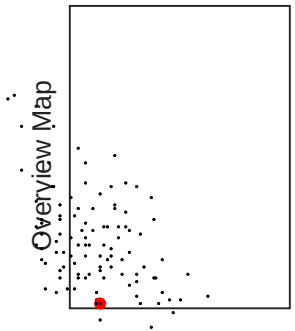

Total RMS = 14461.07

Zxy RMS = 14280.00
Zyx RMS = 14639.91

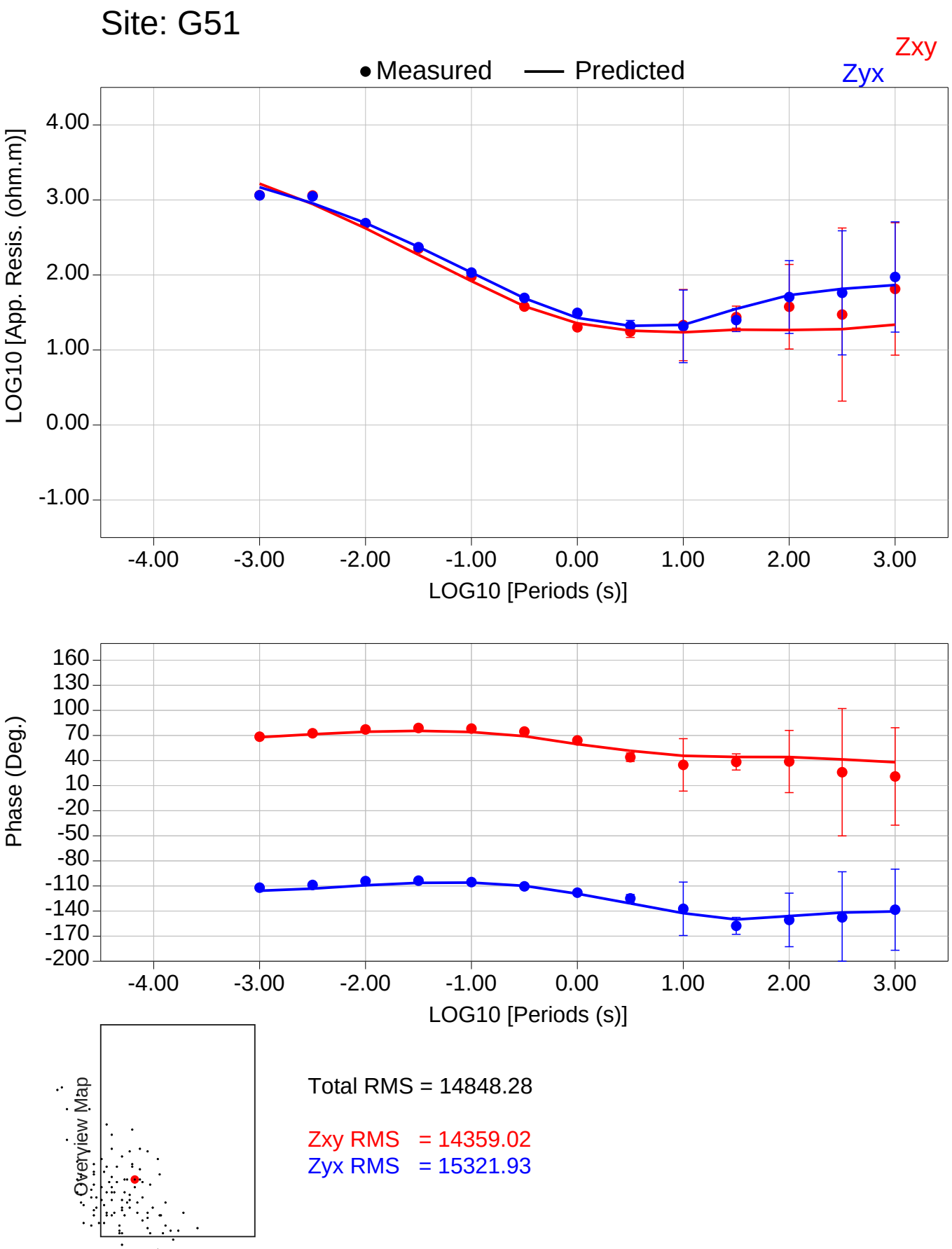
Site: G51
Zxy
Measured
Predicted
Zyx
LOG10 [App. Resis. (ohm.m)]
4.00
3.00
2.00
1.00
0.00
-1.00
-4.00
-3.00
-2.00
-1.00
0.00
1.00
2.00
3.00
LOG10 [Periods (s)]
Phase (Deg.)
160
130
100
70
40
10
-20
-50
-80
-110
-140
-170
-200
-4.00
-3.00
-2.00
-1.00
0.00
1.00
2.00
3.00
LOG10 [Periods (s)]
Overview Map
Total RMS = 14848.28
Zxy RMS = 14359.02
Zyx RMS = 15321.93

Site: G52

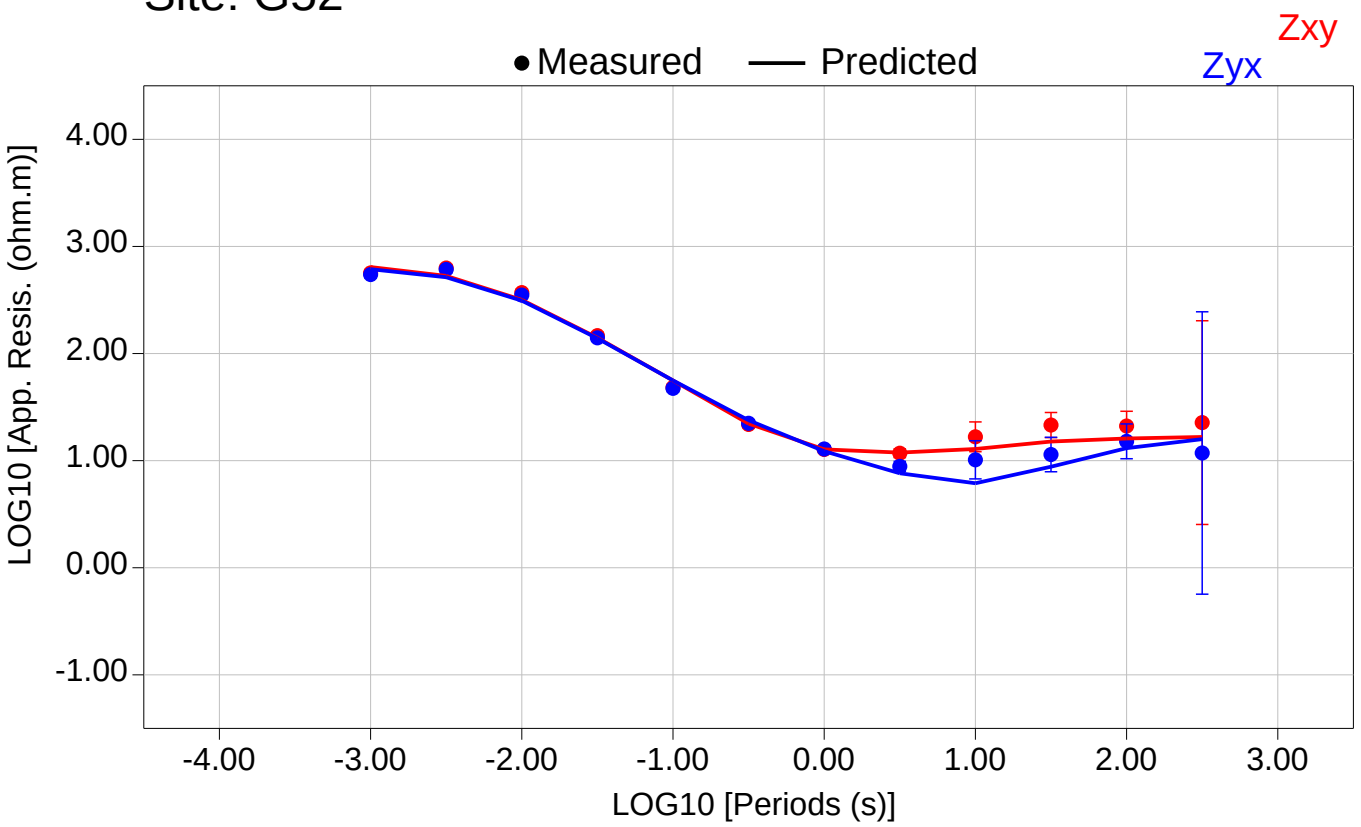

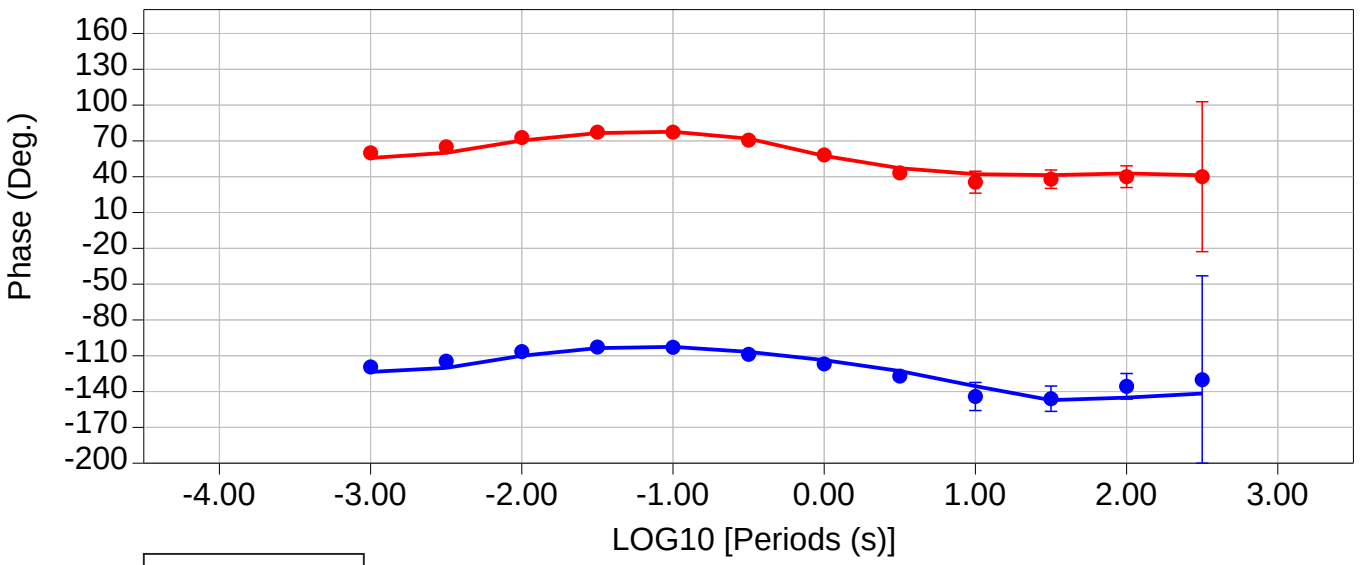

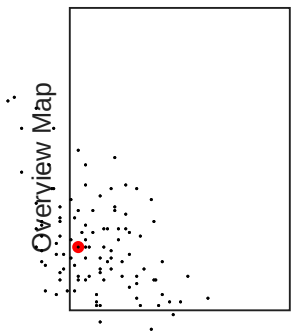

Total RMS = 16028.94

Zxy RMS = 16114.83

Zyx RMS = 15942.59

Site: MT16

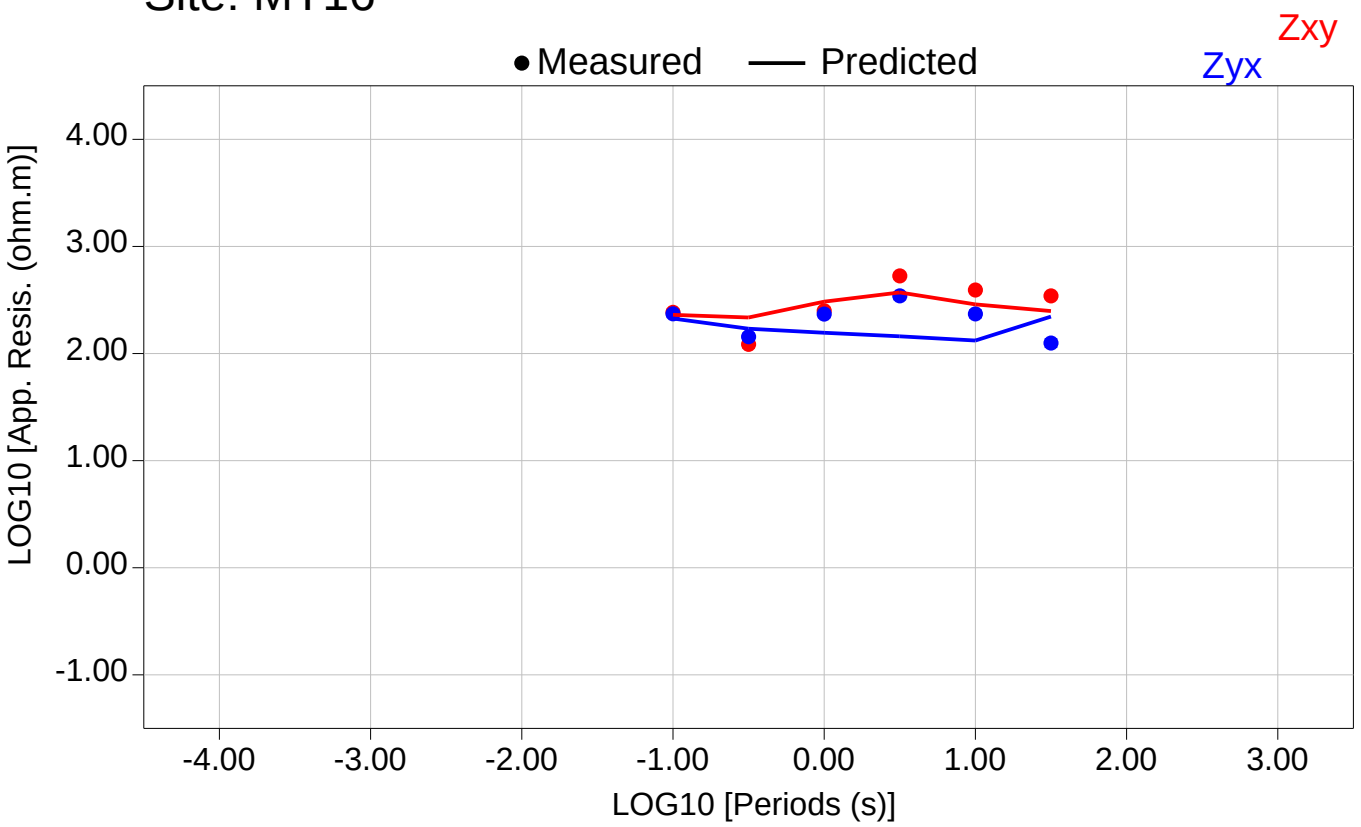

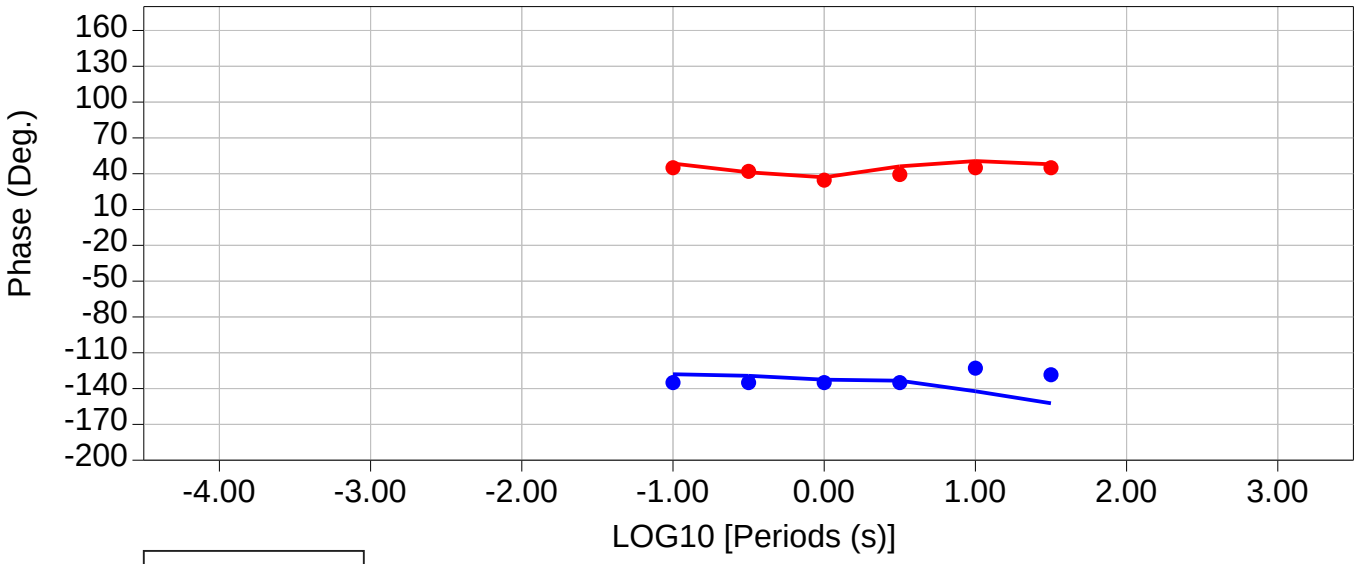

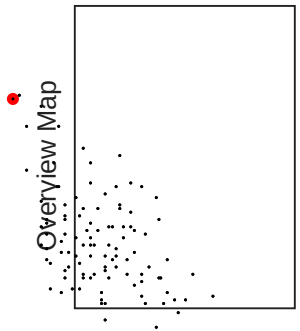

Total RMS = 16398.04

Zxy RMS = 17957.32

Zyx RMS = 14673.99

Site: MT19

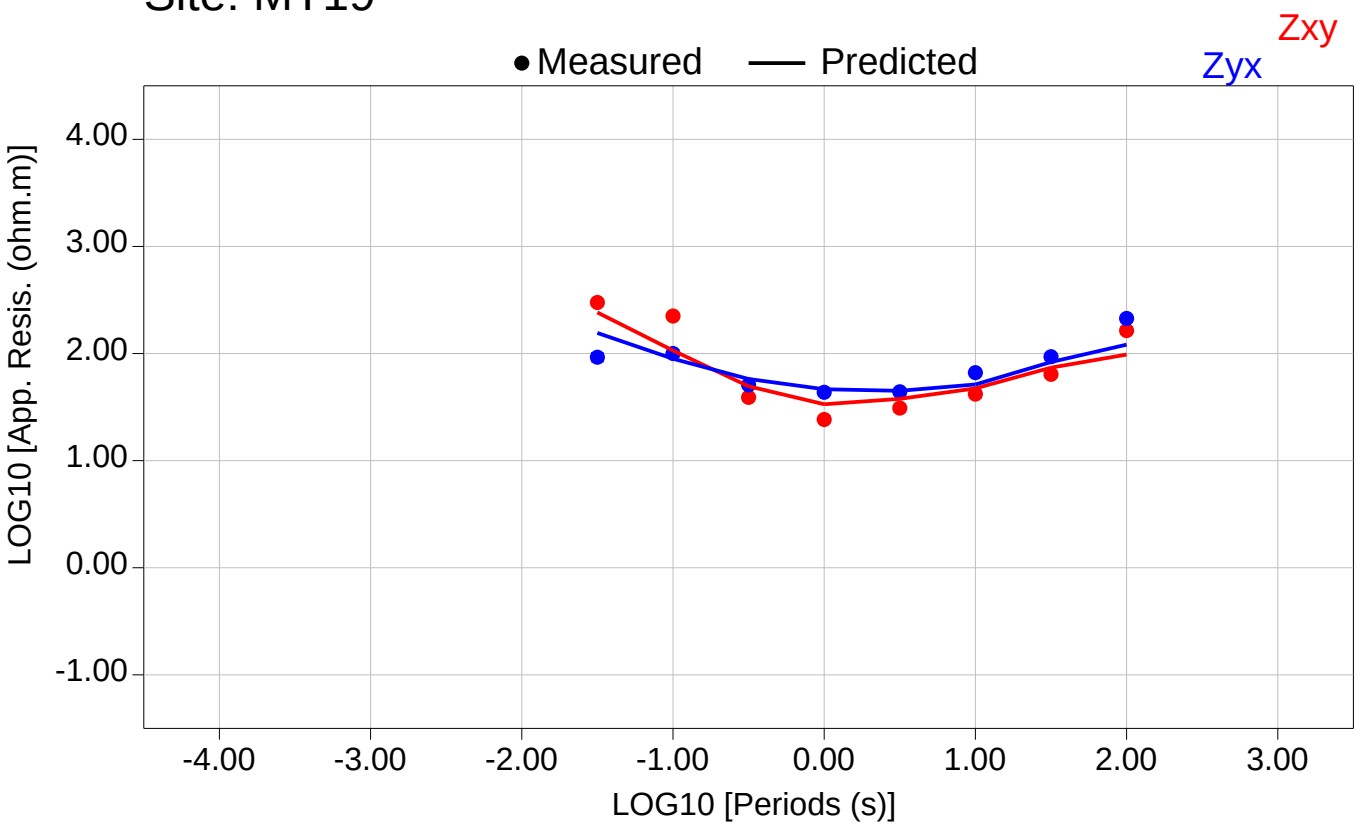

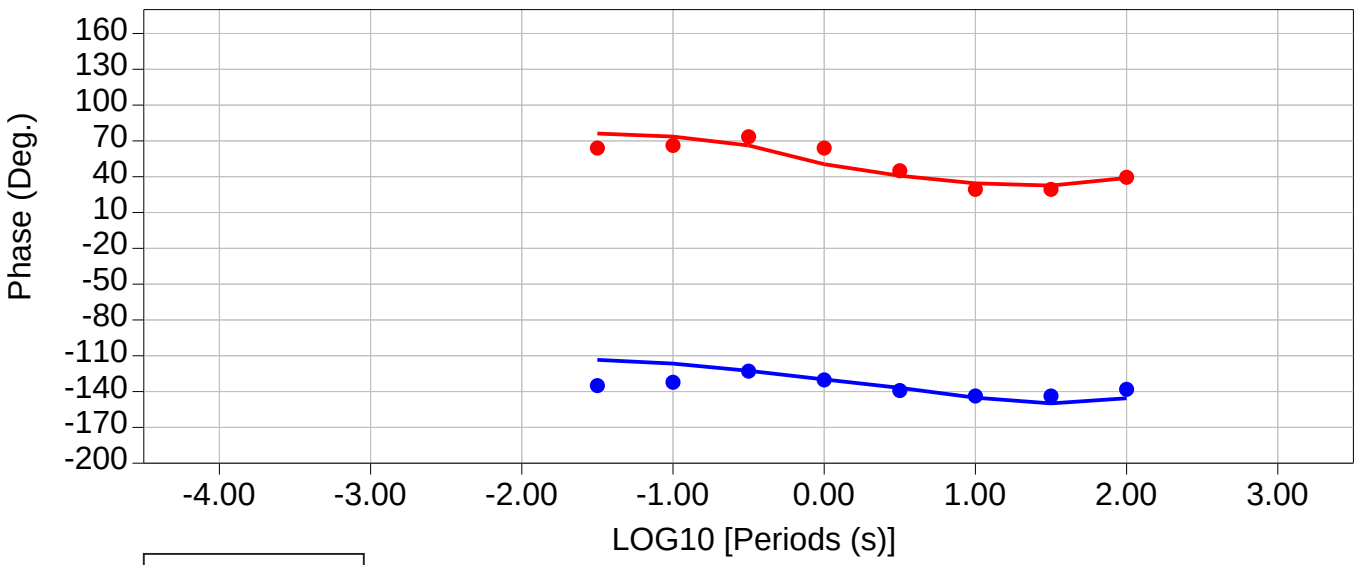

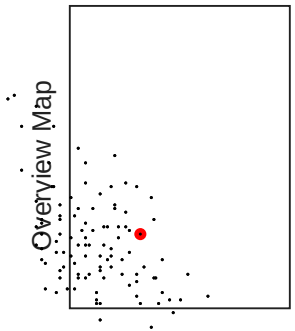

Total RMS = 15821.50

Zxy RMS = 15692.19

Zyx RMS = 15949.77

Site: MT20

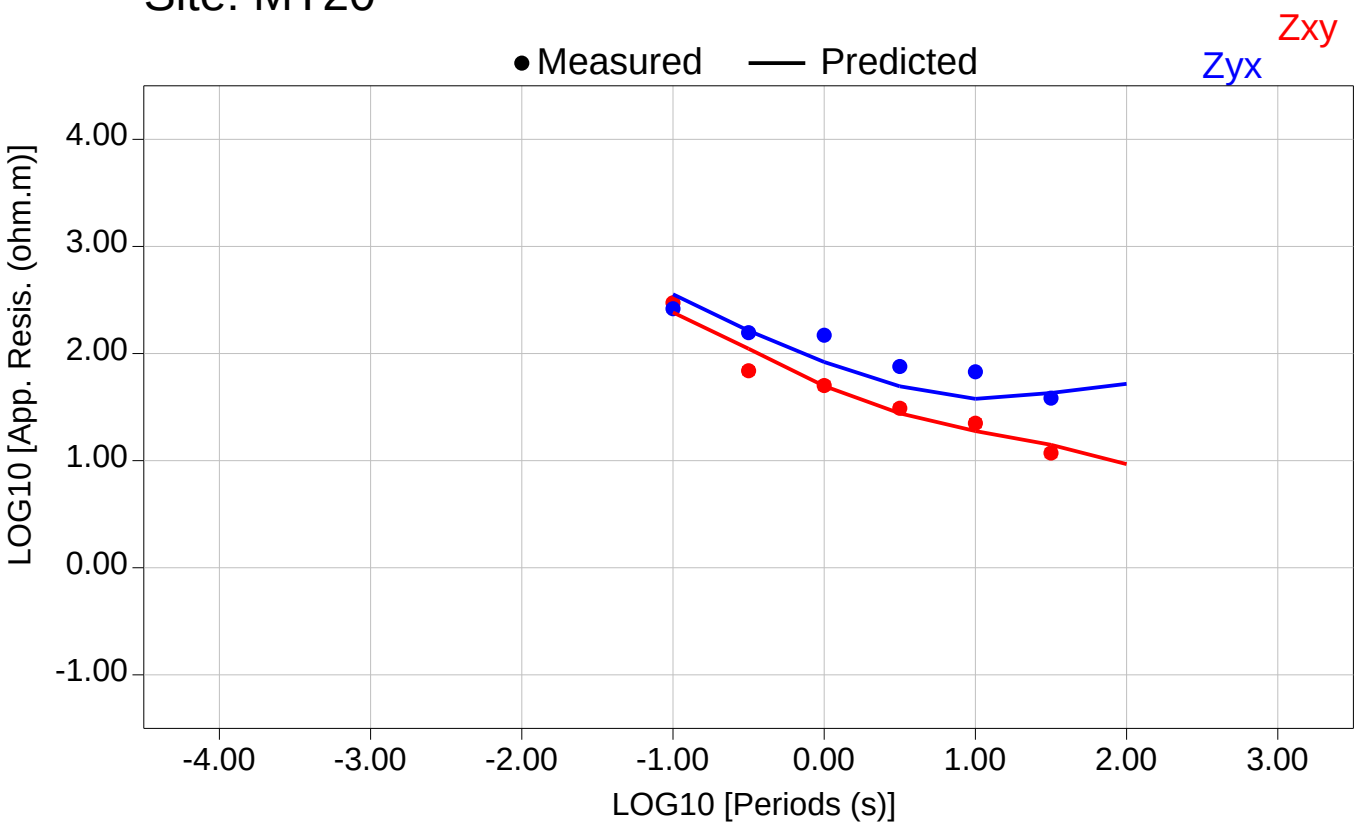

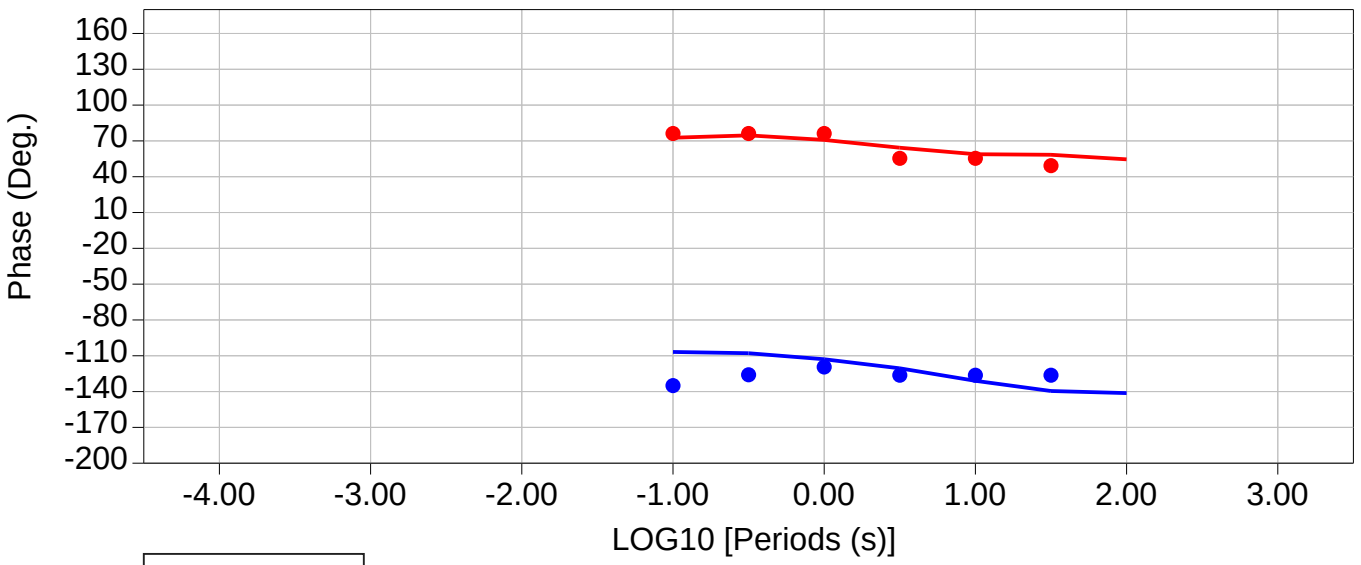

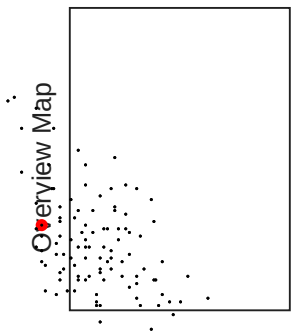

Total RMS = 20672.62

Zxy RMS = 17998.55
Zyx RMS = 23038.36

Site: MT21

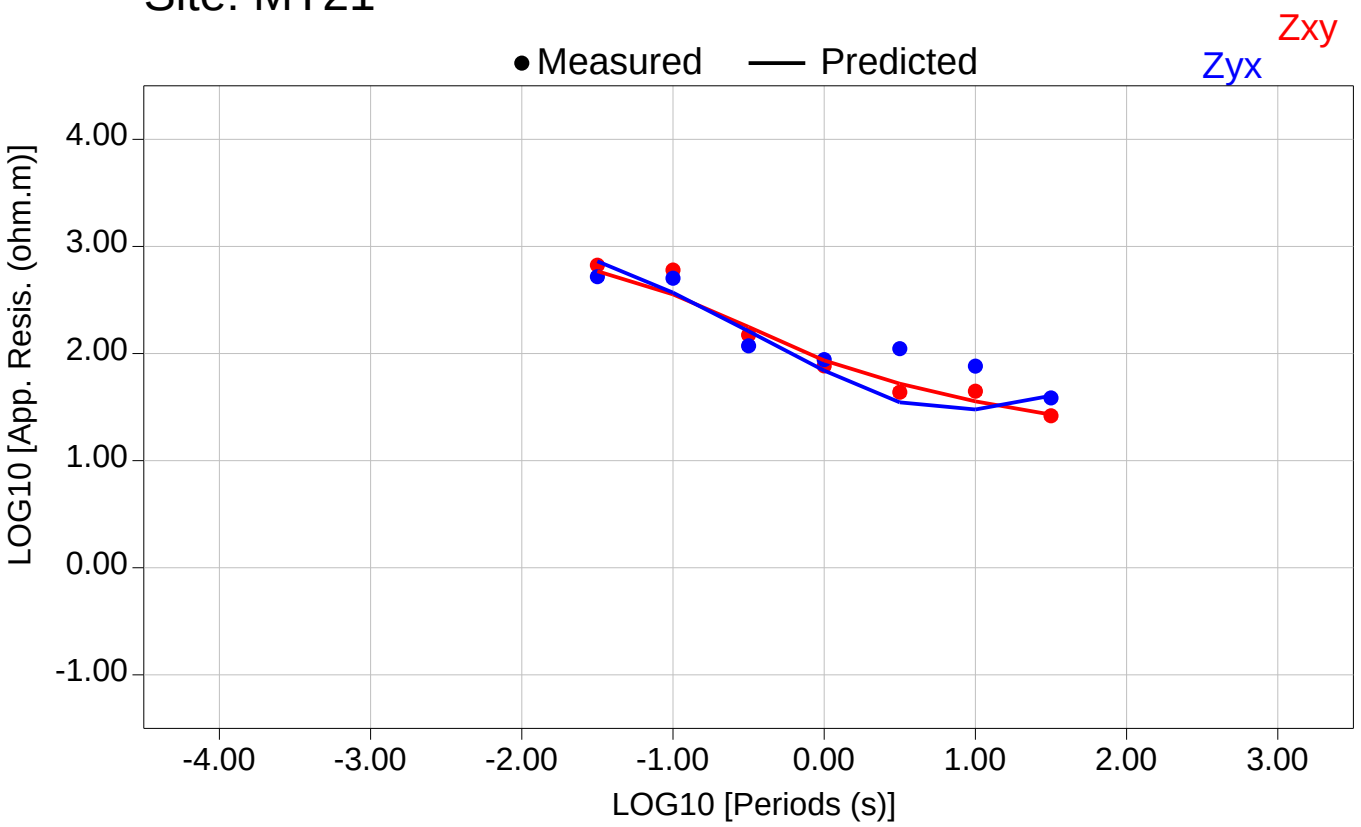

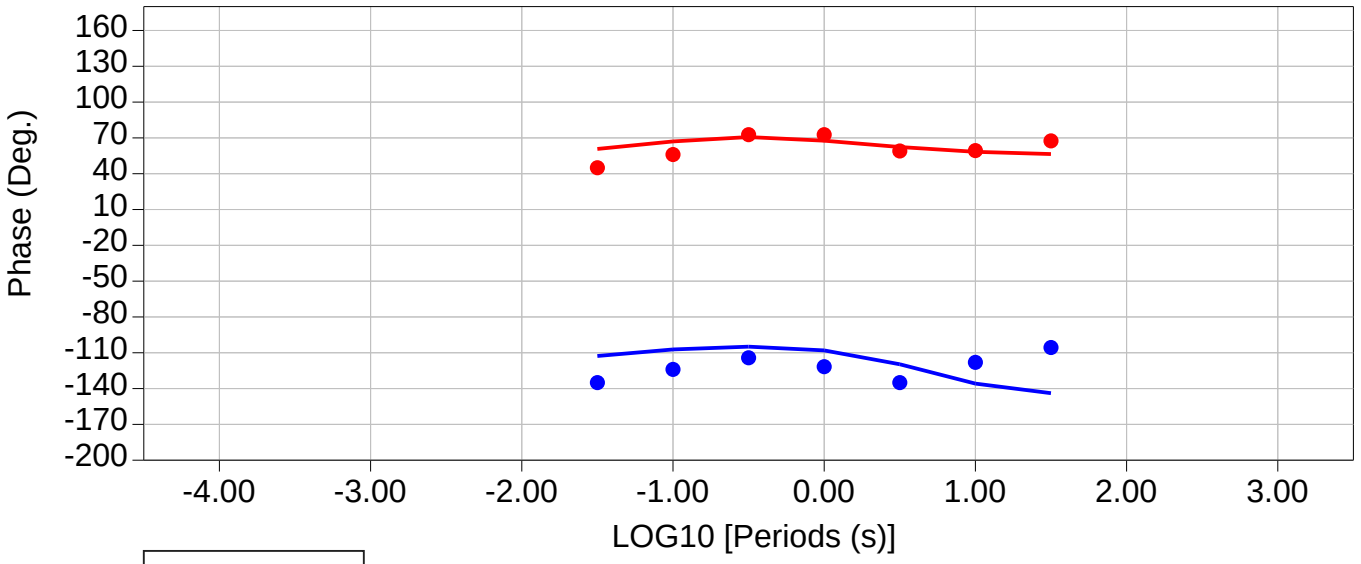

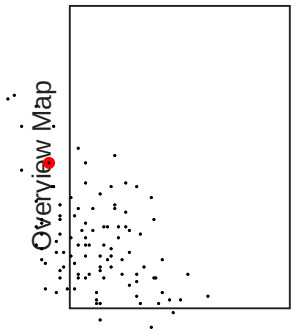

Total RMS = 17862.84

Zxy RMS = 18187.76

Zyx RMS = 17531.91

Site: X03

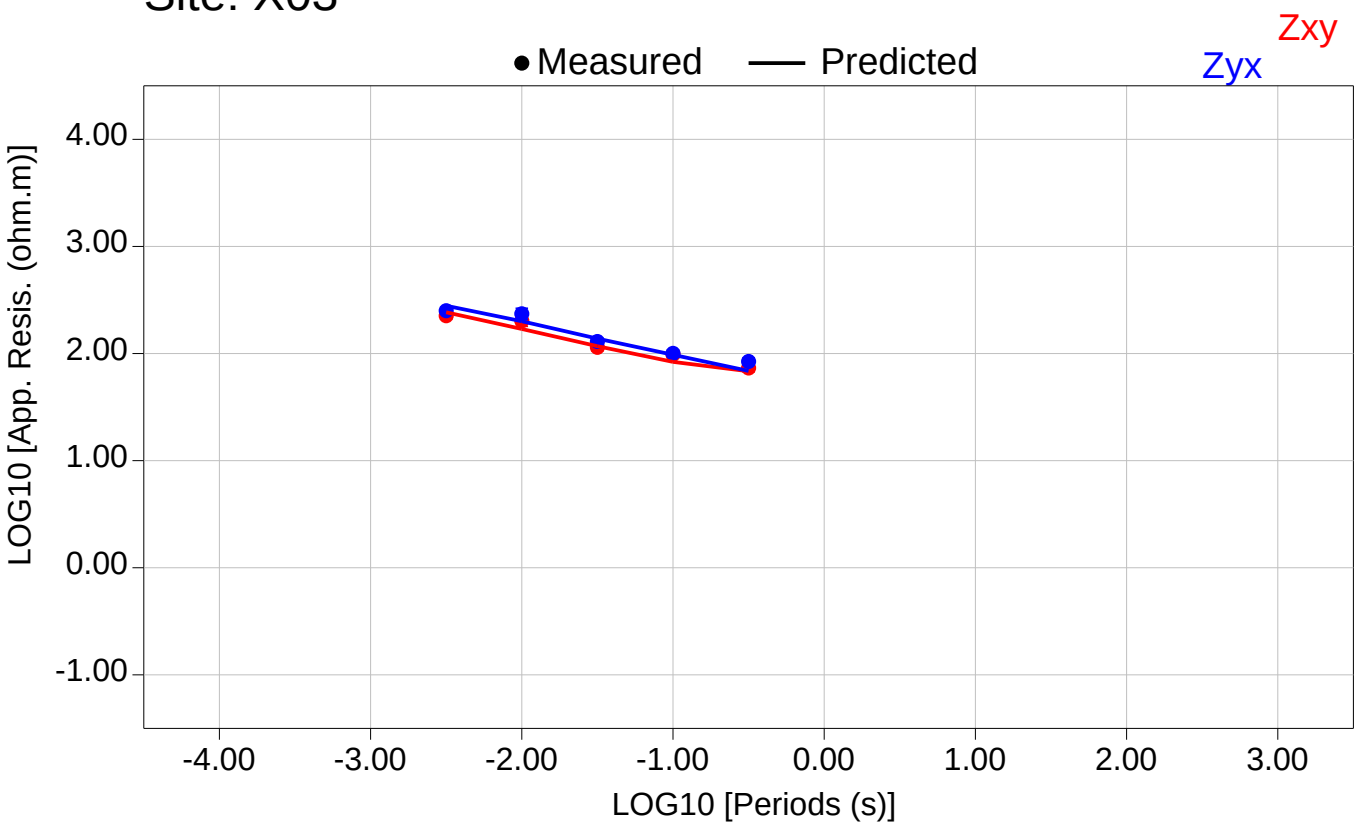

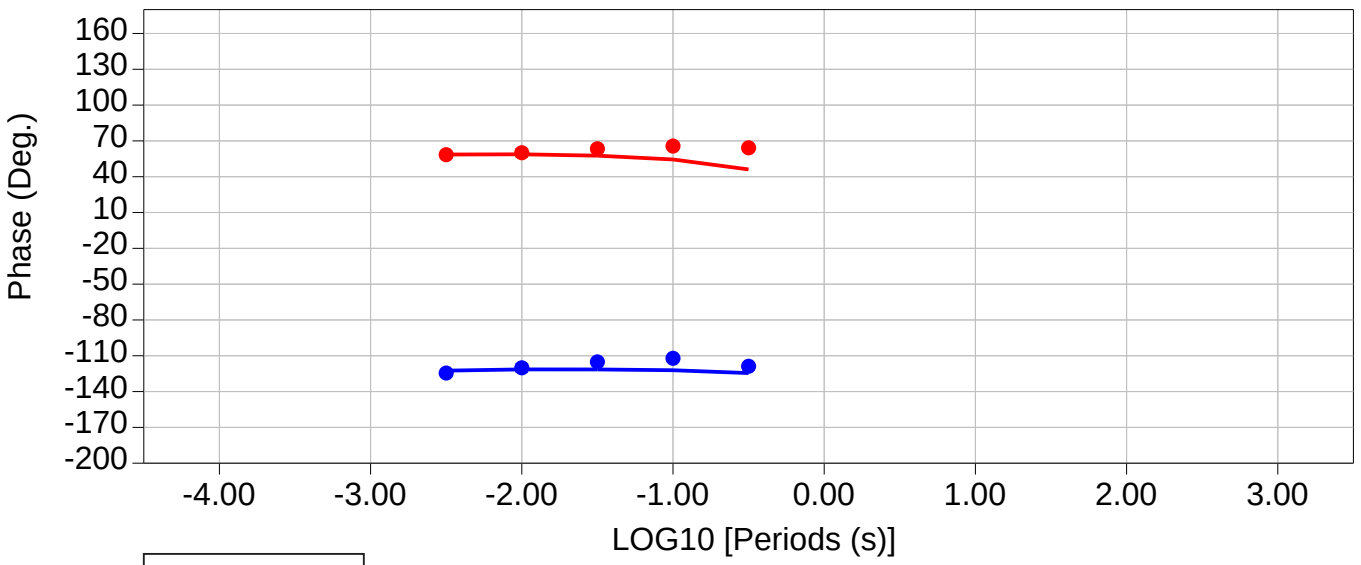

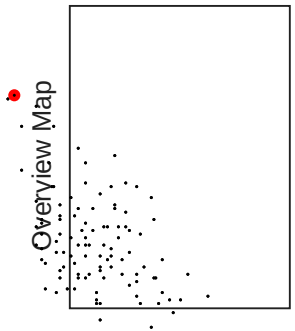

Total RMS = 15019.14

Zxy RMS = 14354.29
Zyx RMS = 15655.79

Site: X05

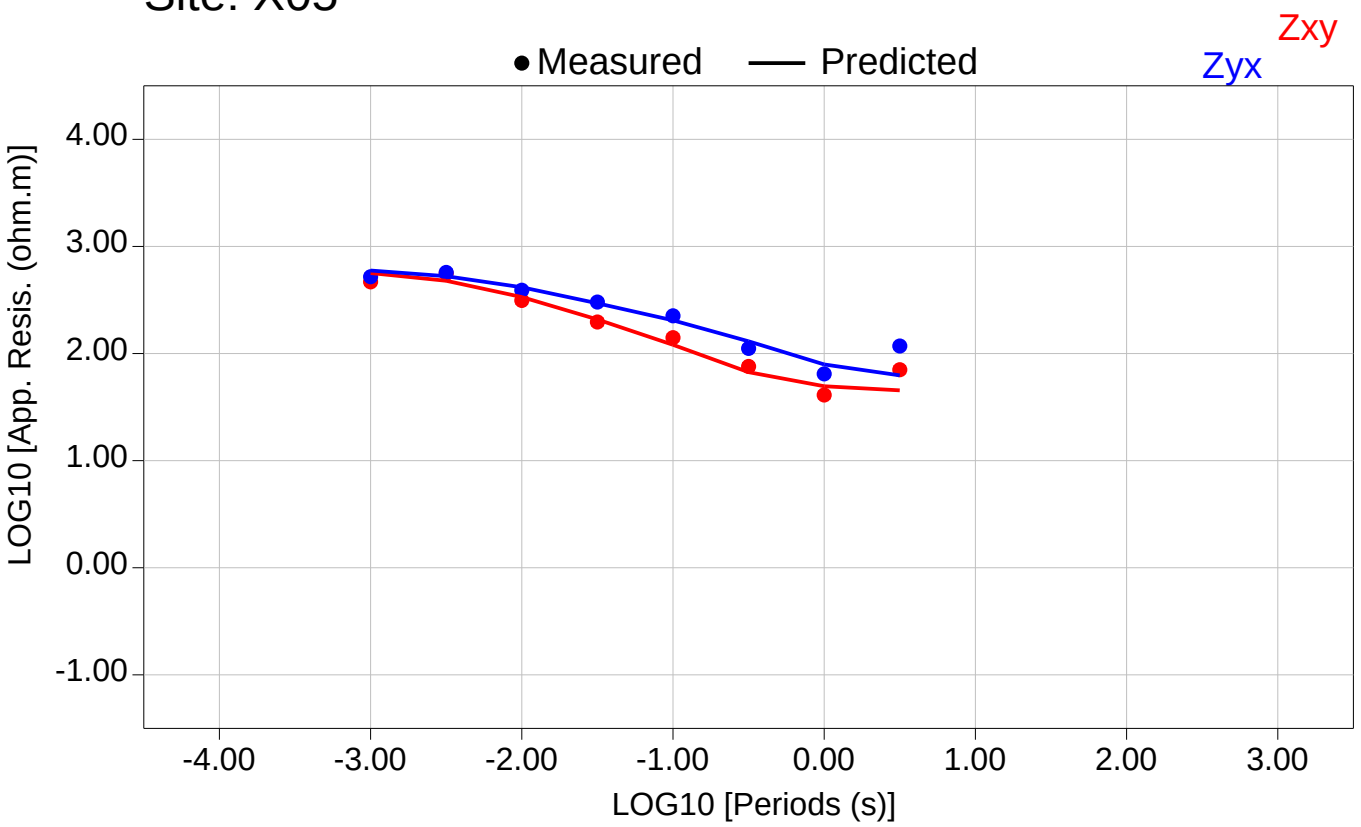

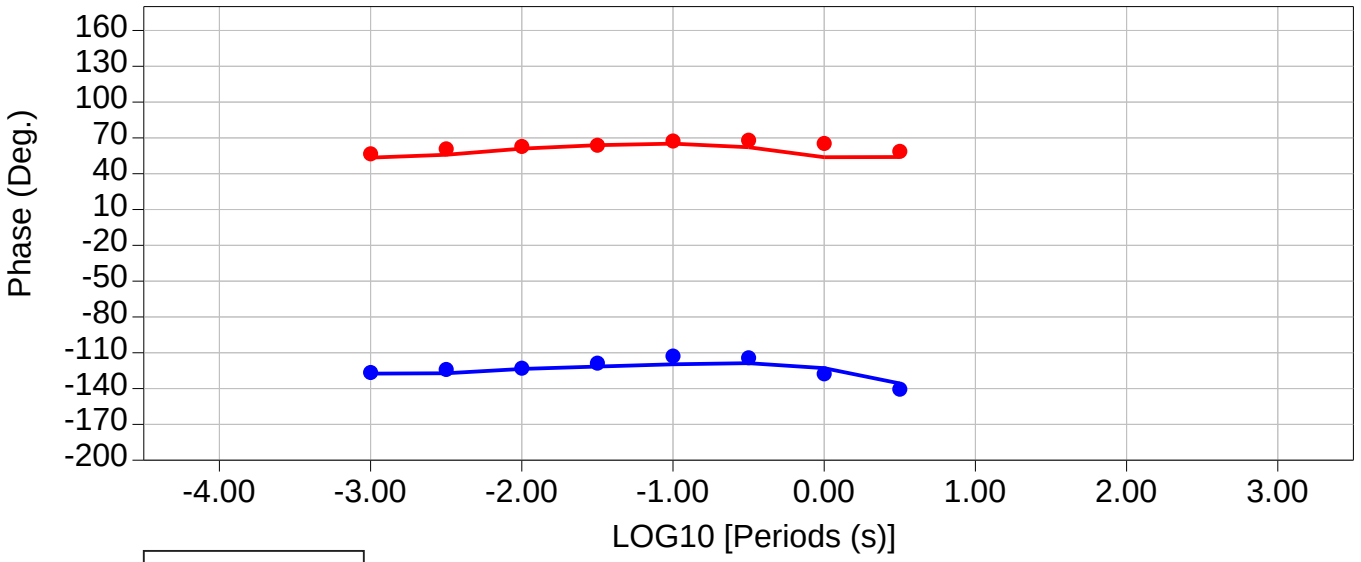

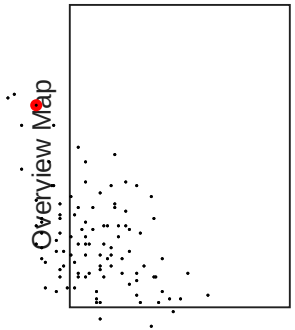

Total RMS = 17940.69

Zxy RMS = 16463.21
Zyx RMS = 19305.43

Site: X06

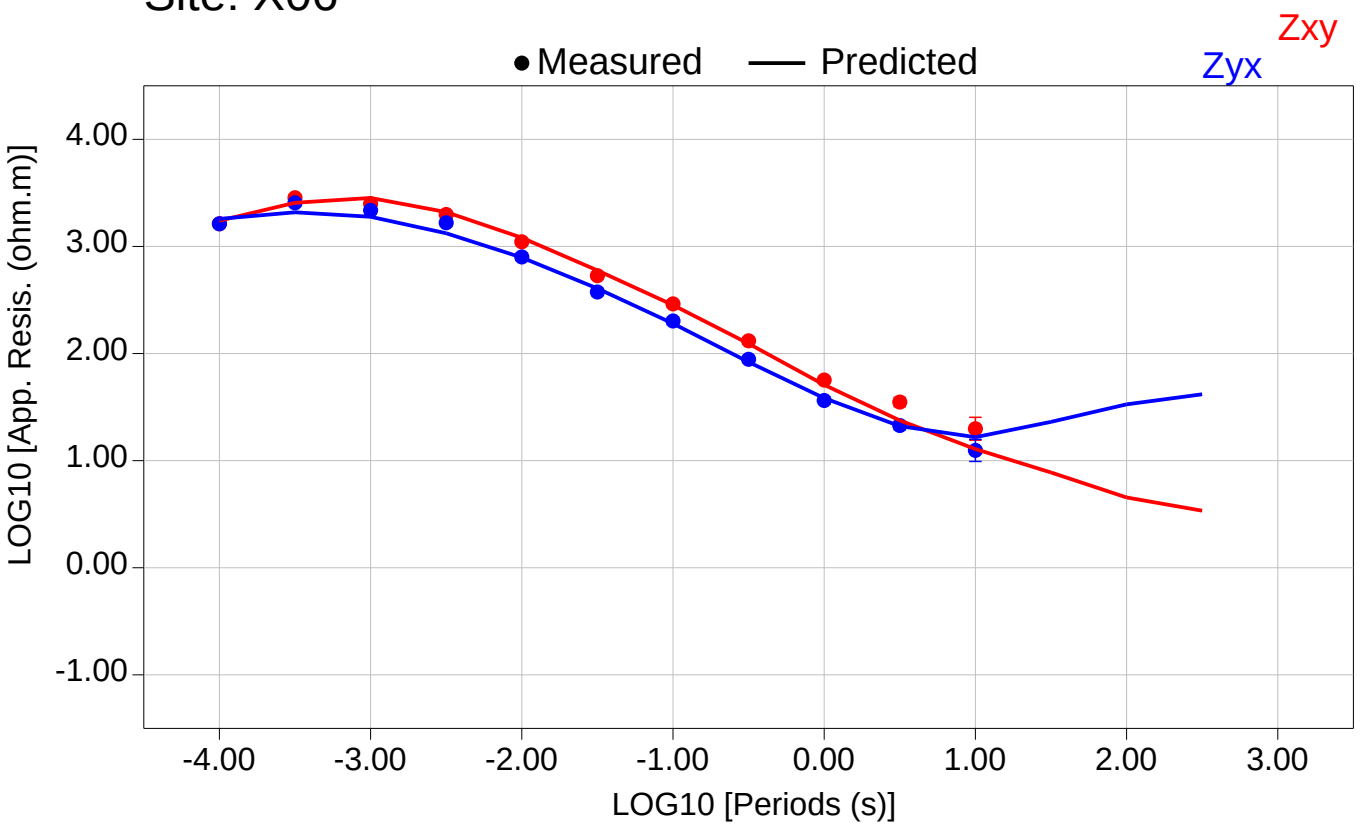

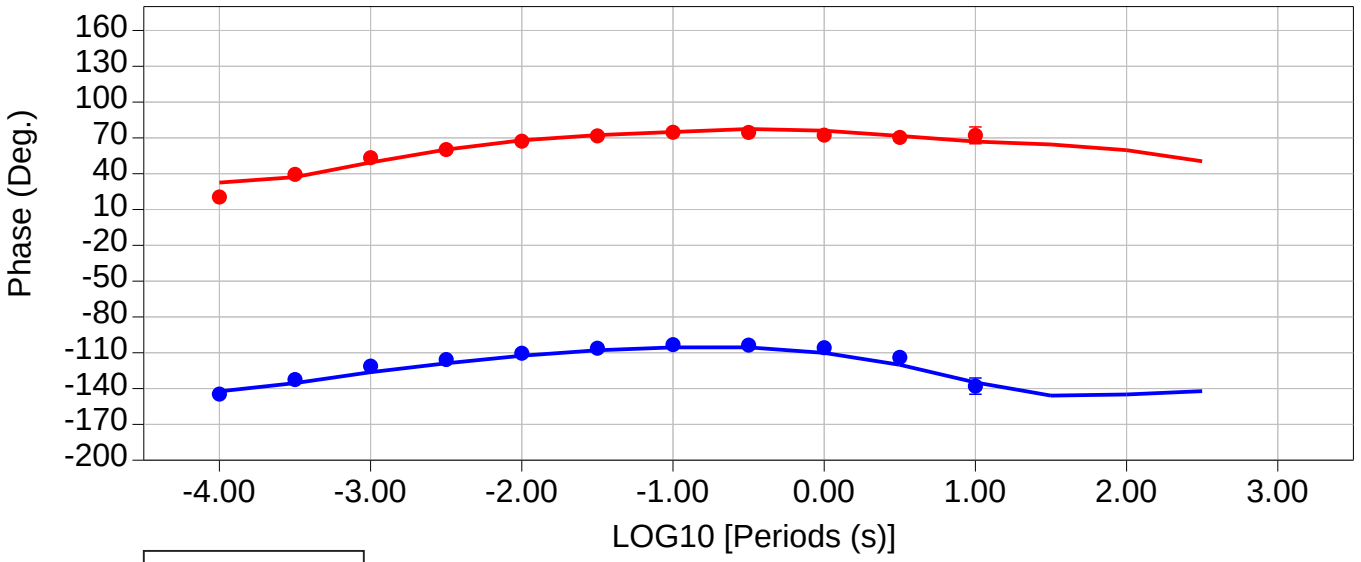

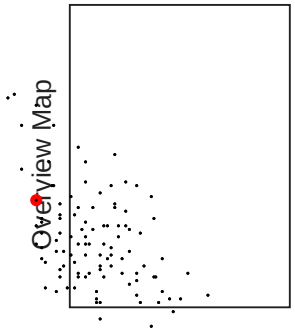

Total RMS = 18029.86

Zxy RMS = 19210.54

Zyx RMS = 16766.24

Site: X07

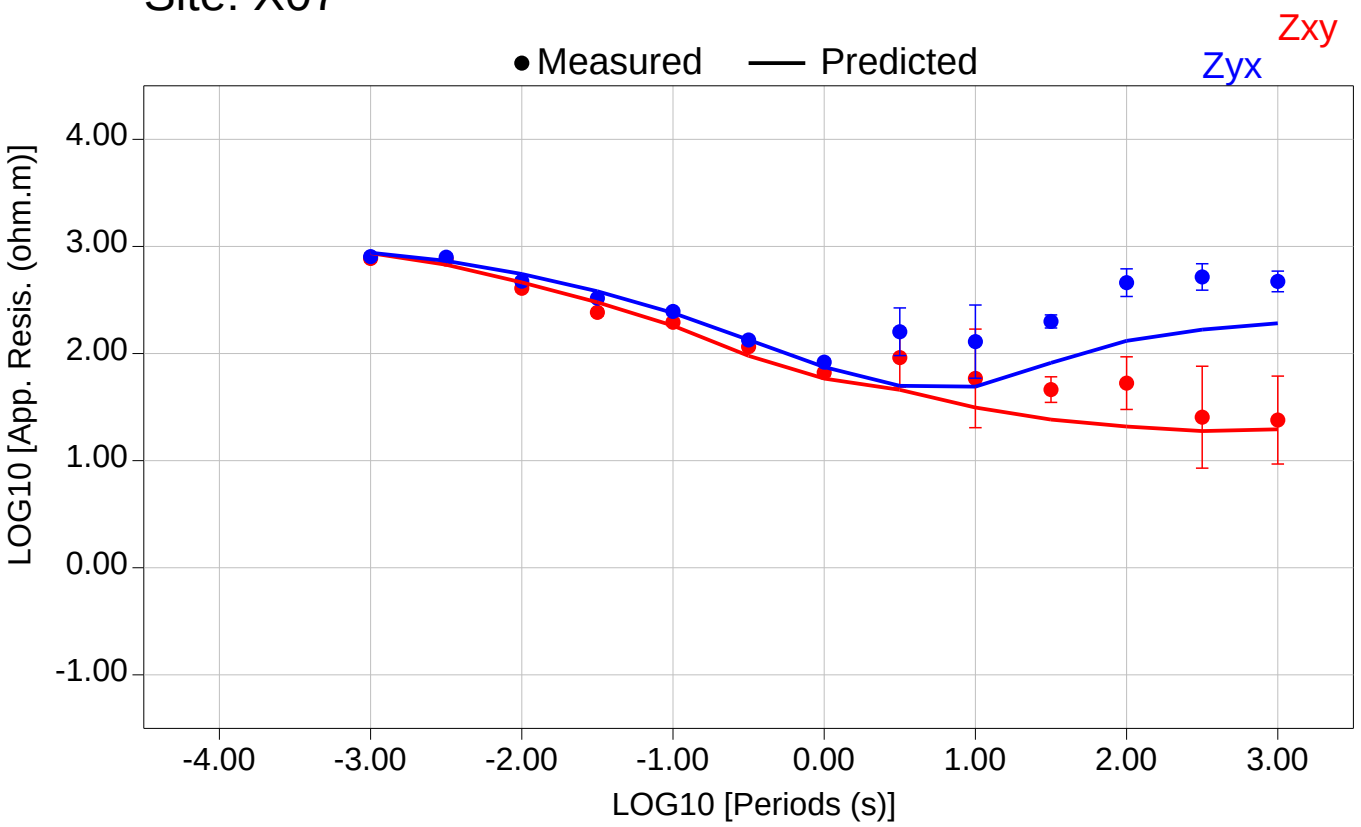

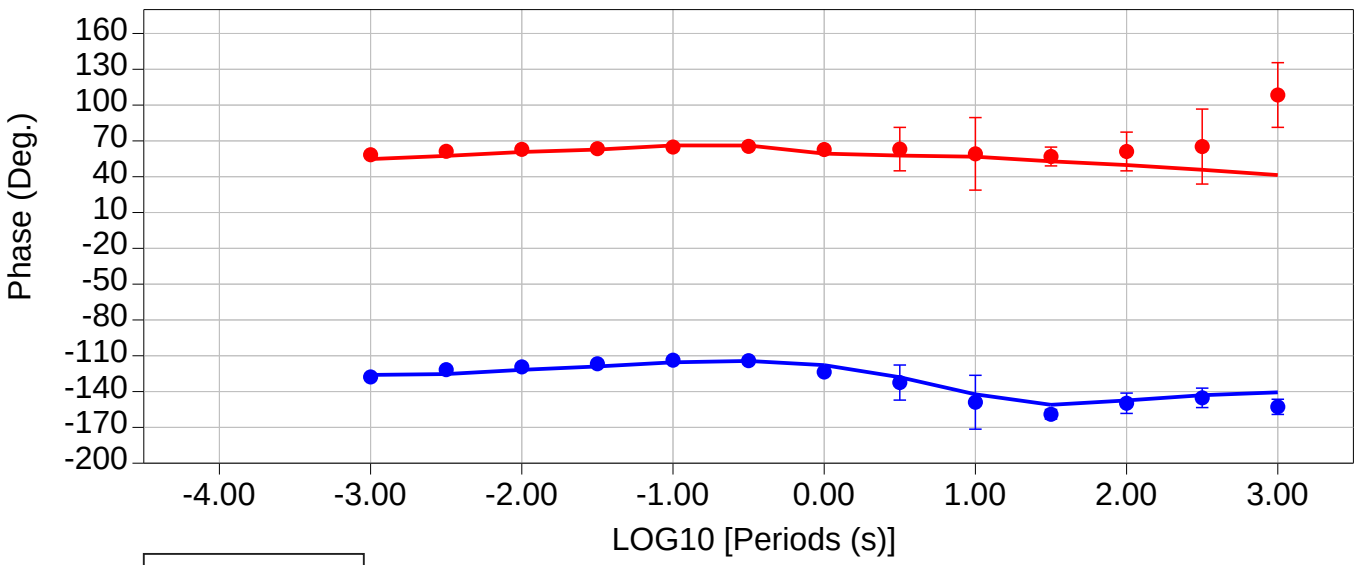

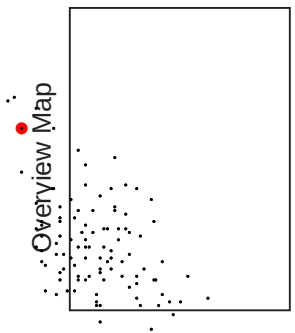

Total RMS = 13583.37

Zxy RMS = 12967.00

Zyx RMS = 14172.95

Site: X11

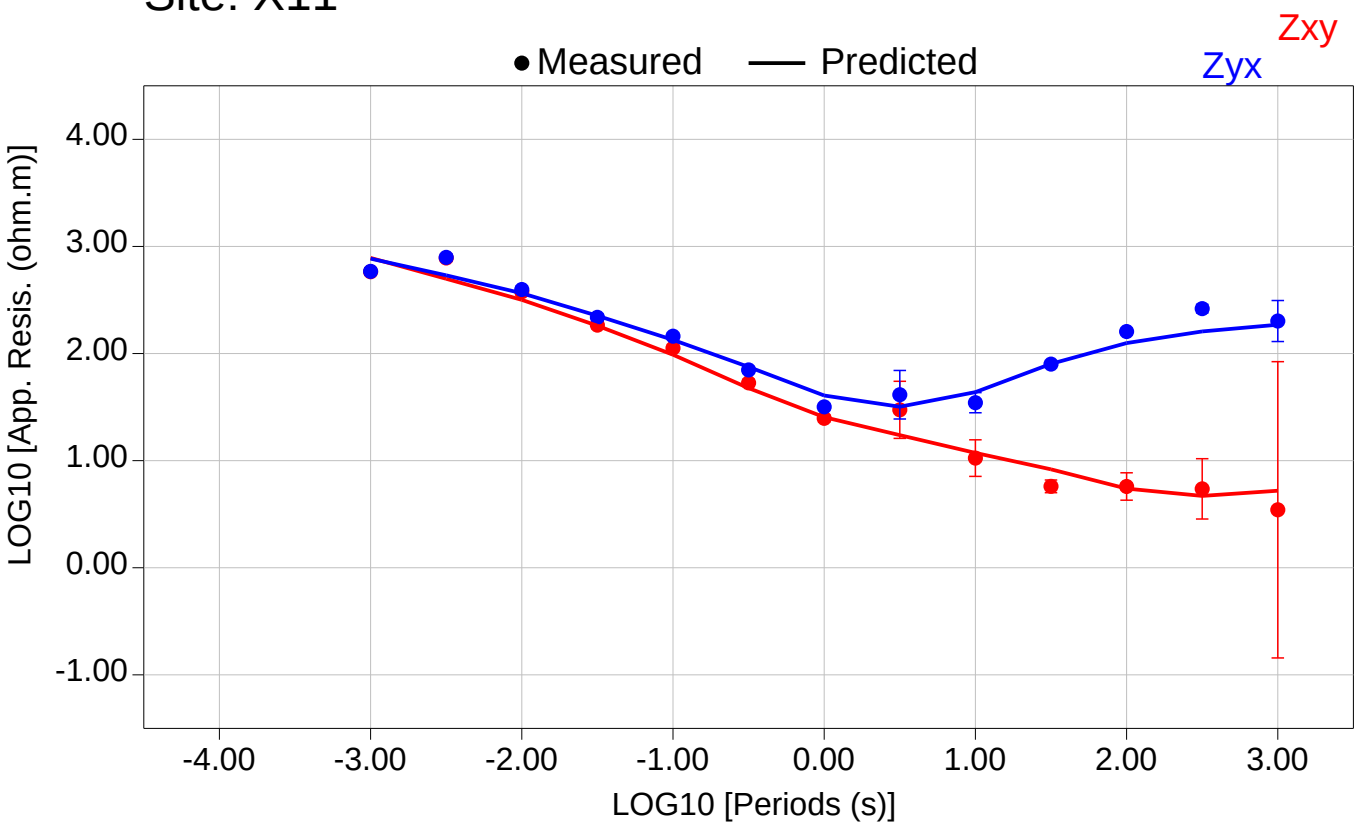

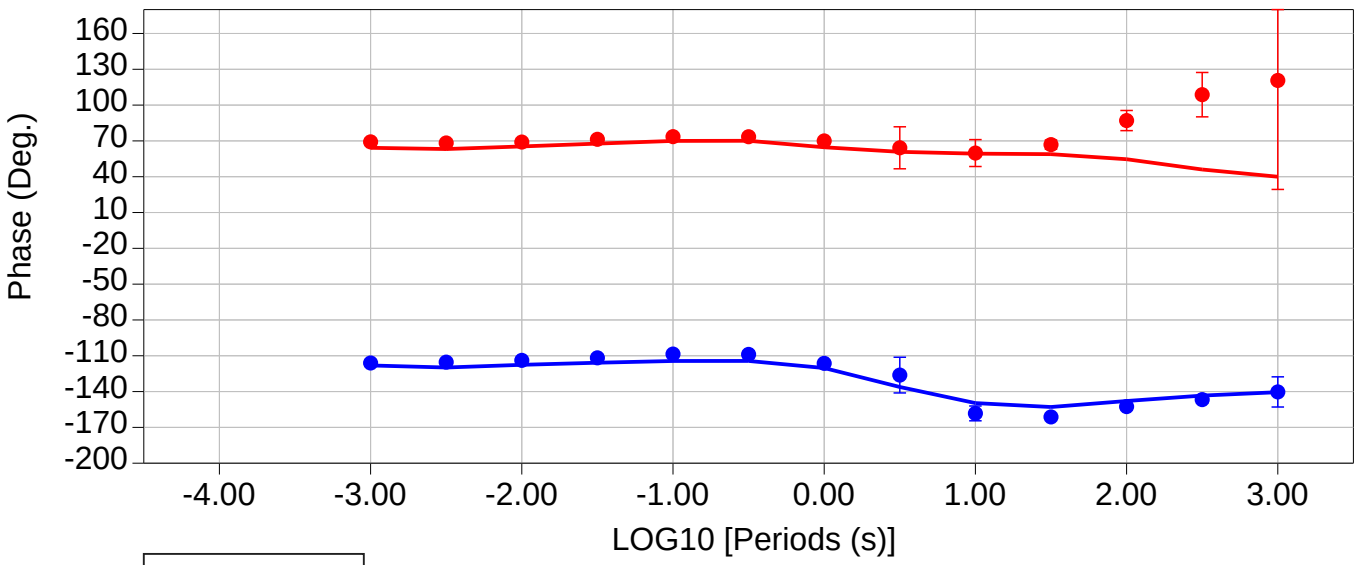

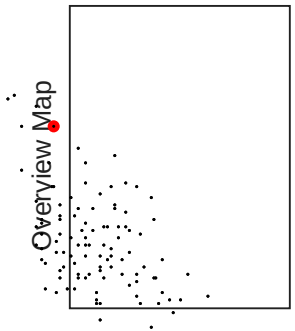

Total RMS = 15324.60

Zxy RMS = 13576.03
Zyx RMS = 16893.14

Site: X12

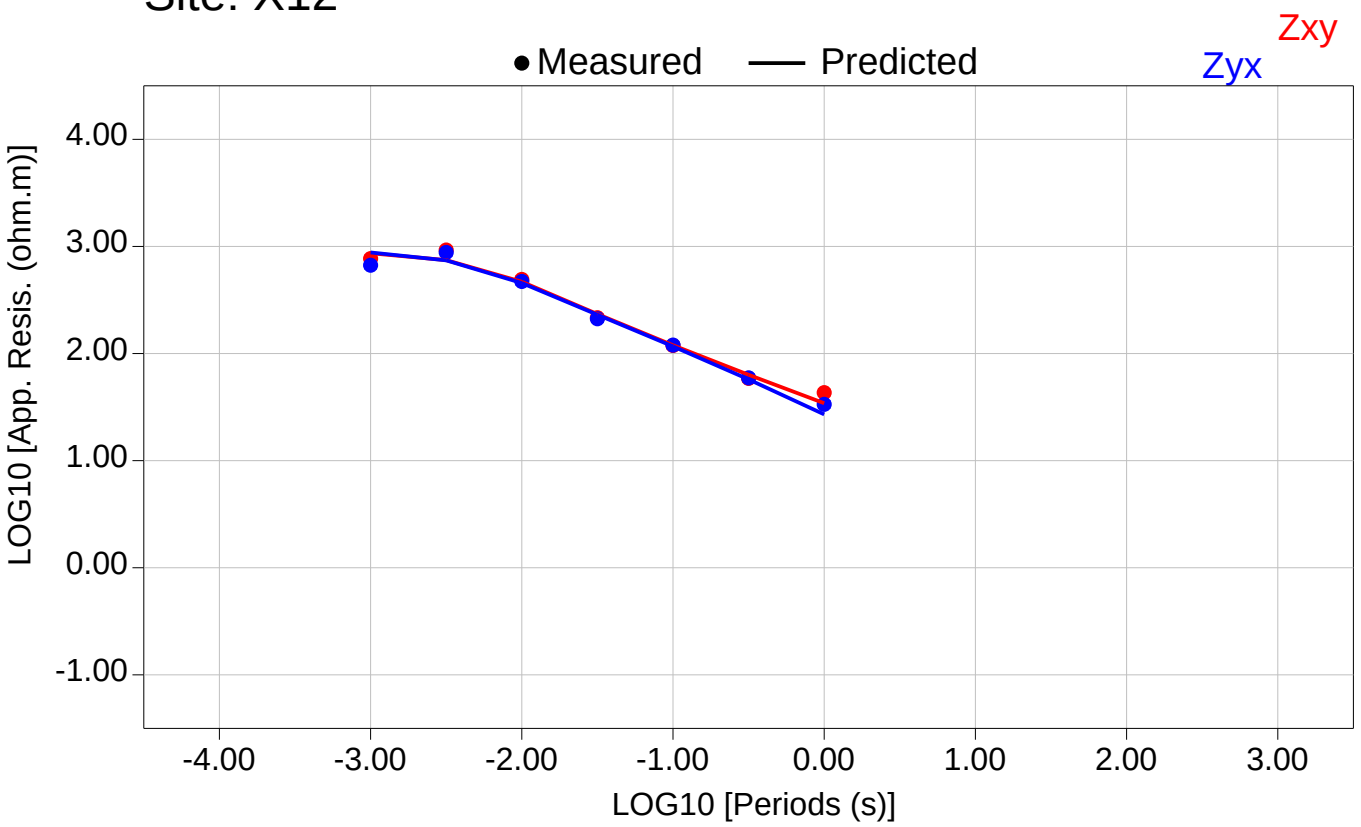

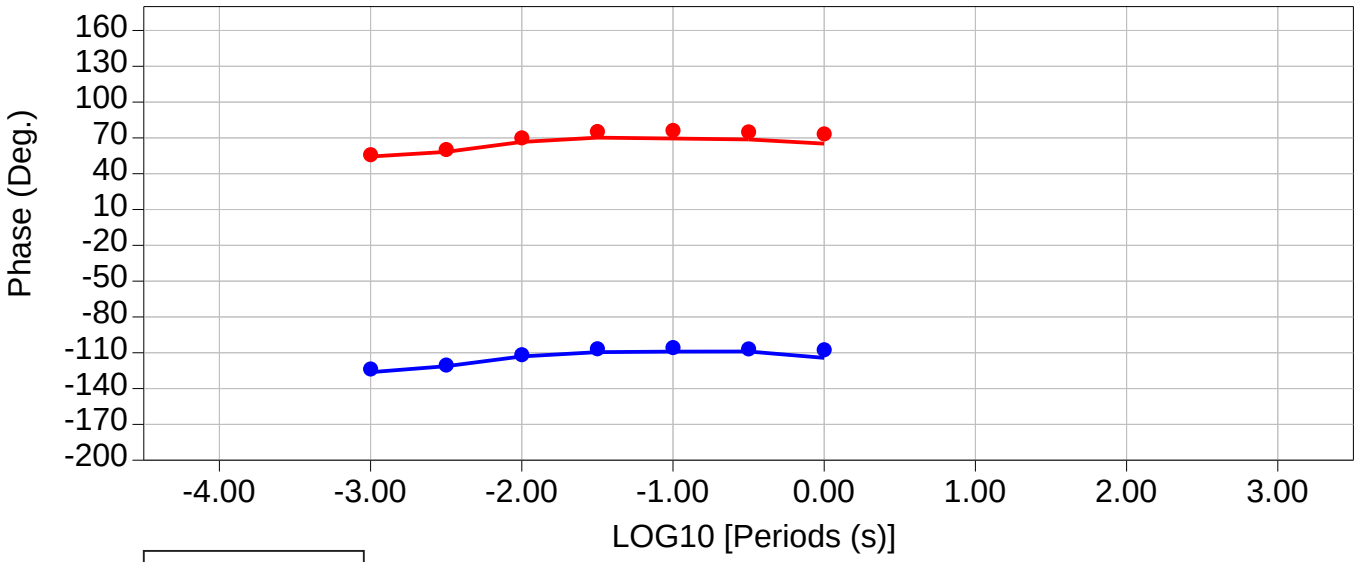

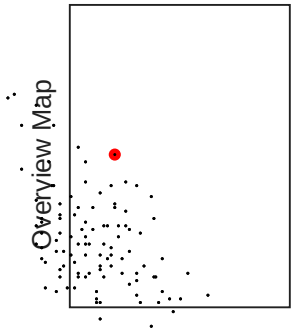

Total RMS = 19107.14

Zxy RMS = 19227.66

Zyx RMS = 18985.86

Site: X14

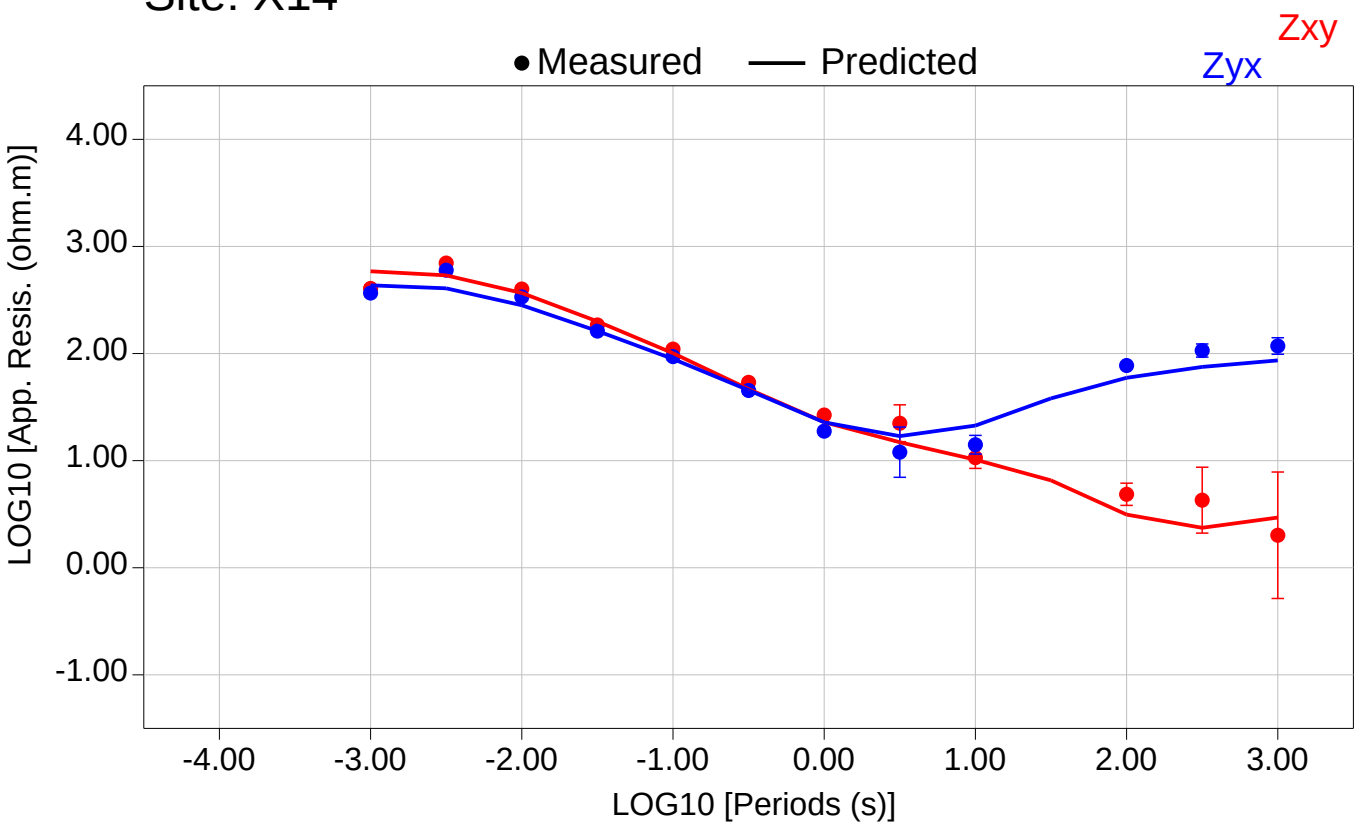

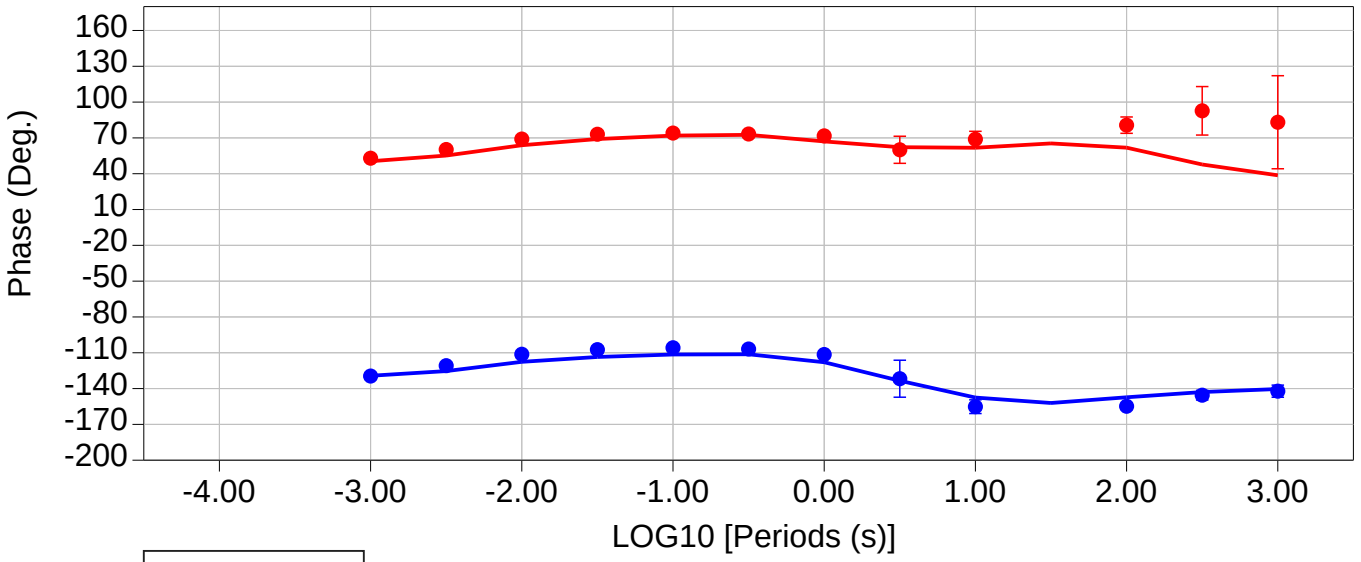

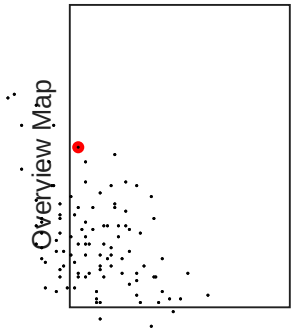

Total RMS = 14438.90

Zxy RMS = 14829.41
Zyx RMS = 14037.53

Site: X15

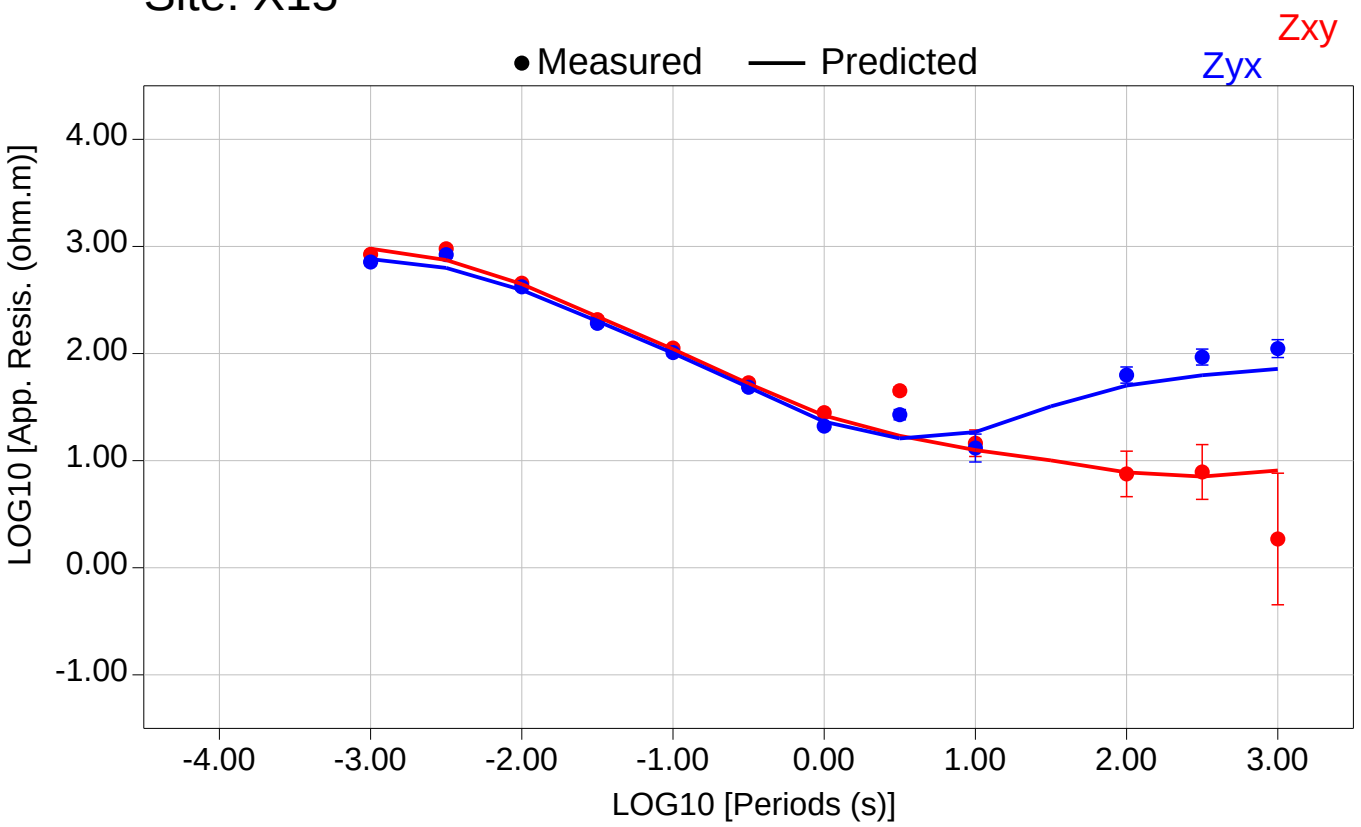

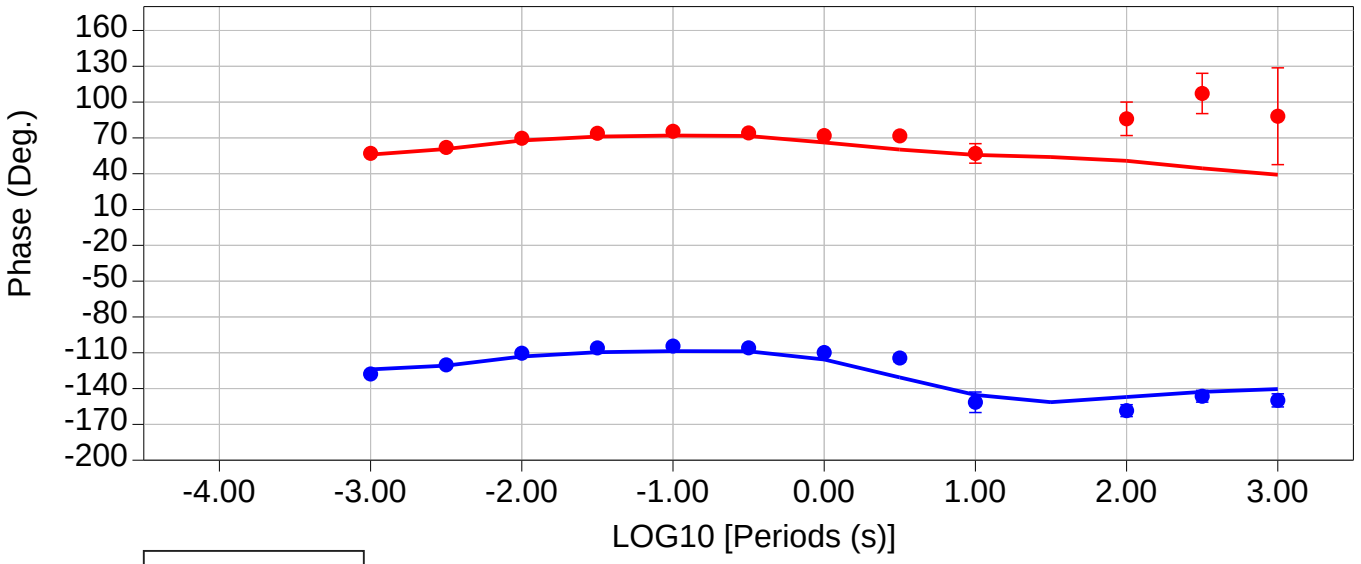

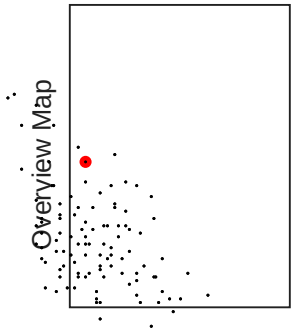

Total RMS = 15184.08

Zxy RMS = 15589.95
Zyx RMS = 14767.07

Site: X16

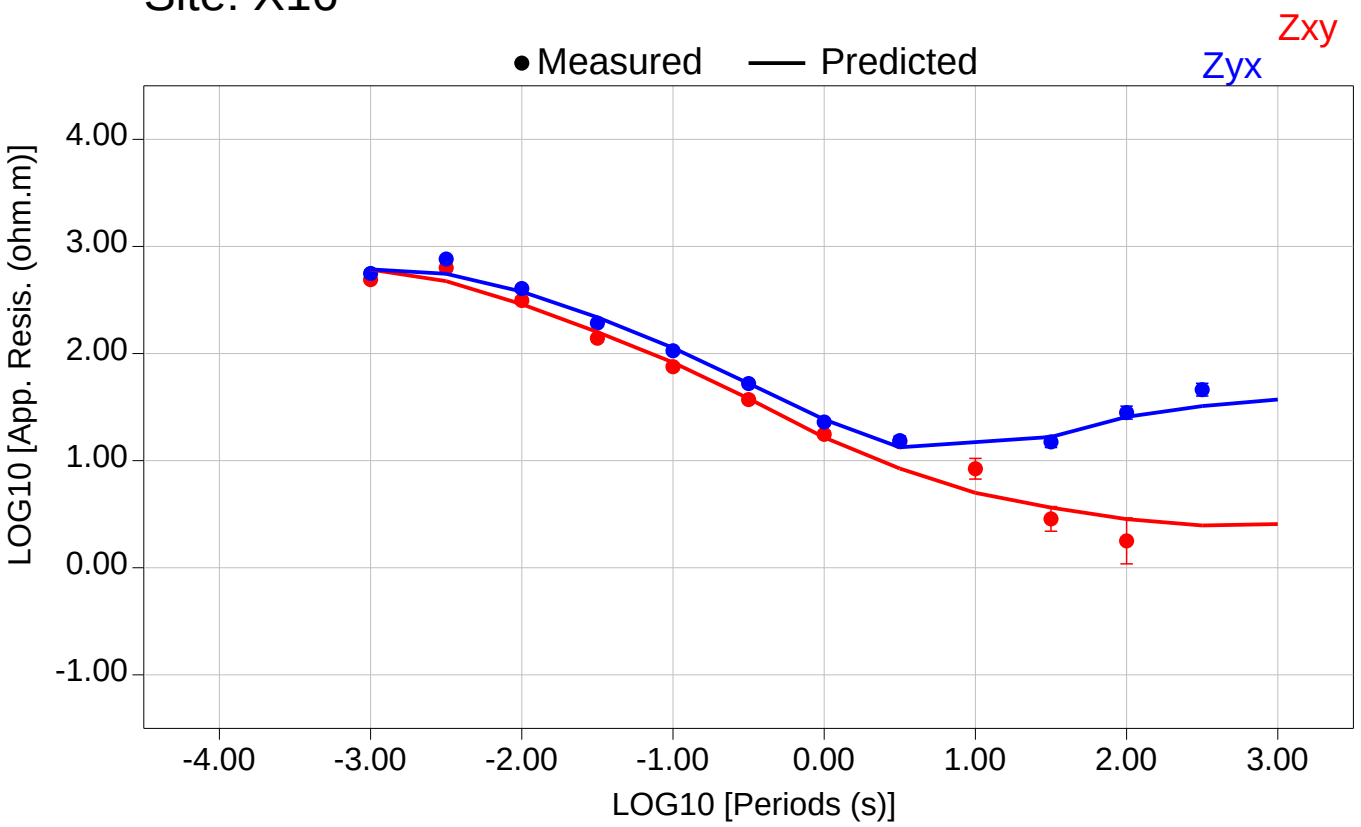

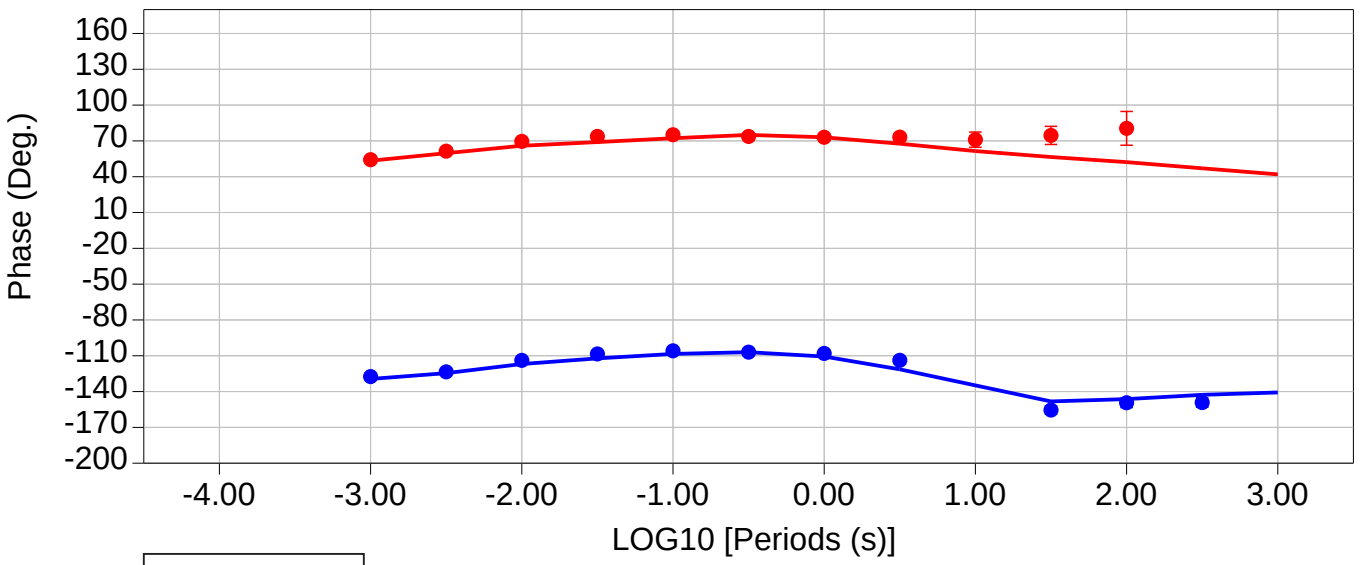

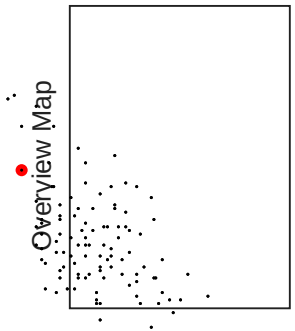

Total RMS = 16329.50

Zxy RMS = 15238.98
Zyx RMS = 17351.61

Site: X19

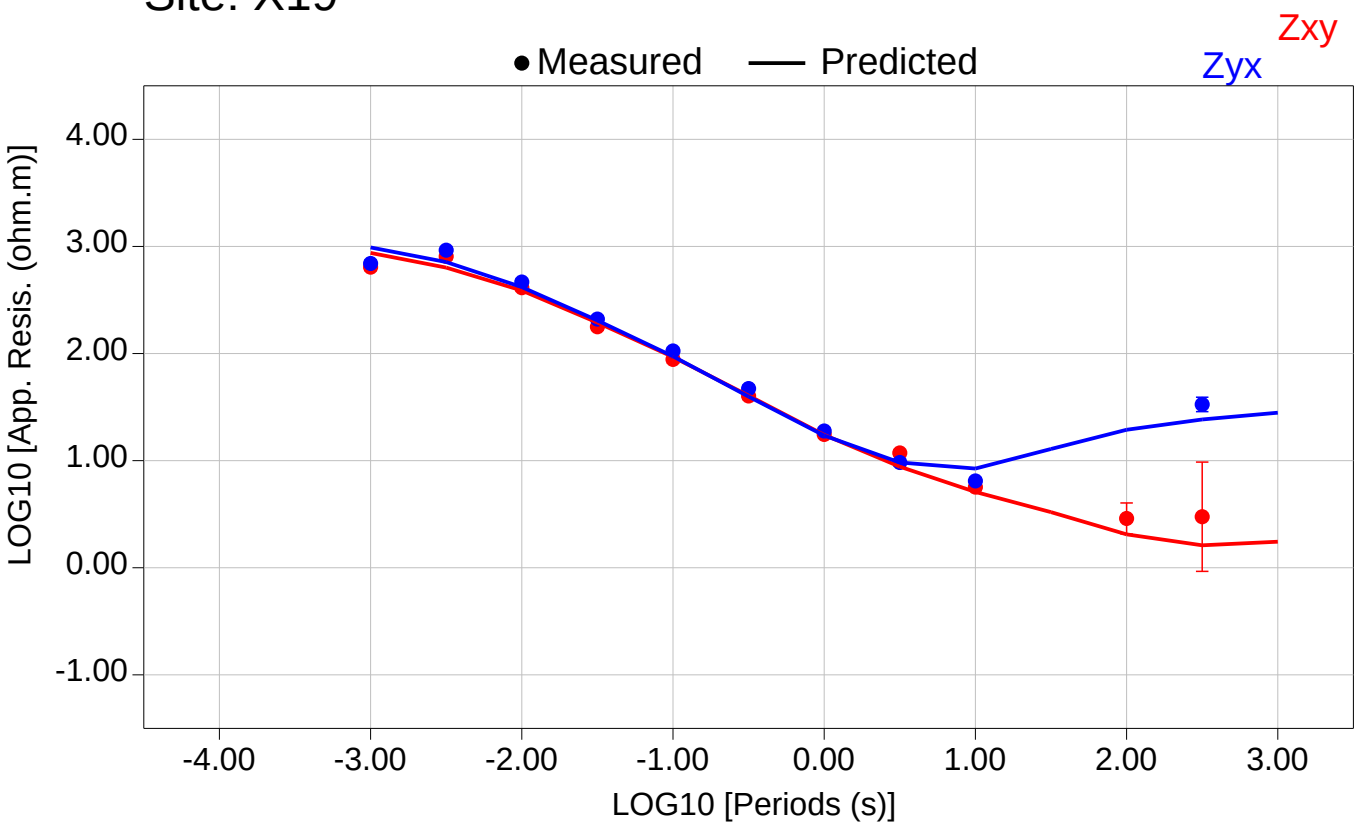

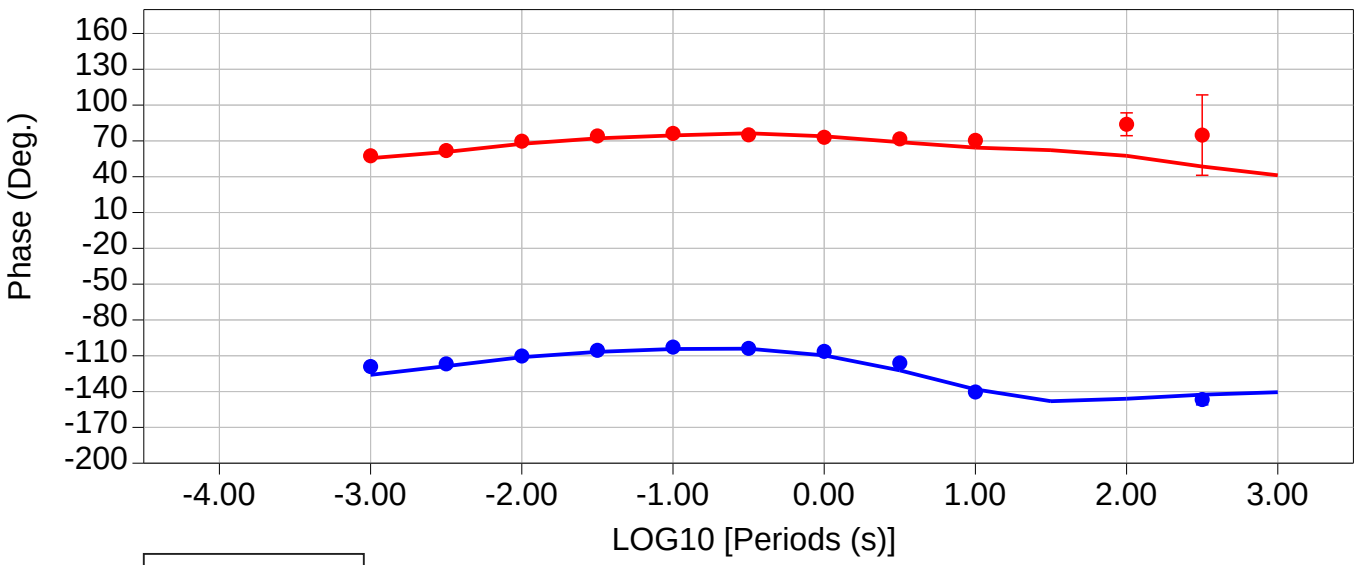

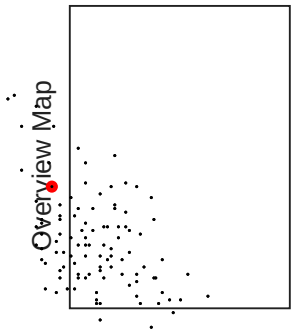

Total RMS = 18192.31

Zxy RMS = 17442.28

Zyx RMS = 18983.14

Site: X20

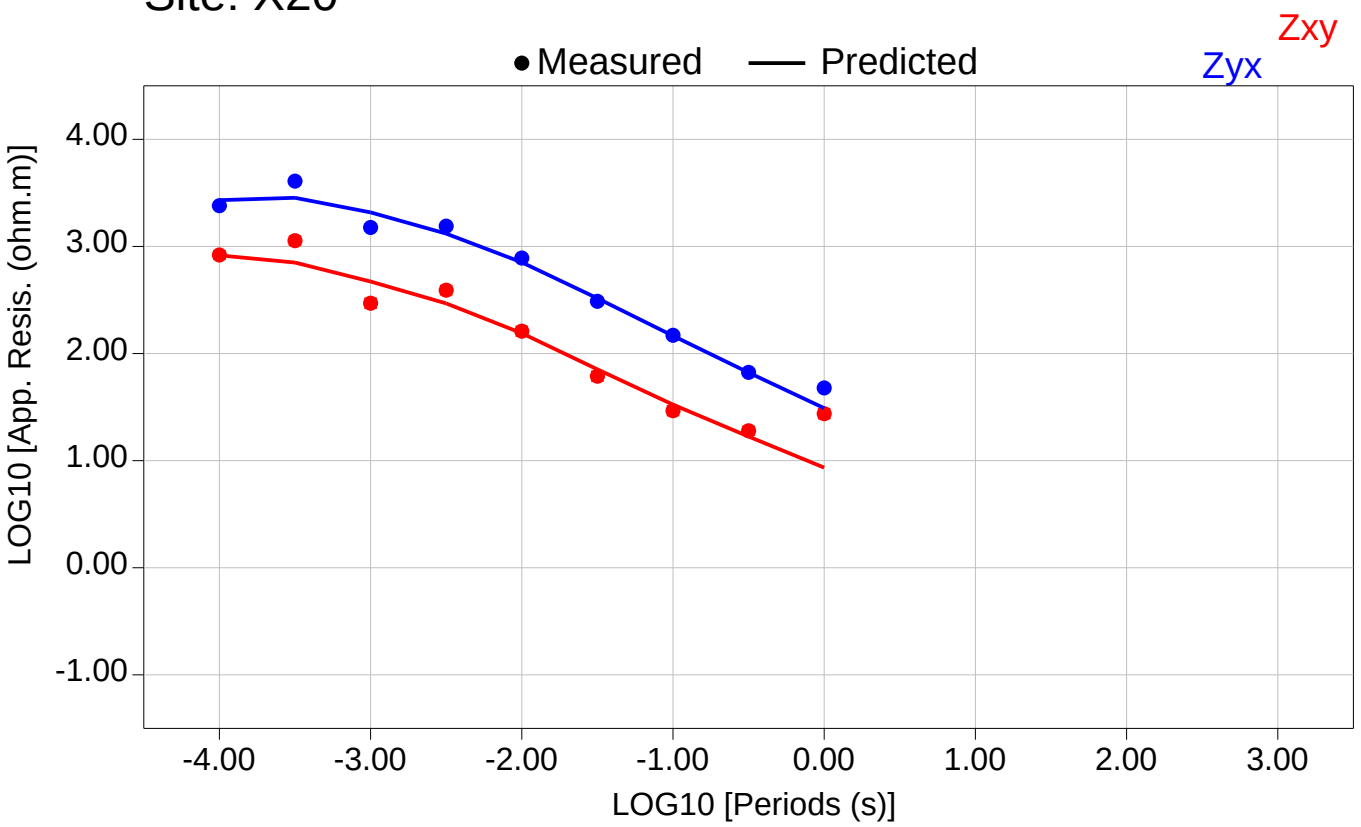

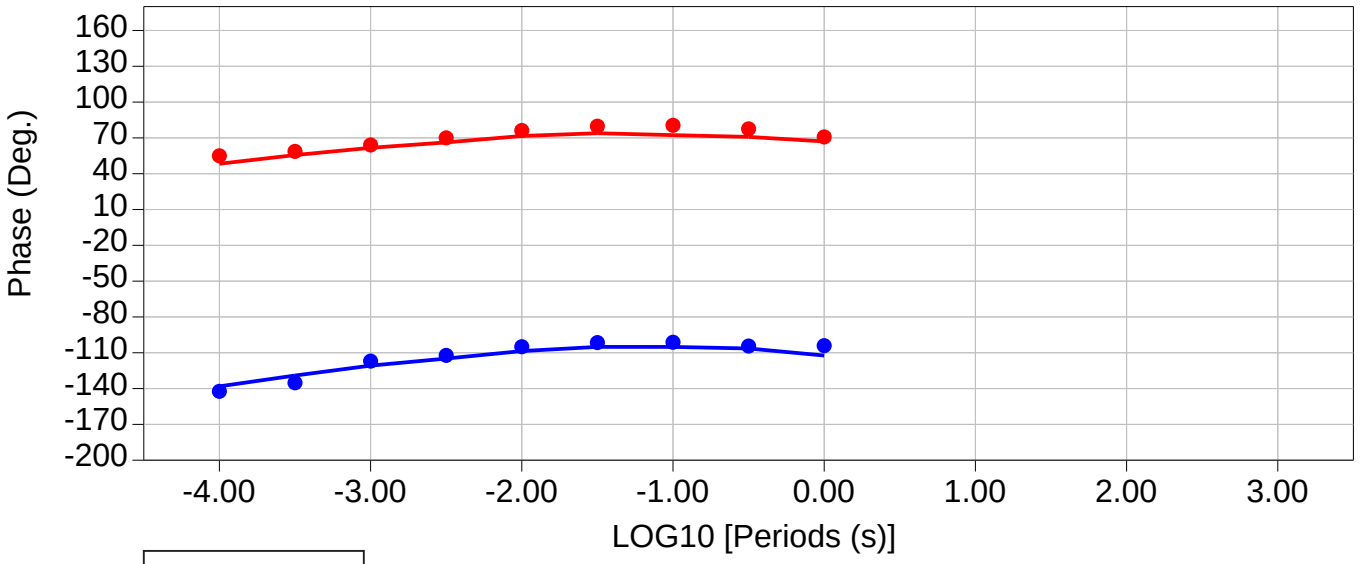

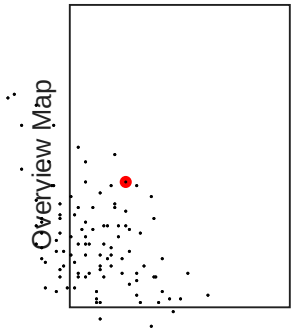

Total RMS = 21161.00

Zxy RMS = 13001.47
Zyx RMS = 26954.36

Site: X21

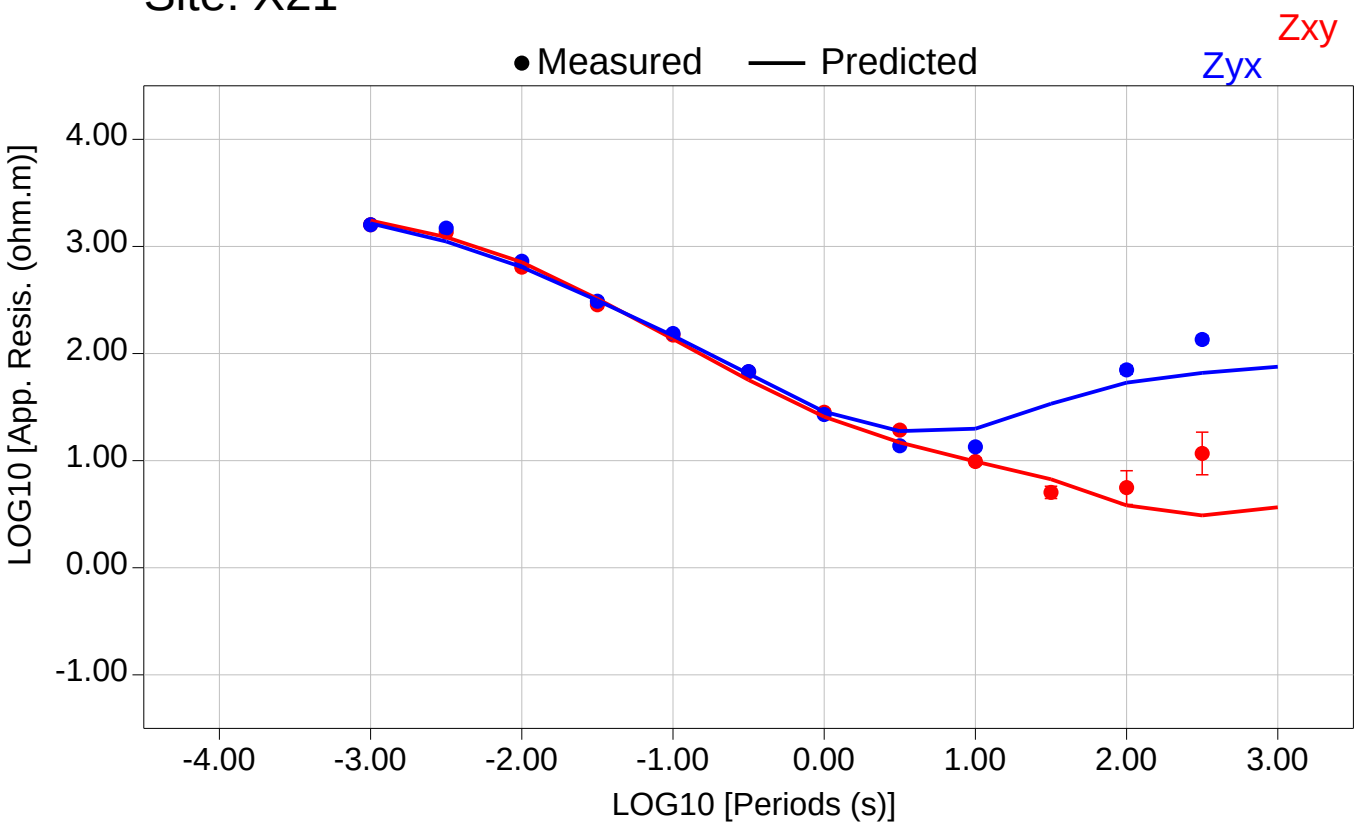

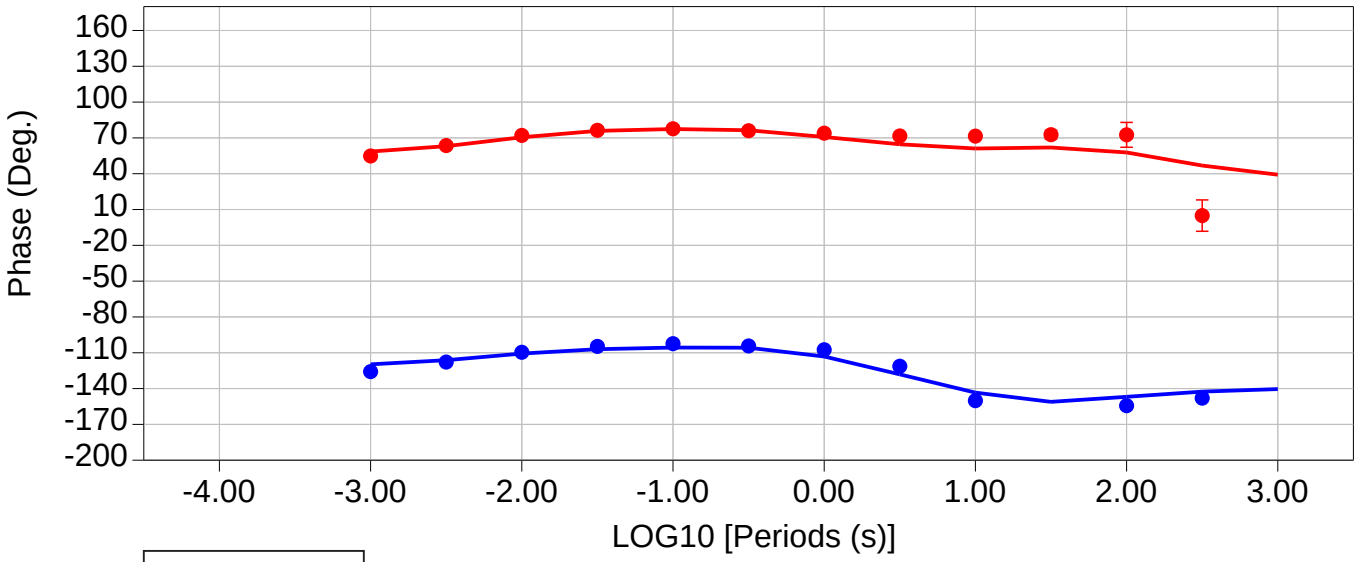

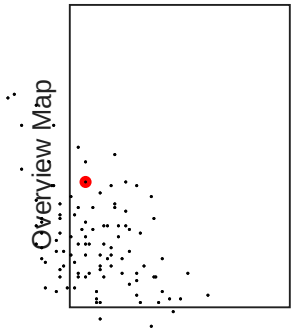

Total RMS = 18083.14

Zxy RMS = 17642.59

Zyx RMS = 18551.81

Site: X22

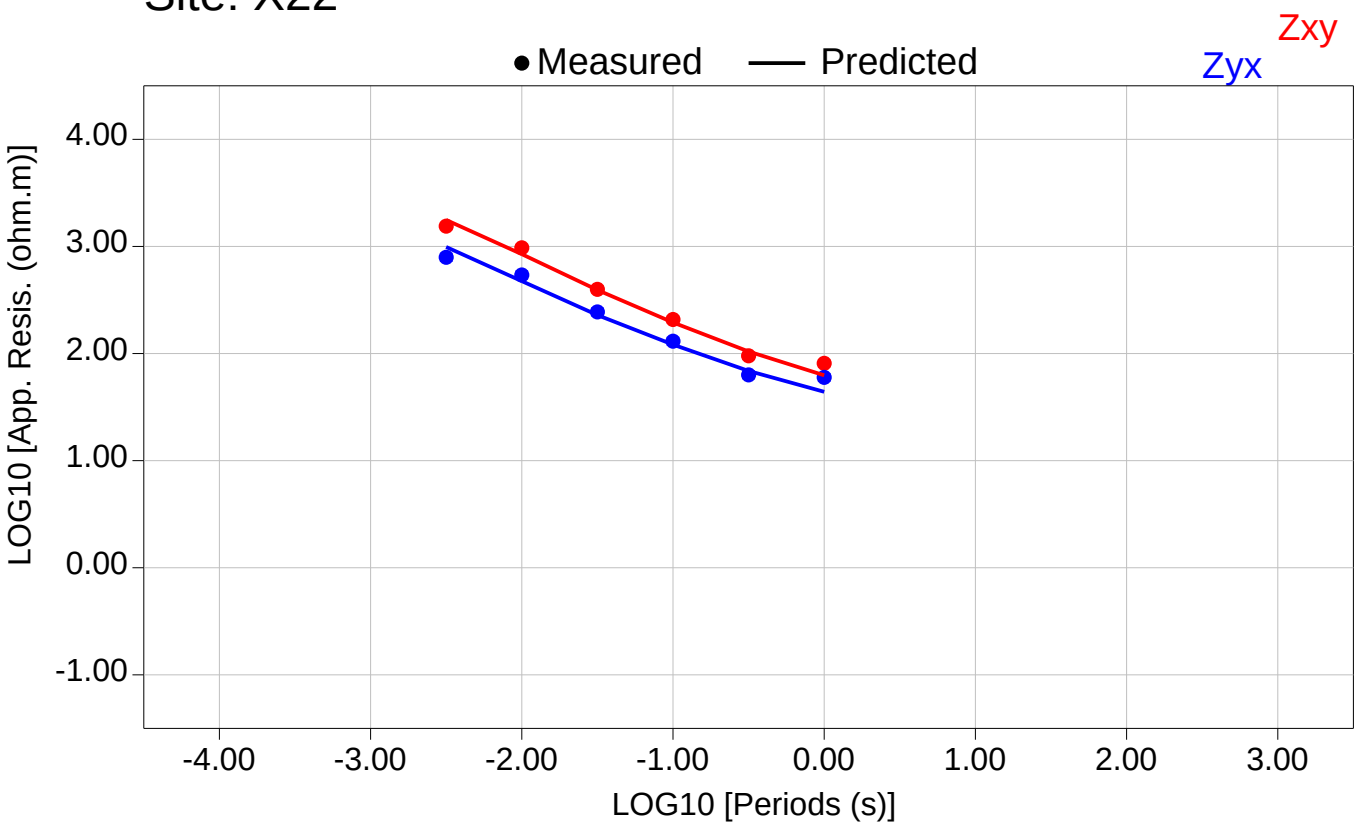

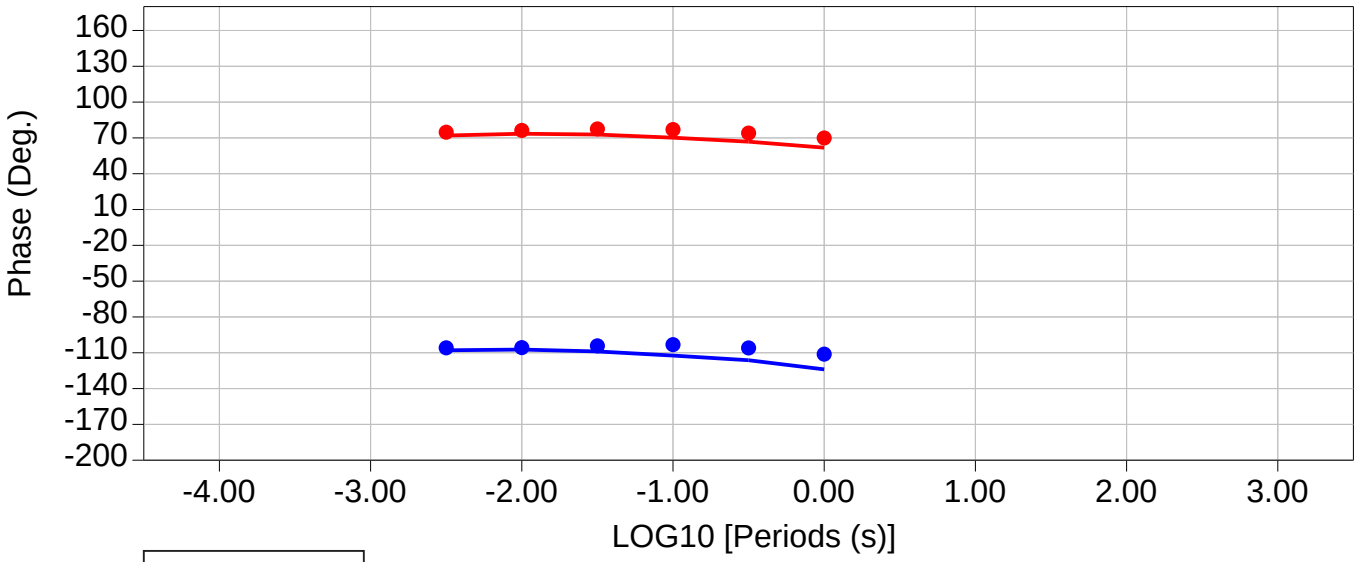

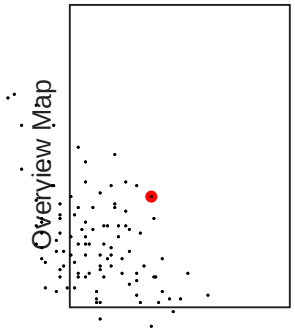

Total RMS = 18245.60

Zxy RMS = 20432.66

Zyx RMS = 15757.86

Site: X23

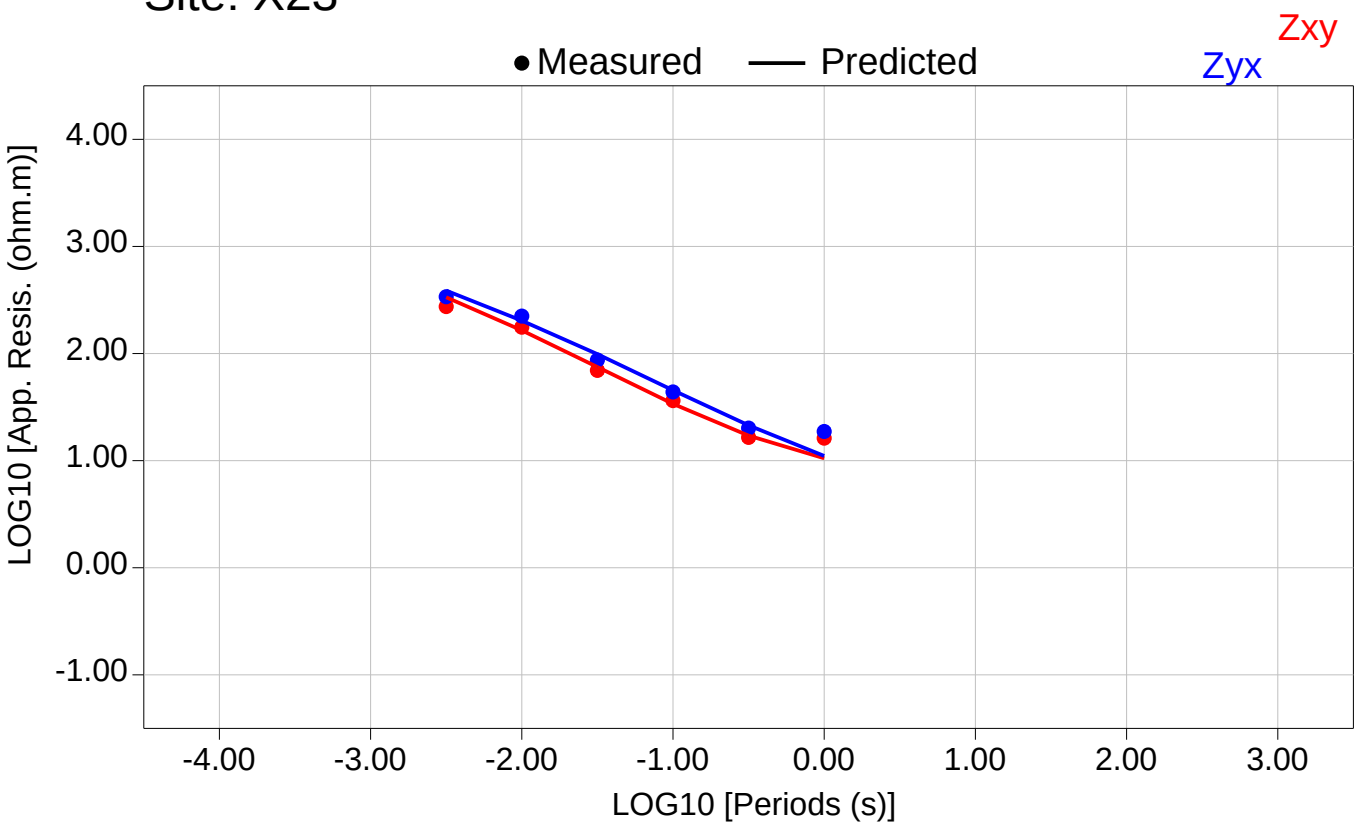

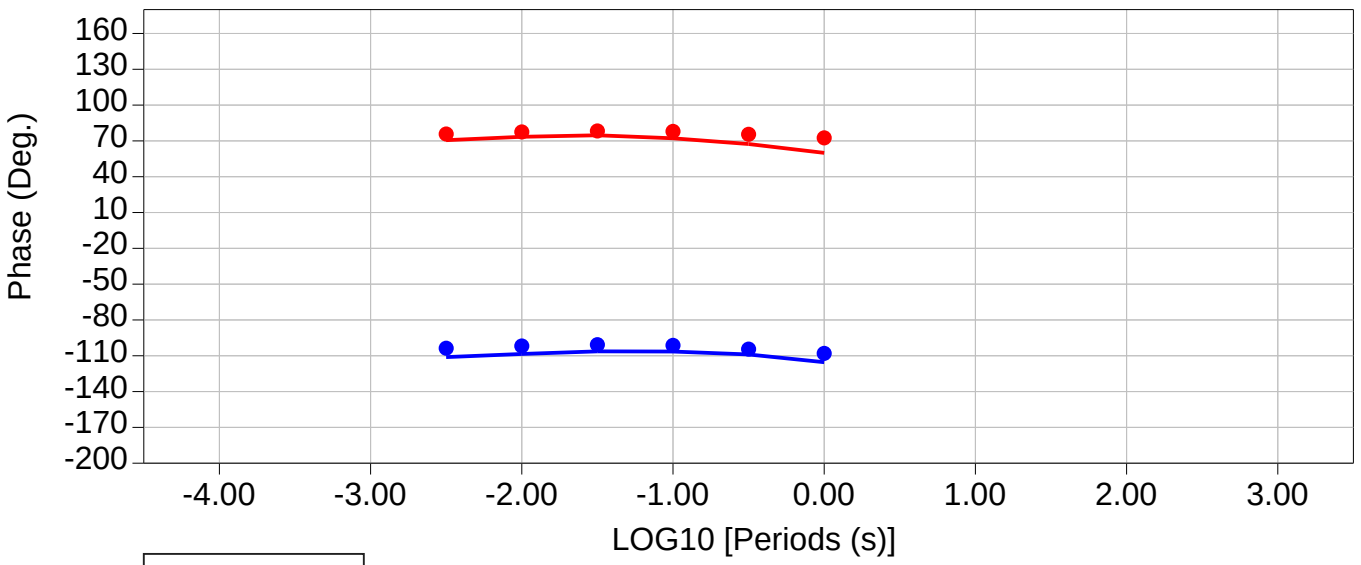

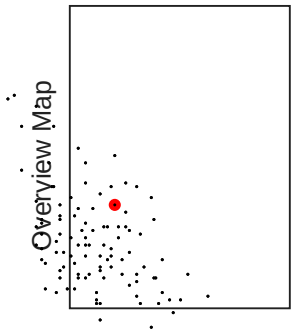

Total RMS = 18875.07

Zxy RMS = 17704.10

Zyx RMS = 19977.52

Site: X27

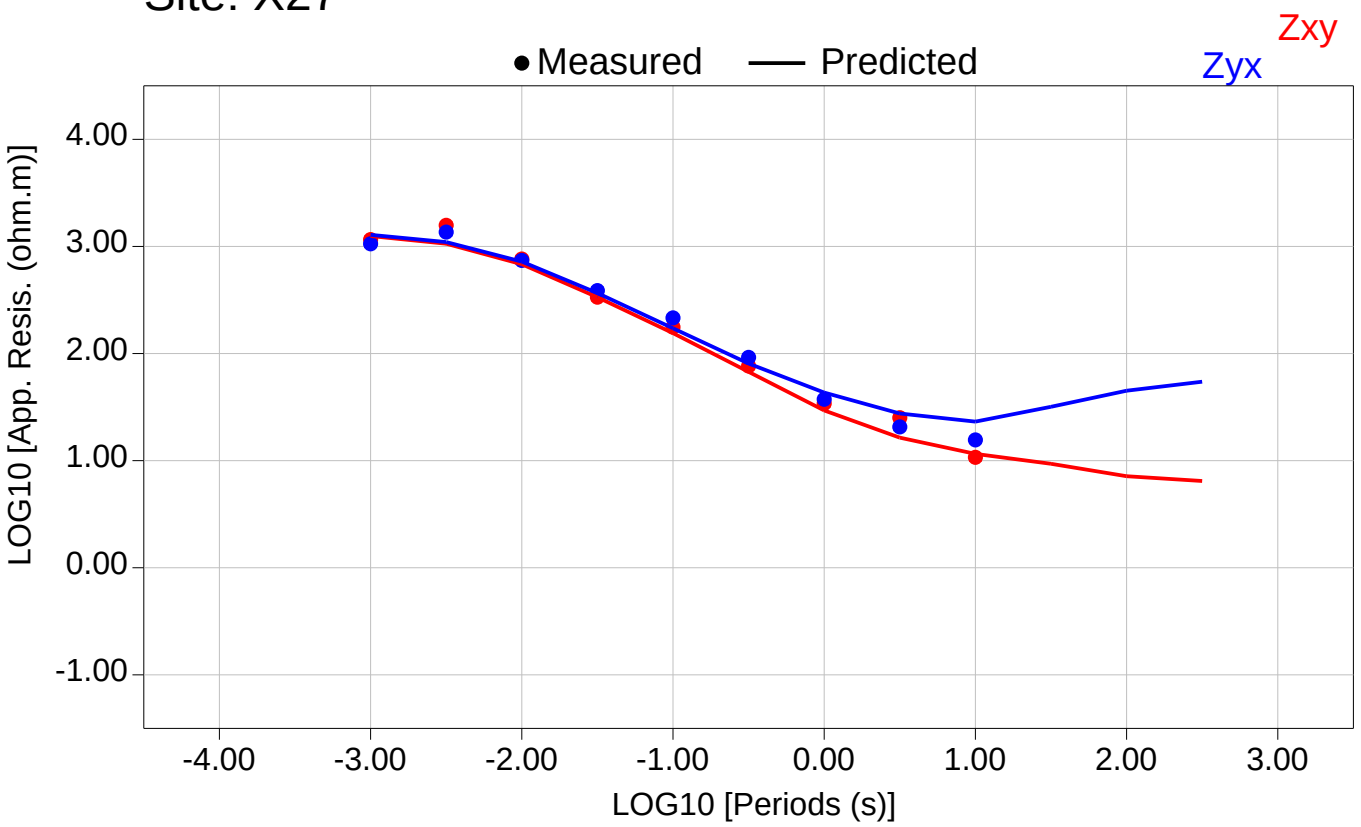

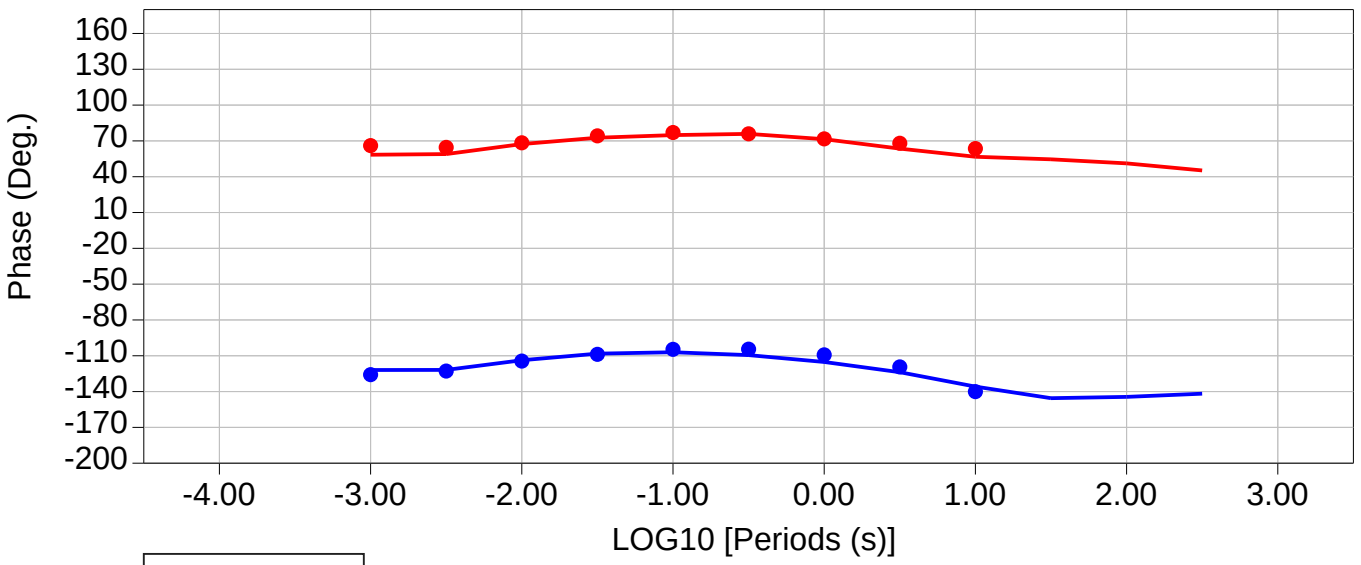

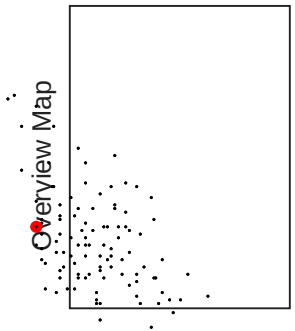

Total RMS = 18886.54

Zxy RMS = 18043.71

Zyx RMS = 19693.33

Site: X28

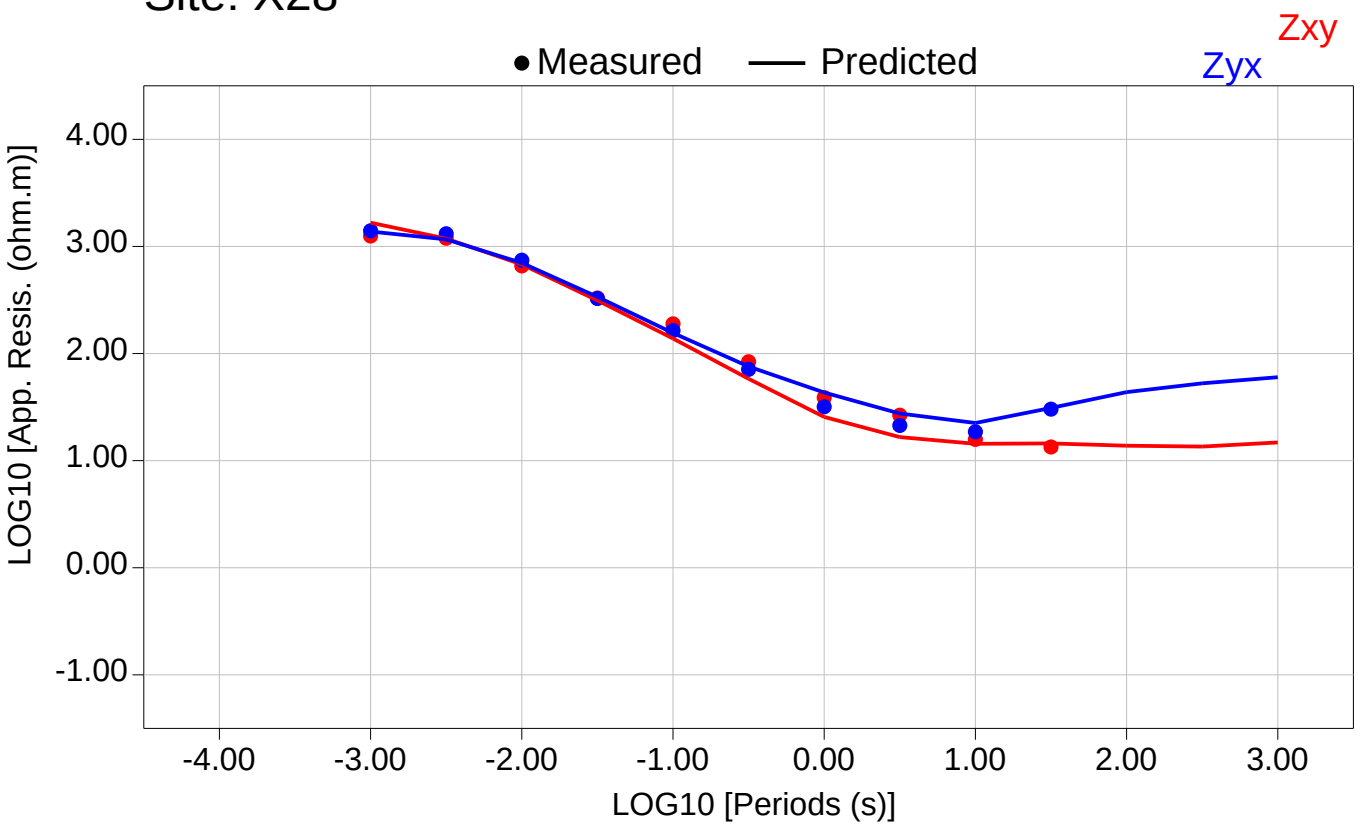

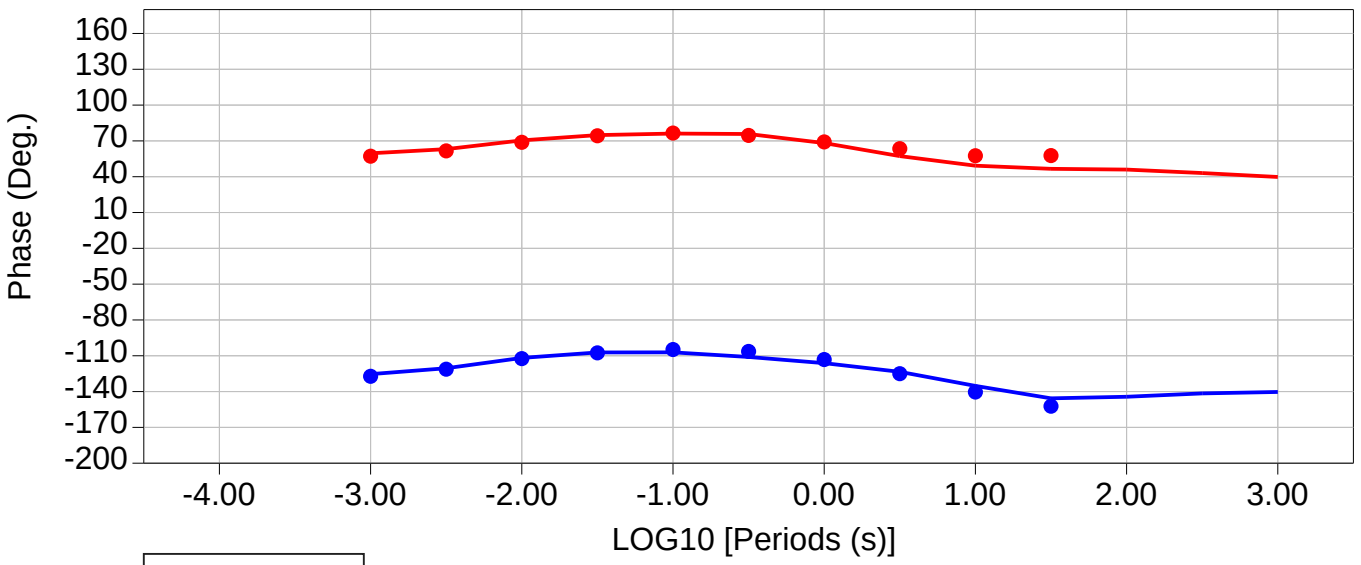

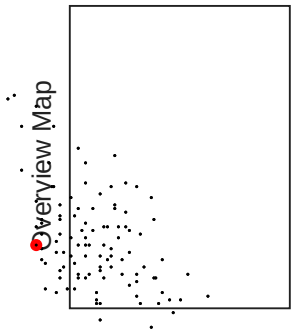

Total RMS = 19157.47

Zxy RMS = 18360.72
Zyx RMS = 19922.39

Site: X29

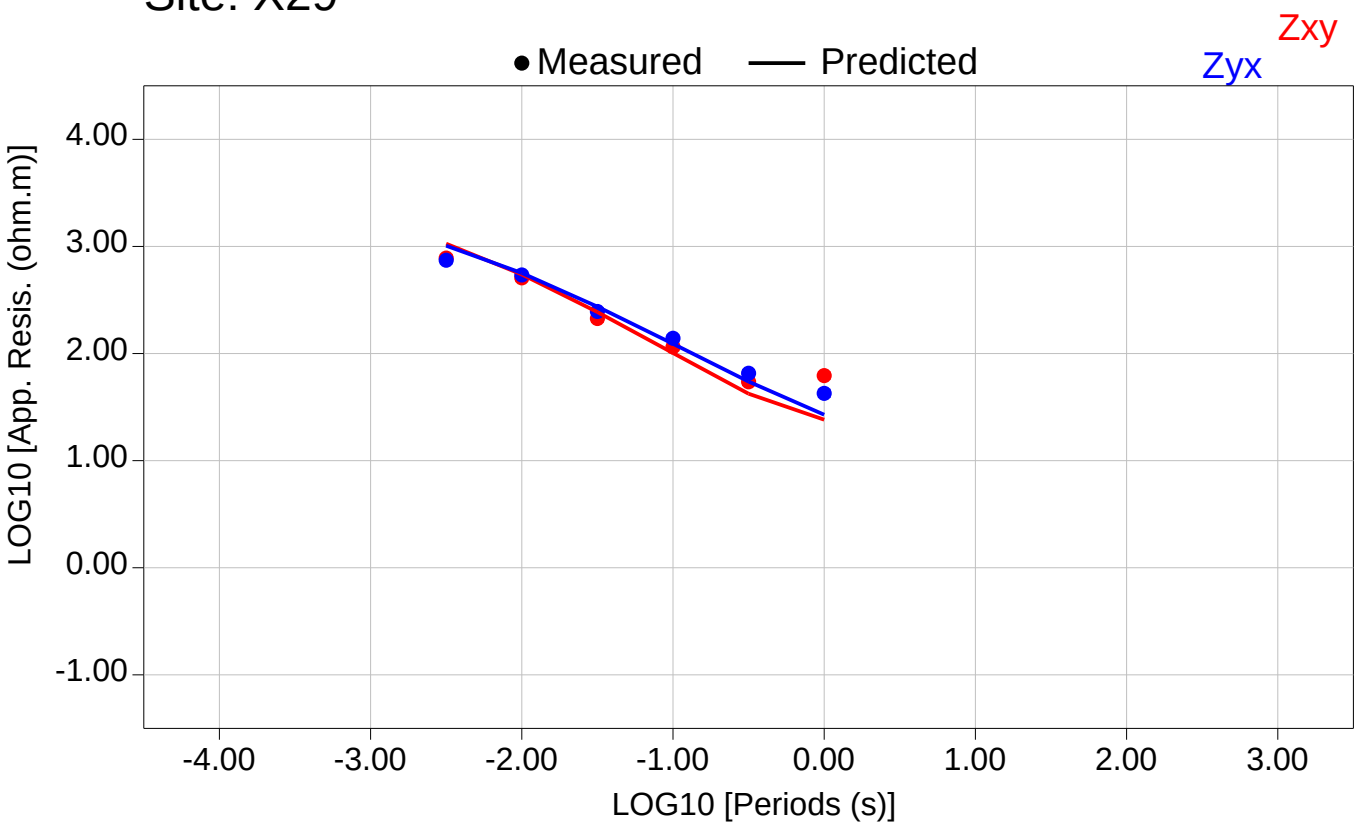

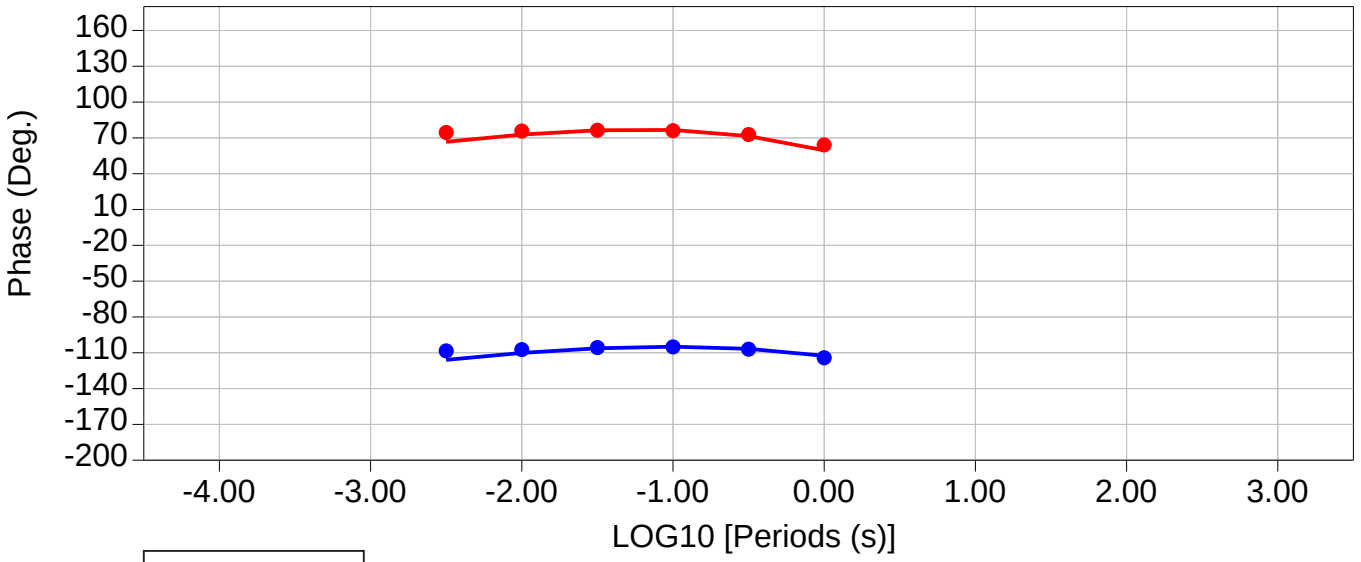

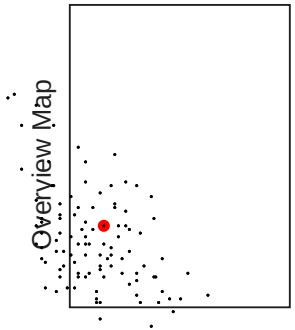

Total RMS = 18356.35

Zxy RMS = 17857.94

Zyx RMS = 18841.59

Site: X30

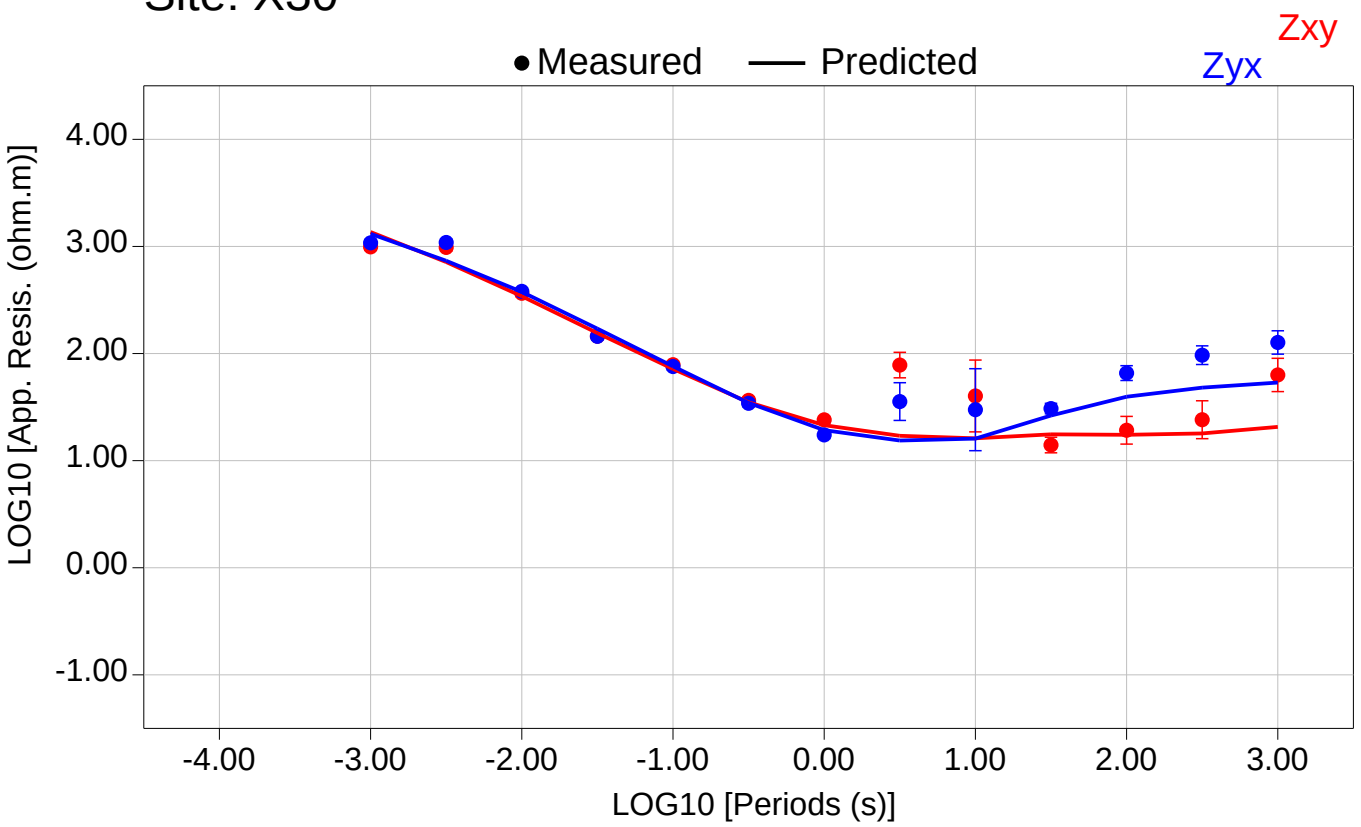

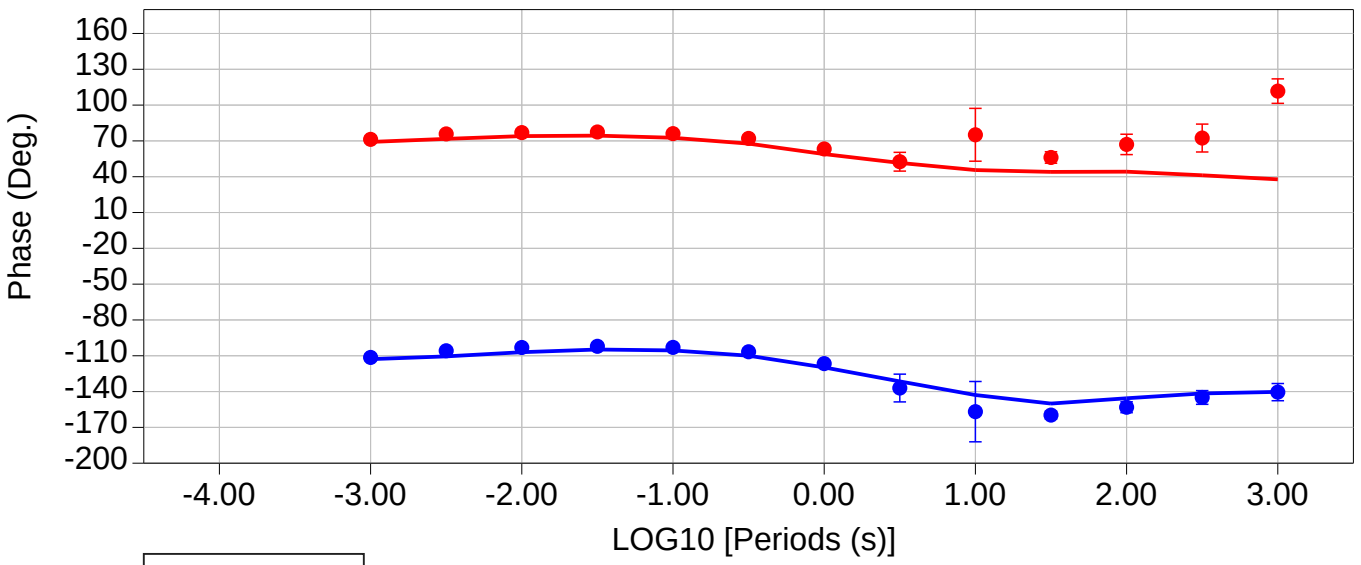

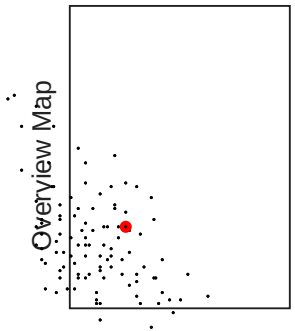

Total RMS = 15183.62

Zxy RMS = 15004.09
Zyx RMS = 15361.06

Site: X31

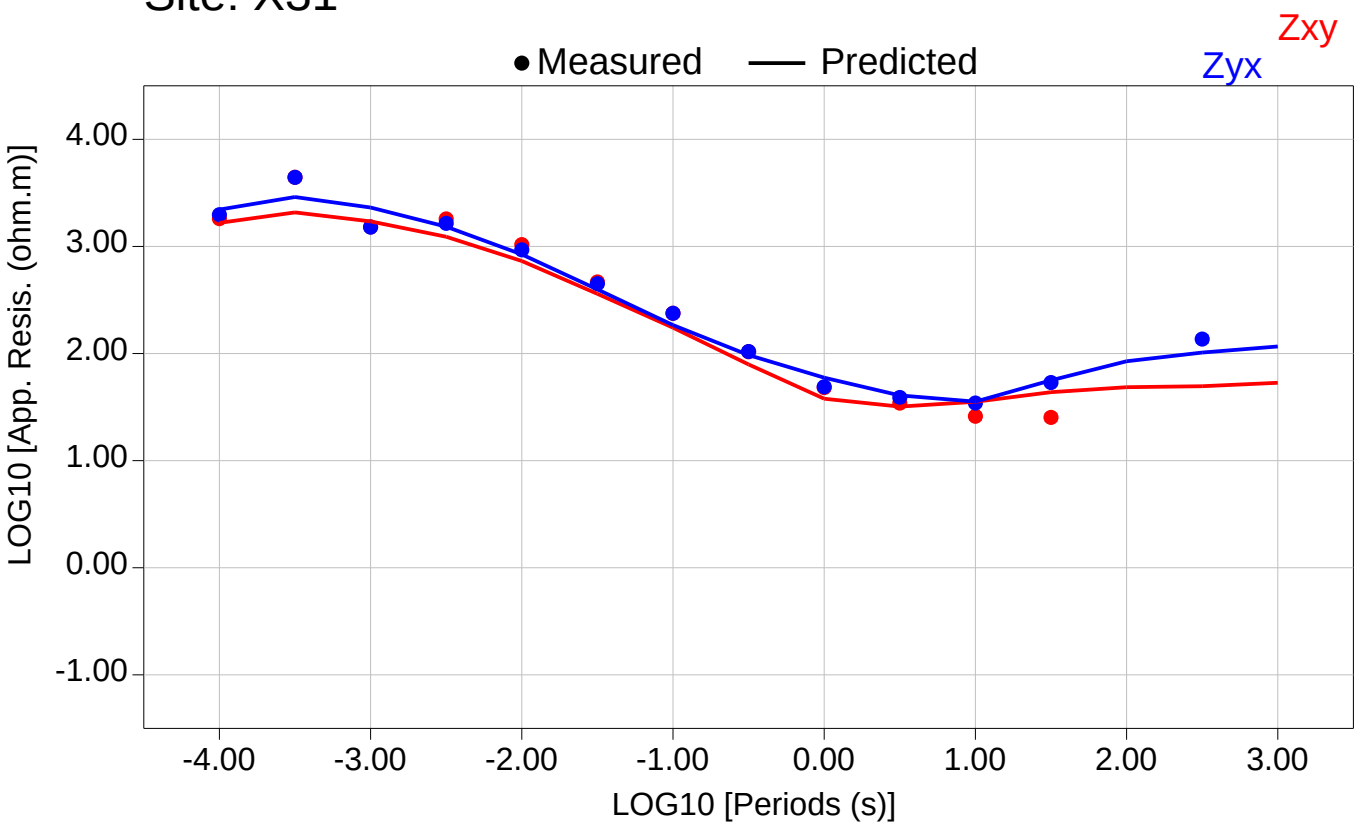

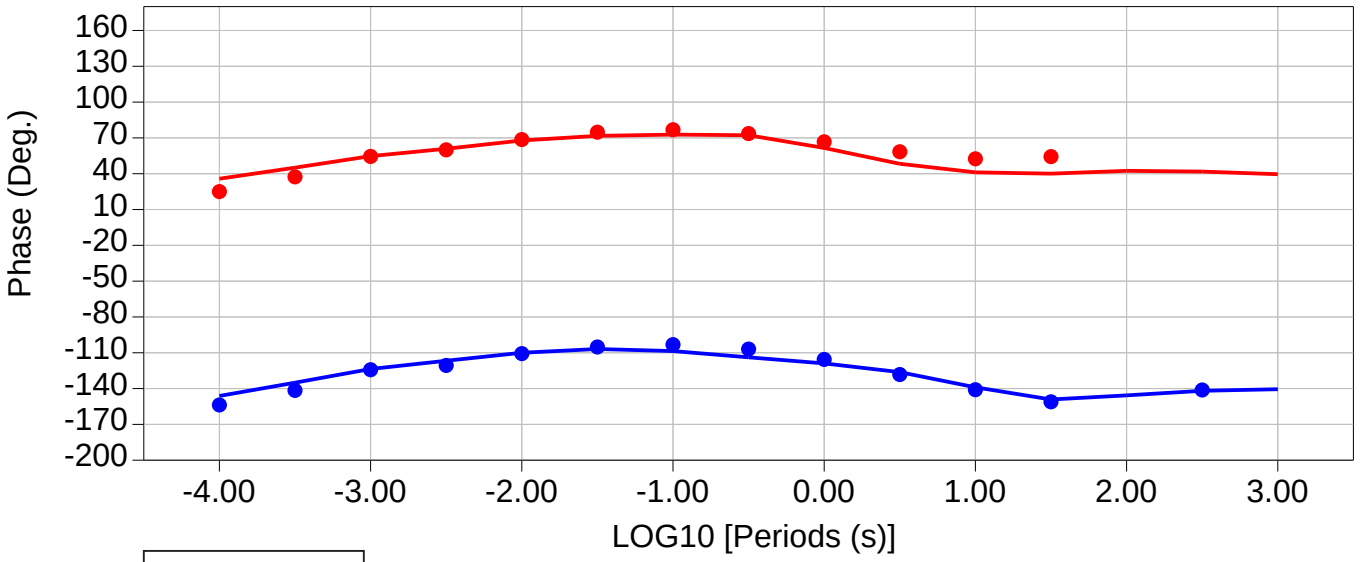

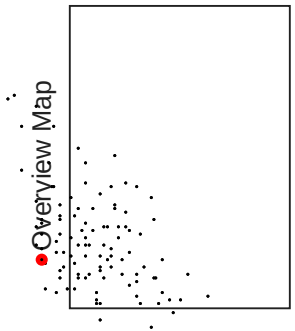

Total RMS = 17432.71

Zxy RMS = 16696.87
Zyx RMS = 18085.40

Site: X32

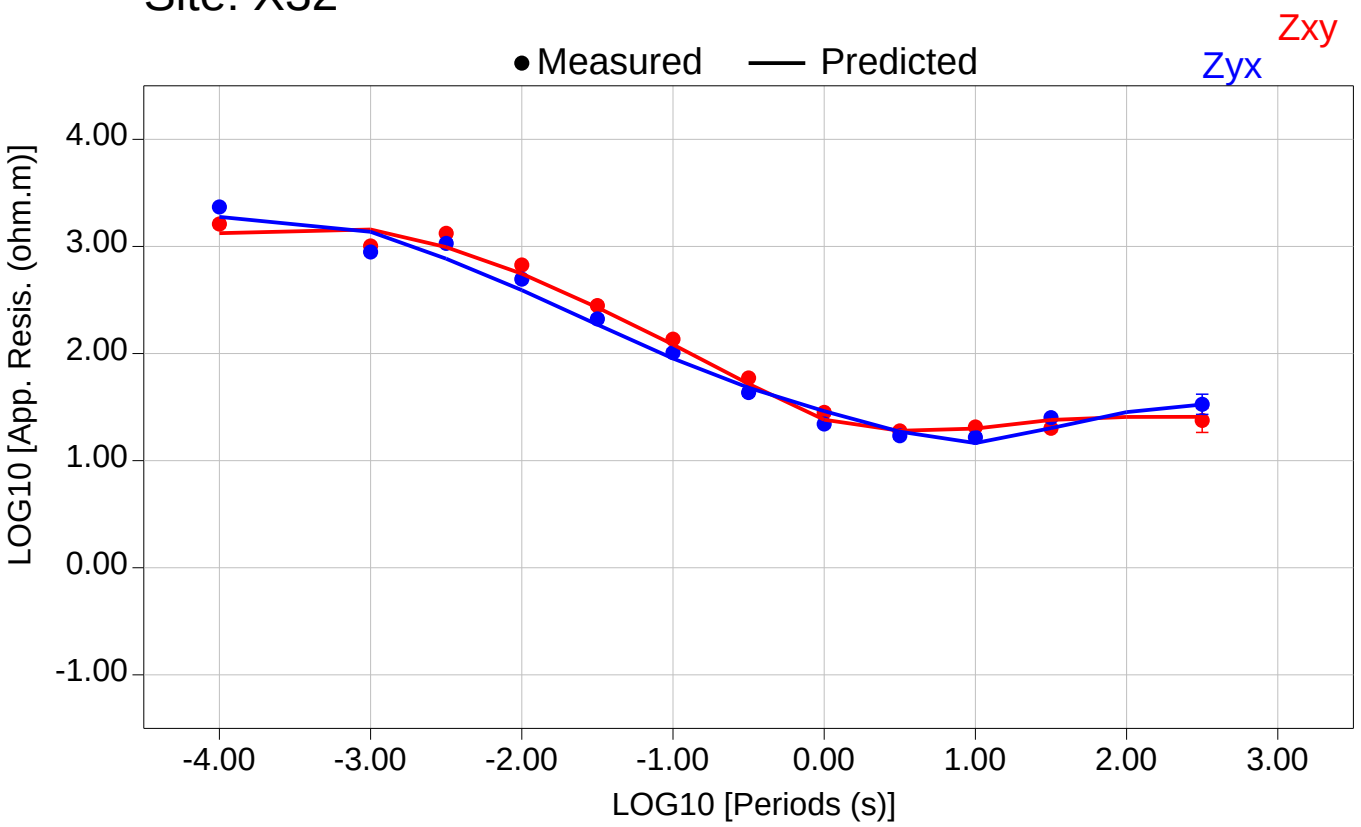

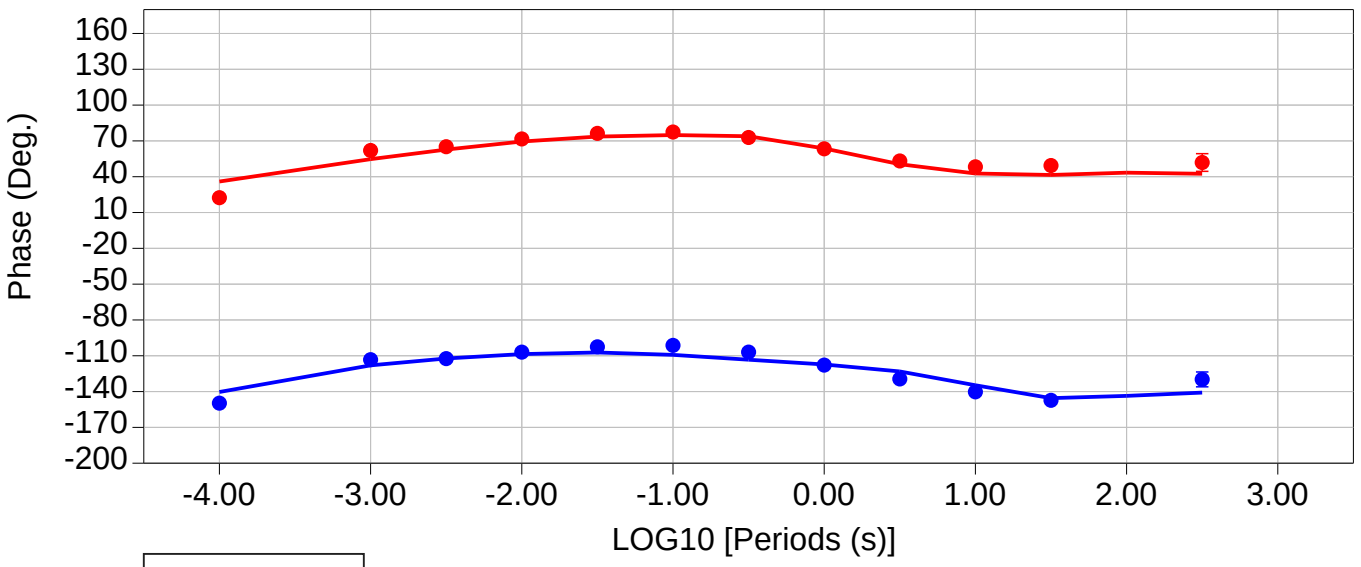

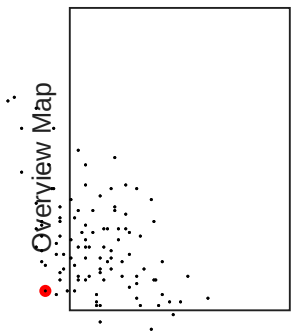

Total RMS = 17754.72

Zxy RMS = 18425.72

Zyx RMS = 17057.35

Site: X33

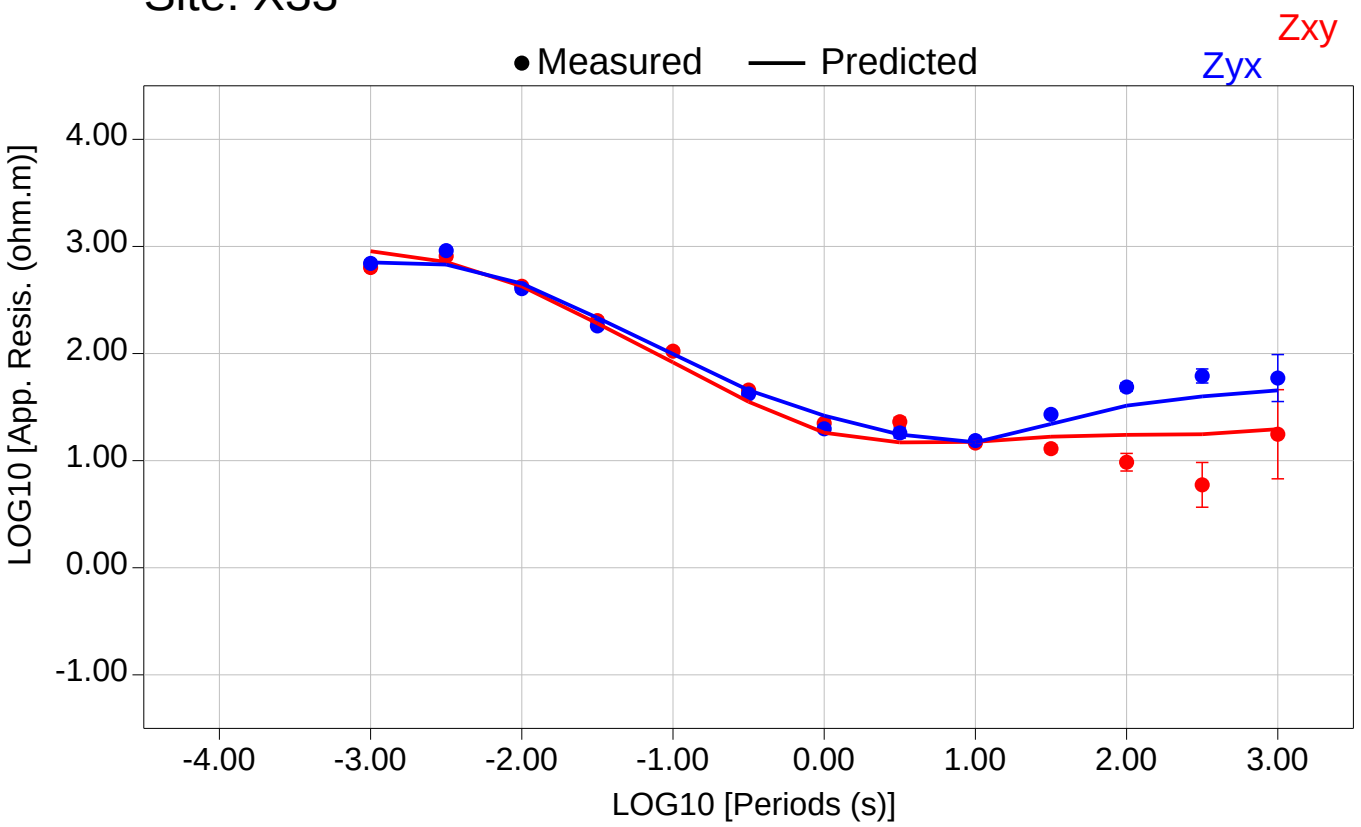

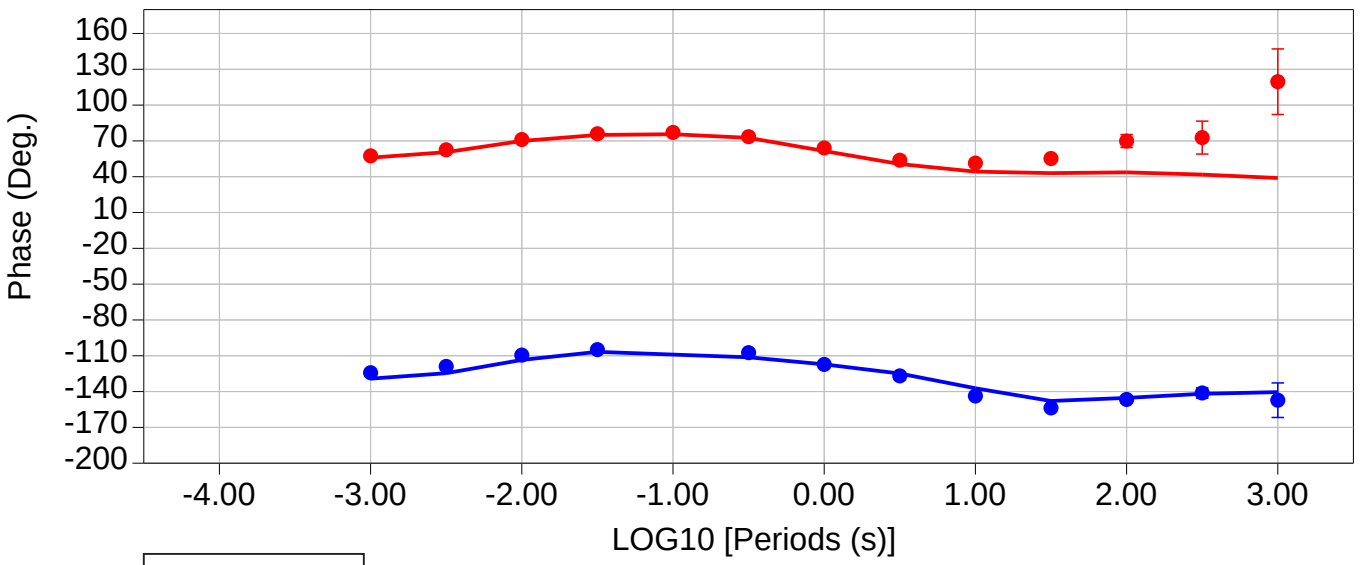

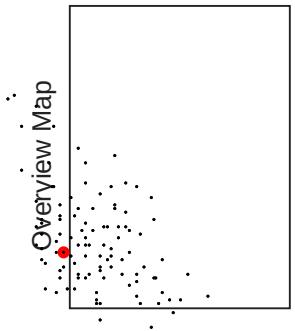

Total RMS = 15148.42

Zxy RMS = 15818.73

Zyx RMS = 14387.06

Site: X34

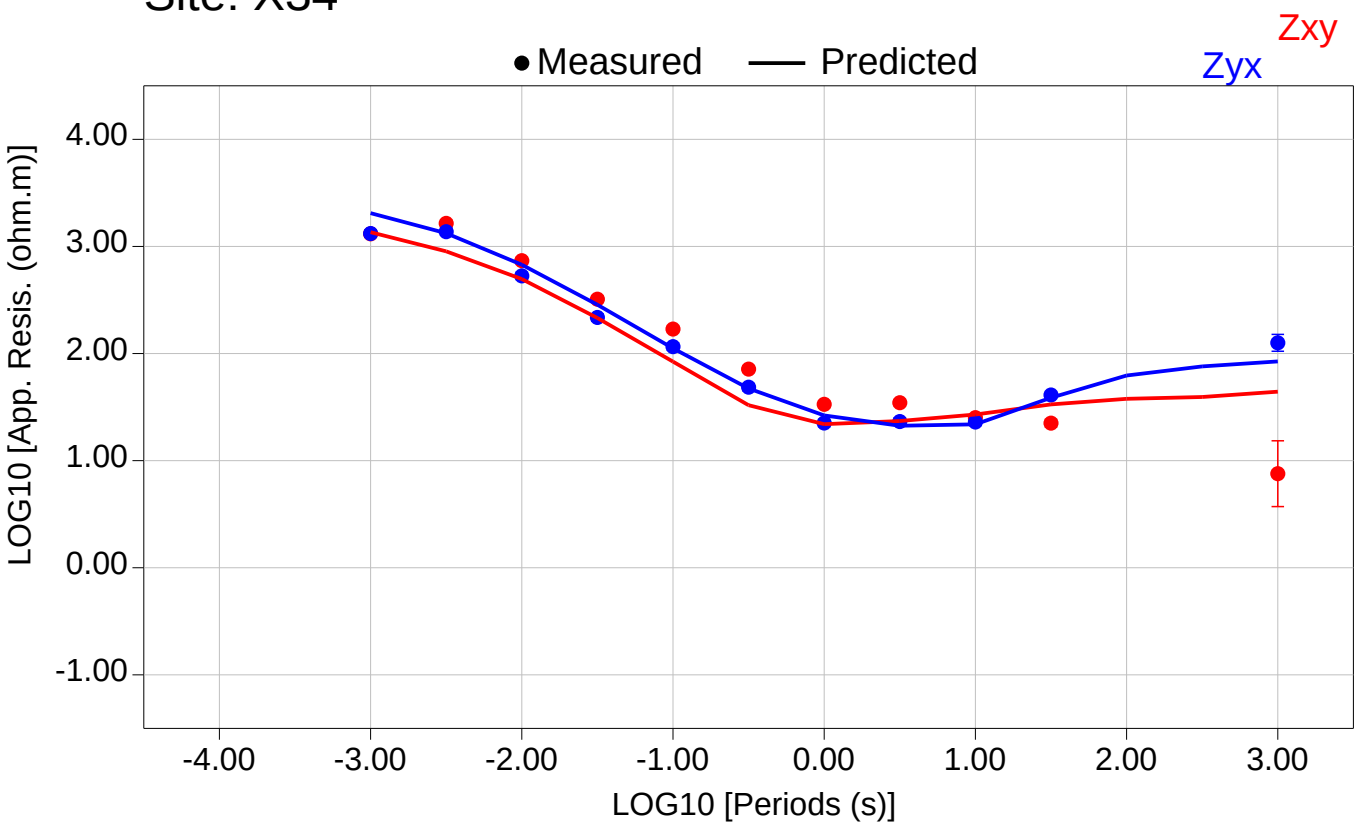

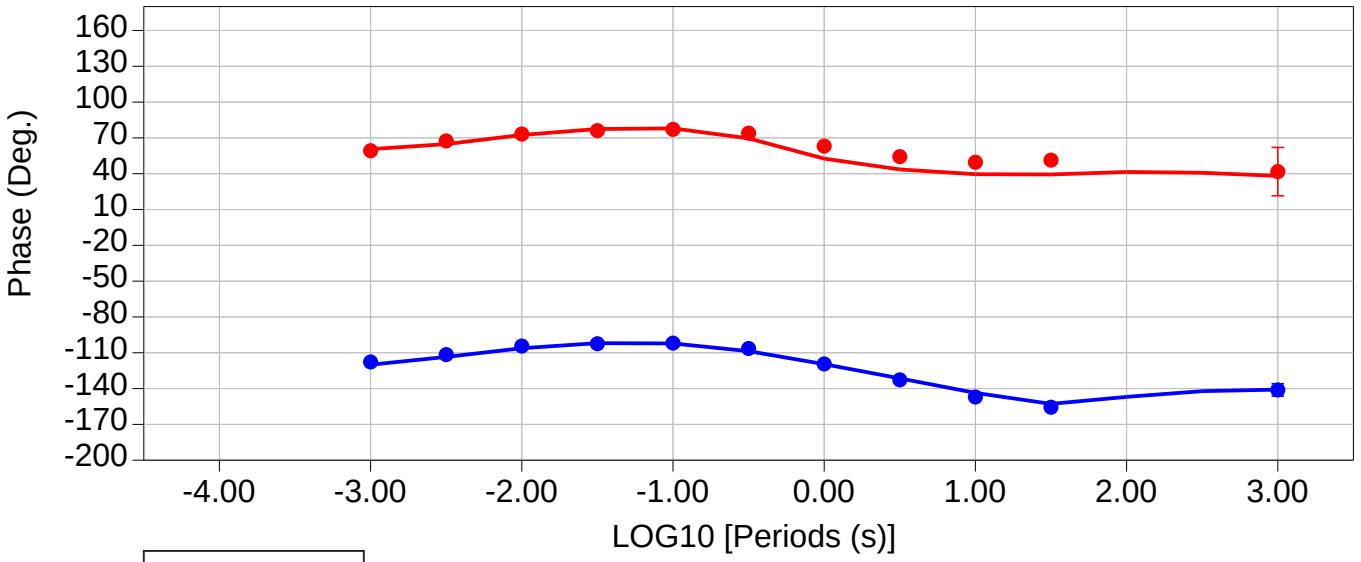

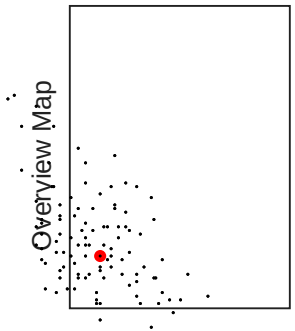

Total RMS = 17292.40

Zxy RMS = 16252.76
Zyx RMS = 18272.99

Site: X35

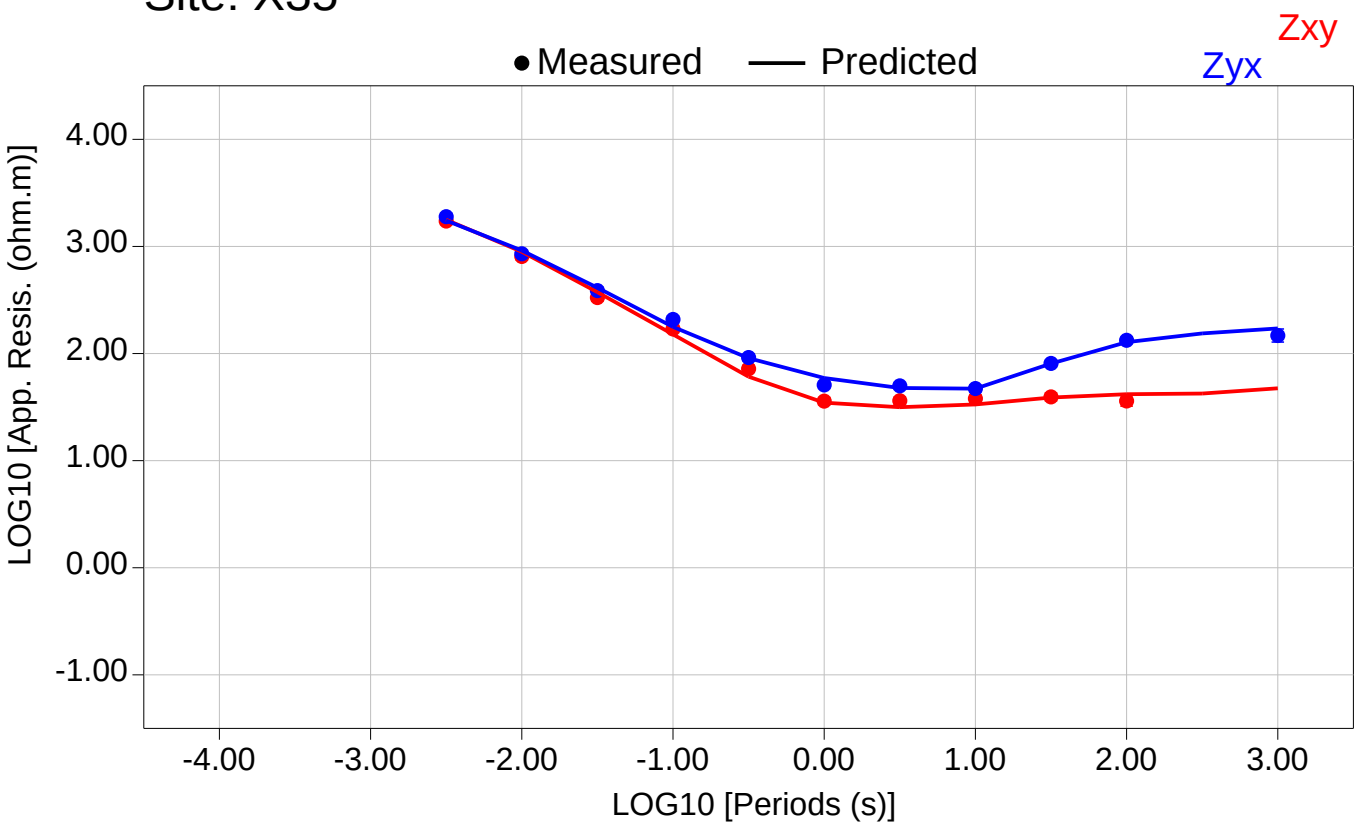

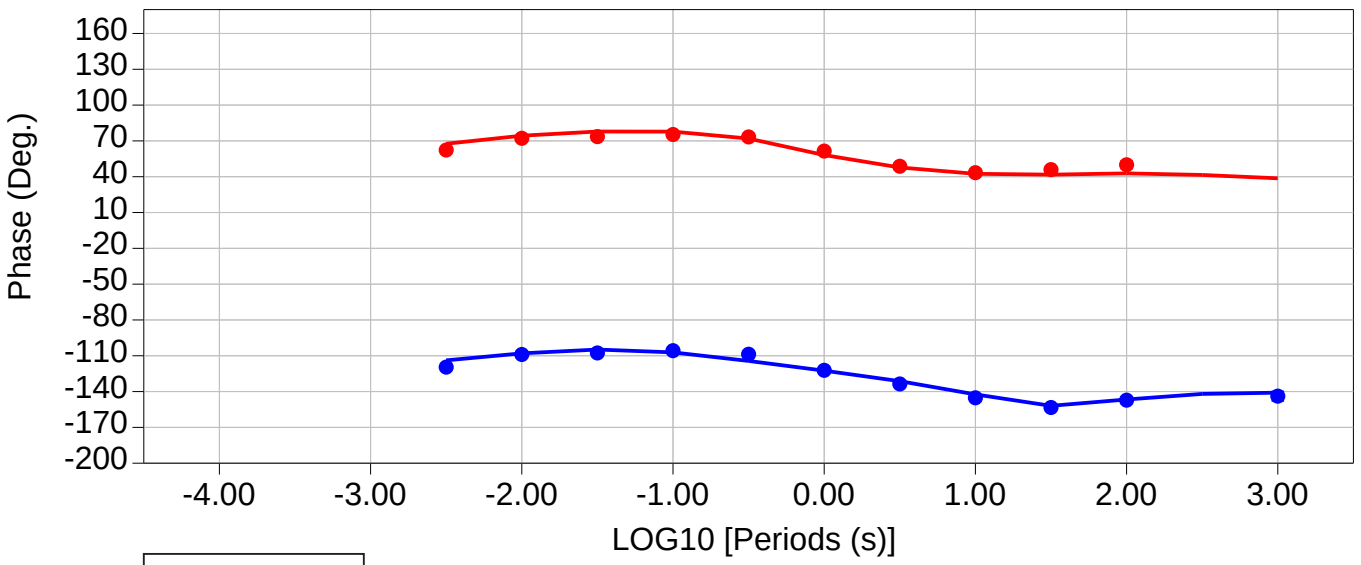

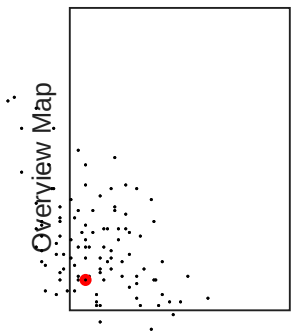

Total RMS = 17449.80

Zxy RMS = 16734.63

Zyx RMS = 18075.41

Site: X40

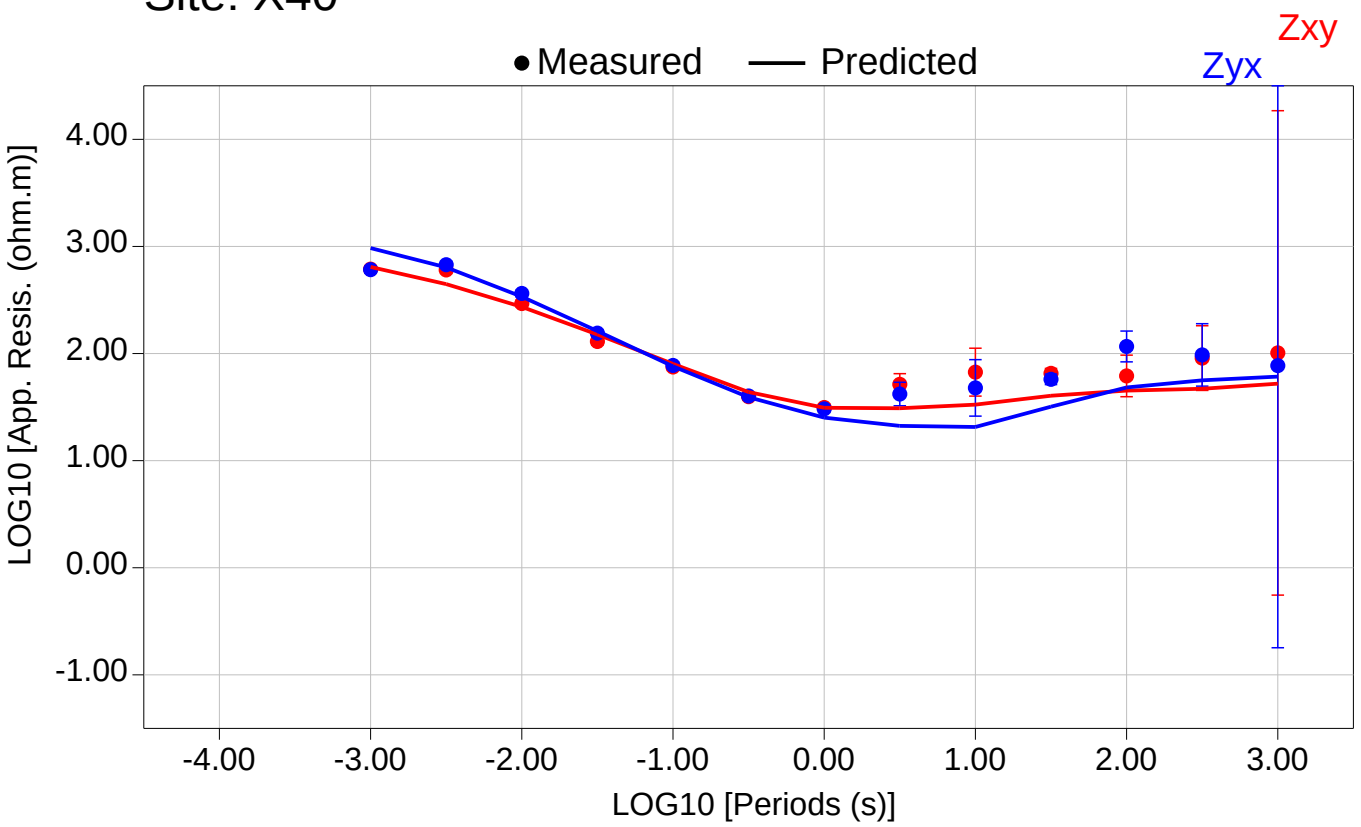

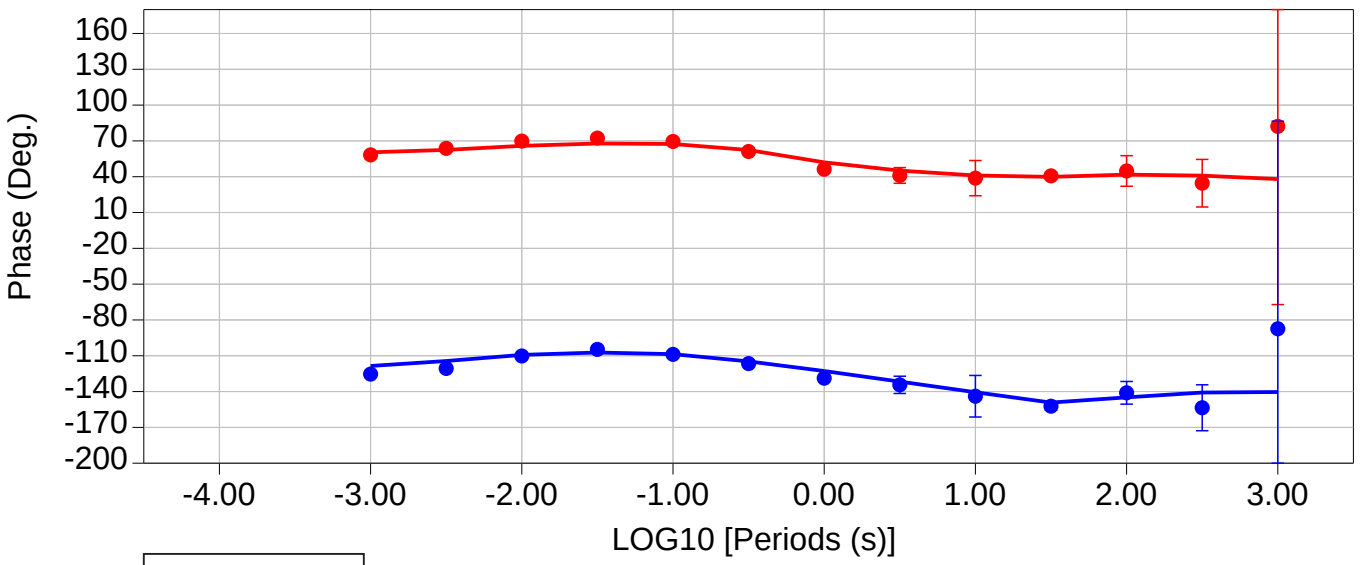

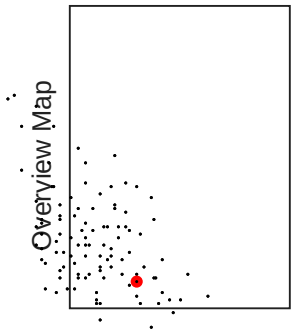

Total RMS = 14628.71

Zxy RMS = 14129.51

Zyx RMS = 15111.43

Site: X41

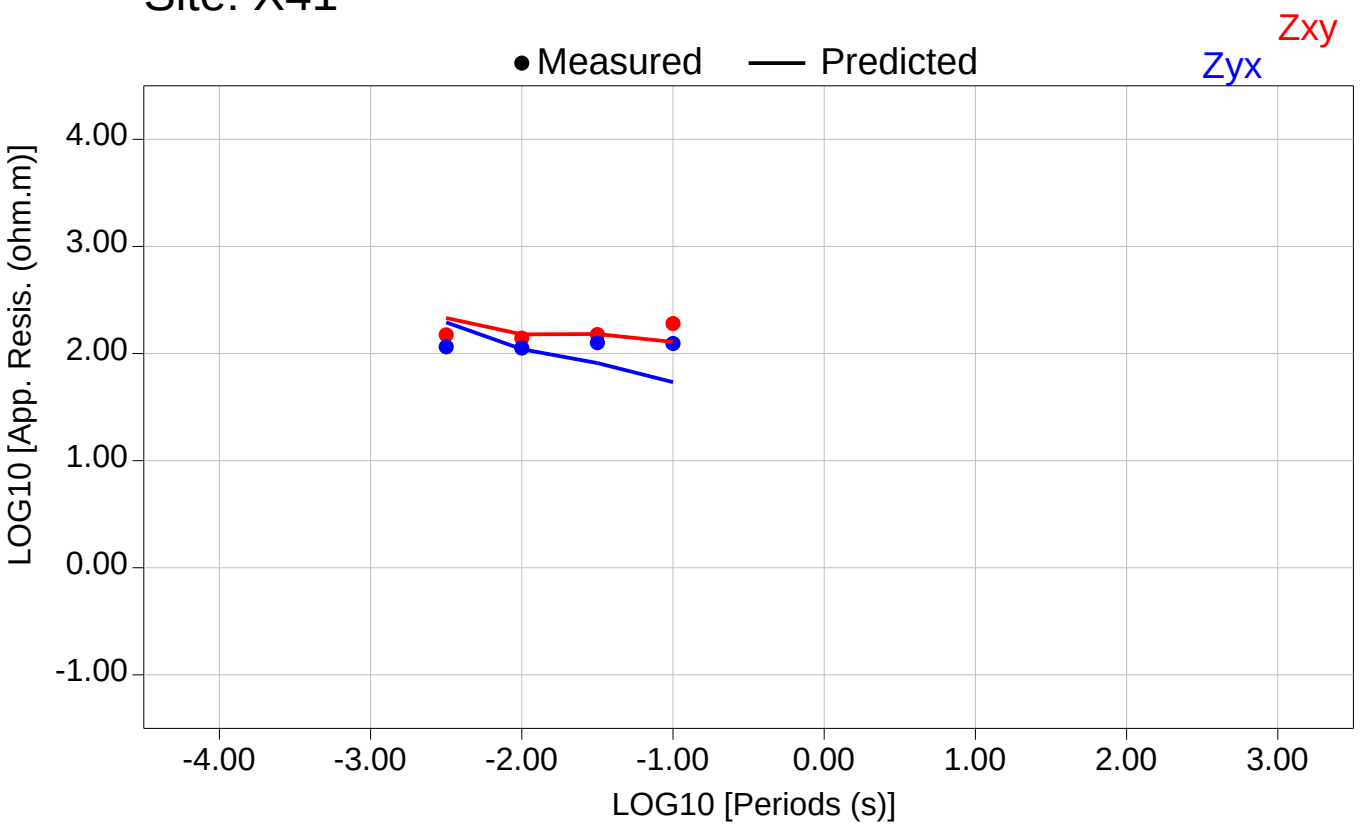

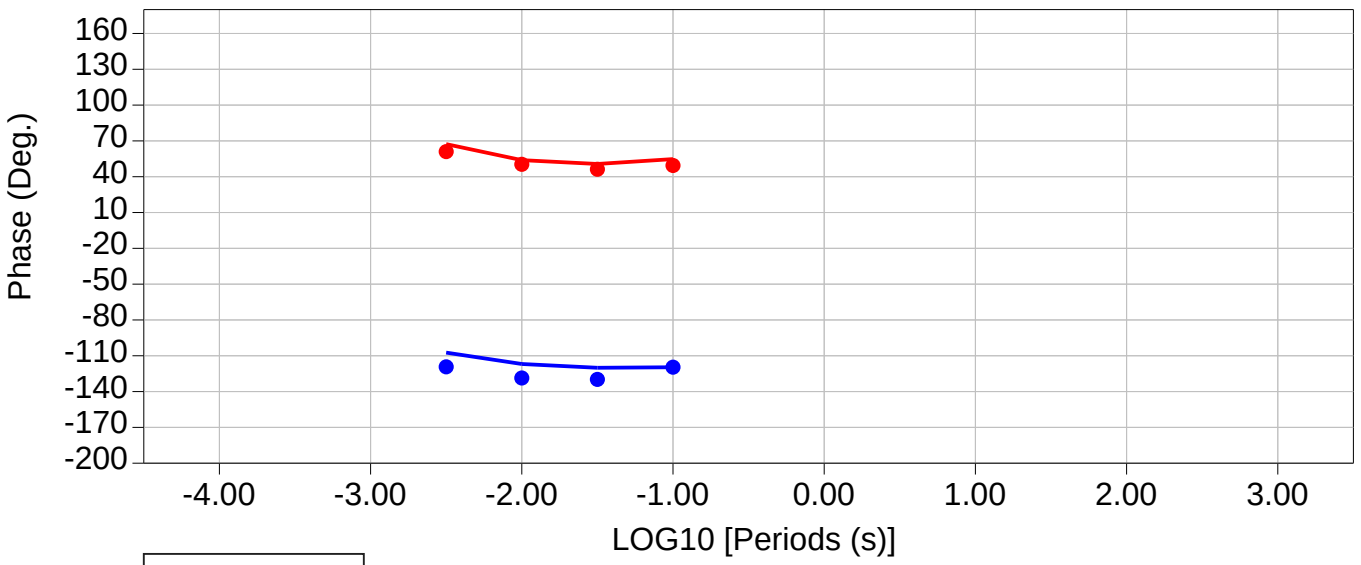

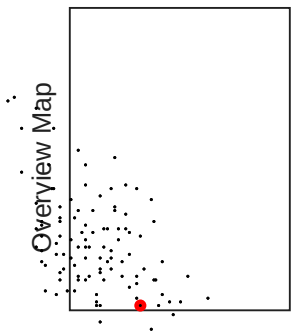

Total RMS = 12094.18

Zxy RMS = 13192.71
Zyx RMS = 10885.36

Site: X87

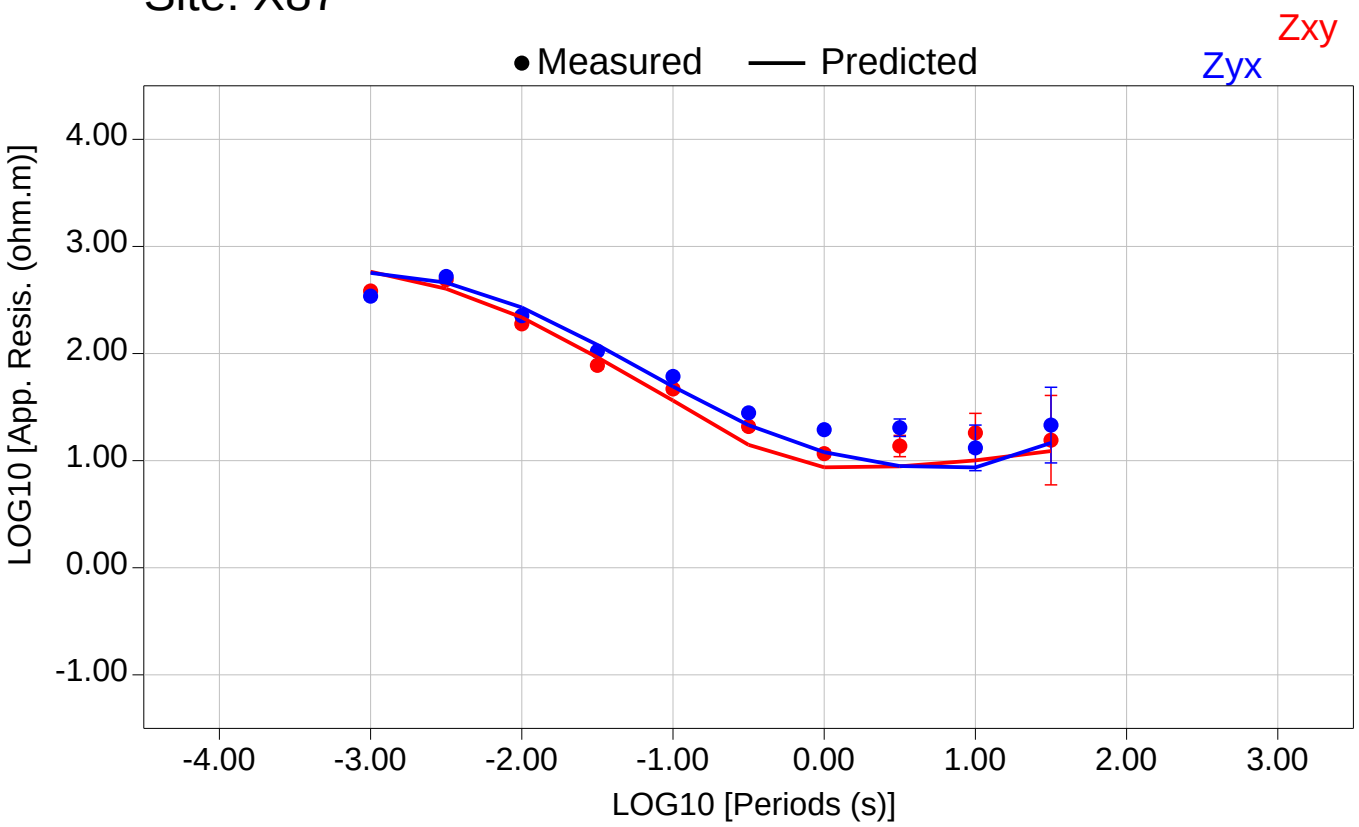

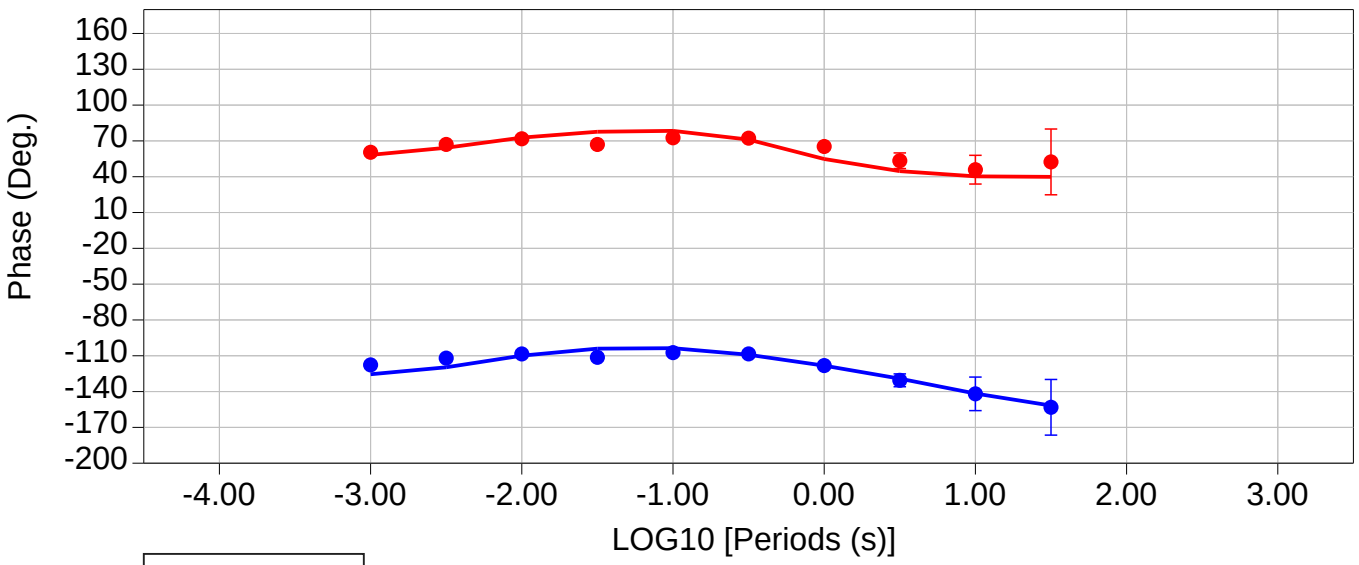

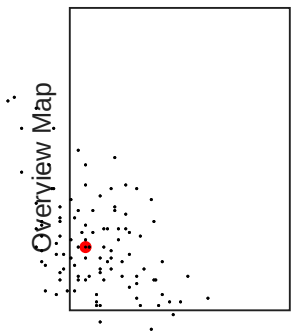

Total RMS = 16765.96

Zxy RMS = 15966.60
Zyx RMS = 17528.92